NANOSCALE OBSERVATIONS OF FINGERPRINTS ON BRASS SUBSTRATES

Thesis submitted for the degree of

Doctor of Philosophy

at the University of Leicester

by

Alex John Goddard MChem

Department of Chemistry

University of Leicester

2013

Nanoscale Observations of Fingerprints on Brass Substrates

Alex J. Goddard

The recovery and visualisation of fingerprints on brass substrates by traditional methods is frequently unsatisfactory, particularly when the samples have been subjected to extreme environmental conditions. This includes items for which surface morphology or exposure to non-ambient conditions compromises traditional recovery methods. To address this challenge, the work in this thesis aims to understand the physical and chemical changes occurring for fingerprint sweat deposited onto brass substrates. This was accomplished by monitoring samples using a range of different surface sensitive techniques, based on optical, physical and chemical phenomena. The main aspects explored were surface structure (topography and morphology, using various microscopies), surface composition (using XPS) and surface dynamics (evolution of surface composition and structure with exposure to diverse conditions). The amount and viscosity of fingerprint sweat deposit changed over time; this was detectable at both the nanoscale (by AFM) and macroscale (optically). The visualisation rate of the fingerprint mark could be enhanced by storage in warm humid environments. The chemical surface composition was also subject to change: this applied to both the substrate and the fingerprint sweat deposit. The Cu:Zn ratio of the substrate was affected by both the sweat type and the storage conditions employed. Surface species also changed when subjected to different storage environments. The fingerprint sweat deposit present on the substrates was difficult to remove; even washing in warm soapy water failed to remove detectable levels of the fingerprint. Non-visible fingerprints could still be detected by surface chemical composition and also *revived* by storage in warm humid environments. The detailed findings should influence laboratory experiment protocols and evidence processing. The outcomes of this work should improve the recovery of fingerprints from brass substrates by optimisation of storage environments and new fingerprint detection methodology.

Acknowledgements

There a great many people that I am grateful to and appreciate all the help and support given throughout my Ph.D. There are too many to mention all by name, however, I am grateful to each and every one of you none the less!

I would like to start by thanking Northamptonshire Police and the University of Leicester for financial support and making this study possible. Also to Prof. A. Robert Hillman and Dr John W. Bond, without whom this project would not have been possible, both offered a great deal of support, faith and guidance. Another thank you goes to all the members of the Hillman group to whom I spent a lot of time with over the last few years, particularly Magda, Ann, Rachel, Charlotte, Abdul and Mo. Also, my thanks go to all of the undergraduate project students that I had the pleasure of working with on a range of different topics.

I am grateful for the company of the entire ground floor write-up room members (electrochemists, fluorine and others), both past and present, with special thanks to Michal Fornalczyk for company and friendship, particularly in the early days!

I also must express my sincere gratitude to Daresbury Laboratory, for access to the NCESS facility and the kind support of Danny Law, Graham Beamson and Bob Bilsborrow whilst on site.

I am indebted to my family for their support and belief in me throughout, but most importantly, my final thanks goes to my partner, Fay, who has been with me all the way and always providing unquestioned support, understanding and belief in me!

Thank you all!

Contents

Abbreviations

AFR	Automatic fingerprint recognition
AFM	Atomic force microscopy
DHM	Digital holography microscopy
DNA	Deoxyribonucleic acid
EFM	Electrostatic force microscopy
ESCA	Electron spectroscopy for chemical analysis
FTIR	Fourier transform infrared spectroscopy
MFM	Magnetic force microscopy
MMD	Multi-metal deposition
NAFIS	National automated fingerprint identification system
RUVIS	Reflective ultraviolet imaging system
SECM	Scanning electrochemical microscopy
SECPM	Scanning electrochemical potential microscopy
SIMS	Secondary ion mass spectrometry
SPM	Scanning probe microscopy
UV/vis	Ultraviolet-visible spectroscopy
XPS	X-ray photoelectron spectroscopy

Chapter One:

Introduction

1.1 Introduction

The phrase "*every contact leaves a trace*" based on the Locard exchange principle summarises in few words the importance of analysing objects contacted during offences[1]. When an individual's finger comes into contact with a surface, secretions of sweat or other materials are deposited and leave behind a mark mirroring that of the pattern present on the finger[2], this mark is known as a fingerprint. The use of such fingerprints deposited at scenes of crime have been used as a means of identifying an offender and hence solving crimes since it was first suggested in the 19th century[3-5]. Fingerprint evidence is an integral part to an investigation of crimes and offences; in the UK evidence from fingerprint identifications detects one and a half times more burglary offenders than DNA identification and over twice as many more in motor vehicle thefts[6].

Fingerprints can be deposited as either a visible or invisible (latent) mark. Those that are visible can be photographed *in situ* but those that are latent must first be enhanced or made visible before recovery or identification can begin. There are two methods of visualisation: invasive (destructive) or non-invasive. Invasive methods include the majority of conventional development techniques, such as the application of powders, metals via deposition, chemical treatments or immersion in small particle suspensions[7-13]. All of these techniques interact directly via chemical or physical means with either the sweat deposit and its components or the substrate surface. Non-invasive methods do not interact directly with either the deposit or substrate and do not degrade the evidence, often allowing for additional enhancement or recovery methods whereas most invasive techniques offer a single attempt. The majority of non-invasive techniques are imaging methods that visualise the fingerprint by either detection of the components in the sweat deposit or by the changes brought about on the substrate surface by the deposit. Examples include FTIR[14], RUVIS[15], UV/vis[16] and Kelvin probe techniques[17, 18].

If the substrate in question is metallic, then the deposited sweat and sample surface can undergo a chemical reaction[19, 20]. Exploitation of this naturally occurring process can itself be used to visualise fingerprints, depending on environmental conditions and substrate material[18, 20-22]. This reaction is effectively corrosion of the metal surface and can result in a change to both the physical and chemical characteristics of the metal surface. If the substrate is brass, then the resulting corrosion can generate a Schottky barrier between the copper or zinc oxide corrosion product and the brass substrate[23-27]. Such Schottky barriers can display good rectifying characteristics and this phenomenon has been used to visualise the fingerprint induced corrosion[17, 18, 21, 24, 28-31].

The reasons that brass substrate has been the focus of previous studies are that, firstly, it is susceptible to corrosion and, secondly, that is the material used for ammunition, both bullet and cartridge cases. Due to the processes involved in loading a cartridge, the amount of contact between a finger and a cartridge case is minimal. This, coupled with the conditions the cartridge is exposed to during firing, causes conventional techniques to fail to detect fingerprints. In part, this is because the majority of the sweat deposit is removed, either by mechanical or environmental (extreme heat) conditions[32].

Rather than seeking to design a new visualisation method for fingerprints, the work in this thesis sets out to understand the processes occurring that cause the Schottky barrier to come into existence as well as seeking to understand the physical and chemical processes occurring when brass samples are subjected to a range of conditions, including those known to promote corrosion and those used in the removal of fingerprints. However, before these findings can be presented, one must review the influences to this field, from the recognition of the significance of fingerprints for identification to methods that enhance before the visualisation of the marks and subsequently improve the rate of identification.

1.2 Fingerprints

The patterned areas observable on the tips of fingers are known as fingerprints. The pattern is formed from a thickened layer of skin known as friction ridge skin. This friction ridge skin is also found elsewhere on a human body, primarily palms of hands, toes and soles of feet; these areas all feature patterned skin. They have been considered to be present in those areas to assist with grip, but this theory was recently challenged[33, 34] and their true purpose is the subject of debate[35-38]. The friction ridges do not consist of regular or uniform markings but rather more complex patterns of raised areas of skin (ridges) separated by furrows visible to the naked eye on the surface of the skin and these patterns are unique to each individual[2]. The friction ridge skin has a greater concentration of nerve endings compared to flat skin found elsewhere on the body[2]. Additionally, the ridges are furnished with sweat pores for the secretion of bodily fluids[39]. When a finger touches a surface, the sweat can be transferred and leaves behind a mark that identically resembles the finger. This is one method of leaving behind a fingerprint; other methods will be discussed in subsequent section 1.2.1.

The observable pattern is formed whilst an individual is in the foetal stage of development, around twenty-eight weeks after conception. The exact arrangement of the ridges is determined by the dermal papillae, which are a layer of cells that separate the outer layer of skin (the epidermis) from the underlying dermis[2]. Once formed, the pattern will persist throughout an individual's lifetime. Minor cuts and similar injuries only cause temporary defects to the fingerprint; upon healing, the original pattern returns. However, injury to the generating layer can cause permanent defects[40]. The fact that the friction ridge skin remains unchanged throughout life makes it extremely useful in the identification of an individual at any stage of their life[2]. The fingerprint pattern detail also persists after death and is one of the last features to be lost as the skin decomposes, enabling them to be used to identify individuals *post mortem*[39].

1.2.1 Fingerprint Marks

Fingerprints are not only a permanent and unchangeable feature present on every human before they are even born, but are also unique to that individual (see section 1.2.3). Whilst these two factors are considerable enough to warrant studies of them, they are of little importance if they are non-transferable. However, when a finger touches a surface it leaves behind a trace of this contact, material and observability irrespective, which resembles the pattern present on the finger. In leaving behind a fingerprint, it can be classified as one of three types: visible, latent or plastic[41].

1.2.1.1 Visible Print

A visible print is a mark or impression made by a finger that is viewable to the naked eye. It involves a transfer of material as either a positive or negative transfer. A positive transfer is the deposition of material, such as a dye or paint from the finger onto a contrasting coloured surface, for instance the deposition of blood or red paint onto a white door. A negative transfer is the removal of material from a surface by a finger, such as a fingerprint in dust. Visible fingerprints can be viewed, photographed and compared *in situ*[41].

1.2.1.2 Latent Print

A latent print is also referred to as an invisible print; it is not visible by eye and requires some kind of enhancement to be seen. Common occurrences of latent fingerprints are the transfer of sweat from the finger onto a surface; a sub-visible amount of sweat is normally transferred each time. Other scenarios could include the transfer of a foreign material onto a similar coloured background, such as blue ink onto a blue wall. A wide variety of techniques can be used to visualise latent fingerprints, including physical powders and chemical dyes. After visualisation enhancement, the fingerprint is usually photographed[41].

1.2.1.3 Plastic Prints

A plastic fingerprint is one where the finger has indented the surface and left behind a three dimensional impression. Plastic fingerprints are usually visible and found in materials such as clay, putty and wet paint. They can be photographed *in situ* or a mould can be taken[41].

1.2.2 Composition of Sweat

As mentioned in section 1.2.1.1, the composition of visible prints is entirely dependent on the material transferred. However, latent fingerprints are mainly composed of deposited sweat. This sweat can be classed as either eccrine or sebaceous based; the difference between these two derives from the areas of the body they originate from and consequently their chemical composition. Eccrine sweat glands are predominantly found on hairless areas of the body, principally the soles of the feet, palms and fingertips. Sebaceous glands are found throughout the exterior of the body, except on areas where eccrine glands are found. The sebaceous sweat gland density is greatest around the face and scalp. Whilst eccrine glands are found in hairless areas, sebaceous glands are generally associated with hair follicles, so the two glands are not found in the same areas on the body[42]. There is a third type of sweat, known as apocrine, that is found close to hair follicles, as with sebaceous glands, however the apocrine is responsible for the odour commonly associated with underarm sweat[43]. The exact composition of the sweat types varies depending on both the individual and circumstances, nonetheless the composition of both eccrine and sebaceous sweat has been well documented by various groups (summarised in Tables 1.1, 1.2 and 1.3, below). The exact composition of apocrine sweat is less well documented due to its close proximity of sebaceous glands but is known to include proteins, carbohydrates, cholesterol and iron[43-48].

1.2.2.1 Composition of Eccrine Sweat

Eccrine sweat is usually in excess of 98% water but it also contains numerous organic and inorganic compounds. Excess secretion of certain chloride salts has been reported to cause corrosion of metal surfaces[49]. Various trace metals and halides have been detected as outlined below in Table 1.1. The sweat pH can vary depending on the rate of sweat generation: at a low sweat rate the pH can be as low as 5.0, however under high sweat rates it can increase to 7.0. This is indicative that the sweat duct itself controls the pH of the excreted sweat, by absorbing bicarbonates or secreting H^+ in exchange for sodium ions[50]. Amino acids are also present in varying amounts, from 0.3 to 2.59 mg/L[51]. As many as 22 different amino acids have been reported in eccrine sweat excretions[52], with serine, glycine and alanine being the most abundant ones[53-59]. Another component is proteins, with amounts in the region of 15-25 mg/dL, a much higher concentration than amino acids. Trace amounts of lipids, such as fatty acids, more commonly associated with sebaceous sweat have also been detected[60, 61].

Table 1.1 – Composition of eccrine sweat

<table>
<tr><th>Type</th><th>Element or Compound</th><th>Concentration</th><th>Type</th><th>Element or Compound</th><th>Concentration</th></tr>
<tr><td rowspan="16">Inorganic (major)</td><td>Sodium</td><td>34-266 mEq/L[62]
avg. 140 mEq/L[63, 64]</td><td rowspan="8">Inorganic (trace)</td><td>Zinc</td><td rowspan="8">Trace[51, 65, 66]</td></tr>
<tr><td>Ammonia</td><td>0.5-0.8 mM[67]</td><td>Copper</td></tr>
<tr><td>Potassium</td><td>5-59 mEq/L[64]
(avg. 8)[62, 68]</td><td>Cobalt</td></tr>
<tr><td>Chloride</td><td>46 mEq/L[64, 69]</td><td>Lead</td></tr>
<tr><td>Iron</td><td>1-70 mg/L[70]</td><td>Manganese</td></tr>
<tr><td>Calcium</td><td>3.4 mEq/L[42]</td><td>Molybdenum</td></tr>
<tr><td>Bicarbonate</td><td>15-20 mM[50]</td><td>Sulphur</td></tr>
<tr><td>Magnesium</td><td>1.2 mEq/L[42]</td><td>Tin</td></tr>
<tr><td>Phosphates</td><td>10-17 mg/L[70]</td><td rowspan="3">Organic</td><td>Amino acid</td><td>0.3-2.59 mg/L[51, 71]</td></tr>
<tr><td>Iodide</td><td>5-12 µg/L[70]</td><td>Proteins</td><td>15-25 mg/dL[72, 73]</td></tr>
<tr><td>Bromide</td><td>0.2-0.5 mg/L[70]</td><td>Glucose</td><td>0.2-0.5 mg/dL[74]</td></tr>
<tr><td>Fluoride</td><td>0.2-1.2 mg/L[70]</td></tr>
<tr><td>Sulphate</td><td>7-190 mg/L[70]</td></tr>
<tr><td>Urea</td><td>10-15 mM[65]</td></tr>
<tr><td>Lactate</td><td>30-40 mM[65]</td></tr>
<tr><td>Fatty acids</td><td>0.01-0.1 µg/mL[60, 61]</td></tr>
</table>

1.2.2.2 Composition of Sebaceous Sweat

The sebaceous sweat contains much less water than its eccrine counterpart, with most of its volume consisting of fatty or waxy material. The total amount of fatty acids in sebaceous sweat is the region of 15-25%, although levels as high as 30% have been reported[75, 76]. Half of the

fatty acids found are saturated straight carbon chains of 14 – 16 carbons long[77], although fatty acid concentration and composition can differ frequently for individuals[78]. The compounds found in sebaceous sweat are listed below in Table 1.2 and Table 1.3.

Table 1.2 – Major organic components of sebaceous sweat

Compound	Relative Amount
Triglycerides	30-40 %[76, 79-85]
Free fatty acids	15-25 %[42]
Saturated	7.5-12.5 %[77]
Monounsaturated	7.2-12 %[86, 87]
Polyunsaturated	0.3-0.5 %[86, 87]
Wax esters	20-25 %[88-90]
Squalene	10-12 %[91, 92]
Cholesterol	1-3 %[76, 79-85]
Cholesterol esters	2-3 %[76, 79-85]

Table 1.3 – Organic trace components of sebaceous sweat[93]

Aldehydes	Amides	Ketones	Pyrazines
Alcohols	Amines	Mercaptans	Pyridines
Alkanes	Furans	Phospholipids	Pyrroles
Alkenes	Haloalkanes	Piperidines	Sulphides

1.2.3 Individuality of Fingerprints

Whilst DNA evidence can differentiate between the majority of people, it is unable to distinguish between identical twins. However, fingerprints can do so. This is because DNA is hereditary and identical twins not only have the same biological parents, but form from the

same cells, so their genetic makeup is identical. Fingerprints, on the other hand, are not hereditary and are a result of the environment an individual experiences inside the womb. Whilst identical twins share the womb, they will have slightly different interactions within it, thus causing them to have distinct fingerprints not only from each other but also between their own fingers. The reason that the fingerprint is unique is that although the interactions cause outwardly similar patterns to be created, they create many minor permutations, known as minutiae, which are predominately responsible for the uniqueness of an overall fingerprint.

To be able to compare fingerprints, although the minutiae provide distinct characteristics, the overall pattern produced can be much more easily categorised. Although many different descriptions of the patterns exist and are the basis of numerous classification, which will be discussed further in section 1.2.6, today the three types of pattern mainly considered are depicted in Figure 1.1, known as loops, arches and whorls[2, 39]:

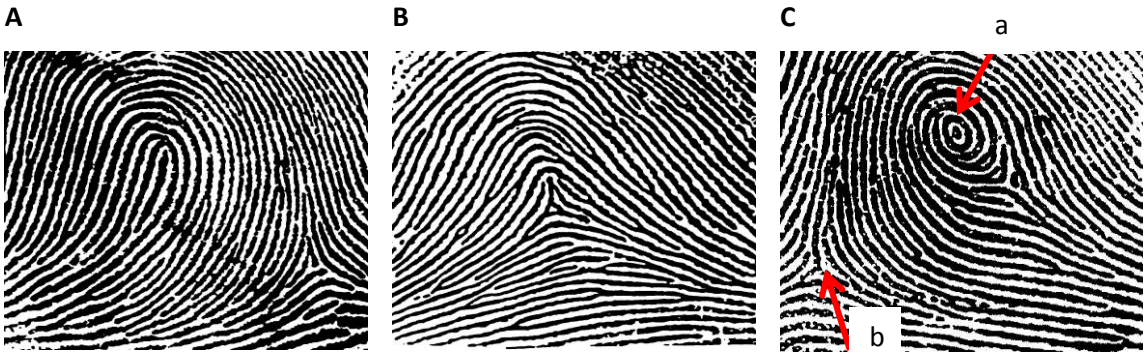

Figure 1.1 – Depiction of various types of fingerprint patterns as inked prints[94], the ridges are represented as black lines; ***A)*** *Left Loop;* ***B****) Tented Arch;* ***C****) Central Pocket Whorl.*

In classifying the fingerprint pattern, one must observe the print as a whole, observing the general flow of the ridges and the shapes that they form. Whilst some patterns are simpler to discern and categorise, some may have characteristics that can fit several profiles. In order to deduce the correct pattern assignment, one may be required to perform a ridge count for the

features. A ridge count starts from the central core pattern, this can be seen in Figure 1.1C above (feature 'a'), in the centre of the pattern as a circle. From here you draw an imaginary line which transverses the gap between the core and the delta (marked 'b'), the total number of ridges that are encountered along this line serve as the ridge count number[2].

1.2.3.1 Loop

A loop is a pattern in which at least one ridge must enter from one side, loop round and exit on that same side. The two sub-types are the radial loop (in the direction of the thumb) and the ulnar loop (in the direction of the little finger); these are named after the bones of the forearm that the loop originates from. To be classified as a true loop pattern, four features must be present[2]:

a single delta (an area where the ridges diverge);

a core (the pattern's centre);

at least one re-curving ridge that flows between the delta and the core;

a minimum ridge count of one.

1.2.3.2 Arch

Arches exist in two forms: the plain arch and the tented arch. The plain arch has the friction ridges flowing from one side of the print to the other, rising smoothly in the centre. The tented arch has an up-thrusting ridge or ridges that meet at 90 or less at the apex of the arch. The tented arch is an intermediate between an arch and a loop and may show some of the loop characteristics[2].

1.2.3.3 Whorl

Whorls are slightly harder to separate into sub-categories unlike the previous two groups. Whorls can be classified into four sub-categories: plain; central pocket; double loop and

accidental. The plain whorl is the simplest of these; it consists of two deltas and at least one ridge that completely encircles the core, describing the shape of circle, oval or spiral in doing so[2].

If one ridge, circling the core, is encountered when passing from one delta to the other, it is classified as a plain whorl. On the other hand if it does not, then it is classified as a central pocket whorl. The double loop whorl consists of two loop patterns in combination. Having a second delta discounts this from the loop pattern type. The final subtype of whorls is the accidental whorl; this is applied to fingerprints that either contain a combination of two or more pattern types or whose pattern simply does not fit into any of the categories already mentioned[2].

1.2.4 Minutiae and Comparisons

When identifying fingerprints and trying to match them to each other, the overall pattern is considered first and is classed as level 1 detail, the minutiae are known as level 2 details and sweat pores are level 3 detail[40]. As mentioned before, the minutiae are the features that give true individuality to a fingerprint. In simple terms they are defects of the ridge skin preventing it from running in a smooth continuous manner throughout the pattern. The appearances of some characteristic second level details are outlined in Figure 1.2.

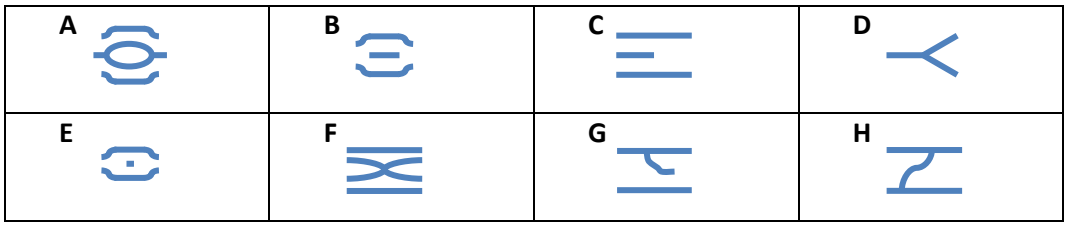

*Figure 1.2 – Representations of minutiae features as second level details observed in fingerprint patterns; **A**) Lake; **B**) Short Independent Ridge; **C**) Ridge Ending; **D**) Bifurcation; **E**) Dot; **F**) Ridge Crossing; **G**) Spur; **H**) Bridge.*

The appearance of the minutiae is not the only consideration in comparisons of fingerprints: the locations of all minutia must also match in each of the separate fingerprints. UK legislation previously required a minimum of 16 of these features to match with no contradicting features present for use in criminal courts[2]. However, in 2000 this minimum count rule was abolished in the UK following a review of the 16 count system[95] and today no minimum count rule exists. The decision over the identification rests solely with the individuals who complete the identification of the recovered fingerprints and who may later have to defend their decision in court[2].

1.2.5 History of Fingerprinting

The significance and incorporation of fingerprints as identifying marks is considered a recent revelation. However, their presence has been found on hand formed building materials dating back to 7000 B.C. in the excavation of the ancient city of Jericho[5]. A Chinese clay seal dated to before 300 BC had a thumb impression on one side, whilst the other side contained ancient Chinese script representing the person who had made the impression[5]. This use by the Chinese suggests that they considered fingerprints at least partially exclusive to an individual. Nevertheless, the first documented study of fingerprints was by Nehemiah Grew (1641-1712), an English plant morphologist, who not only wrote on the subject but also published accurate drawings of finger patterns in 1684[5].

Following the siege of Londonderry in 1691, 255 citizens petitioned London for compensation for loss and damage incurred by the siege. Each of the claimants not only signed their name but accompanied the signature with an inked impression of their finger. This suggests that the citizens considered their finger mark of equal status to their signature in identifying them as an individual[5]. Another individual that is deemed to hold the finger pattern as an identifier was Thomas Bewick (1753-1828) who was considered England's finest engraver and was highly

regarded worldwide for his skills. The books and works that he engraved used an engraving of his fingerprint as his signature. It is thought that his love of nature and the intricate detail there caused him to notice the intricacies in fingerprints; as he used an engraving of his fingerprint often overlaid by "*Thomas Bewick his Mark*" it is likely that he considered his fingerprint unique to himself[96].

The first recorded academic study of fingerprints was by a Bohemian named Dr Joannes Evanelista Purkinje (1787-1869) who published a thesis in 1823 on the topic of the functions of the ridges, furrows and pores present on the tips of the fingers. Purkinje also attempted to classify patterns and described nine characteristic patterns: one arch, one tent, two loops, and five whorls[5, 96]. Today, we still generally identify patterns in the same way except with only 4 whorls in place of Purkinje's five. The next recorded academic study was by Sir William Herschel (1833-1917) and was on the effect that aging had on the patterns present on an individual's hands. By taking impressions of his own fingers in 1860 and then again in 1890, Herschel found that, with the exception of a few extra crease lines, the prints were identical[5]. Welker, a German anthropologist performed the same study but over a larger time period, between 1856 and 1897, and came to the same conclusion. In 1877, Herschel insisted that the criminals incarcerated by the Indian justice system should have their fingerprints recorded for means of identification instead of signatures or Bertillon measurements (Bertillon measurements involved ten physical measurements of an individual, including height, stretch, bust and cranial measurements)[97]. Although Herschel saw fingerprints as a means to identify an individual as well as the fact they would not change throughout an individual's lifetime, he did not foresee any applications for the use of fingerprints in crime scenes or criminal proceedings[5].

During the late 1870's Dr Henry Faulds was working as a medical missionary in Japan and found the inspiration to study fingerprints from finding ancient shards of pottery bearing the finger imprints of the potters. Whilst in Japan, Faulds fingerprinted several of his patients and then removed the printed skin from their fingers. Once the skin had regrown they were fingerprinted again. Faulds discovered that the pattern impressions from the regenerated skin identically matched the impressions from the original finger patterns[5]. This discovery, coupled with Welker's and Herschel's, demonstrates that not only does a fingerprint pattern remain the same throughout a lifetime, it will also be regenerated after sustaining injury or damage. In 1880 the link between fingerprints and their use in criminal proceedings was realised and was documented by Faulds, along with other fingerprint related discoveries, in a letter to Nature[3]. Whilst in Japan, Faulds twice assisted the Japanese authorities in comparing imprints obtained at a crime scene to the suspects; upon identifying the perpetrators, in both cases they confessed to the crime. Faulds was certain that fingerprints were crucial in assisting in criminal proceedings to the extent that in both 1886 and 1888 he attempted to establish a fingerprint bureau in Scotland Yard at his own expense; however at this time, fingerprints were not regarded highly enough to warrant a bureau[5].

Sir Francis Galton (1822-1911) was a Bertillon authority and it was not until 1888 that Galton took an interest in fingerprints and in particular, thumb impressions. By 1890 Galton's interest had increased and he started to collect full sets of finger impressions[5]. From this point, Galton started working on a system to categorise and classify the fingerprint patterns present (see section 1.2.6.2). In 1892 Galton published his work in a book entitled "Finger Prints"[98]; in this, Galton demonstrated that the odds of two individuals having identical fingerprints were 64 billion to 1[2, 98]. Considering that there has been no known case where two individuals have had matching prints since fingerprint studies began[2, 5] and that the world population is approximately 6.9 billion[99], this calculation clearly demonstrates the individuality and

significance of fingerprints. A year after this publication, Galton was called before the Asquith Committee in 1893 to give evidence for the strength and validity of fingerprints over Bertillon measurements. The committee envisaged problems when classifying and matching large quantities of fingerprints and so fingerprint information was added to Bertillon cards rather than replacing them entirely[5].

By the 1890s Sir Edward Henry (1850-1931) used fingerprints as a means of identify his workforce in India and ensuring that each worker only got paid once. To classify the fingerprints, Henry used a more comprehensive system than that of Galton's (section 1.2.6.4). In 1900 Henry was called before the Belper Commission, whose purpose was to decide which fingerprint identification system should be used in Great Britain. The Belper Commission decided to recommend the use of Henry's system and by 1901 it had been adopted by the first Fingerprint Bureau in Scotland Yard[2, 5, 39]. The following year, the UK had its first trial, a burglary, involving fingerprint evidence[96, 100] and in 1905 the first murder trial to use fingerprints and subsequently the first murder conviction[96].

In these cases a match between two impressions was declared by a fingerprint expert alone. By 1920 Scotland Yard introduced the minimum of 16 matching characteristics for all fingerprints placed before the courts. This minimum count was calculated based on calculations by Sir Edward Henry in that each finger had on average 80 to 100 characteristic features. Henry had allowed for a one-in-four probability for each characteristic feature and calculated that for any 10 characteristics in sequence, then the probability was 1 in a million. Taking 16 points, the chances then became 1 in 4,294,967,296. Although introduced in 1920, the 16 point rule became the national standard in 1953[100] and was determined as the minimum number required to match a print exclusively[39].

Whilst the individuality of fingerprints had been recognised by some for over a century and used to confirm identity for decades, little development of enhancing and recovering fingerprints took place. Until the 1950s only basic enhancement techniques were used, most notably using powders, and photography of the fingerprints *in situ* was not routinely available. In order to improve the evidentiary worth of fingerprints, improvements to both the resources available and the techniques applied was vital. Currently, there are a wide variety of techniques available, with each specialising in enhancing a mark from a specific scenario. An overview of some of the recent research is discussed in section 1.2.8.

1.2.6 Classification Systems

Comparing and matching two fingerprints can be a difficult task when they have the same pattern. However, trying to establish the identity of the person responsible for leaving a fingerprint at a crime scene is a much greater challenge, more so when there are no suspects. In order to identify a fingerprint there needs to be a concise and logical method for describing the fingerprint in such a way that a search through a collection can avoid having to examine every single print. As this task is an empirically subjective one, many different systems of classification have been suggested. Here we focus on a selective few that are considered to be the most influential on today's classification system[2, 39, 96, 101].

1.2.6.1 Purkinje

In the course of his work, Purkinje examined the patterns present on the finger tips and identified nine unique patterns. Although this is not strictly a detailed classification system, it is considered the precursor to other systems[96, 101]. The nine classifiable fingerprint patterns Purkinje identified, with today's interpretation in brackets, are: (1) transverse curve (plain arch), (2) central longitudinal stria (tented arch), (3) oblique stria (mixed loop and arch) , (4) oblique sinus (standard loop pattern), (5) almond (central pocket loop), (6) spiral (central

pocket loop), (7) ellipse (plain whorl), (8) circle (plain whorl), and (9) double whorl (double loop whorl)[101].

1.2.6.2 Galton

In the publication of his book "Finger Prints" in 1892, Galton established that fingerprints are both permanent and unique. Galton also attempted to classify a collection of 1008 thumb imprints, half of which are from the right hand and the other half from the left[98]. Galton started off trying to categorise them according to the nine classes that Purkinje identified (section 1.2.6.1), but failed due to being unable to discern certain patterns. After much experimentation on possible groupings, Galton arrived at using three main pattern classification types: arch, loop, and whorl. Whilst each of these sections is broken down further into 19 distinct pattern types, the fingerprints would only be recorded as a single letter: A for arch, L for loop or W for whorl[98]. The assignment was recorded in the following order: right hand index, middle and ring followed by left hand index middle and ring, then right thumb and little finger and finally left thumb and little finger. For example, a person with the right hand possessing all whorls except for the little finger having a loop, and the left hand having all loops except for the little finger having a whorl, would have the following classification: WWWLLLWLLW. This classification code would then be recorded on a card and the card filed alphabetically by this classification[96, 101].

Whilst Galton did attempt to classify fingerprints further, he was not confident of his system and admitted that a further breakdown of the categorisation became too subjective and imprecise[98]. Due to the storage method of the fingerprint cards, although they would be effective in establishing the identity of someone already on record, it would be extremely inefficient to search the entire collection with only a single fingerprint, such as one recovered from a crime scene.

1.2.6.3 Vucetich

Vucetich, although considered a fingerprint pioneer, was omitted from the section on the History of Fingerprints (section 1.2.5) for one main reason. Much of his research and work took place in Argentina around the 1890s and although he was influenced by Galton's system described above, Vucetich's classification system and research was mainly restricted to South America. Vucetich's classification system was the main system employed within much of South America and is still in use today[5]. The Vucetich system consists of a basic classification, known as the primary system, and a more descriptive secondary classification system[101]. The primary system categorises the fingerprint pattern into one of four pattern types (Table 1.4):

Table 1.4 – Primary assignment of pattern types for the Vucetich classification system[101]

Pattern	Thumbs	Other Fingers
Arch	A	1
Internal loop	I	2
External loop	E	3
Whorl	V	4

An internal loop is a left sloped loop, whereas the external loop is a right sloped loop. The primary classification is divided into two groups and was expressed in ratio form. The numerator represents the right hand and the denominator represents the left hand. The assignments for each hand are performed from the thumb through to the little finger. For example, if both the numerator and denominator were assigned V4414, then both the right and the left hands have all whorls on all of the fingers except the ring fingers, which have arches[101].

The secondary classification further subdivided the fingerprints into five subtypes: 5, 6, 7, 8, and 9. Each number represents a further description of the pattern (Table 1.5); if the pattern

type is classified as a normal loop, then the secondary classification defaults to ridge count values (Table 1.6)[101].

Table 1.5 – Secondary classification numeral assignment for the Vucetich system[101]

Pattern	Value	Description
Arch	5	Vaulted/Normal
	6	Left-inclined
	7	Right-inclined
	8	Tent-shaped
	9	All others
Internal loop	5	Normal flow
	6	Invaded
	7	Interrogatory
	8	Hooked
	9	All others

Pattern	Value	Description
External loop	5	Normal flow
	6	Invaded
	7	Interrogatory
	8	Hooked
	9	All others
Whorl	5	Normal
	6	Sinuous
	7	Ovoid
	8	Hooked
	9	All others

Table 1.6 – Vucetich's ridge count values[101]

Ridge Count Spread	Value
1 - 5	5
6 - 10	10
11 - 15	15
16 - 20	20
Over 20	25

The secondary classification values are added as superscript values alongside the corresponding primary classification. For example, a person whose right-hand fingers all have a pattern type as external loops and the left-hand as all internal loops, they would have the following classification:

$$\frac{E^{20}3^{15}3^{10}3^{5}3^{15}}{I^{10}2^{10}2^{5}2^{5}2^{10}} \qquad 1.1$$

By collecting fingerprints and classifying them according to this system, it is quite possible to identify an unknown without having to sort through an entire database. The Vucetich system is very efficient for matching complete sets of fingerprints, for example in identity verifications,

but is fairly inefficient if the finger responsible for the fingerprint mark is unknown, such as marks commonly found at crime scenes.

1.2.6.4 Henry

Henry had seen the research material from Galton, Herschel and Faulds before commencing on devising a classification system of his own. Henry assigned two police officers to the fingerprint classification project, Azizul Haque and Hem Chandra Bose. Whilst Henry took full credit for this classification system, both Haque and Bose are retrospectively credited for their work in devising it.

As with previous systems, Henry's system starts with assigning a primary value to each of the fingers, arranged from the right thumb through to the left little finger. The value assigned was determined by the finger on which a whorl pattern was present (Table 1.7). If there was no whorl present, then the finger was assigned a value of zero.

Table 1.7 – Primary values for the Henry classification system[101]

Finger	Number	Value if Whorl
Right thumb	1	16
Right index	2	16
Right middle	3	8
Right ring	4	8
Right little	5	4
Left thumb	6	4
Left index	7	2
Left middle	8	2
Left ring	9	1
Left little	10	1

The primary was expressed as a ratio form with the numerator representing the values of the even fingers plus one and the denominator representing the values of the odd fingers plus 1. If an individual had whorls as the only pattern, then the primary classification would be 32 over

32, however if an individual has loops in the right and left index fingers, with the remainder still being whorls, then their fingerprint record card would resemble the following:

Table 1.8 – Representation of an individual's primary classification according to the Henry System

Right thumb	Right index	Right middle	Right ring	Right little
16	0	8	8	4

Left thumb	Left index	Left middle	Left ring	Left little
4	0	2	1	1

Taking the sum of the even numbered fingers for the numerator (right index, right ring, left thumb, left middle, left little) and adding one, results in a numerator value of 16. Taking the sum of the odd numbered fingers and adding one results in a denominator value of 30. This would then be represented as:

$$\frac{\mathbf{1}+(\boldsymbol{Sum\ of\ even\ finger\ values})}{\mathbf{1}+(\boldsymbol{Sum\ of\ odd\ finger\ values})} = \frac{\mathbf{1}+(\mathbf{15})}{\mathbf{1}+(\mathbf{29})} = \frac{\mathbf{16}}{\mathbf{30}} \qquad 1.2$$

Categorising in this way allowed for 1024 primary variations. However, there was a secondary category shown in the formula by capital letters determined by the pattern types of the index fingers of each hand. The assignment of pattern was designated by: A for arch, T for tented arch, R for radial loop, U for ulnar loop, and W for whorl. As certain patterns were considered rarer than others, if a non-index finger contained an arch, tented arch or radial loop, these patterns were added to the formula as a lower case letter after the capital letters for the pattern of the index fingers. However, the exception is that if the rare pattern was found on a thumb, then the letter was to the left of the primary. The sub-secondary was to the right of the secondary and represented the ridge counts for loops or ridge tracing for whorls in the remaining fingers[101].

When needing to compare a full set of fingerprints, such as in identity checking, using the Henry system would result in the correct grouping being searched and was a very efficient system for performing such operations. When dealing with a single print from an unknown finger or individual, then it would be impossible to find a match by using this system.

1.2.7 Current Approaches to Fingerprint Characterisation and Comparisons

In the UK, prior to 1970, all fingerprint information was held on a series of card indices. When a criminal was arrested, their full set of fingerprints, known as ten-prints, were taken as ink impressions onto the record card. These cards were then filed, searched and retrieved by hand. Locating the cards was a slow and labour intensive process and was only generally effective for complete sets of fingerprints. Whilst a fingerprint recovered from a crime scene could easily be compared directly to a suspect's, it was virtually impossible to find a suspect using the card method with a recovered fingerprint alone. Additionally, each police force held local records and it was common practice to share records between different regions[2].

With the onset of technological and computational developments, an automated system to replace the cards called the automated fingerprint recognition (AFR) technology was developed. This technology was the foundations for the National Automated Fingerprint Identification System (NAFIS), which by 2001 had become available to all police forces in England and Wales. This system withdrew the need to store hardcopies of fingerprints as well as a much improved and more efficient and accurate search mechanism[2].

In 2005, NAFIS was replaced by IDENT1, which also incorporated the Scottish fingerprint database as well. IDENT1 offered improved features and a larger database than was available with NAFIS. The database in April 2010 held 8.3 million individuals' ten-print sets[102].

The search process can be used in one of two main ways, to verify identity and check for criminal history of an individual or to compare a fingerprint recovered from a crime scene to those stored on the database to help narrow down the list of suspects. The first was possible with the card indices method and the digital databases just offer improved efficiency. The latter was the aspect that was near impossible with the card indices method, but is now a routine operation for the IDENT1 database. Upon recovering a fingerprint from a crime scene, a digital copy is made to enable database searching. A fingerprint expert will examine the fingerprint and identify ridge characteristics and mark these on the digital copy. These marked characteristics and their relative locations are used to search the database, IDENT1 will return a list of approximately 8 prints ranked as percentage matches. From this point, it is up to the fingerprint expert to deduce the identity of the individual responsible for leaving the fingerprint. Before being admissible in court, two other fingerprint experts must perform their own individual comparison and arrive at the same conclusion. Although there is no minimum requirement for the number of matching characteristics, there can be no conflicting features[2].

1.2.8 Recent Innovations

Although the research into patterns and classification of fingerprints is not fully exhausted, with the advent of computer databases and more efficient methods of searching for fingerprints, fingerprint research today has taken on a different approach. With the knowledge that fingerprints are a permanent characteristic of each finger of an individual, their importance in identity of unknown victims or perpetrators is of paramount significance. Therefore, rather than focusing on classification and identification of fingerprints, the focus has been on understanding, visual enhancement and subsequent recovery of fingerprints from scenes of crimes.

In the 1970s, Thomas and Reynoldson started studying the physical appearance of fingerprint sweat deposits and the behaviour of the sweat deposit over time[103]. Thomas continued the research by examining the visual appearance of sweat deposits under optical magnification[104]. His observations showed that, although the fingerprint ridges made by sweat deposits might appear as solid entities to the naked eye, in fact they consist of tightly packed clusters of the deposit material. By being able to understand the physical properties and behaviour of the fingerprint material transferred, Thomas hoped that it would enable increased detection and recovery of fingerprints from crime scenes.

There are many factors to consider when trying to visually enhance a latent fingerprint and subsequently improve the quality of the mark. These include the nature and colour of the substrate, environmental factors, as well as the material transfer involved in depositing a fingerprint. Due to the range of influencing factors, there are a wide variety of enhancement techniques to cover most scenarios, such as optical, chemical and physical methods.

1.2.8.1 Physical Enhancement and Visualisation Techniques

Physical development methods are typically rudimentary and involve the addition of a substance to the substrate material to enhance the latent mark. A typical example of this is the use of powders, which when applied to a fingerprint mark stick to the sweat and sticky matter transferred in the contact between the finger and the substrate[2]. There is a wide range of powders, each suited to particular situations, although most powders are mainly used to develop fingerprints on non-porous surfaces. The correct powder to use in a given situation is often determined by colour alone so that a good contrast is provided by the enhanced ridges compared to the substrate[105]. The use of powders has been extended beyond the typical range of objects and has been proven useful for developing fingerprints on fruit and vegetables[106].

An alternative to powders is the use of multi-metal deposition (MMD) developed by Saunders in the late 1980s[107]. MMD involves the application of a colloidal gold solution followed by a weak solution of silver physical developer. The colloidal gold adheres to the fingerprint deposit and forms catalytic nucleation sites for the silver physical developer; in essence the silver amplifies the visualisation of the gold deposit[108]. Zhang et al then took the MMD technique further and imaged the MMD using a scanning electrochemical microscope (SECM)[109, 110]. The advantage that this offers over traditional photography of the developed fingerprint is that it offers much higher resolution images and, due to selectively imaging the silver deposit, the colour of the background becomes irrelevant. SECM has also been used to image fingerprints after they were either silver-stained[110, 111] or tagged with dyes such as benzoquinone[111].

1.2.8.2 Chemical Enhancement and Visualisation Techniques

Chemical development treatments are similar in that they also introduce an alien substance to the substrate. However, where they differ is that rather than the enhancement being from physical adhesion, the introduced substance reacts either with the fingerprint deposit or the substrate. Regardless of the reaction type, both result in an enhanced visualisation of the latent fingerprint.

1.2.8.3 Enhancement by Sweat Interactions

Chemical reactions that target the sweat usually require a certain substance to be present in the fingerprint residue, such as amino acids[112, 113], and can also work on a wider range of surface types than with physical development treatments. Kelly *et al.* have found that S_2N_2 polymerises on contact with latent fingerprint residues and works on a vast range of substrates including paper, pottery, cotton cloth, plastics and metals[114]. Taking the idea of targeted aspects one step further, Legget et al have developed an anti-body nanoparticle detection method[115]. The anti-bodies are selected to bind to certain drug metabolites excreted with

sweat and so can be used as a lifestyle analysis tool as well as visualising latent fingerprints. The use of a chemical treatment that not only dyes the fingerprint, as with ninhydrin, but also causes it to fluoresce have been used on various porous samples[116].

1.2.8.4 Enhancement by Substrate Interactions

Whilst using techniques that require specific substances to be present in the fingerprint for them to aid visualisation, in some cases these substances may not be present and so a visualisation by these methods is not possible. Instead of reacting with the fingerprint deposit, there are a range of enhancement techniques that chemically react with the substrate, although the majority of these chemical enhancement techniques require a metal substrate. In these cases, the fingerprint residue acts as a barrier and protects the surface directly under its deposit. The rest of the metal substrate is exposed and is either dyed[12] or deposited on with polymers[10, 117, 118] or metals[13, 119].

1.2.8.5 Visualisation by Optical and Spectroscopic Means

As discussed before, a latent fingerprint is invisible to the naked eye and requires some enhancement to become visible. However, that enhancement does necessarily require the application of additional material. The visual enhancement can be caused by using non-invasive spectroscopic methods. The advantage of non-invasive techniques is that they can be used as an early detection method before subsequent chemical or physical treatments. As the majority of spectroscopic techniques do not damage or alter the sample in any way, they are not detrimental to other detection methods.

Spectroscopic methods can be used to generate an image of a latent fingerprint, provided the chosen technique is sensitive to at least one constituent of the latent fingerprint deposit. Several groups have looked at fingerprint detection using FTIR in spatial acquisition mode to

detect and image the fingerprint based on illicit substances, such as drugs[120-122] and explosive residue[120-123], being present. Raman spectroscopy[124, 125] and gas and liquid chromatography linked with mass spectrometry[126] have also been used in identifying drugs in fingerprint sweat deposits. Using the natural constituents of sweat, Bhargava was able to map a fingerprint using FTIR[127] and Norimitsu similarly imaged a fingerprint but by using a tuneable laser to excite the components of the deposit and was able to image by fluorescence[128]. Williams also examined natural sweat deposits using SIMS[18] and a Kelvin Probe microscope[17, 18] to generate images of latent fingerprints. The Kelvin probe differs from the other spectroscopic methods mentioned as it generates the images based on surface potential differences rather than the surface deposit.

1.2.8.6 Understanding the Fingerprint Deposit

Aside from using spectroscopic techniques as enhancement tools, they can also be incorporated into the study of fingerprint deposits and increasing our understanding of the sweat deposited material and its variation between donors. It is known that the composition of a child's and adult's fingerprint deposit varies greatly[129]. Several groups have attempted to identify a few of the constituents in the deposit that can indicate the age of the individual[130-133]. Hemmila[129] and Stewart[134-136] have identified the fatty acid chain lengths as the greatest indicator of the age of an individual: young people have free fatty acids whereas older people have longer chain fatty acids[129].

1.3 Surface Characterisation Techniques

Whilst the apparatus and operation of techniques are described in more detail in subsequent chapters (Chapter 2 - Methodology and Chapter 3 - Experimental), an overview of the techniques employed during the course of this study is presented here.

1.3.1 Atomic Force Microscope

An atomic force microscope (AFM) is part of the scanning probe microscopy (SPM) family. An SPM is typically a microscope that uses a mechanically moved probe to image a sample. SPM's have been in use since the tunnelling microscope was developed in 1981. The AFM uses a cantilever with a sharp tip on the underside to scan the sample surface. The tip can measure various surface-tip interactions including van der Waals forces, electrostatic forces and magnetic forces. The sharper the tip, the higher the resolution of data obtained, both laterally and of the interaction being measured. The AFM is routinely used to analyse surfaces from metals to biological samples. The choice of cantilever material and the mode of operation may vary depending on the scenario and is discussed in more detail in section 2.1 of the methodology chapter. The AFM has been commercially available since 1989 and one of its more common uses is to provide topographical information of a surface.

1.3.2 Digital Holography Microscopy

Digital holography microscopy (DHM) is a laser-based optical microscopy technique. Instead of recording the projected image from reflected light, the DHM records the reflected light wave front from the object as a hologram. Computer calculations and reconstruction algorithms allow the reassembly of the object appearance in 3D. The advantage over SPM is that the 3D image can be generated and displayed in real time, whereas SPM have a slight time delay caused by longer acquisition times. Due to the speed of data capturing and image regeneration, it makes the DHM suited to monitoring changes in real time, particularly for biological living cells behaviour. More details are available in section 2.2 of the methodology chapter.

1.3.3 X-Ray Photoelectron Spectroscopy

X-ray photoelectron spectroscopy is a quantitative spectroscopic technique for measuring elemental composition of a sample. An X-ray source is used to irradiate the sample and the ejected photoelectrons are recorded; further details can be found in section 2.3 of the methodology chapter. XPS allows one to study and analyse the surface chemistry of samples (top 10 nm of the sample), including the deduction of elemental composition, oxidation states and empirical formula. XPS can be used to either collect information for the whole surface or in a spatially resolved (centimetre width with tens of micron resolution) manner, where it is possible specifically to pinpoint areas of differing chemical composition.

1.4 Metal Substrates

As with most materials, a metallic substrate can be affected by its environment. The type of metallic substrate and environmental factors both play a role in determining the consequence of any interactions. Very few metals exist naturally in elemental form. Gold is one that can exist in this form; it is extremely stable and can be exposed to air or water without being oxidised. More reactive metals are found naturally occurring in either compounds or as oxides. Metals that are reactive and exposed to air in their elemental form will spontaneously and instantaneously react with water vapour in the air, to give a range of oxides and hydroxides[137]. This new oxide or hydroxide layer can act as a protective barrier and cause reactive metals to become stable in otherwise harsh environments.

1.4.1 Corrosion and Corrosion Pathways

A reaction between a metal and another material does not necessarily mean that a corrosion reaction has occurred; although metals are prone to corrosion they have various reactions and reaction pathways they are susceptible to. In order to discuss this properly, a definition of

corrosion is required. Whilst different authors each provide slightly varying descriptions, the most apt for this thesis is:

"Corrosion is an irreversible interfacial reaction of a material with its environment, resulting in the loss of material or in the dissolving of one of the constituents of the environment into the material. The corrosion of metals is due to an irreversible redox reaction between the metal and an oxidising agent[138]."

Other materials beside metals can also undergo corrosion processes including ceramics, plastics and polymers[139], however, in this section metal degradation by corrosion is the primary focus.

For a corrosion reaction to occur, four essential components are required: an anode, a cathode, an electrolyte and electrical connections[140]. If a single one of these components is omitted, then a corrosion based reaction cannot occur. The anode and the cathode can both be part of the same metal substrate and in this instance the bulk material can provide the electrical connections. Corrosion is usually considered an electrochemical process as corrosion processes usually proceed with the oxidation of metal atoms to form ionic species with higher oxidation states, as well as the liberation of electrons[141]. In defining corrosion, the term 'environment' was introduced; the environment simply refers to a medium that can be considered an electrolyte, such as a liquid containing dissolved ionic species[141].

Corrosion covers a wide range of different metal reactions, below in Table 1.9, the most commonly occurring corrosion pathways are described.

Table 1.9 – The various types of corrosion pathways with brief explanations

Corrosion type	**Short description**
Uniform attack	A chemical or electrochemical reaction that proceeds uniformly over the exposed area[142]
Galvanic attack (bi-metallic)	Dissimilar metals with a potential difference which allows electron flow[142]
Crevice corrosion	Corrosion proceeds at the site where a trapped solution becomes stagnant[142]
Pitting	Extreme localised attack, resulting in small holes in the metal; can be initiated by metallurgical factors alone[140]
Intergranular corrosion	Localised attack at or adjacent to grain boundaries, caused by impurities[142]
Selective leaching	Selective removal of one element from a solid alloy by corrosion processes[142]
Erosion corrosion	Accelerated deterioration due to relative movement between the material and a corrosive fluid[142]
Stress corrosion	Cracking caused by tensile stress and corrosive medium[142]
Hydrogen damage	Mechanical damage of a metal caused by the presence of hydrogen[142]
Deposit corrosion	Corrosion associated with a deposit of the corrosion products or other substances which takes place under or immediately around the deposit[143]
Differential aeration corrosion	A difference in oxygen accessibility between two parts of a metallic structure can induce a corrosion cell[139]. This can be caused by corrosion products growing over a pit and its immediate surroundings, forming a scab. This isolates the environment within the pit from the bulk electrolyte, assisted by a concentration of Cl^- [140]

1.4.2 Corrosion Rates

All corrosion reactions result in the formation of corrosion products. The physical nature of these products can affect the rate at which the corrosion reaction proceeds. Corrosion products can be grouped into three categories[139]:

- dissolved ions
- porous films
- compact films

However, the product depends on the corrosion occurring as well as the environment. Metals corroding in an acidic environment usually produce hydrated cations or complexes, which dissolve in the electrolyte and diffuse away. Due to the effective removal of the products, their production does not affect corrosion rate in a noticeable way[139].

In neutral or basic environments, the corrosion products are usually not as soluble; therefore they precipitate on the surface of the metal in the form of hydroxides or metal salts. These precipitates can be either porous or non-compact films and do not protect the metal from corrosion. However, because the products are not removed, they do cause a decrease in the rate of corrosion[139].

Compact films are the only one of the three corrosion products that can protect the metal surface as a result of their production. Depending on the metal, compact films can form in both dry and humid or liquid environments, typically as oxide films. These films are commonly referred to as passive films since they form a protective barrier between the metal surface and the environment[139].

1.4.3 Bi-Metallic Corrosion

Corrosion can be initiated by potential difference alone. The potential difference can arise due to a number of reasons but all rely on having two (or more) metals possessing different potential values being connected[142].

When two dissimilar metals are (directly or electrically) connected as well as being in a solution that is either conductive or corrosive, an electron flow is produced between the two metals. This process is known as galvanic or bimetallic corrosion. The least resistant metal becomes anodic and the more resistant metal is cathodic. The cathodic metal usually corrodes very little in this configuration. The only driving force for this corrosion type to occur is the potential between the two metals and the mechanism is not dissimilar to battery cells[142].

Corrosion by dissimilar metals tends to imply that the materials in question always had a difference in potential, however this difference in potential can arise long after production and can be caused by other corrosion pathways such as differential aeration corrosion and pitting corrosion[139]. The onset of one of these corrosion pathways can cause a difference on the oxidation/reduction properties of a metal and so a potential difference can be established.

1.4.4 Copper Containing Metals

Copper is a commonly available material and is used in electrical wires/connectors, roofing and plumbing. Copper can also be used to form a variety of alloys such as brasses, bronzes, cupronickel and alloys with gold and silver. These alloys have a variety of applications including jewellery, decorations, coinage and ammunition.

Some copper alloys are corrosion resistant, such as aluminium bronze, whilst others are susceptible to corrosion, such as brass. The forms of copper that are susceptible to corrosion are of not only scientific interest but also of forensic interest[144]. For reasons not yet fully understood, if a corrosion susceptible copper alloy is contaminated with human sweat and exposed to appropriate environmental factors, the sweat can cause a corrosion process to occur and leave behind a permanent mark only where direct transfer of the sweat material occurred. The exact corrosion mechanism or pathway occurring is not known.

While copper will follow some of the pathways outlined in Table 1.9 it is more likely to undergo the following with these specific conditions required. Copper will not undergo corrosion by acids unless in the presence oxygen or other oxidising agents[145]. However, copper and brass are susceptible to erosion corrosion (and impingement attack)[145]. Regardless of the corrosion pathway, the evolution of hydrogen is not a part of the corrosion process[145].

1.4.4.1 Pitting Corrosion

One of the corrosion processes copper based alloys are prone to is pitting corrosion. The majority of corrosion pits in copper based materials are caused by chlorides and chloride containing ions such as chloride salts[142]. Copper (II) chloride is extremely aggressive and will cause pitting corrosion. Whilst sodium chloride and calcium chloride are less aggressive, they will still cause pitting to occur. These latter two salts are extremely common as cooking additives as well as being present in excreted human sweat[42, 62-64, 69, 146] and can cause sweat to behave as an electrolyte[146]. It is therefore possible that contaminating a copper based material with human sweat could initiate pitting corrosion.

1.4.4.2 Selective Leaching

Selective leaching can only occur when the substrate is not a single metal. There must be a chemical or physical difference between at least two metals present in the substrate. In copper-zinc alloys, the zinc component will be preferentially removed, leaving behind a copper-rich surface to the substrate. This process is commonly referred to as dezincification since the zinc is removed. Dezincification can occur either on a localised scale or on a uniform scale.

For dezincification to occur on a uniform scale there needs to be a high zinc content in the bulk material, as well as exposure to an acidic environment[142]. Localised corrosion or plug type

corrosion is more likely to occur when there is low zinc content but can occur in neutral, alkali or slightly acidic conditions[142].

The corrosion mechanism for dezincification is believed to occur as a three step process. Firstly, the brass surface is dissolved into the solution, then the zinc ions remain in solution whilst the copper ions are re-plating. The zinc metal then corrodes slowly in water, by the cathodic reduction of H_2O into hydrogen gas and hydroxide ions. This process can occur in the absence of oxygen[142].

1.4.5 Advantages of Metallic Substrates in Fingerprinting

Fingerprints are known to leave behind material after contacting a surface[2]. The material commonly deposited is human sweat, which often contains hygroscopic salts as well as water[22, 42]. When this is deposited onto a copper surface, differential aeration cells can develop and cause a dark, discolouring copper oxide to form[143]. This process is not instantaneous and can take several days to occur depending on environmental factors.

Most metals are attacked under acidic conditions and although acidic conditions may not be present upon initial deposition of a material, acidification can arise by evaporation. Furthermore, the process of acidification of localised corrosion cavities will continue as long as the metallic ions formed are precipitated as oxides or hydroxides. However, the acidification will cease as soon as the metallic ions are precipitated as salts[147].

1.5 Objectives

As can be seen in section 1.2.8, there has been considerable research into the enhancement and development of fingerprints on a variety of surfaces but little research into the sweat residue itself. The work presented in this thesis seeks to investigate changes occurring to and

within the sweat deposited material when on a brass substrate. The study can be split into two lines of enquiry; the first is the effect of aging and storage environment on the fingerprinted samples and the second is the effect of post-deposition attempts at removal of fingerprints.

The first set of specific objectives comprises the physical and optical changes occurring on the substrate surface as a function of time. This will require examination of the evolution of the sweat residue and identification of the chemical species present on the surface (with particular emphasis on changes occurring as a result of aging and storage environments) and the metal oxidation states and metal-bound species. These objectives are addressed in chapters 4 and 5.

The second set of specific objectives involves the effect of post-deposition treatments of the fingerprinted samples, notably attempts at removing the fingerprints. The detailed aims here are the covering physical, optical and chemical changes occurring to both the fingerprint deposit material and the brass substrate. These objectives are addressed in chapter 6.

1.6 References

1. A. R. W. Jackson and J. M. Jackson, Pearson, Harlow, 2004, p. 398.
2. A. R. W. Jackson and J. M. Jackson, *Forensic Science*, Pearson, Harlow, 2004, pp. 79-94.
3. H. Faulds, *Nature*, 1880, **22**, 605.
4. W. J. Herschel, *Nature*, 1880, **23**, 76.
5. J. Berry and D. A. Stoney, in *Advances in Fingerprint Technology*, eds. H. C. Lee and R. E. Gaensslen, CRC Press, Boca Raton, 2nd edn., 2001.
6. *Finger mark identifications for burglary and motor vehicle offences*, Home Office, 2005.
7. V. Bowman, *Manual of fingerprint development techniques*, 2nd rev. edn., Police Scientific Development Branch, Home Office, Sandridge, UK, 2004.
8. P. Czekanski, M. Fasola and J. Allison, 58th Annual Meeting of the American-Academy-of-Forensic-Sciences, Seattle, WA, 2006.
9. H. Bandey and T. Kent, *Superglue treatment of crime scenes* 30/03, Police Scientific Development Branch, Home Office, Sandridge, UK, 2003.
10. C. Bersellini, L. Garofano, M. Giannetto, F. Lusardi and G. Mori, *J. Forensic Sci.*, 2001, **46**, 871-877.
11. A. A. Cantu, D. A. Leben, R. Ramotowski, J. Kopera and J. R. Simms, *J. Forensic Sci.*, 1998, **43**, 294-298.
12. C. Kauffman and K. Smith, *J. Forensic Ident.*, 2001, **51**, 9-15.
13. Y. Migron and D. Mandler, *J. Forensic Sci.*, 1997, **42**, 986-992.
14. N. J. Crane, E. G. Bartick, R. S. Perlman and S. Huffman, *J. Forensic Sci.*, 2007, **52**, 48-53.
15. A. A. Cantu, in *Optics and Photonics for Counterterrorism and Crime Fighting III*, ed. C. Lewis, Spie-Int Soc Optical Engineering, Bellingham, 2007, vol. 6741, p. D7410.
16. D. L. Exline, C. Wallace, C. Roux, C. I. Lennard, M. P. Nelson and P. J. Treado, *J. Forensic Sci.*, 2003, **48**, 1047-1053.
17. G. Williams, H. N. McMurray and D. A. Worsley, *J. Forensic Sci.*, 2001, **46**, 1085-1092.
18. G. Williams and N. McMurray, *Forensic Sci. Int.*, 2007, **167**, 102-109.
19. M. W. Pascoe and M. O. W. Richards, *Wear*, 1971, **18**, 76-78.
20. J. W. Bond, *J. Forensic Sci.*, 2008, **53**, 1344-1352.
21. J. W. Bond, *J. Forensic Sci.*, 2008, **53**, 812-822.
22. S. Virtanen, I. Milosev, E. Gomez-Barrena, R. Trebse, J. Salo and Y. T. Konttinen, *Acta Biomater.*, 2008, **4**, 468-476.
23. J. W. Bond, *J. Forensic Sci.*, 2009, **54**, 1034-1041.
24. J. W. Bond, *J. Phys. D-Appl. Phys.*, 2008, **41**, 125502.
25. A. Bar-Lev, *Semiconductors and electronic devices*, Prentice Hall, Hemel Hempstead, 1993, pp. 96-124.
26. S. M. Sze, *Semiconductor devices*, Wiley, Danvers, 2002, pp. 224-253.
27. D. A. Fraser, *The physics of semiconductor devices*, Oxford University Press, New York, 1986, pp. 132-163.
28. J. W. Bond, *J. Phys. D-Appl. Phys.*, 2009, **42**, 235301.
29. J. W. Bond and C. Heidel, *J. Forensic Sci.*, 2009, **54**, 892-894.
30. J. W. Bond, *Rev. Sci. Instrum.*, 2009, **80**, 075108.
31. E. Halahmi, O. Levi, L. Kronik and R. L. Boxman, *J. Forensic Sci.*, 1997, **42**, 833-841.
32. E. Paterson, J. W. Bond and A. R. Hillman, *J. Forensic Sci.*, 2010, **55**, 221-224.
33. R. Ennos and P. Warman, *Comp. Biochem. Phys. A.*, 2009, **153**, S123-S124.
34. P. H. Warman and A. R. Ennos, *J. Exp. Biol.*, 2009, **212**, 2015-2021.
35. S. E. Tomlinson, R. Lewis and M. J. Carre, *Wear*, 2009, **267**, 1311-1318.
36. S. E. Tomlinson, M. J. Carre, R. Lewis and S. E. Franklin, *Wear*, 2011, **271**, 2346-2353.
37. S. Derler, L. C. Gerhardt, A. Lenz, E. Bertaux and M. Hadad, *Tribol. Int.*, 2009, **42**, 1565-1574.

38. R. K. Sivamani, J. Goodman, N. V. Gitis and H. I. Maibach, *Skin Res. Technol.*, 2003, **9**, 227-234.
39. K. Barnett, in *Crime Scene to Court: the essentials of forensic science*, ed. P. White, The Royal Society of Chemistry, Cambridge, 1st edn., 1998, pp. 98-104.
40. D. Charlton, in *Crime Scene Management: Scene Specific Methods*, eds. R. Sutton and K. Trueman, Wiley-Blackwell, Chichester, 2009, pp. 99-130.
41. P. V. D. Haan, *Contemp. Phys.*, 2006, **47**, 209-230.
42. R. S. Ramotowski, in *Advances in Fingerprint Technology*, eds. H. C. Lee and R. E. Gaensslen, CRC Press, Boca Raton, 2nd edn., 2001.
43. Victoria Police, *Fingerprint branch training manual, module nine, latent fingerprint composition*, Melbourne, 2002.
44. D. Robertshaw, in *Physiology, Biochemistry and Molecular Biology of the Skin.*, ed. L. A. Goldsmith, Oxford University Press, New York, 2nd edn., 1991.
45. W. B. Shelley, *J. Invest. Dermatol.*, 1951, **17**.
46. A. M. Knowles, *J. Phys. E. Sci. Instrum.*, 1978, **11**, 713-721.
47. I. Toth and I. Faredin, *Acta Med. Hung.*, 1985, **42**, 21-28.
48. J. N. Labows, G. Preti, E. Hoelzle, J. J. Leyden and A. M. Kligman, *Steroids*, 1979, **34**.
49. O. Jensen and E. Nielsen, *Acta Derm.-Venereol.*, 1979, **59**, 139-143.
50. D. Kaiser and E. Drack, *Eur. J. Clin. Invest.*, 1974, **4**, 261-265.
51. F. Bayford, *Fingerprint Whorld*, 1976, **1**.
52. M. Miklaszewska, *Pol. Med. J.*, 1968, **7**, 617-623.
53. N. Liappis, S. D. Kelderbacher, K. Kesseler and P. Bantzer, *Eur. J. Appl. Physiol.*, 1979, **42**, 227-234.
54. P. H. Gitlitz, F. W. Sunderman and D. C. Hohnadel, *Clin. Chem.*, 1974, **20**, 1305-1312.
55. C. A. Coltman, H. J. Rowe and R. J. Atwell, *Am. J. Clin. Nutr.*, 1966, **18**, 373-378.
56. D. Jenkinson, R. M. Mabon and W. Manson, *Brit. J. Dermatol.*, 1974, **90**, 175-181.
57. B. Hadorn, F. Hanimann, P. Anders, H.-C. Curtius and R. Halverson, *Nature*, 1967, **215**, 416-417.
58. P. B. Hamilton, *Nature*, 1965, **205**, 284-285.
59. J. Oro and H. B. Skewes, *Nature*, 1965, **207**, 1042-1045.
60. T. Takemura, P. W. Wertz and K. Sato, *Brit. J. Dermatol.*, 1989, **120**, 43-47.
61. T. C. Boysen, S. Yanagawa, F. Sato and K. Sato, *J. Appl. Physiol.*, 1984, **56**, 1302-1307.
62. K. Sato, C. Feibleman and R. L. Dobson, *J. Invest. Dermatol.*, 1970, **55**, 433-438.
63. E. Seutter, N. Goedhart-De Groot, H. M. Sutorius and E. J. M. Urselmann, *Dermatologica*, 1970, **141**, 226-233.
64. K. Sato and R. L. Dobson, *J. Invest. Dermatol.*, 1970, **54**.
65. K. Sato, *Rev. Physiol. Bioch. P.*, 1979, **79**, 52-131.
66. R. D. Olsen, *Fingerprint and Identification Magazine*, 1972, **53**.
67. S. W. Brusilow and E. H. Gordes, *Am. J. Physiol.*, 1967, **214**.
68. T. Verde, R. J. Shephard, P. Corey and R. Moore, *J. Appl. Physiol.*, 1982, **53**, 1540-1545.
69. I. J. Schultz, *J. Clin. Invest.*, 1969, **48**, 1470-1477.
70. H. H. Mitchell and T. S. Hamilton, *J. Biol. Chem.*, 1949, **178**.
71. M. Miklaszewska, *Pol. Med. J.*, 1968, **7**, 1313-1318.
72. T. Marshall, *Anal. Biochem.*, 1984, **139**, 506-509.
73. N. Nakayashiki, *J. Exp. Med.*, 1990, **161**, 25-31.
74. L. Forstrom, M. E. Goldyne and R. K. Winkelmann, *J. Invest. Dermatol.*, 1975, **64**, 156-157.
75. R. R. Marples, A. M. Kligman, L. R. Lantis and D. T. Downing, *J. Invest. Dermatol.*, 1970, **55**, 173-178.
76. K. M. Nordstrom, J. N. Labows, K. J. McGinley and J. J. Leyden, *J. Invest. Dermatol.*, 1986, **86**, 700-705.
77. S. C. Green, M. E. Stewart and D. T. Downing, *J. Invest. Dermatol.*, 1984, **83**, 114-117.

78. L. Boniforti, S. Passi, F. Caprilli and M. Nazzaro-Porro, *Clin. Chimica Acta*, 1973, **47**, 223-231.
79. G. C. Goode and J. R. Morris, *AWRE report No. 022/83*, 1983.
80. D. T. Downing, J. S. Strauss and P. E. Pochi, *J. Invest. Dermatol.*, 1969, **53**, 322-327.
81. C. A. Lewis and B. Hayward, in *Modern Trends in Dermatology, Vol 4.*, ed. P. Borrie, Butterworths, London, 1971.
82. E. Haahti, *Scand. J. Clin. Lab. Inv.*, 1961, **13**.
83. N. Nicolaides and R. C. Foster, *J. Am. Oil Chem. Soc.*, 1956, **33**, 404-409.
84. C. B. Felger, *J. Soc. Cosmet. Chem.*, 1969, **20**.
85. D. J. Darke and J. D. Wilson, *AERE report No. G 1528*, 1979.
86. M. Nazzaro-Porro, S. Passi, L. Boniforti and F. Belsito, *J. Invest. Dermatol.*, 1979, **73**, 112-117.
87. N. Nicolaides, *Science*, 1974, **186**, 19-26.
88. F. Kanda, E. Yagi, M. Fukuda, K. Nakajima, T. Ohta and O. Nakata, *Brit. J. Dermatol.*, 1990, **122**, 771-776.
89. N. Nicolaides, *Lipids*, 1966, **2**, 266-275.
90. N. Nicolaides, H. C. Fu, M. N. A. Ansari and G. R. Rice, *Lipids*, 1972, **7**, 506-517.
91. R. Summerly, H. J. Yardley, M. Raymond, A. Tabiowo and E. Ilderton, *Brit. J. Dermatol.*, 1976, **94**, 45-53.
92. W. J. Cunliffe, J. A. Cotterill and B. Williamson, *Brit. J. Dermatol.*, 1971, **85**.
93. U. R. Bernier, D. L. Kline, D. R. Barnard, C. E. Schreck and R. A. Yost, *Anal. Chem.*, 2000, **72**.
94. *Ridges and Furrows*, http://ridgesandfurrows.homestead.com/fingerprint_patterns.html, Accessed June 2012.
95. I. W. Evett and R. L. Williams, *J. Forensic Ident.*, 1996, **46**, 49-73.
96. J. G. Barnes, in *The Fingerprint Source Book*, ed. A. McRoberts, National Institute of Justice, Washington, 2011.
97. A. Bertillon, *Identification Anthropometrique: Instructions Signaletiques*, Imprimerie Administrative, Melun, 1893.
98. F. Galton, *Finger Prints*, Macmillan and Co., London, 1892, p. 216.
99. Worldbank, *World Population*, http://data.worldbank.org/indicator/SP.POP.TOTL/countries?cid=GPD_1&display=graph, Accessed August 2012.
100. G. Lambourne, *The Fingerprint Story*, Harrap, London, 1984, p. 138.
101. L. A. Hutchins, in *The Fingerprint Source Book*, ed. A. McRoberts, National Institute of Justice, Washington, 2011.
102. NPIA, *Fingerprint Database*, http://www.npia.police.uk/en/10504.htm, Accessed May 2012.
103. G. L. Thomas and T. E. Reynoldson, *J. Phys. D-Appl. Phys.*, 1975, **8**, 724-729.
104. G. L. Thomas, *J. Phys. E. Sci. Instrum.*, 1978, **11**, 722-731.
105. G. S. Sodhi and J. Kaur, *Forensic Sci. Int.*, 2001, **120**, 172-176.
106. M. Trapecar and M. K. Vinkovic, *Sci. Justice*, 2008, **48**, 192-195.
107. G. C. Saunders, *Los Alamos National Laboratory Guidelines*, 1989.
108. A. A. Cantu and J. L. Johnson, in *Advances in Fingerprint Technology*, eds. H. C. Lee and R. E. Gaensslen, CRC Press, Boca Raton, 2nd edn., 2001, pp. 262-263.
109. M. Zhang, A. Becue, M. Prudent, C. Champod and H. H. Girault, *Chem. Commun.*, 2007, 3948-3950.
110. M. Zhang and H. H. Girault, *Analyst*, 2009, **134**, 25-30.
111. F. Cortes-Salazar, M. Q. Zhang, A. Becue, J. M. Busnel, M. Prudent, C. Champod and H. H. Girault, *Chimia*, 2009, **63**, 580-580.

112. R. Jelly, E. L. T. Patton, C. Lennard, S. W. Lewis and K. F. Lim, *Anal. Chim. Acta*, 2009, **652**, 128-142.
113. M. J. Plater and W. T. A. Harrison, *J. Chem. Res.-S*, 2009, 384-387.
114. P. F. Kelly, R. S. P. King and R. J. Mortimer, *Chem. Commun.*, 2008, 6111-6113.
115. R. Leggett, E. E. Lee-Smith, S. M. Jickells and D. A. Russell, *Angew. Chem. Int. Edit.*, 2007, **46**, 4100-4103.
116. J. Almog, A. Klein, I. Davidi, Y. Cohen, M. Azoury and M. Levin-Elad, *J. Forensic Sci.*, 2008, **53**, 364-368.
117. A. L. Beresford, R. M. Brown, A. R. Hillman and J. W. Bond, *J. Forensic Sci.*, 2012, **57**, 93-102.
118. A. L. Beresford and A. R. Hillman, *Anal. Chem.*, 2009, **82**, 483-486.
119. Y. Migron, G. Hocherman, E. Springer, J. Almog and D. Mandler, *J. Forensic Sci.*, 1998, **43**, 543-548.
120. P. H. R. Ng, S. Walker, M. Tahtouh and B. Reedy, *Anal. Bioanal. Chem.*, 2009, **394**, 2039-2048.
121. S. Bell, *Annu. Rev. Anal. Chem.*, 2009, **2**, 297-319.
122. Y. Y. Mou and J. W. Rabalais, *J. Forensic Sci.*, 2009, **54**, 846-850.
123. T. C. Chen, Z. D. Schultz and I. W. Levin, *Analyst*, 2009, **134**, 1902-1904.
124. M. J. West and M. J. Went, *Spectroc. Acta Pt. A-Molec. Biomolec. Spectr.*, 2009, **71**, 1984-1988.
125. E. Widjaja, *Analyst*, 2009, **134**, 769-775.
126. D. A. Kidwell, J. C. Holland and S. Athanaselis, *J. Chromatogr. B*, 1998, **713**, 111-135.
127. R. Bhargava, R. S. Perlman, D. C. Fernandez, I. W. Levin and E. G. Bartick, *Anal. Bioanal. Chem.*, 2009, **394**, 2069-2075.
128. A. Norimitsu, S. Naoki and K. Kenro, *J. Forensic Sci.*, 2007, **52**, 1103-1106.
129. A. Hemmila, J. McGill and D. Ritter, 43rd Annual Meeting of the Missouri-Academy-of-Science, St Joseph, MO, 2007.
130. D. Noble, *Anal. Chem.*, 1995, **67**, A435-A438.
131. A. Yamamoto, S. Serizawa, M. Ito and Y. Sato, *J. Invest. Dermatol.*, 1987, **89**, 507-512.
132. G. M. Mong, C. E. Petersen and T. R. W. Clauss, *Advanced Fingerprint Analysis Project: Fingerprint Constituents* PNNL-13019; R&D Project: 28471; TRN: AH200136%%340, Richland, WA, 1999.
133. G. Sansone-Bazzano, B. Cummings, A. K. Seeler and R. M. Reisner, *Brit. J. Dermatol.*, 1980, **103**, 131-137.
134. M. E. Stewart and D. T. Downing, *J. Invest. Dermatol.*, 1990, **95**, 603-606.
135. M. E. Stewart and D. T. Downing, *J. Invest. Dermatol.*, 1985, **84**, 501-503.
136. M. E. Stewart, W. A. Steele and D. T. Downing, *J. Invest. Dermatol.*, 1989, **92**, 371-378.
137. C. Leygraf, in *Encyclopedia of Electrochemistry: Corrosion and Oxide Films*, eds. A. J. Bard, M. Stratmann and G. S. Frankel, Wiley-VCH, Cambridge, 2003.
138. D. Landolt, *Corrosion and Surface Chemistry of Metals*, EPFL Press, Lausanne, 2007, p. 2.
139. D. Landolt, *Corrosion and Surface Chemistry of Metals*, EPFL Press, Lausanne, 2007.
140. K. R. Tretheway and J. Chamberlain, *Corrosion for Science and Engineering*, Longman, Harlow, 1995.
141. G. S. Frankel and D. Landolt, in *Encyclopedia of Electrochemistry: Corrosion and Oxide Films*, eds. A. J. Bard, M. Stratmann and G. S. Frankel, Wiley-VCH, Cambridge, 2003, vol. 4.
142. M. G. Fontana, *Corrosion Engineering*, International edn., McGraw-Hill Book Co, Singapore, 1987, pp. 39-152.
143. E. Mattsson, *Basic Corrosion Technology for Scientists and Engineers* Institute of Materials, London, 1996.
144. A. J. Goddard, A. R. Hillman and J. W. Bond, *J. Forensic Sci.*, 2010, **55**, 58-65.

145. M. G. Fontana, *Corrosion Engineering*, International edn., McGraw-Hill Book Co, Singapore, 1987, pp. 240-243.
146. G. L. Thomas, *J. Forensic Sci. Soc.*, 1975, **15**, 133-135.
147. Pourbaix, in *Corrosion Chemistry Within Pits, Crevices and Cracks: Proceedings of a Conference Held at the National Physical Laboratory, Teddington, Middlesex, on October 1-3, 1984* ed. A. Turnbull, HMSO, London, 1987.

Chapter Two:

Methodology

2.1 Introduction

The data presented in this thesis combines results from varying techniques, notably topographical techniques and techniques that can derive chemical information. In order to produce a concise account of what each technique is capable of this chapter includes discussion of modes of operation not actively pursed for the data presented in later chapters.

2.2 AFM Methodology

2.2.1 Introduction

The atomic force microscope (AFM) is part of the scanning probe microscopy (SPM) family and is a tip-surface force based device. Unlike some other members of the SPM family (notably the scanning tunnelling microscope), the AFM is able to measure the topography of both insulating and conductive samples at near-atomic resolution. This is because the AFM is capable of measuring both physical features and the effects of surface forces, such as Van der Waals force, due to the nature of the interaction.

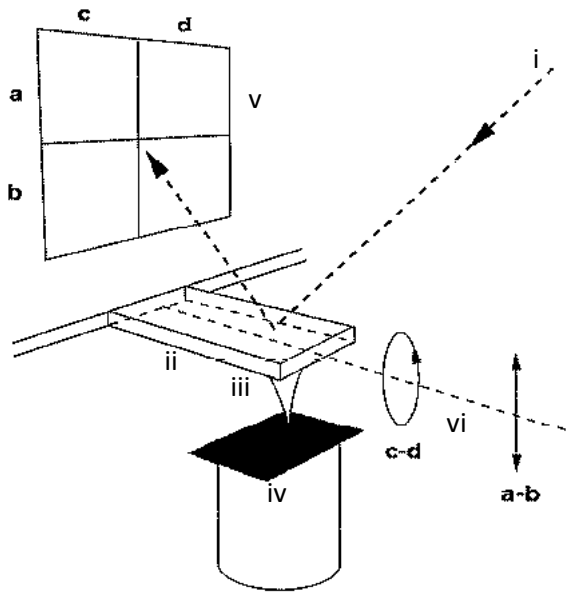

Figure 2.1 – Schematic depiction of the basic components of an AFM[1]. i) Laser pathway; ii) cantilever; iii) probe; iv) sample and sample stage; v) segmented photodiode; vi) plane of movement available to cantilever, where a-b) the direction of normal bending on the cantilever and the resultant effect on reflected laser position in the segmented diode; c-d) the effect of torsion on the cantilever and the resultant effect on the reflected laser position in the segmented photodiode.

The AFM is made up of three main parts: cantilever, sample stage and optical detection system. The last of these consists of a laser diode and segmented photodiode. The laser beam is reflected off the back side of the cantilever and is detected by a four quadrant photodiode detector, as observed in Figure 2.1. By using a four quadrant system, it provides the opportunity to measure both normal bending (Figure 2.1, labels a-b) as well as torsion (Figure 2.1, labels c-d) of the cantilever.

On the underside of the cantilever is a sharp, conical or pyramidal, tip (the probe) that is used to scan the sample's surface. The material that the cantilever is made of is chosen according to the application, but is usually silicon based. Typical cantilever dimensions are 100-300 µm in length, 10-30 µm wide and 0.5-3 µm thick. This results in spring constants typically between

0.01 and 100 N/m. In order to obtain topography measurements, the cantilever is rastered across a sample's surface. During the course of scanning, bending of the cantilever due to variations in surface forces or physical features are detected by the segmented photodiode.

The position of the cantilever is controlled by three piezoelectric controls, one for each axis. Real time monitoring of the *x* and *y* positions during the raster scan allows the topographical measurements to be portrayed as a three dimensional topographical map of the sample surface. Due to the forces present on a surface, the probe to sample distance is crucial to the type of information to be obtained. This gives rise to three main modes of operation for the AFM: contact mode, in which the probe is in direct contact with the surface; non-contact mode, in which surface contact is avoided and lastly; tapping mode, in which the probe is oscillated and intermittently directly contacts the sample surface.

2.2.2 Contact Mode

Contact mode AFM operates, as the name suggests, with the probe in direct constant contact with the sample surface and the probe is effectively dragged across the surface[2].

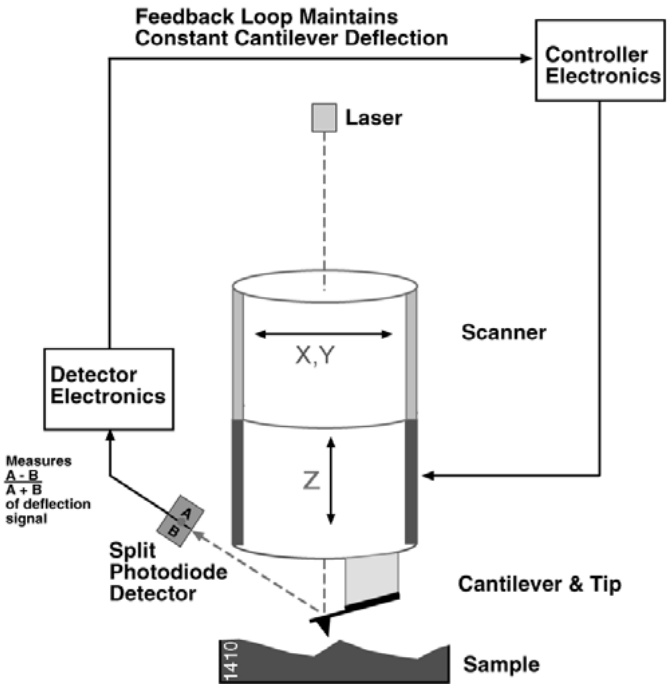

Figure 2.2 – Schematic of a contact mode AFM system with a feedback loop (image courtesy of Veeco Instruments Inc.).

A feedback loop maintains a constant deflection between the cantilever and the surface by vertically moving the scanner unit at each lateral data point (Figure 2.2). By maintaining a constant cantilever deflection, the force between the sample and probe remains constant and so the topographical height information is recorded by the physical height of the scanner unit[3].

The obvious drawback of operating in this mode relates to hardness comparisons. If there is a significant difference in the hardness of the probe and sample being studied, then damage and deformation may occur to the softer material. Additionally, soft material present on a sample surface can be dragged across it. Deformation and damage are equally undesirable as they causes permanent changes to the surface features of the sample, as well as causing incorrect topography measurements to be recorded. Consequently, this mode is typically used to measure the physical features of a hard surface (glass) under vacuum or ambient conditions and its use is avoided for soft pliable samples, such as biological material or polymers containing plasticising components.

2.2.3 Non-Contact Mode

Rather than directly measuring the surface features, this mode measures the forces present on the sample surface. The probe is kept clear from contacting the sample surface, typically 5-10 nm away[2]. Rather than being in contact and dragged over the surface by constant force (contact mode), the cantilever is kept at a constant height and is oscillated slightly above its resonant frequency, with an amplitude of typically <10 nm. This generates an AC signal from the cantilever monitored by the optical deflection system[3].

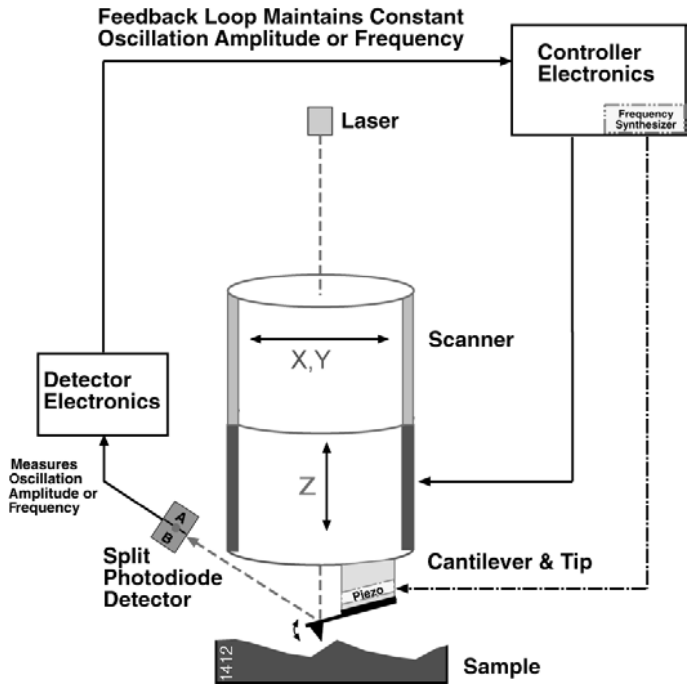

Figure 2.3 – Schematic of a non-contact mode AFM system with a feedback loop (image courtesy of Veeco Instruments Inc.).

As the cantilever moves across the sample surface in a raster fashion, a feedback loop is employed to maintain oscillation frequency (Figure 2.3). Van der Waals forces and other long range forces interact with the oscillating cantilever by attractive or repulsive forces. These forces will either dampen or extend the oscillation amplitude. Upon detecting a variation in the oscillation, the height of the cantilever and scanning head is adjusted. The forces are

therefore recorded as a function of the scanning head height along with the associated lateral dimensions.

Due to the lack of physical interaction between the cantilever and the sample surface, there is no degradation of the cantilever during the course of a scan. However, if the surface is not particularly smooth and has a sharp height contrast, the cantilever is liable to crash sideways into these features causing damage to either the sample or the probe, and in some cases both.

Due to the monitoring of forces, non-contact mode can be successfully employed to distinguish multiple materials present on a surface as well as imaging liquid layers. Conversely, it cannot be as accurately employed to monitor the physical features present, compared to other modes of operation, because it is mainly affected by force variation rather than surface height changes. Interpretation is therefore reliant on knowledge of the force-distance relationship, which may vary for different materials. Although ideally simply related, this is not always straightforward for complex samples, with spatially variant composition.

2.2.4 Tapping Mode

Rather than operating at constant height (non-contact mode) or constant force (contact mode), this final mode of operation is a hybrid of the two. A cantilever is oscillated at or near its resonant frequency, with the amplitude typically between 100-200 nm. At one extreme of each oscillation, the probe on the cantilever underside lightly contacts the sample surface, see Figure 2.4A. As the cantilever is rastered across the sample, the probe continually taps the surface, so this probe behaviour gives rise to this mode of operation being known as intermittent-contact or tapping mode. The effect of tapping the surface causes a reduction in the oscillation amplitude and monitoring of this enables the oscillation dampening to become

the feedback control, which in turn enables the surface topography to be measured (Figure 2.4B).

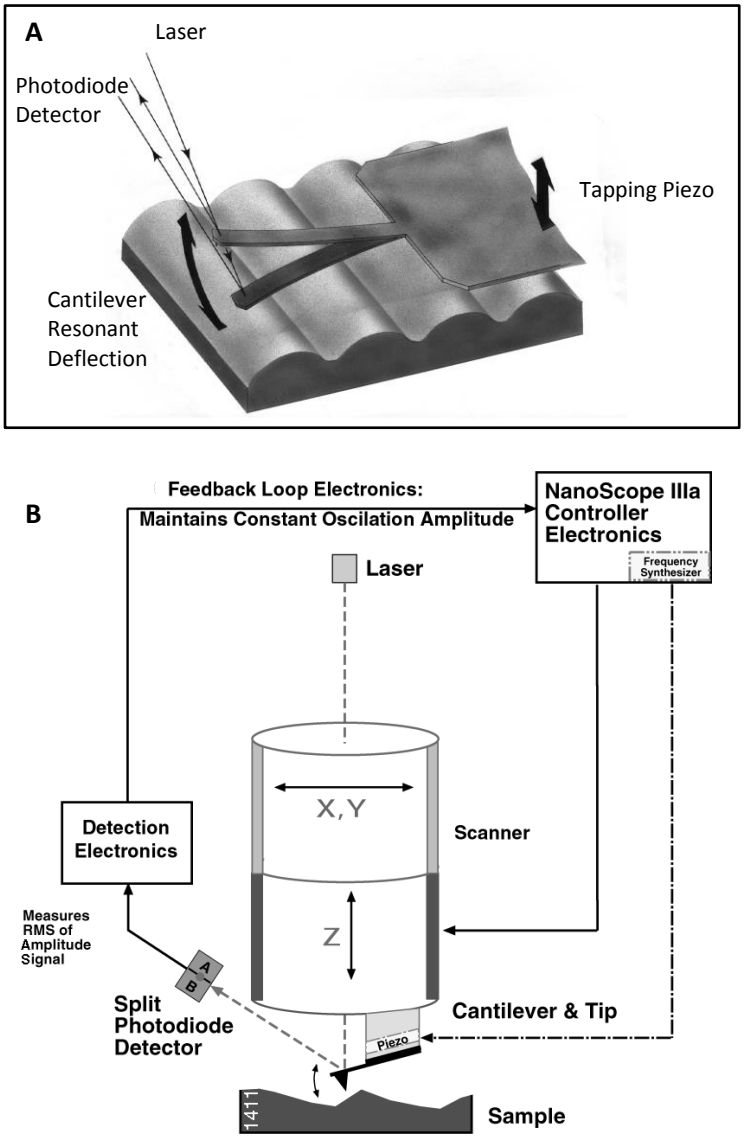

*Figure 2.4 – Schematics of tapping mode AFM: **A**) depiction of cantilever and laser movements as the cantilever traverses the surface; **B**) schematic of a non-contact mode AFM system with a feedback loop (images courtesy of Veeco Instruments Inc.).*

The advantage of this mode is that it is possible to achieve very accurate information about physical surface features as well as force variations and the presence of multiple materials. Additionally, due to the light tapping nature, the sample is not as easily damaged as may occur in contact mode and, although the probe does degrade, it typically has a longer lifetime.

Tapping mode can also be used to acquire topographical data from both ambient and liquid environments.

2.2.5 Other Modes of Operation

The modes described above cover the basic operation modes of the AFM, however, by modifying the material of the cantilever and probe, other measurements can be made. Almost all of the modes of operation outside of basic topography measurements employ a non-contact mode for measurements[2].

Using cobalt and chromium based magnetic probes and cantilevers allows for magnetic force microscopy (MFM). MFM uses a non-contact mode AFM set-up with the magnetic probe and can be used to measure magnetic dipole-dipole interactions and other magnetic surface forces[3-5]. Similarly, electrostatic force microscopy (EFM) works on the same principles and set-up but measures electrostatic attractions and repulsions rather than magnetism effects; EFM can even work on submerged as well as non-conducting samples[3, 6].

With slight modifications to the feedback loop system, scanning electrochemical potential microscopy (SECM/SECPM) can also be performed, using either W or Pt/Ir based probes in liquid media[7]. This form of microscopy is operated in non-contact mode, keeping a constant height but close enough to the surface of the material for the electrochemical exchanges to occur between the probe and the sample surface with the resulting current measured. SECPM can be used to study solid/liquid interfaces[8] as well as variations in surface composition or electrical potential profiles[9-11] amongst other applications.

2.3 DHM Methodology

2.3.1 Introduction

Digital holography microscopy (DHM) is an optical microscopy method which utilises laser interference principles to enable imaging and topographic measurements of a sample. The technique incorporates a single laser beam (of known wavelength), which is split into two beams. One of the beams serves as the reference beam whilst the other serves as the objective beam. In order for accurate measurements and reconstruction of the refracted laser, the distance travelled by each part of the split beam must be the same. The objective laser beam is directed at the sample. If the sample is translucent, such as a glass slide, then the objective beam is directed at the underside of the sample with the detector on the other side of the sample. This is referred to as transmission configuration (Figure 2.5A). Alternatively, if the sample is opaque or reflective, is it not possible to pass the beam through, therefore a reflective configuration is required. In this case the objective beam is directed at the topside of the sample with the detector above as well (Figure 2.5B). By measuring the change in intensity of the light beam reflected from the sample compared to the reference beam, a hologram, and subsequently an image, can be generated.

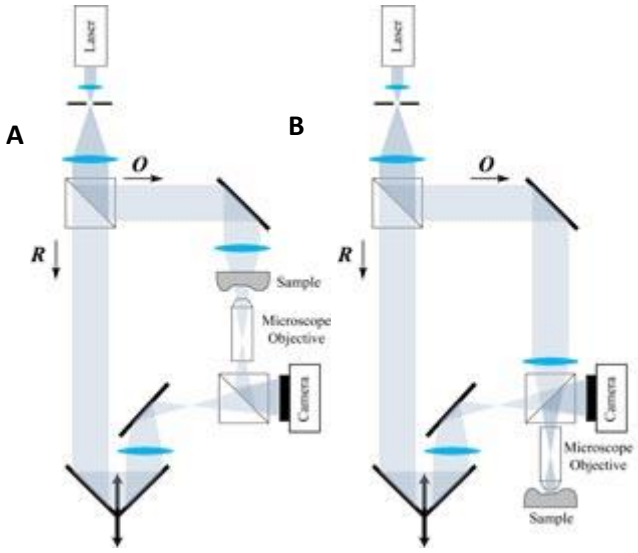

*Figure 2.5- Schematics of DHM instrumentation in two different configurations: **A**) transmission configuration; **B**) reflection configuration*[12].

2.3.2 Image generation

A DHM is capable of portraying the topography of the sample in two ways: by intensity or phase. Intensity images are similar to those obtained by classical optical microscopes, but with a monochromatic source rather than white light. This can provide more contrast than white light images. However it cannot provide any information about the colour of the sample[12].

A phase image provides quantitative data of the sample surface; it is used for accurate and stable measurements. In reflection configuration, the phase image reveals the surface topography. In transmission, the phase image reveals the phase shift induced by a transparent specimen, which depends on its thickness and refractive index[12].

The two laser beams (objective and reference) are coherent due to having the same path length. This means that they can interfere with each other and enable a topographical hologram to be generated as well as the phase image information to be recorded. The

wavefront from the objective beam changes after encountering the sample (Figure 2.6), this is then compared to the reference beam and the differences recorded[12].

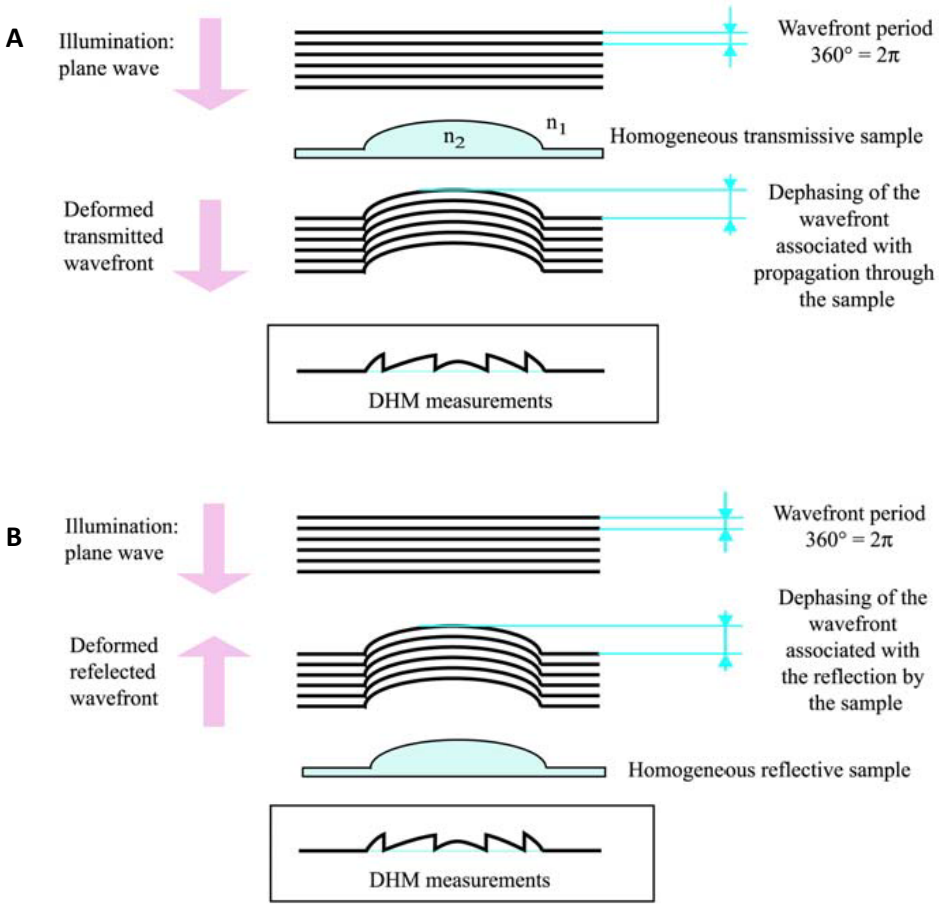

Figure 2.6 – Principle of phase measurements in DHM, showing how wavefronts are generated after interaction with surface features: ***A****) Transmission configuration;* ***B****) Reflective configuration*[12].

Figure 2.6 shows how the measurement received by the DHM does not initially resemble the sample surface. However, the angles and step heights are accurately recorded relative to the wavelength of the beam. Viewing of the phase measurement would give some idea of what the surface was like with regards to topographical variation, but would not display the information in a fully interpretable image (Figure 2.7A). The phase image is then converted

into the topographical image by a series of equations (see appendix C), which then allows the topographical image obtained to be viewed (Figure 2.7B).

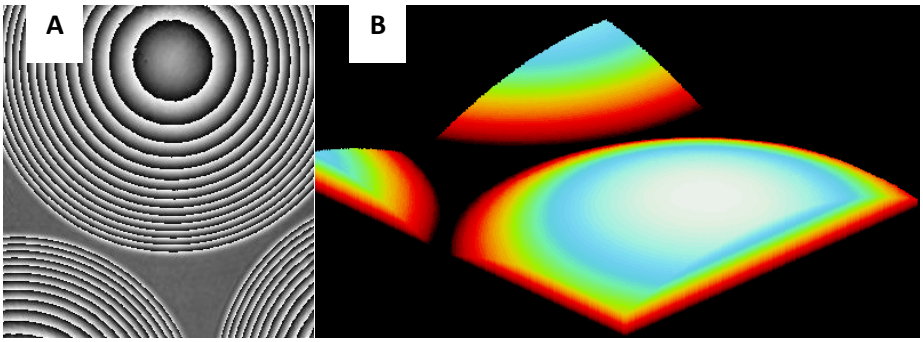

*Figure 2.7 – Images obtained from a DHM instrument: **A**) phase image of micro lenses; **B**) 3D topographical representation of the phase image in **A**[12].*

If the step height or features of the sample are greater than half the wavelength (λ/2) of the laser, then the height information may be incorrectly recorded. This is due to the way the laser portrays the surface features encountered (Figure 2.6). Figure 2.8, below, depicts a cross section through a "staircase" of varying step heights, as some of the step increases are greater than λ/2 they are misrepresented by the wavefront and therefore the phase data is misinterpreted (Figure 2.9). The final step is completely invisible when viewed as a 3D representation. This is because the height of the step matches the λ/2 function of the laser. As the step height is approximately 1300 nm, the wavelength of the laser could be 650 nm with λ/2 being 325 nm[12].

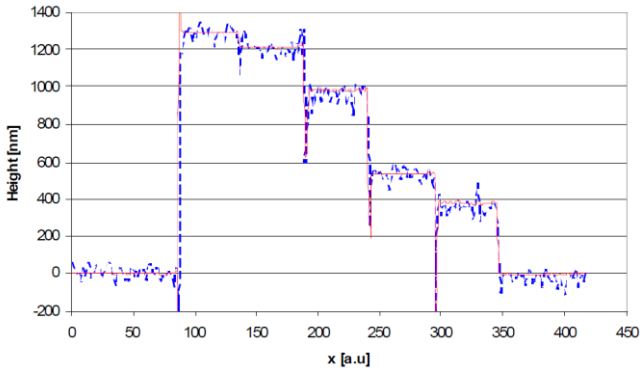

Figure 2.8 – Cross section of a "staircase" on a sample surface, obtained by DHM measurements incorporating dual wavelength lasers[12].

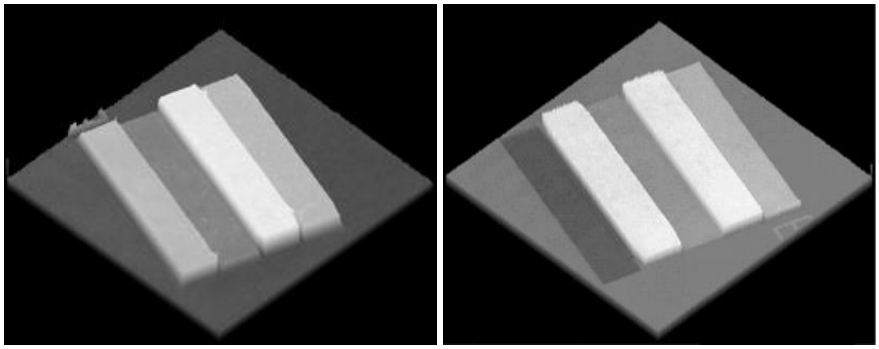

Figure 2.9 – 3D topographical image of the "staircase" from Figure 2.8. ***A)*** *imaged using a single laser wavelength;* ***B)*** *imaged using a different wavelength than that seen in* ***A***[12].

The staircase feature is not recognisable in either image in Figure 2.9, however they are both depictions of this same feature but imaged using a laser of single wavelength. To avoid this type of misinterpretation, a second laser beam can be employed that has a slightly different wavelength; each image obtained by different laser wavelengths may show different surface feature heights. This means that the value assigned to λ/2 is different for each laser and so different step heights can be measured. By combining the information between the two, the true step heights can be determined, as was seen originally in Figure 2.8, this is an example of data acquisition by dual wavelength DHM measurements.

2.3.3 Sample types

Image acquisition in reflective configuration is highly dependent on the reflective properties of the surface. If the surface has a mirror-like finish, then it makes it an ideal surface to image. If, however, the surface is dull or scratched then imaging of surface features can be slightly more problematic. Materials suitable for reflective measurements are those that are reflective or semi-reflective, excepting those that diffuse strongly. These materials, such as powders, paper and certain ceramics, by their nature, "fog" the phase information and cannot form holograms. The maximum roughness of surfaces that can be measured by a reflective DHM should have a surface roughness profile (Ra) of less than 200 nm[12].

In transmission configuration, in order to obtain measurements, the samples must be able to at least partially transmit the light, excepting those that diffuse strongly. The materials that diffuse light "fog" the phase information and prevent the formation of holograms. The maximum roughness of surfaces that can be measured by a DHM in transmission configuration is less than a surface roughness profile (Ra) of 400 nm[12].

2.4 XPS Methodology

2.4.1 Introduction

X-ray photoelectron spectroscopy (XPS), sometimes referred to as electron spectroscopy for chemical analysis (ESCA), is a highly sensitive surface chemical analysis technique that is used to analyse the surface composition of the sample in terms of elemental composition, chemical state and electronic state. This is performed by using an X-ray beam to excite the sample and then measuring the quantity and energy of the electrons that escape from the sample. Electrons do not travel very far in air, due to the presence of other atoms. Therefore to be effectively used for analysis XPS is carried out under ultra-high vacuum conditions.

The X-ray beam is used to irradiate the sample surface, providing the energy needed to enable electrons to escape; the X-ray source is commonly an Al Kα, Cr Kβ or Cu Kα X-ray generator. The atoms in the sample absorb the energy and in turn promote electrons. If the energy absorbed is greater than the work function of the electron, then the electron is ejected. This ejected electron is known as a photoelectron. The photoelectrons travel with a characteristic velocity, determined by the energy required to be ejected. The main reason that XPS is so surface sensitive, even though the X-rays penetrate much deeper, is because the photoelectrons ejected deeper in the sample are re-captured or trapped by the layers nearer the surface and so it is only the photoelectrons emitted from very close to the surface (~10 nm) that can actually escape the sample[13, 14]. The photoelectrons are essentially emitted in every direction above the sample. In order to accurately analyse the photoelectrons, only those emitted with a particular trajectory will be detected due to the path length to the detector (up to a metre away). This means that only the area directly irradiated will be analysed, which practically eliminates background contamination. Due to the distance of the detector from the sample surface, an ultra-high vacuum has to be used, otherwise very few electrons would reach the detector. A schematic of an XPS instrument is shown in Figure 2.10.

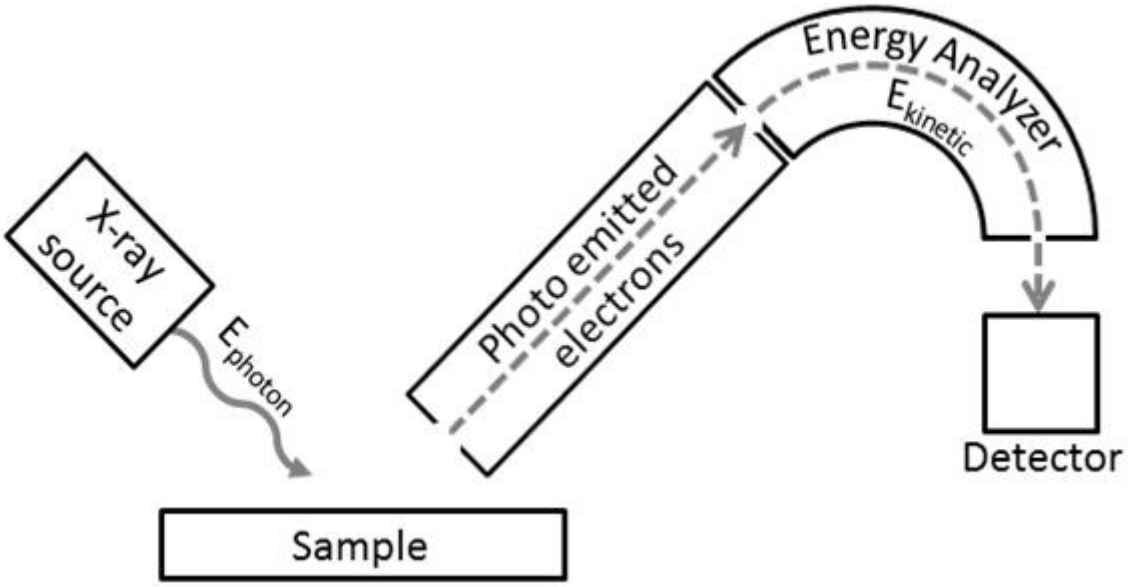

Figure 2.10 – Schematic of XPS instrumentation set-up. The dashed line shows the pathway for the emitted photoelectrons that are detected.

2.4.2 Qualitative Surface Analysis

Aside from just counting the number of photoelectrons, the kinetic energy is also measured. By knowing the kinetic energy of the photoelectrons as well as the energy of the X-ray beam, it is possible to deduce the binding energy of the electrons (Equation 2.1)[13]. The binding energy values enable the deduction of not only the identity of the atom that the electron escaped from, but also the oxidation state of that atom. The variation of binding energies with oxidation states is on the order of a few electron volts per unit change in oxidation state and is therefore readily measureable.

$$E_{binding} = E_{photon} - (E_{kinetic} + \emptyset) \qquad 2.1$$

Where $E_{binding}$ is the binding energy of the electron prior to ejection, E_{photon} is the energy of the X-ray photon beam, $E_{kinetic}$ is the kinetic energy of the electron after ejection as measured by the instrument and Ø is the work function of the spectrometer and not the material [13].

Each element has a characteristic set of binding energies associated with it. By plotting the binding energy against the number of electrons detected, a spectrum is generated and this can be used to identify the elements present. These characteristic peaks correspond to the electron configuration of the electrons within the atoms. The number of detected electrons is directly proportional to the amount of that element present in the irradiated area[13].

An example of an XPS spectrum for carbon is shown below (Figure 2.11):

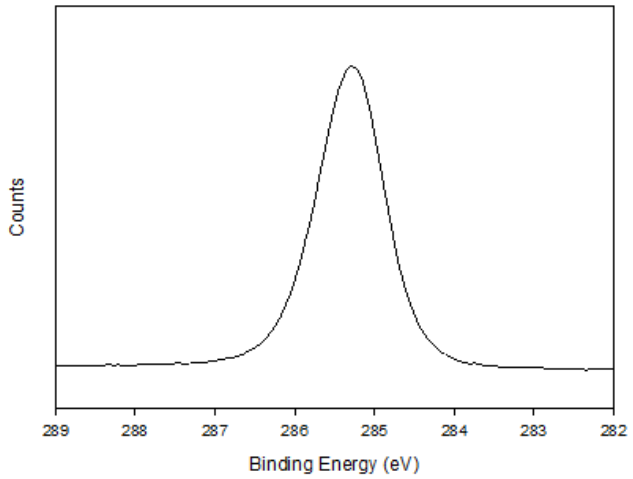

Figure 2.11 – An XPS spectrum for Carbon 1s, between 282 and 289 eV. The sample is a polished brass substrate.

The carbon spectrum in Figure 2.11 shows a clear single peak, a symmetrical peak with smooth slopes on either side. The assignment of such a peak is relatively simple. One merely records the binding energy value for the mid-point of the peak. However, not all such peaks are as easily assigned, as more variations of the selected element are present on the sample surface, the more complex the spectrum becomes. For instance, if there were two different carbon based bonds present, such as in acetone, then one would expect to see a peak for each. The peak separation is attributable to the difference in binding energies between the two bound forms of carbon. When spectra for metallic elements are examined, the splitting of a peak or

multiple peaks can indicate different oxidation states of the metal being present. This is illustrated by the copper spectrum in Figure 2.12.

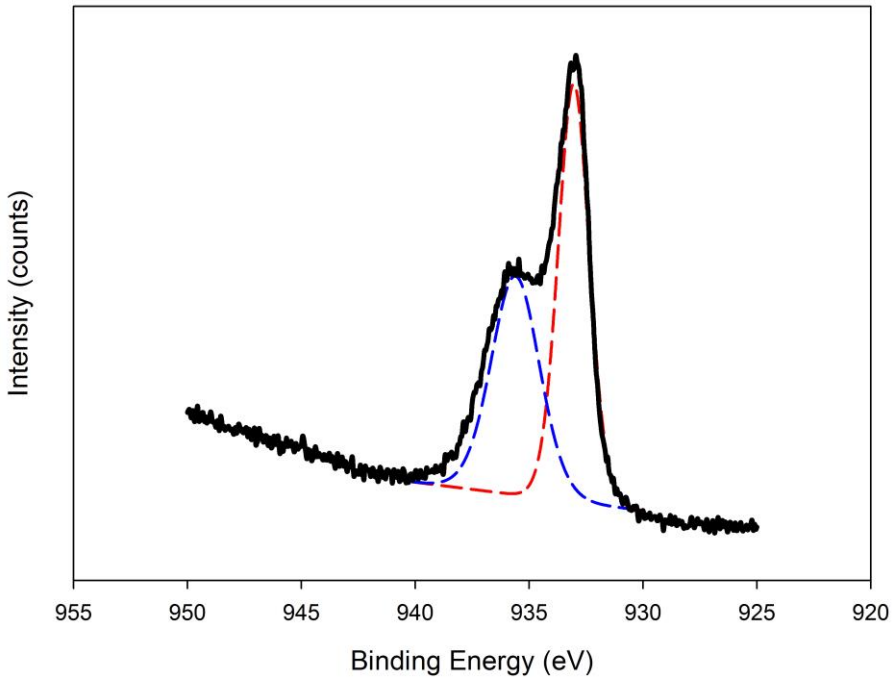

Figure 2.12 – XPS spectrum for copper 2p3/2 region of a sebaceous fingerprinted brass substrate, original spectrum is the solid black line, two potential deconvoluted options are the red and blue dashed lines.

In the above figure (Figure 2.12), the original peak (the black solid line) can be seen to possess two distinct features with clear separation, with binding energy values of *ca*. 935 eV and 930 eV. In order to fully assign the peaks, they must be de-convoluted and the signal producing each peak extracted. In this same figure, two dotted lines can be seen, one red and the other blue, these lines represent two potential signals or profiles which could be attributed to be the cause of the split peak. The red line at the lower binding energy value can be attributed to either Cu(0) or Cu(I) whereas the blue line is at binding energy values associated with copper in a higher oxidation state, Cu(II). Just from this breakdown it is possible to identify that two distinct oxidation states for copper are present; more accurately identifying the peak positions

then enables one to identify that particular compound. The peak of the red profile is at 933.0 eV and the blue is at 935.5 eV, which can be attributed to copper as Cu(0)[15-17] and $Cu(OH)_2$[18] respectively.

2.4.3 Spatially Resolved Surface Analysis

What Figure 2.11 shows, is a spectrum acquired in standard acquisition mode, with the surface composition averaged over a relatively wide area (typically several millimetres) with no information relating to the spatial composition variance. If one were interested in identifying specific areas of different compositions or oxidation states, this would not be adequate (see Figure 2.13). However, it is possible to obtain spatially resolved XPS spectra. A physical filter is placed between the sample and the detector to narrow the studied area to a rectangular area in the order of several centimetres long, the spectra are resolved as vertical slices and dependent on settings can allow for 1024 spectra along the area of interest, with each slice representing a segment tens of microns wide (see Figure 2.14).

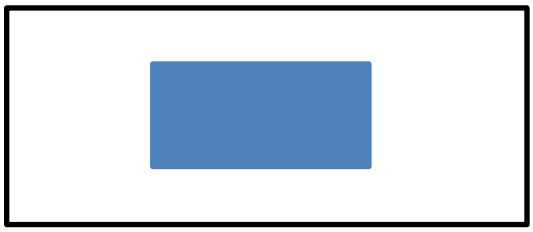

Figure 2.13 – A simple diagram to show the area standard XPS measures; the black rectangle represents the sample whilst the blue rectangle represents the area that data is collected from. Image is not drawn to scale.

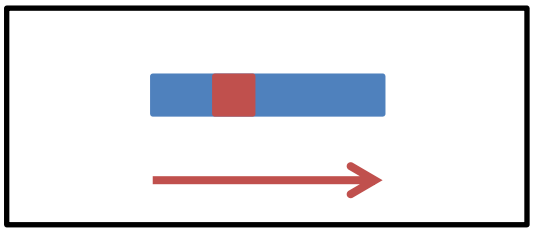

Figure 2.14 – A simple diagram to show how spatial XPS operates; the large black rectangle is the sample, the inner blue rectangle is the area imaged with slices obtained along the flow of the arrow. The red segment is representative of a single spectrum slice. Image is not drawn to scale.

The spectra from each slice can be viewed individually; however the most visual representation is obtained when they are viewed altogether focusing on specific energy bands at a time. Spatially resolved spectra are discussed further in Chapter 5.

2.5 References

1. R. J. Colton, D. R. Baselt, Y. F. Dufrene, J.-B. D. Green and G. U. Lee, *Current Opinion in Chemical Biology*, 1997, **1**, 370-377.
2. G. T. Barnes and I. R. Gentle, *Interfacial Science: an introduction*, 2nd edn., Oxford University Press, Oxford, 2011, pp. 195-198.
3. J. S. Murday and R. J. Colton, in *Chemistry and Physics of Solid Surfaces VIII*, eds. R. Vanselow and R. Howe, Springer-Verlag, Berlin, 1990, pp. 356-362.
4. A. C. Wright, M. K. Faulkner, R. C. Harris, A. Goddard and A. P. Abbott, *J. Magn. Magn. Mater.*, 2012, **324**, 4170-4174.
5. U. Hartmann, *Annu. Rev. Mater. Sci.*, 1999, **29**, 53-87.
6. S. Xu and M. F. Arnsdorf, *P. Natl. Acad. Sci. USA*, 1995, **92**, 10384-10388.
7. A. J. Bard, F. R. F. Fan, J. Kwak and O. Lev, *Anal. Chem.*, 1989, **61**, 132-138.
8. H. Wolfschmidt, C. Baier, S. Gsell, M. Fischer, M. Schreck and U. Stimming, *Materials*, 2010, **3**, 4196-4213.
9. R. F. Hamou, P. U. Biedermann, A. Erbe and M. Rohwerder, *Electrochim. Acta*, 2010, **55**, 5210-5222.
10. R. F. Hamou, P. U. Biedermann, A. Erbe and M. Rohwerder, *Electrochem. Commun.*, 2010, **12**, 1391-1394.
11. C. Hurth, C. Li and A. J. Bard, *J. Phys. Chem. C*, 2007, **111**, 4620-4627.
12. Lyncee Tec, *Digital Holography Microscope: user operating manual*, Lausanne.
13. E. A. Leone and A. J. Signorelli, in *A Guide to Materials Characterisation and Chemical Analysis*, ed. J. P. Sibilia, Wiley-VCH, New York, 2nd edn., 1996, pp. 221-235.
14. P. W. Atkins, *Physical Chemistry*, 5th edn., Oxford University Press, Oxford, 1995, pp. 617-619.
15. H. M. Liao, R. N. S. Sodhi and T. W. Coyle, *J. Vac. Sci. Technol. A-Vac. Surf. Films*, 1993, **11**, 2681-2686.
16. P. Marcus and M. E. Bussell, *Appl. Surf. Sci.*, 1992, **59**, 7-21.
17. C. D. Wagner, W. M. Riggs, L. E. Davis and J. F. Moulder, *Handbook of x-ray photoelectron spectroscopy: a reference book of standard data for use in x-ray photoelectron spectroscopy*, first edn., Physical Electronics Division, Perkin-Elmer Corp., 1979.
18. L. S. Dake, D. E. King and A. W. Czanderna, *Solid State Sci.*, 2000, **2**, 781-789.

Chapter Three:

Experimental

3.1 Introduction

In this chapter, the experimental conditions and protocols used throughout this thesis are presented. This includes sample preparation, fingerprint deposition methods, data acquisition and instrumentation operating procedures.

3.2 Techniques

3.2.1 Atomic Force Microscopy

3.2.1.1 Instrumentation

The instrumentation used was a Digital Instruments Nanoscope IV, Dimension 3100 Scanning Probe Microscope (Veeco Instruments Inc., Santa Barbara, CA), operated using Nanoscope version 6.12r1 software (Veeco Instruments Inc.). This was used in only tapping mode, using a tap300 probe type; the probe tips were phosphorus doped silicon, with a nominal tip radius of 10 nm and their operation was calibrated before each use with a silicon wafer reference sample (full probe and scan settings are available in Appendix C).

3.2.1.2 Data Acquisition

Samples were loaded on to the sample stage and data acquired in accordance with the operating procedures outlined in the users handbook[1-5]. All data was acquired in ambient environments. Acquired topographical images were tilt corrected using the Nanoscope software.

Multiple combined AFM images were acquired individually as above and then exported to SigmaPlot version 10.0 (Systat Software Inc., Chicago, IL) for collation and image generation. Baseline correction for these images was performed by a static addition or subtraction to the data set.

For each sample, a minimum of three different areas were examined to ensure topography measurements were representative of the whole surface.

3.2.2 Digital Holography Microscopy

The instrumentation used was a Lyncee Tec R1000 series Digital Holography Microscope (Lyncee Tec, Lausanne) coupled with a Baumer TxD14 CCD camera. The instrument was operated using Koala V4 software (Lyncee Tec). The DHM images shown in this thesis were acquired by the reflective configuration and incorporated the use of dual wavelength image acquisition, with the wavelengths of the two lasers being 682.5 nm and 660.0 nm.

Samples were loaded on to the sample stage. Images were acquired using the Koala software program with the dual wavelength mode enabled, to ensure accurate measurements of surface feature heights. The DHM was operated according to standard operating procedures[6]. No post-acquisition manipulation of the images was performed.

For each sample, a minimum of three different areas were examined to ensure measurements were representative of the whole surface

3.2.3 Optical Microscopy

Optical microscopy images were obtained using a Meiji Techno MT7100 trinocular microscope with a CCD camera attached for digital acquisition of images. Samples were loaded on to the sample stage and images were captured using uEye V3.2 software (IDS imaging Development Systems), according to standard operating procedures.

3.2.4 Photography

The camera used for acquisition of images was a Panasonic DMC-FS3 Lumix digital camera operated in macro mode. The camera was placed on a tripod and images taken at oblique angles to avoid capturing reflections on the samples. The camera was white balanced and ambient lighting was used.

3.2.5 X-Ray Photoelectron Spectroscopy

3.2.5.1 Instrumentation

The instrument used to obtain XPS measurements was a Scienta ESCA300 spectrometer at the National Centre for Electron Spectroscopy and Surface Analysis (NCESS) at Daresbury Laboratory. The ESCA300 uses a high power rotating anode and a monochromatic Al K_α X-ray source (hv = 1486.7 eV). The detection system consists of a 300 mm hemispherical analyser and a multi-channel detector, giving a minimum resolution of *ca*. 0.3 eV. All measurements were obtained under UHV conditions.

3.2.5.2 Data Acquisition

Samples were loaded to the sample delivery chamber and then degassed and the pressure lowered. Samples were then moved to an intermediate chamber, whose purpose is to further increase the vacuum prior to delivery to the data acquisition chamber. Samples were aligned by eye, using the viewing windows available. Samples were positioned with a take-off angle of 90° and a slit width of 0.8 mm was used.

Prior to the acquisition of any data, low resolution and broad energy step sample surveys were captured with a pass energy of 150 eV. The binding energy range was 0 eV to 1325 eV with energy steps of 1 eV and a step dwell time of 0.533 seconds (1325 steps in 11.9 minutes), with only a single pass for data acquisition.

Individual high-resolution spectra (non-spatially resolved) were obtained using a transmission lens mode and a swept acquisition mode, taken at a pass energy of 150 eV with an energy step of 0.0183 eV. Binding energy ranges for acquisition were dependent on the region chosen, for example the C 1s region would be between binding energy values of 282 eV to 290 eV. Typically, the energy range of interest was swept multiple times in order to increase the photoelectron count and hence signal strength.

For the acquisition of spatially resolved spectra, a spatial imaging cone was fitted over the detector inside the data acquisition chamber, enabling specific areas of the sample to be selected for elemental analysis. Spatially resolved spectra were obtained using spatial lens mode and fixed acquisition mode. A pass energy of 300 eV and an energy step of 0.0183 eV were used. Acquiring the data would take *ca*. 11.1 minutes per region selected, regions would typically have a single pass for data collection. The area over which data would be acquired is approximately 4 mm long, with spectra obtained approximately every 4 µm. Therefore *ca*. 1000 slices of spectra would comprise a single spatial image, with a dwell time per spectra of *ca*. 0.66 seconds.

3.2.5.3 Data Interpretation

Acquired images were exported to SigmaPlot (Systat Software Inc.), for image generation purposes, the data was baseline corrected and signal intensity was scaled for ease of comparison. Deconvolution of the spectra was performed using CasaXPS version 2.3.15 (Casa Software Ltd) software program and peak positions extracted using this software, with assignments being made primarily using La Surface[7] and NIST[8] online databases. All sources of spectral identities are referenced accordingly in the main body of the text.

Surface ratios were calculated using:

$$C_A = \frac{\left(\frac{I_A}{S_A}\right)}{\sum_n \left(\frac{I_n}{S_n}\right)} \qquad 3.1$$

Where C_A is the atomic percentage of all peaks determined, I_A is the intensity of the element (peak area) and S_A the sensitivity factor (cross-section) of the element in question and performed for *n* elements[9]. However, only the relative amounts of surface copper and zinc were desired and so the equation can be expressed in terms of the surface amounts as a ratio function:

$$Cu : Zn \text{ as } 1 : \frac{\left(\frac{I_{Zn}}{S_{Zn}}\right)}{\left(\frac{I_{Cu}}{S_{Cu}}\right)} \qquad 3.2$$

Thus, surface amounts of the two metal elements are displayed as a relative amounts. The peaks chosen for obtaining the intensities were the $2p_{3/2}$ peaks and were taken from the same spectrum, to ensure equality in terms of data acquisition.

3.2.5.4 Uncertainties

There are many uncertainties that can be considered when performing high resolution chemical interpretation of a sample by XPS. One factor is the position of the peak and the deduction of the species responsible for that signal. A difference of at least 0.2 eV is required to fully differentiate between different chemical species of similar binding energies. Deconvolution of peaks containing multiple species also requires some subjective interpretation; the exact location of multiple peaks in certain spectra can be interpreted in different ways. Interpretation was preformed based on results published in various journals and also those found on online databases.

Another cause of uncertainty can arise from lack of use of a flood gun; charge build-up can occur on the surface due to semi-conductor properties of ZnO and organic material present. This can cause widening of peaks in acquired spectra.

Additionally, there is an uncertainty when determining the ratio of Cu:Zn by peak area. Depending on the intensity of the signal and experimental set-up, the magnitude of the uncertainty in the measurements will vary. There is approximately a 5-10% error in acquiring the peak area and an associated error in determining the sensitivity factor. Due to the calculation to determine the ratio, this error is essentially doubled. As such, all ratio values given possess an error value on the order 10-20%.

In order to produce accurate measurements, each sample had at least 3 areas studied, this enable the data presented to be statistically representative of the total sample surface. Broad survey spectra were obtained for all samples but have not been included within this work; other elements and orbital studies were also studied but not included either, although were commented about where appropriate.

3.3 Samples and Procedures

3.3.1 Substrate Preparation

Brass discs (68% copper; 32% zinc); of diameter 3 cm and thickness 1 mm were obtained from Nobles Engineering, Northamptonshire UK. The discs were supplied with protective plastic films adhered to both sides. Prior to use, the films were removed and the discs washed in warm water (*ca*. 50°C) containing detergent (Fairy® washing-up liquid), followed by rinsing with acetone and spraying dry with nitrogen gas.

Unpolished samples were used immediately following the film removal and cleaning regime outlined above. Polished samples were then rubbed with Brasso™ for 10 to 15 minutes, until a pale gold and mirror like finish was achieved. After polishing, the samples were re-washed in warm water with detergent and rinsed with acetone, followed by drying with nitrogen gas.

3.3.2 Fingerprint Deposition

3.3.2.1 Eccrine Fingerprints

The fingerprints used throughout this thesis were provided by a single donor. For each deposition of eccrine based sweat the donor washed their hands with liquid soap and dried them with paper towel. A time period of 15-20 minutes elapsed before deposition. Immediately prior to deposition, the donor rubbed fingers with the palm of the hand to help spread a uniform composition and amount of sweat across the finger tips. The fingerprints were deposited onto the samples by touching them in a firm but careful manner. All eccrine fingerprint deposited samples used contained latent fingerprint marks.

3.3.2.2 Sebaceous Fingerprints

For each deposition of sebaceous based sweat, the donor washed their hands with liquid soap and dried them with paper towel. The fingers were then wiped across the hairline, sides of the nose and behind the ears to collect the sebaceous sweat. The finger tips were then rubbed with the thumb to evenly distribute the sweat, followed by deposition by touching the samples in a firm but careful manner. All sebaceous fingerprint deposits were considered to be latent fingerprints, although angling samples correctly in natural light coupled with viewing at oblique angles could in some cases reveal traces visible by eye.

3.3.3 Storage Conditions

Samples were stored in a range of different environments throughout this thesis; specific details relating to temperatures and storage times are presented in each case at the relevant point in the main body of the thesis. These storage conditions were selected based upon preliminary findings. A summary of the conditions is presented here.

Ambient samples were stored in an office environment. The temperature was not fully controlled; average day time (08:00 to 18:00) temperatures varied between 17°C and 21°C, depending on the time of year. These samples were left uncovered.

Sample storage in humid environments consisted of being placed in a sealable container with liquid water present. Warm humid storage environments used the same set-up but placed inside an oven with temperatures spanning 45°C to 80°C. A dry (oven) environment consisted of the sample being placed directly inside an oven.

The samples that were subjected to direct heat were held at the top of the blue section of the Bunsen burner flame, for the time indicated in the relevant result sections.

3.3.4 Post-Deposition Treatments

The fingerprinted samples described in Chapter 6 were also subjected to post-deposition treatments, the selection of these treatments in based upon preliminary research along with the findings reported by Paterson *et al.*[10]. A sample that was subjected to being wiped was rubbed 10 times in a lateral motion with blue paper towel, using a moderate force. An acetone rinsed treatment means that the sample was rinsed by a steady flow of acetone for approximately 10 seconds. Similarly, a water rinse means that the sample was placed under running water for 10 seconds with a moderate flow rate. Washing in warm soapy water

involved the sample being placed in a bowl of warm water (*ca*. 50°C) containing a few drops of detergent (Fairy® washing-up liquid) and then rubbed firmly with a gloved hand. Following removal from the soapy water, the sample was rinsed with clean water. Where acetone followed a wash in warm soapy water, the acetone rinse was only a few seconds in length. Post treatment, the samples were left exposed to ambient conditions unless otherwise specified.

3.3.5 Summary of Sample Conditions

Due to the varied storage and post-deposition treatments of the samples used to generate the data portrayed in the following results chapters, in the following series of tables is a concise list of all relevant conditions used. For all conditions explored, a minimum of two samples were studied to monitor the impact of either the storage environment or post-deposition treatment. In each case, fingerprints were deposited simultaneously, such that ambient conditions would be identical and sweat composition and volume of deposit would be similar. Potential sweat deposit variations between fingers was minimised by evenly distributing the sweat prior to deposition.

Table 4. 1 – Summary of sample information for samples used in Chapter 4

Sweat type	Substrate finish	Storage conditions	Time stored	Treatment
Eccrine	Unpolished	Ambient	10 days	
Eccrine	Unpolished	Humid	10 days	
Sebaceous	Unpolished	60°C Humid	5 days	
Eccrine	Unpolished	Ambient	9 days	Detergent washed
Sebaceous	Unpolished	60°C Humid	5 days	Detergent washed
Eccrine	Polished	Ambient	17 days	
Eccrine	Polished	Ambient	8 days	
Eccrine	Polished	Ambient	35 days	
Eccrine	Polished	45°C	8 days	
Eccrine	Polished	50°C Humid	11 days	
Eccrine	Polished	75°C Humid	5 days	

The samples used to chapter 4 cover a range of conditions, beside those included in this thesis, other conditions were also explored. These include limiting the humidity (dry conditions), studying temperatures from ambient to 100°C, at regular intervals. The effect of ambient storage environments on eccrine fingerprinted samples was studied for a total duration of 54 days. Samples were studied periodically through the aging process.

Although mostly eccrine fingerprinted samples were examined in Chapter 4, similar experiments were performed on sebaceous fingerprinted samples. However, these were of less intrinsic value due to being of a visible (non-latent) nature shortly after deposition.

Table 4. 2 – Summary of sample information for data displayed in Chapter 5

Sweat type	Substrate finish	Storage conditions	Maximum Time stored	Treatment
Control	Unpolished	Ambient	3 weeks	
Control	Polished	Ambient	5 weeks	
Control	Freshly polished	Ambient	>5 minutes	
Sebaceous	Polished	Ambient	4 weeks	
Fresh Sebaceous	Polished	Ambient	>5 minutes	
Eccrine	Polished	Ambient	5 weeks	
Fresh Eccrine	Polished	Ambient	>5 minutes	
Eccrine	Polished	Humid	5 days	
Sebaceous	Polished	Humid	5 days	
Control	Polished	75°C Humid	6 hours	
Eccrine	Polished	75°C Humid	6 hours	
Sebaceous	Polished	75°C Humid	6 hours	
Control	Polished	Ambient	4 weeks	Bunsen
Eccrine	Polished	Ambient	4 weeks	Bunsen
Sebaceous	Polished	Ambient	4 weeks	Bunsen

The data presented in Chapter 4 is intended to concisely show the effects of varying environmental storage conditions. Whilst not included, other storage environments and storage lengths were also investigated. Such conditions include temperatures spanning the range between ambient and 100°C, both with and without excess humidity.

Table 4. 3 – Overview of samples and storage environments as well as post-deposition treatments for samples in the first part of Chapter 6

Substrate information	Storage conditions	Time stored	Treatment	Additional storage conditions	Time stored	Second treatment
Sebaceous; Unpolished	60°C Humid	5 days	Detergent wash			
Eccrine; Unpolished	Ambient	5 weeks	Water and acetone	100°C	2 hours	Detergent wash
Eccrine; Unpolished	Ambient	4 days	Acetone rinse	60°C Humid	5 days	
Eccrine; Unpolished	Ambient	4 days	Detergent wash	60°C Humid	5 days	
Eccrine; Unpolished	Ambient	5 weeks	Water and acetone			
Eccrine; Polished	Ambient	4-8 days	Acetone rinse			
Eccrine; Polished	Ambient	4-8 days	Detergent wash			
Eccrine; Polished	Ambient	9 days	Acetone rinse			
Eccrine; Polished	Ambient	9 days	Detergent wash			
Eccrine; Polished	Humid	9 days	Acetone rinse			
Eccrine; Polished	Humid	9 days	Detergent wash			
Eccrine; Polished	Ambient	7 days	None	80°C Humid	1 hour	
Eccrine; Polished	Ambient	35 days	Various treatments	80°C Humid	1 hour	
Eccrine; Polished	Ambient	2 days	Detergent washed			
Eccrine; Polished	50°C Humid	11 days	Detergent washed			
Eccrine; Polished	45°C Humid	7 days	None	80°C Humid	2.5 hours	
Eccrine; Polished	Humid	8 days	Bunsen			Detergent washed

The first part of Chapter 6 primarily focuses on the effects of attempting to remove surface sweat deposit after the sample has been stored in varying conditions for varying amounts of time. Preliminary data that investigates the effectiveness of these removal attempts is also presented here.

Table 4. 4 – Overview of samples and storage environments as well as post-deposition treatments for samples in the latter part of Chapter 6

Sweat type	Treatment after deposition	Storage conditions	Time stored	Treatment after storage
Eccrine	None	Humid	7 days	Detergent washed
Sebaceous	None	Humid	7 days	Detergent washed
Eccrine	None	75°C Humid	2 days	Detergent washed
Sebaceous	None	75°C Humid	2 days	Detergent washed
Eccrine	Wiped	75°C Humid	20 hours	Detergent washed
Sebaceous	Wiped	75°C Humid	20 hours	Detergent washed
Eccrine	Detergent washed	75°C Humid	20 hours	Detergent washed
Sebaceous	Detergent washed	75°C Humid	20 hours	Detergent washed

In the latter part of Chapter 6, there is a focus on the comparison of eccrine and sebaceous fingerprinted samples with respect to varying storage environment and removal treatments.

In order to present data that can provide an overview of the effects of the varying treatments, not all samples studied have been included. Such conditions omitted from this chapter include: storage temperatures exceeding 75°C; varying time between deposition and removal treatment; varying time lengths for image revival; effects of acetone washing both before and after washing with detergent.

Those results presented in all three results chapters are intended to present a concise overview of a range of storage environments and treatments with respect to the surface changes observed by physical, chemical and optical monitoring methods.

3.4 References

1. Digital Instruments Veeco Metrology Group, *Dimension 3100 Manual, Version 4.43C*, Santa Barbara, CA, 2003.
2. Digital Instruments Veeco Metrology Group, *Fine Calibration Procedures for the SPM - a User's Guide*, Santa Barbara, CA, 1996.
3. Digital Instruments Veeco Metrology Group, *Nanoscope IV Controller Manual*, Santa Barbara, CA, 2002.
4. Veeco Instruments Inc., *NanoScope Software 6.12 User Guide*, Santa Barbara, CA, 2004.
5. Veeco Instruments Inc., *NanoScope Version 6 Addendun*, Santa Barbara, CA, 2004.
6. Lyncee Tec, *Digital Holography Microscope: user operating manual*, Lausanne.
7. P. D. Sawant, Y. M. Sabri, S. J. Ippolito, V. Bansal and S. K. Bhargava, *Phys. Chem. Chem. Phys.*, 2009, **11**, 2374-2378.
8. G. S. Sodhi and J. Kaur, *Forensic Sci. Int.*, 2001, **120**, 172-176.
9. D. Briggs, in *Surface Analysis by Auger and X-Ray Photoelectron Spectroscopy*, eds. D. Briggs and J. T. Grant, IM Publications, Chichester, 2003, p. 44.
10. E. Paterson, J. W. Bond and A. R. Hillman, *J. Forensic Sci.*, 2010, **55**, 221-224.

Chapter Four:

Physical and Optical Analysis of Sweat Deposits on Brass Substrates as a Function of Time

4.1 Outline

From the first moment of contact between a finger and a substrate, some sweat residue is transferred and deposited onto the substrate. Factors such as contact area and force affect the amount of material deposited[1]. Other factors, including but not limited to cleanliness of hands, diet and environmental conditions affect the composition and distribution of the transferred sweat[2]. When viewed by eye, such transfers can appear as a pattern of solid lines (ridges), mirroring the pattern of the finger (see Chapter 1, section 1.2), dependent on the substrate, amount of material deposited and other factors mentioned above[3]. However, when studied at the micro- and nanoscale, it becomes clear that the apparent solid ridge lines in fact consist of a densely packed series of spikes, akin to stalagmites[3, 4]. The space between them is less than the wavelength of light and so they visually appear as one entity. Not all contact between a finger and substrate leaves behind a visible trace when studied by eye; this invisible (latent) fingerprint can materialise into a visible fingerprint under certain conditions, notably when significant time has passed and when the substrate is susceptible to corrosion[5].

As mentioned above, the deposition can give vastly different appearances depending on the deposition circumstances. With light contact and minimal perspiration, only the faintest of traces of the sweat residue will be detectable; traditionally these fingerprints would be developed by a range of techniques (see chapter 1, section 1.1) to enhance them visually. However, using non-destructive visualisation techniques such as optical microscopy, digital holography microscopy (DHM) and atomic force microscopy (AFM), one can study the transferred material *in-situ* without any contamination or deformation of either the deposit or substrate. Although these techniques can detect trace amounts of sweat and provide information beyond the capabilities of the human eye, they cannot always be used to image a whole fingerprint instantaneously. An optical microscope can image the majority of the fingerprint, down to several ridges (magnification dependent); a DHM can be used to image

several ridges down to a single ridge; whereas an AFM can only be used to study part of a ridge in a single scan. Thus, the use of these techniques in a coordinated manner allows one to focus on parts of a fingerprint at different resolutions.

Fingerprints on brass substrates have been found to develop with time and more so with increased temperatures[5, 6]; surfaces that were fingerprinted and then cleaned can still have fingerprints recovered from them[5]. In order to deduce the mechanisms occurring, it is necessary to investigate the conditions known to cause visualisation of fingerprints from metal substrates. Storage environments that include heat and humidity conditions above ambient are known to accelerate the visualisation of latent fingerprints on brass substrates[7]. However, visualisation can also occur at room conditions, but this requires a significantly longer time period[8].

4.2 Results

4.2.1 Observations of Fingerprints on Brass Substrates

After the initial deposition of a fingerprint onto the brass substrate, the deposit was not visible when viewed by eye. However, after significant time had elapsed, the fingerprint pattern started to materialise as a dark colouring on the brass sample. Below in Figure 4.1 is a collection of photographs taken of fingerprints that were initially latent marks but have become visible after exposure to a range of environments, including increased humidity and heat.

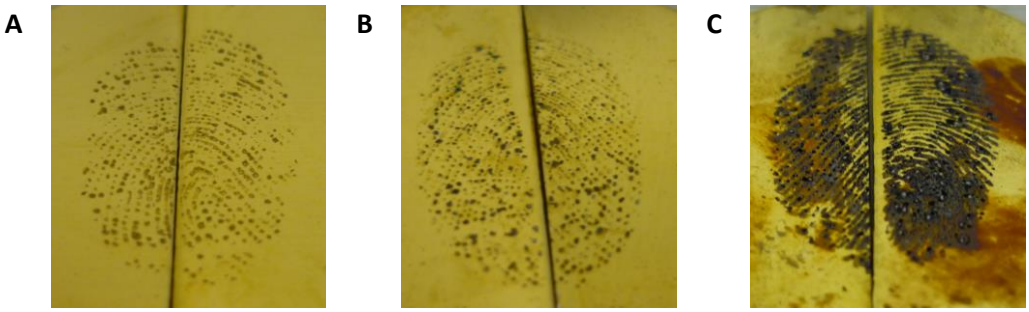

Figure 4.1 – Photographs of fingerprinted unpolished brass substrates stored in different conditions; ***A****) Eccrine fingerprint 10 days after deposition, stored at ambient conditions (approximately 17°C) ;* ***B****) Eccrine fingerprint 10 days after deposition, stored in humid conditions at approximately 17°C;* ***C****) Sebaceous fingerprint 5 days after deposition, stored in humid conditions at elevated temperature (60°C).*

Figure 4.1A is a photograph of a brass substrate on which a latent fingerprint was deposited; after 10 days of being exposed to 17°C in an ambient environment, the fingerprint became visible as a dark brown mark, strongly contrasting against the brass. This brown mark is an identical representation of the features of the friction ridge skin of the finger used for the deposition, with no presence of marks outside of this pattern. Although the fingerprint is fully recognisable, the ridge lines are discontinuous and comprise a tightly clustered series of dots rather than a solid line. Increasing just the humidity and keeping all other factors identical (Figure 4.1B), causes the ridge detail to be of a darker colouring and contain more ridges of a solid nature. Some incomplete dotty ridges are still present, which suggests that the dots increase in size and eventually merge together, but only in the confines of the areas directly contacted by the friction ridge skin.

Increasing the temperature, and keeping the humid conditions, results in a more visible fingerprint than at ambient temperatures, as seen in Figure 4.1C. The fingerprint also became visible over a much shorter time period than samples stored at humid or ambient conditions. The ridge colour is of a darker brown-black colour than seen previously, with the majority of the ridges consisting of continuous lines. A side effect of this environment seems to have

caused some overdevelopment of the ridges on the fingerprint periphery, resulting in slight loss of detail. It is not clear if this can be attributed to ridges merging by continual development and spreading or as a result of smudging in the deposition process. There is also a noticeable change to the appearance of the substrate in Figure 4.1C, which is not present on either of the other samples. Small areas of brown discolouring are present that can be found on both the fingerprinted and non-fingerprinted sections of the sample. This suggests that the brass substrate has been degraded, which is unrelated to the presence of any sweat residue or material transfer in the deposition of the fingerprint.

4.2.2 The Effects of Ambient Environments on Fingerprinted Substrates

The process responsible for the visualisation of a latent fingerprint on metal substrates is not amenable to study by photography alone. Rather than trying to track the changes occurring on a fingerprint as a whole, focusing on a smaller area with higher resolution may provide more information. Digital holography microscopy (DHM) is able to capture an image that is several hundred microns wide whilst retaining sub-micron detail. The DHM has been utilised to time capture the development of a fingerprint from shortly after deposition, to when the fingerprint is visible and recognisable to the naked eye. The two figures below (Figure 4.3 and Figure 4.4) show how the fingerprint material changes in visible appearance over the course of seven days when stored in an ambient environment; both sets of images are from the same eccrine fingerprinted sample but are of different areas.

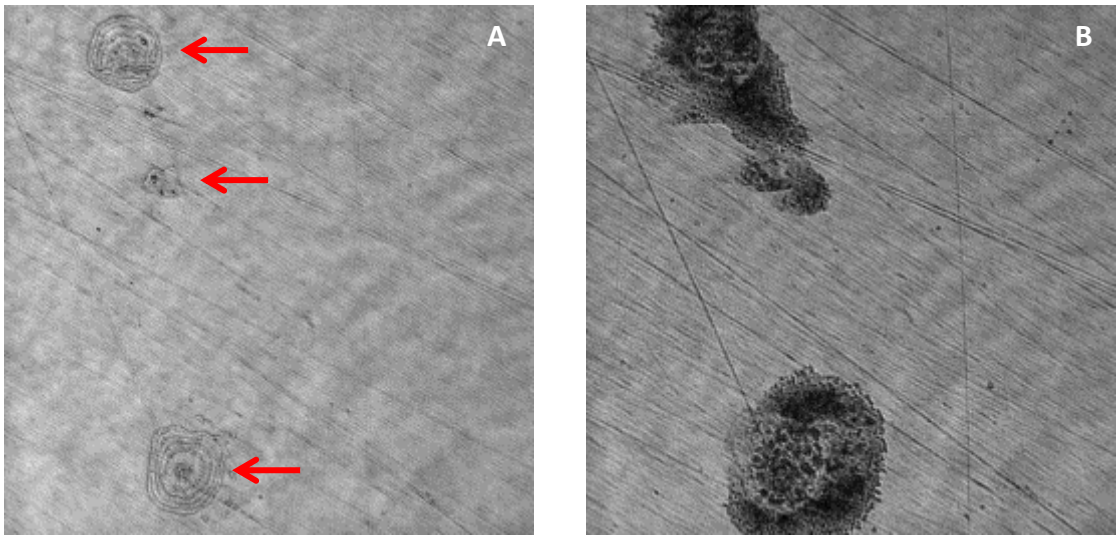

Figure 4.2 – DHM images of an eccrine fingerprint on polished brass substrate stored in an ambient environment with a temperature of ca. 17°C. Both images are of the same area but at different times since deposition: ***A****) several minutes after deposition;* ***B****) seven days after deposition. Images are 450 µm wide.*

Figure 4.2A shows three surface blemishes, as indicated by the arrows, that are all that remain from the contact and are the faintest of signs that sweat residue could be present. These three areas are isolated from each other and no clear ridge line direction can be deduced; a ridge could either run vertically encompassing all 3 blemishes, or two ridges in parallel, separated by a gap of *ca*. 200 µm, from between the bottom mark and the second from top mark. However, after seven days (Figure 4.2B), the suspected sweat residue marks at the top left of Figure 4.2 have merged together and seem to be stretching towards the bottom one, thus it can be proposed that the ridge would run vertically and therefore encompass all three marks. Aside from merging, the marks have increased in size and spread in all directions, although mostly in the boundaries of the now partially formed ridge. Despite this, the positions of the original traces are observable in the centre of their respective growths. The marks are also more visible and therefore have changed consistency from being opaque to a more solid nature, thus causing the diffraction of light rather than transmittance, since DHM is a light based measuring instrument.

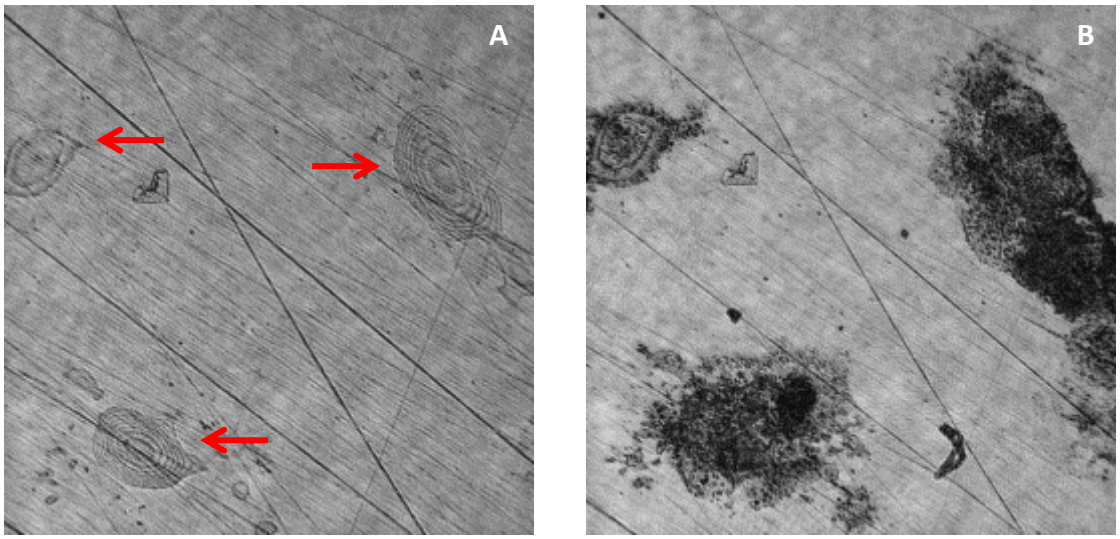

Figure 4.3 – DHM images of an eccrine fingerprint on polished brass substrate stored in an ambient environment with a temperature of ca. 17°C (same sample as Figure 4.2). Both images are of the same area but at different times since deposition: ***A****) ca. 12 minutes after deposition;* ***B****) seven days after deposition. Images are 450 µm wide.*

The images in Figure 4.3 are of the same sample but of a different region from those in Figure 4.2, Figure 4.3A was taken *ca.* 10 minutes after Figure 4.2A. As a result of this slight delay, the three blemishes present in the captured area appear slightly larger and more detectable (indicated in the figure), although still invisible to the naked eye. Due to their arrangement resembling the points of an equilateral triangle (*ca.* 250 µm apart), it is unlikely that all three marks belong to the same ridge section. The relative amounts of material seen in Figure 4.2B and Figure 4.3B are similar despite them being captured *ca.* 8 minutes apart. This difference in time shortly after the deposition resulted in subtle changes; however, over a long time period this same time difference has far less effect. Each of the three areas in Figure 4.3B has expanded away from the initial marks, although the initial marks are still observable amongst the new expansion. The area captured appears to have two ridges running near-vertically, the two marks from the left of the image comprise the first ridge, and the lone right mark has expanded greatly only in the vertical ridge direction; with the right mark and ridge showing the greater expansion. However, in part this could be attributed to marks or deposited material

outside the captured area but in close enough proximity to the captured mark to influence it. Conversely, deposit on the left hand side of the captured area may be further apart or even contain less deposited material.

Although the gap between the left and right sides has narrowed slightly, there is far more growth vertically than horizontally in Figure 4.3B, this supports the suggestion that ridge growth only expands in areas directly contacted by the friction ridge skin of the finger. This controlled direction of expansion seen in both Figure 4.2 and Figure 4.3 could be due to minimal material transferred during the contact, which is undetectable by optical means.

Although DHM has successfully captured the onset of the fingerprint visualisation from a latent mark to a recognisable fingerprint on a brass substrate, it is unable to provide accurate information about the nature of the deposit material, or dimensional changes seen during the course of the development of the fingerprint.

4.2.3 Combining Physical and Optical Measurements of Samples

Monitoring the fingerprinted surface by a single technique limits the information and data obtainable. When viewed on the micron scale (Figure 4.2 and Figure 4.3), the fingerprint ridges were observed to not be fully formed but still visible to the naked eye. To further understand what is occurring on the substrate surfaces immediately after deposition of the fingerprint sweat, fingerprinted brass samples were studied using a light based microscope (DHM) in order to view large sections of ridges. In addition, physical topographical monitoring (AFM) was also used to provide information relating to the interface between the ridge edge and bare substrate with an improved resolution but a smaller capture area than the DHM.

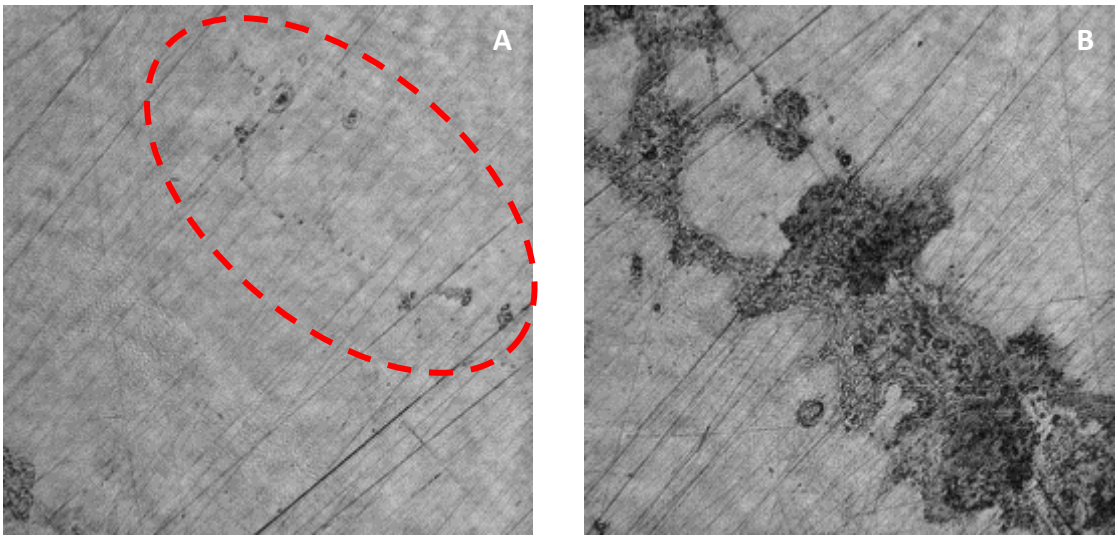

Figure 4.4 – DHM images showing an eccrine fingerprint on polished brass substrate. ***A****) The area captured immediately following deposition;* ***B****) The same area after 17 days stored at ambient conditions. Images are 450 µm wide.*

From the circled area in the DHM image, Figure 4.4A, traces of deposit can be observed. There is sufficient material in close enough proximity to suggest a single ridge running diagonally across the image area. This level of deposit is sub-visible and barely detectable by microscopic techniques. After 17 days (Figure 4.4B), a continuous ridge line can be seen, where before only small traces were present. This ridge has expanded in a specific linear direction, rather than a random or uniform expansion in all directions, however, imperfections are present in this ridge line. These imperfections seen are most likely to be attributed to the finger used for the deposition, either as damages or inconsistencies in the friction ridge skin itself, although they could also be caused by an incomplete spreading of sweat across the finger before and/or during deposition.

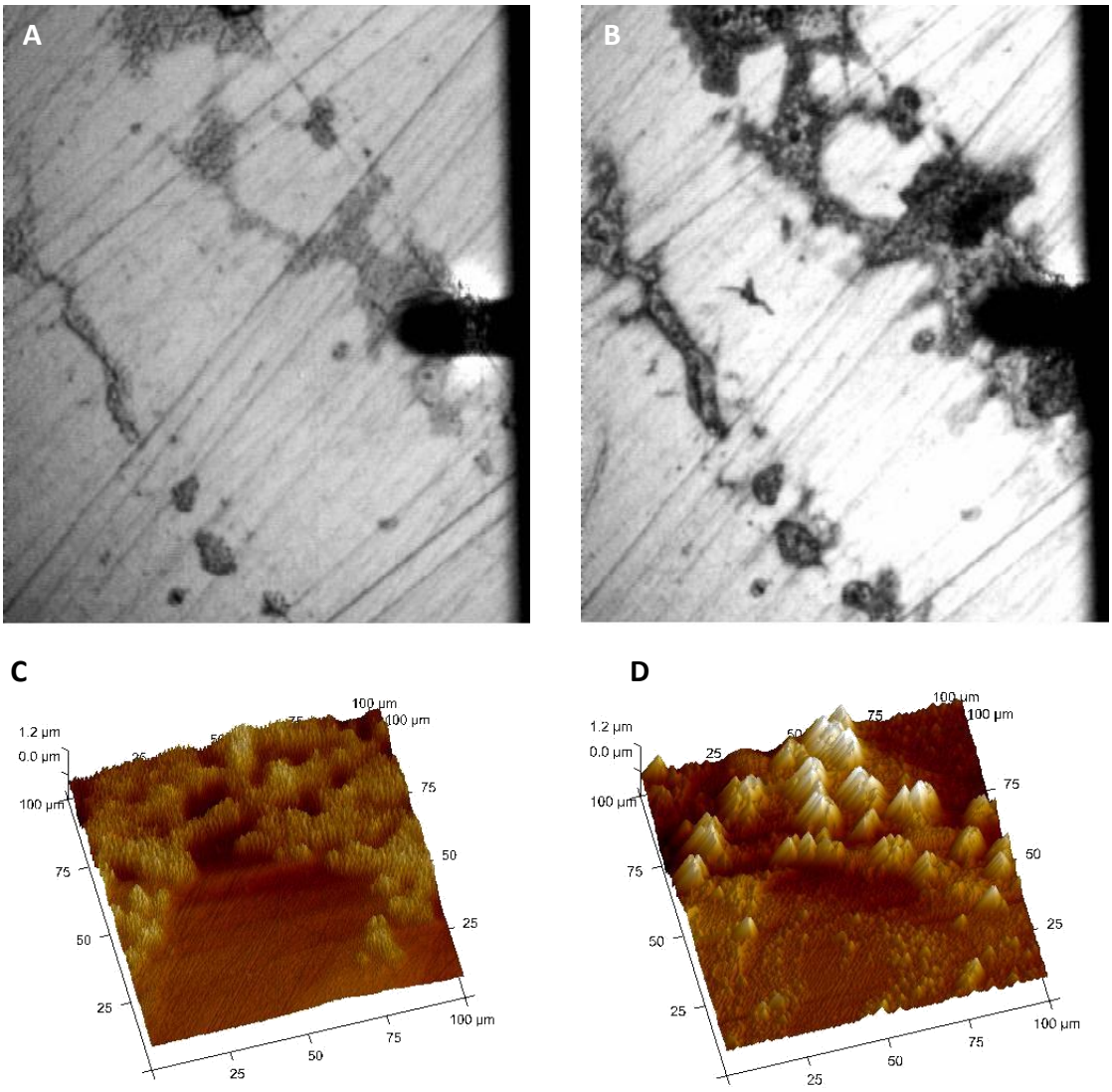

Figure 4.5 – Optical and topographical images of the same eccrine fingerprint sample in Figure 4.4, acquired using the AFM and on-board optical system. Optical image area is ca. 550 µm by 600 µm. ***A****) optical image of the initial fingerprint mark taken ca. 30 minutes after deposition;* ***B****) the same area acquired 14 days later;* ***C****) the AFM topographical information acquired from the area beneath the cantilever in* ***A****, taken ca. 30 minutes after deposition;* ***D****) the same area acquired 14 days later, after the sample was stored at ambient conditions.*

The same area as Figure 4.4A was captured using the optical microscope attached to the AFM following imaging by DHM (Figure 4.5A). This shows how quickly the latent and barely detectable trace deposit starts to resemble a ridge. The images were captured only 30 minutes apart and already partially complete ridges are present and readily viewable compared to the

minute traces captured by DHM. Two ridges are present, running in parallel. The left hand ridge is thinner and of a less consistent and more dotty nature than the right ridge. Although, this right ridge is not a solid line either, nor does it have a straight hard edge, there are many notches present as well as a patchy appearance to the bulk material (Figure 4.5A). The AFM topographical image, Figure 4.5C, was acquired by tapping mode AFM and is of a small section on the edge of the ridge (below the cantilever seen in Figure 4.5A), this AFM image shows a clear distinction between the deposit material and the metal substrate. The deposit is of a viscous nature and has a varying thickness from *ca*. 100 nm to 400 nm. This viscous nature is shown by the fuzzy appearance on the raised areas in the topographical images, which can be attributed to a liquid or soft material that has caused the probe to stick slightly on each pass.

The initial changes to the visual appearance of the residue occur rapidly as demonstrated by the stark contrast in appearance of the same area in the time taken to change apparatus (Figure 4.4A, Figure 4.5A and C). This indicates that the AFM could display inexact scan images if acquiring data for fresh deposits (*ca*. 8 minutes), since the AFM acquisition time is of a similar time period for the apparatus change over (*ca*. 10-30 minutes). However, the capture rate of the DHM is several frames per second and so is not complicated by this issue.

Under the AFM optical microscope attachment, the ridge in Figure 4.5B is of a much darker appearance as well as having thicker and more distinctive markings than seen fifteen days previously (Figure 4.5A). The gap between the two ridges still persists and no apparent closing of this gap has occurred. There is a noticeable change between the AFM topographical data during the 15 day capture period (Figure 4.5C and D); the acquisition area and settings are the same, but the appearance of the residue is vastly different. Small traces of new material are present (Figure 4.5D) in the bottom left of the image; this was previously recorded as bare substrate. Additionally, the bulk deposit (encompassing the area mentioned previously), is

harder and no longer appears to consist of a liquid material. This is due to the smoother finish to the raised area in the topographical images. A liquid or soft material may cause the probe to stick slightly and produce the fuzzy or hazy finish, as seen in Figure 4.5C. The raised area has also increased in height by several hundred nanometres, with some features being *ca*. 900 nm high.

With the images captured after a significant time delay (14 days), no noticeable changes can be seen between imaging of the samples by DHM and AFM as was seen immediately after deposition (Figure 4.4 and Figure 4.5). This suggests that the visualisation rate of the fingerprint follows a non-linear progression as seen in Figure 4.2 and Figure 4.3; this is not surprising since it would be very unlikely that a linear progression for this type of process would be in effect. Immediately after deposition, the rate of surface change is very quick, with the sweat deposit going from being barely detectable to resembling fingerprint ridges in a matter of minutes (from Figure 4.4A to Figure 4.5A). As the fingerprint becomes more visible, the rate of change is reduced to the extent that changes are only noticeable when viewed several days apart.

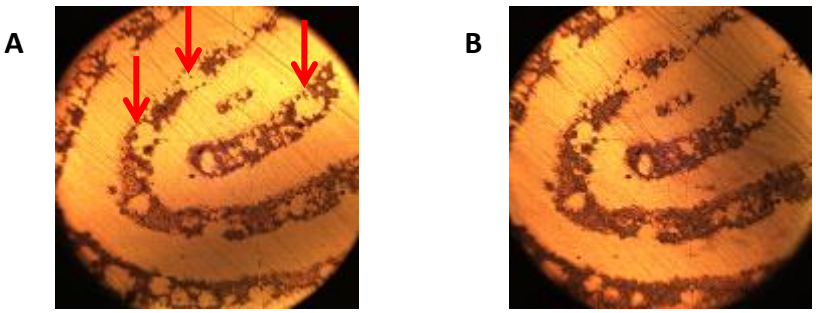

Figure 4.6 – Images of an eccrine fingerprint on polished brass substrate stored at ambient conditions. Image area is ca. 2.2 mm by 2.2 mm. The same sample and fingerprint as captured in Figure 4.4 and Figure 4.5, although of a different area. ***A****) 12 days after deposition;* ***B****) 15 days after deposition.*

After twelve days, the fingerprint is fully visible with clear ridge detail observable by the naked eye, although under magnification it can be seen that the ridges still consist of varying colour and density (Figure 4.6A). Each ridge, as well as sweat pores, can be easily identified (as indicated in Figure 4.6A). After a further three days, image Figure 4.6B was captured; a slight darkening of the ridges has occurred and a solidification of the ridge on the outer edge is noticeable.

From the images seen in Figures 4.5 and 4.6, a change to the fingerprint material can be observed, from a sub-visible mark to one that is readily seen by eye. However, this transformation is not merely of an optical nature, since the AFM data suggests that a state change is occurring, from a soft sticky or viscous liquid based material to a firmer more solid material. All imaging techniques suggest that the initial deposit has expanded in volume, vertically as well as laterally, but that it is also confined to the areas contacted directly by the friction ridge skin, thus forming a mirror image of the finger's pattern without distortion. Although no trace had previously been detected, there must be a very thin layer present. If this was not the case, there would be nothing to prevent the spread of the visible deposit in any direction. The cause of the growth can be attributed to an interaction between the substrate and components of the sweat deposit. This interaction could be of a corrosive nature, as speculated by Bond *et al.*[6-14]. A simple way to test this hypothesis is to subject the deposited substrate to certain conditions. For corrosion to occur, several factors need to be considered, one of which is the reactive nature of the substrate. In this case the copper component of the brass samples is a possible candidate. There also needs to be an oxidising agent; atmospheric oxygen is sufficient to be the source. Lastly there must be a conductive or electrolyte containing medium, such as the components of eccrine sweat, with both water and metal salts present. Additional water can be sourced from both atmospheric and humid environments. If one of these factors were to be removed, then the development of the

fingerprint would not occur; if one was to be limited then visualisation of the fingerprint may take longer to occur.

4.2.4 Effect of Heat on Fingerprinted Substrates

The previous studies in sections 4.2.2-4.2.3 were performed at ambient temperatures (*ca*. 17-20°C) with no control over the humidity. Figure 4.4 and Figure 4.5 demonstrate the short time period in which a latent fingerprint can become visible. If this visualisation is caused by a corrosion based process, limiting the humidity should have a detrimental effect and may increase the time frame in which the fingerprint becomes visible by eye. Also, if the environment is sufficiently dry, the visualisation process may even be quenched. In order to investigate this, a brass disc was split in half and a single fingerprint was deposited over the combined halves, such that each brass half contains approximately half of the same fingerprint. This ensures that factors relating to sweat composition, deposition volume and pressure are identical on both samples. One sample was kept at ambient conditions whilst the other was subjected to dry conditions, in an oven kept at 45°C. The samples were primarily monitored by optical microscopy, with supporting AFM observations.

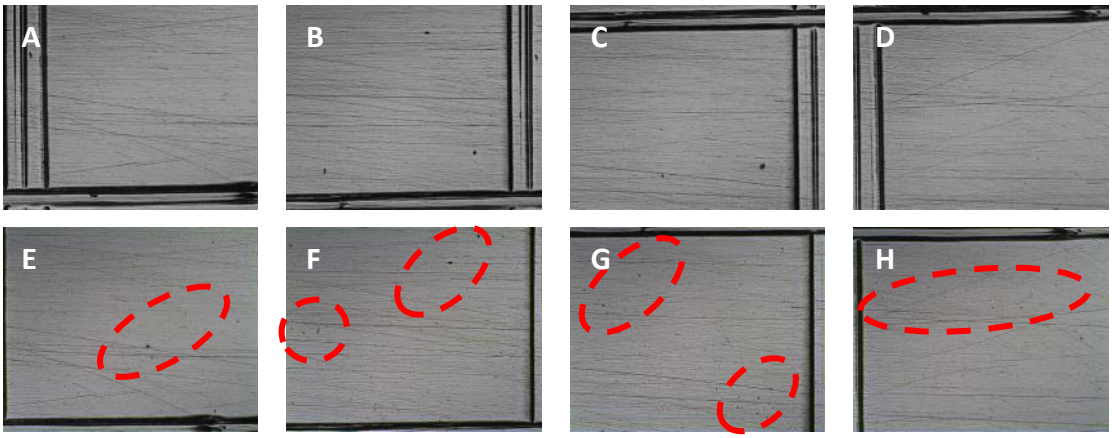

Figure 4.7 – Optical microscopy images of four different areas of an eccrine fingerprint on a polished brass substrate. Magnification used was a 5x objective lens, image area is ca. 5.6 mm by 4.5 mm. ***A to D)*** *ca. 30 minutes after deposition;* ***E to H)*** *after 8 days stored at ambient conditions.*

In Figure 4.7A-D, no trace of the fingerprint deposit immediately after deposition can be seen. Even after 8 days stored at ambient conditions, the fingerprint is still not visible (Figure 4.7E-H), although, some traces of potential fingerprint growth spots can be seen in the highlighted areas above. The absence of heat to initiate any visualisation may be a controlling factor, although at similar temperatures, fingerprints still became visible over this time period (Figure 4.4). One possibility could be an insufficient amount of sweat residue was initially deposited, however the fingerprint examined below (Figure 4.8) was deposited simultaneously under the same conditions and yielded typical fingerprint marks, but slightly underdeveloped.

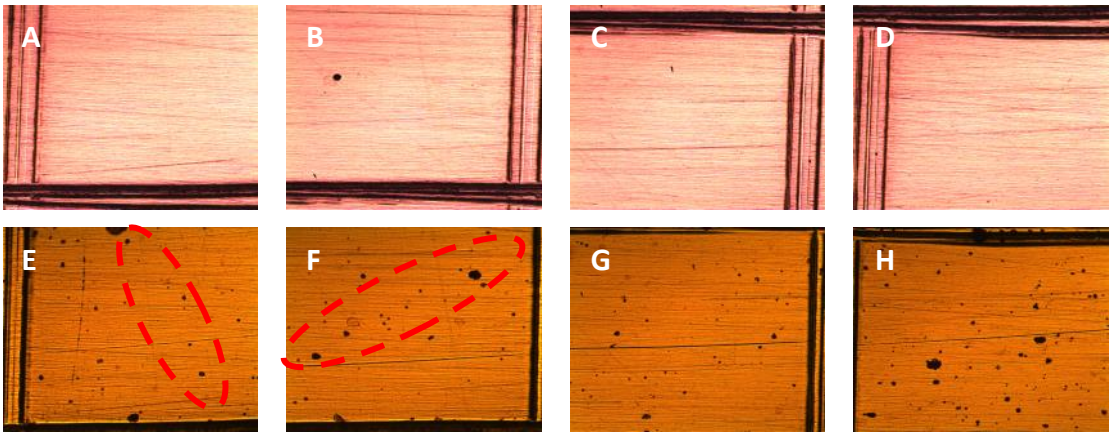

Figure 4.8 – Optical microscopy images of four different areas of an eccrine fingerprint on polished brass substrate. Magnification used was a 5x objective lens, image area is ca. 5.6 mm by 4.5 mm. ***A to D)*** *ca. 30 minutes after deposition;* ***E to H)*** *after 8 days stored in an oven at 45°C.*

As in Figure 4.7A-D, immediately after deposition no trace of the fingerprint sweat deposit can be seen in Figure 4.8A-D. After storage at 45°C for 8 days, the same areas display changes (Figure 4.8E-H). A seemingly random collection of dark spots are now visible across the sample, although some are clustered in a linear fashion, as indicated on the images above. Full ridge details are still not present, despite both the application of heat and a significant time period for development to occur. Two possible explanations can be suggested. The first is that the sweat deposition contained less reactive or corrosive components than on previous deposited

samples, although such variance in the sweat composition is unlikely. The other, more likely, possibility is that the environment had effectively limited the humidity, and hence the water component of the corrosion process, and so hindered the naturally occurring corrosion based visualisation of the fingerprint image.

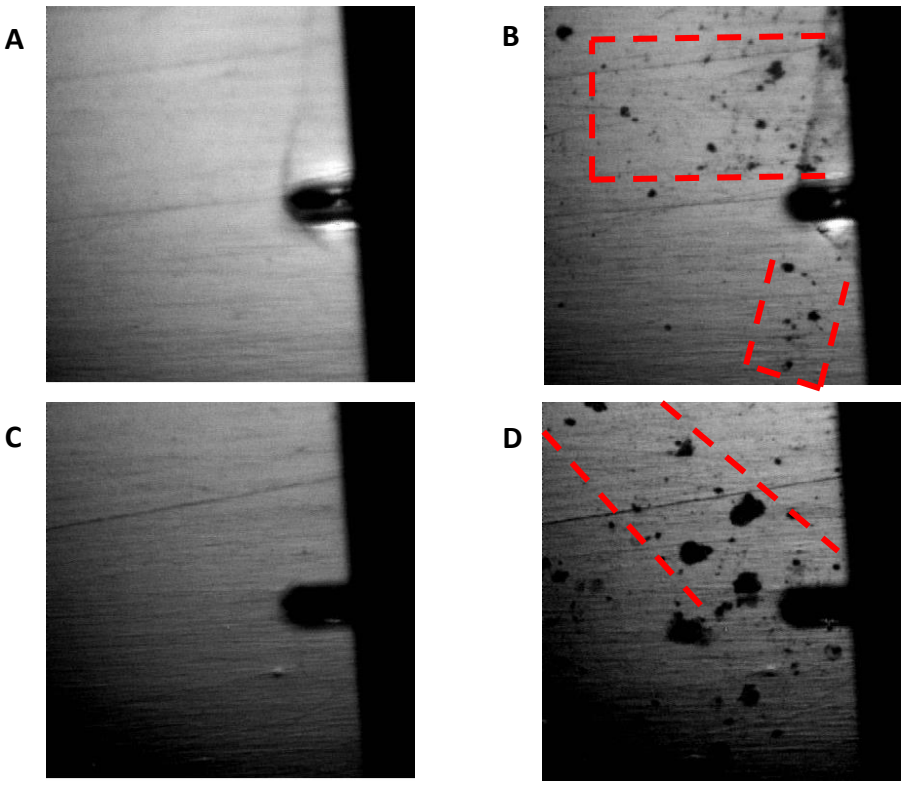

Figure 4.9 – Images captured using the optical microscope system built into the AFM instrument, image area is ca. 550 µm by 600 µm. All images are from the same eccrine fingerprinted brass sample seen in Figure 4.8, but from two different areas. This sample was stored in an oven at 45°C. ***A****) taken ca. 20 minutes after deposition;* ***B****) the same area as* ***A*** *taken 8 days after deposition;* ***C****) taken ca. 25 minutes after deposition;* ***D****) the same areas as* ***C*** *but taken 8 days after deposition.*

Figure 4.9A is of particular interest since it is the only captured image to show a substantial trace of the fingerprint deposit shortly after deposition (*ca.* 20 minute delay). The trace material appears as an oval shape, with the elongated axis running vertically, the other half of the oval is obscured by the AFM cantilever. Figure 4.9C bares no trace of the contact as expected by previously displayed images in Figure 4.8. The most obvious change from Figure

4.9A-B, after being stored for eight days in an oven at 45°C, is the prominent black spots of varying size that have arisen in Figure 4.9B. However, a more subtle change is that of the oval feature observed shortly after deposition. This feature persists and has become more distinct. Rather than having an opaque border, it is now of a darker colour peppered with small dark spots. It does not appear to be part of a ridge section as it runs perpendicular to the ridge present (highlighted in Figure 4.9B). The appearance of the oval in Figure 4.9A and B suggests that it could be a water droplet, possibly caused by an excess of moisture on the finger used; if it was caused by excess moisture it would contain less concentrated sweat components and so after prolonged exposure to warm dry conditions, the water has vaporised leaving behind the non-volatile sweat components.

The transition observed from the areas in Figure 4.9C to D is equally remarkable; from no observable trace of any deposit material, the image area is now filled with new surface marks. After the sample was stored in the warm conditions, a ridge section can be observed originating from the top left corner of Figure 4.9D (highlighted). It is not clear if the marks at the bottom right of this image are part of this ridge section or another ridge running perpendicular, as found in features like spurs (chapter 1, section 1.2.4). The loss of detail observed mainly in the bottom left corner of this same image is a result of splitting the brass discs in half; this resulted in some substrate deformation and bending along the cut line.

The dry warm conditions do not seem to hinder the rate of the visualisation process of the fingerprint mark as new features are present, compared to the ambient stored sample, where, after 8 days, no trace of a fingerprint could be found. Although the oven conditioned sample was stored in a dry environment the majority of the time, it was continually removed from this each time it was subjected to an examination. The removal of this sample from this environment, although detrimental to the proposed dry environment, was necessary to record

the changes. Each time the sample was removed, it was exposed to ambient environment and hence water vapour. Being exposed to this whilst still warm could have been enough to promote the interaction between the deposited material and the substrate; any adsorbed moisture would then continue to promote the interaction shortly after being returned to the oven.

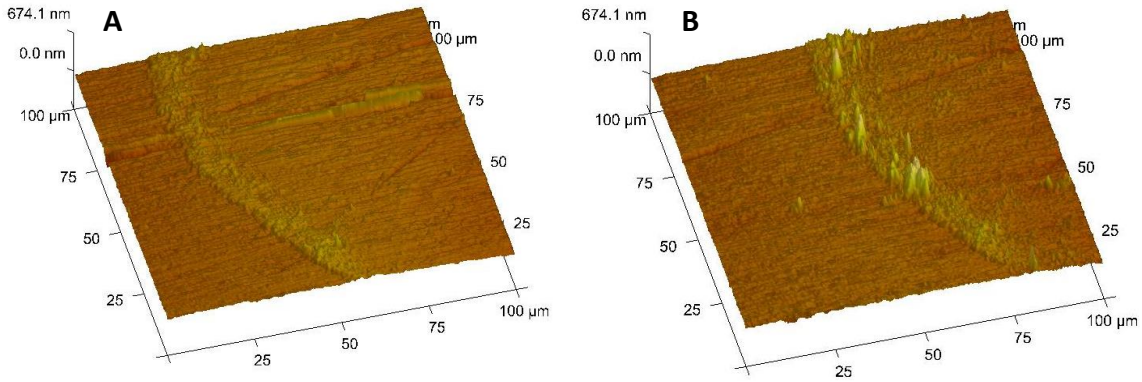

*Figure 4.10 – AFM topographical image from part of the oval feature observed in **Figure 4.9A** and **B**, from the area directly below the cantilever; **A**) taken ca. 20 minutes after deposition; **B**) the same area as **A** but after 8 days at 45°C.*

The majority of AFM images obtained did not show any surface changes, this is in part due to the areas selected being offset from the actual areas of change. The locations of the areas examined with the AFM are small squares centred around the cantilevers seen in Figure 4.9; as can be perceived, the cantilevers do not lie on the developed ridge material. Whilst AFM images of the new material could be displayed, its value would be diminished as there would be no reference data to compare to, from which to deduce the changes occurring. However, due to the visible nature of the oval from Figure 4.9A, an AFM image was obtained of part of this (AFM taken directly below the cantilever in Figure 4.9A). The oval has a very narrow border, *ca*. 10 µm wide in both the image taken shortly after deposition and after 8 days at 45°C (Figure 4.10). Additionally there is no noticeable difference between the substrate inside or outside of the encompassed area, thus refuting the assumption that it could be a water

droplet. The main change observed is in height: initially the highest feature is on the magnitude of tens of nanometres. However, after 8 days at 45°C, the height of some of the peaks is much greater, with several *ca*. 600 nm high.

4.2.5 Effects of Warm Humid Storage Environments on Fingerprinted Substrates

The effect that elevated temperature has on the development and visualisation of ridge detail was conclusively proved in section 4.2.4 and can clearly be seen Figure 4.9. Conversely, the effect of minimal humidity was inconclusive due to the difficulties of maintaining this environment, whilst imaging and studying the samples. The effect of alternately heating and cooling a sample also remains an interesting factor. Therefore a sample was split in half, as before, with the same fingerprint deposited on each section. Both samples were placed inside a sealed container with excess water present (open vial of liquid water) and the container placed inside a warm oven (*ca*. 75°C). One sample was removed at periodic intervals throughout the study; the other sample was kept undisturbed in the heated and humidified environment after the initial deposition and subsequent images were acquired.

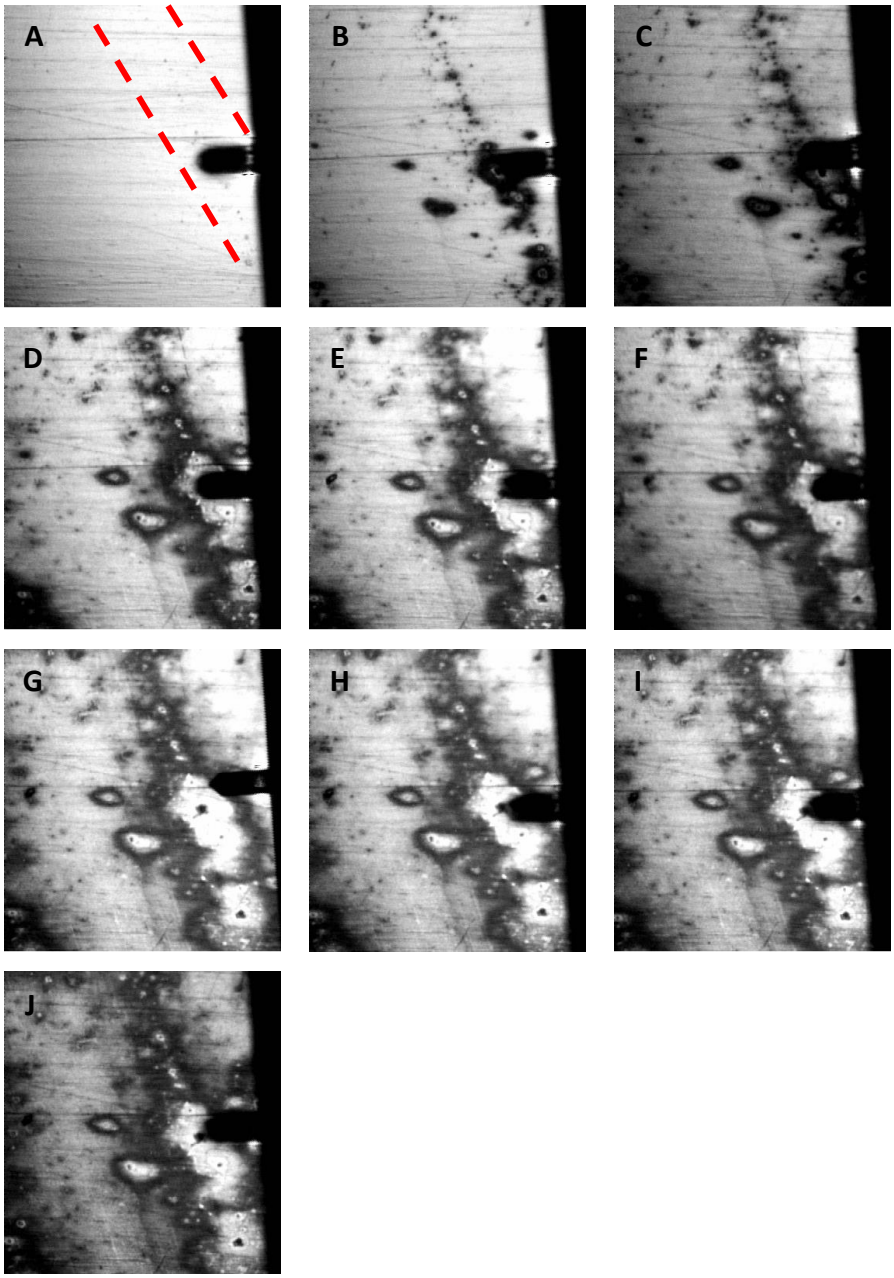

Figure 4.11 – Images obtained using the optical microscope on the AFM instrument, image area is ca. 550 µm by 600 µm. Images are of the same area of a polished brass disc fingerprinted with eccrine deposit studied at varying times since deposition: ***A)*** *ca. 20 minutes;* ***B)*** *two hours;* ***C)*** *4.5 hours;* ***D)*** *24 hours;* ***E)*** *27.5 hours;* ***F)*** *29 hours;* ***G)*** *45 hours;* ***H)*** *48 hours;* ***I)*** *53 hours;* ***J)*** *5 days. Sample was stored at 75°C and 100% relative humidity between imaging.*

The collage of images above (Figure 4.11) shows the progression of a single area on a fingerprinted brass substrate as a function of time. After the initial deposition (Figure 4.11A), a faint trace of small dots can be seen running linearly close to the cantilever, this is the only

trace of any contact having occurred. After approximately two hours in the heated and humidified environment, ridge markings are already apparent (Figure 4.11B); the faint traces of a ridge on the extreme left are also now discernible. The structure of the main ridge is already visible; a vertical line of dark black spots surrounded by scatterings of smaller lighter spots. From Figure 4.11B through to D, the ridge line has widened. The level of detail found in Figure 4.11D is also found across the entire sample and a vivid half fingerprint is visible by eye after 24 hours since deposition of the fingerprint. The clusters and spots on the outer edge of the ridge body have continued to merge together but not all of these outliers are encompassed by the ridge section. After two days at 75°C (Figure 4.11H), the ridge can be perceived as a solid entity on the micron scale; this level of development is greater than seen in the previous studies (sections 4.2.2-4.2.4). By the conclusion of the study, Figure 4.11J, the main body of the ridge section has widened: however, it has not widened to the extent that it has merged with neighbouring ridges, as a clear gap can be seen on either side.

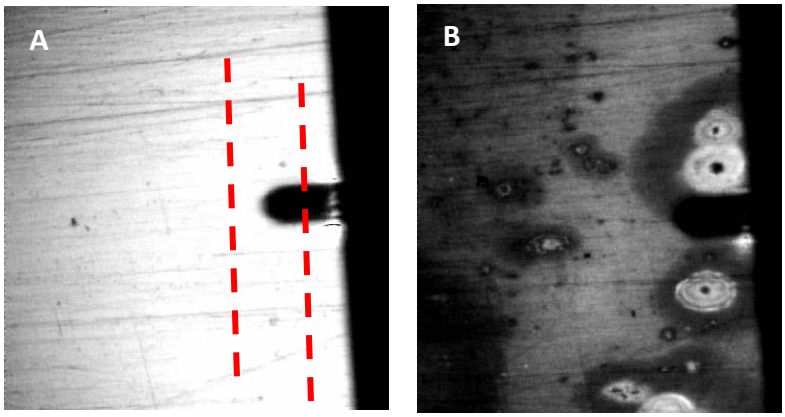

Figure 4.12 – Optical images of part of an eccrine fingerprint deposit onto polished brass substrate, image area is ca. 550 µm by 600 µm. ***A****) taken ca. 40 minutes after deposition;* ***B****) the same area as* ***A*** *taken after five days of being stored at 75°C in an humidified environment.*

Similarly to the previous sample (Figure 4.11A), the sample in Figure 4.12 also displays a very faint trail of dots, observable between the marked area running vertically to the top and

bottom centre of the image in Figure 4.12A. This faint trace suggests that only one latent ridge is present in the captured area. After the sample (Figure 4.12B) had been kept for five days in the warm and humidified environment without removal or interference, a ridge comprised of a dotty line can be seen on the right, with a second ridge on the left hand side, also of a very dotty nature. The ridges are not as thick or developed as those in Figure 4.11 and although they were stored in the same conditions (75°C humidified environment), the sample in Figure 4.11 was continually removed and replaced in the warm humid environment during the imaging process. This suggests that this variation to the environment enhances visualisation more than being kept in a single stable environment.

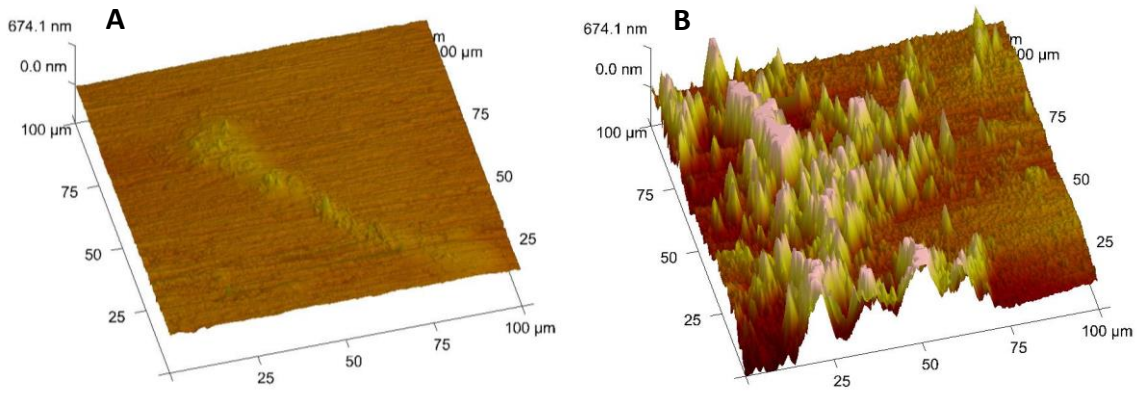

Figure 4.13 – AFM topographical images are of the eccrine fingerprint on polished brass substrate as seen in Figure 4.11, stored in a warm (75°C) humid environment; ***A****) taken 20 minutes after deposition;* ***B****) taken five days later and is of the same sample and area as* ***A****.*

From the AFM topographical images in Figure 4.13, there is a distinctive change in height and amount of material present on the sample surface; the features have increased in height from 10 nm to 700 nm and have gone from covering a 10 µm wide, 70 µm long, sliver to encompassing the entire scan area (100 µm x 100 µm). The regions that previously showed no signs of material other than substrate are now covered in new features. The original feature can be seen amongst the peaks in Figure 4.13B with similar width but vastly increased height. Most of the new material seems to stem from this region as it is denser around there. The way

in which this feature has increased in size suggests that the original deposit acts as a growth site from which the new material develops.

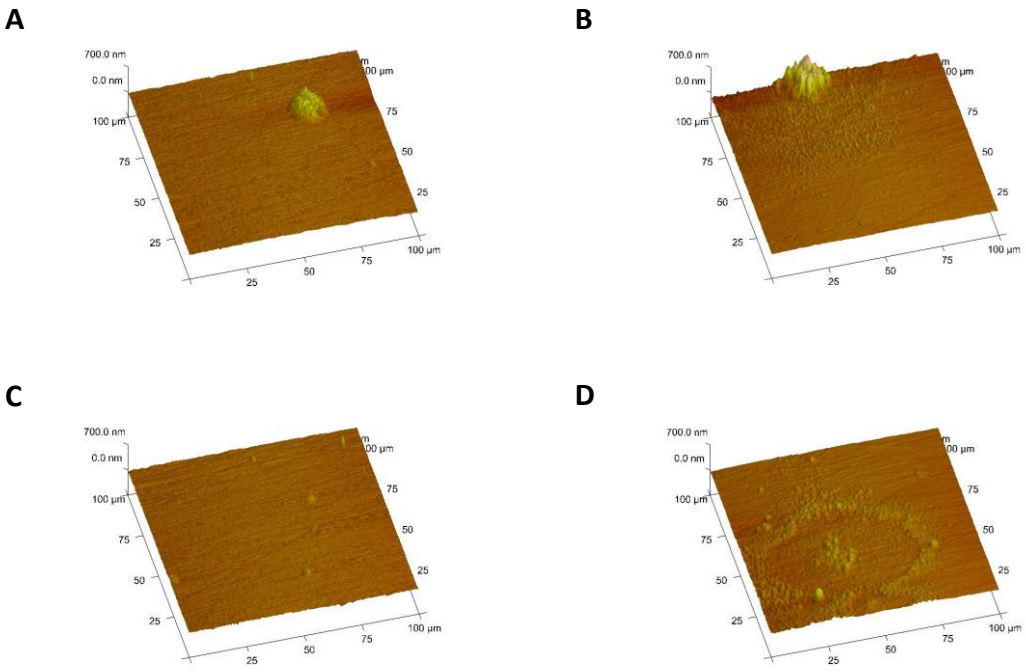

Figure 4.14 - AFM topographical images are of two areas of the same eccrine fingerprint on polished brass substrate as Figure 4.12; ***A****) taken 40 minutes after deposition;* ***B****) taken five days later and is of the sample and area as* ***A****;* ***C****) taken 50 minutes after deposition;* ***D****) taken five days later and is of the sample and area as* ***C****.*

In the first area studied, Figure 4.14A and B, the change in height is fairly subtle; an increase of only several hundred nanometres is observed, compared to over double this in Figure 4.13A-B. More important is the presence of new material present below the main peak; small peaks of *ca*. 50 nm in height are found extending down 50 µm as a dense cluster and span the width of the scanned area. This new material has a similar appearance to that found in Figure 4.5D. These features in Figure 4.14D are small peaks of *ca*. 100 nm in height and densely clustered together. However, these clusters are arranged differently to those in Figure 4.14B. In Figure 4.14D, a small cluster (15 µm diameter) is encircled by a thin ring of clustered peaks; the peak

heights are slightly higher for the central cluster than the ring, by *ca*. 10 nm. This ring is a thin circle of material, approximately 5 µm wide but with a diameter of 80 µm. The shape and size of this feature has a resemblance to a sweat pore, seen above in Figure 4.6. As is the case with previous samples, the final formation and location of material cannot be deduced from the findings of the area imaged immediately following fingerprint deposition.

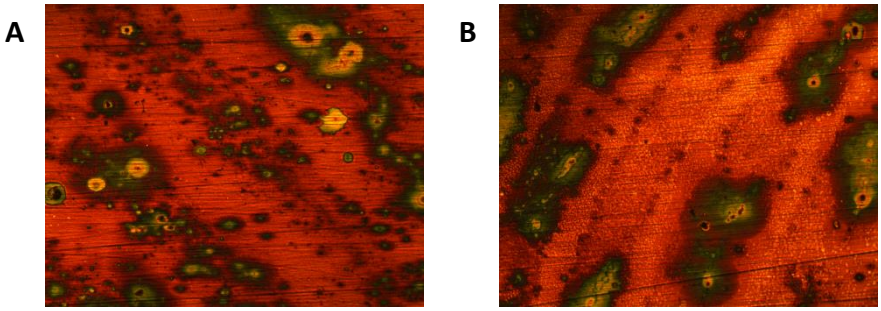

Figure 4.15 – Optical microscopy images of eccrine fingerprint ridges on polished brass substrates, samples were stored at 75°C with 100% relative humidity for 5 days. Image dimensions are ca. 1.5 mm by 1.2 mm. ***A)*** *is the same sample as Figure 4.11;* ***B)*** *is the same sample as Figure 4.12.*

In Figure 4.15, image A is of the sample that was frequently removed from the environment for progressive imaging, whereas the sample shown in image B was constantly kept in the warm humid environment for a period of 5 days. The level of development of the fingerprint ridges is quite different between the two samples, but in both cases multiple ridges can easily be seen. There is more development of the ridges in image A than B, as well as some spattering present between the respective ridges. Image B has very clearly defined ridge boundaries and whilst a ridge can be discerned, the level of development of the material is inconsistent and of a patchy nature. Despite being stored for the same amount of time and in the same storage conditions, the level of development is different at all levels of imaging. The removing of the samples from the warm humid environment does promote the natural visualisation process of the fingerprint mark and varying humidity and temperature do not have a detrimental effect on this.

4.2.6 Composite AFM Imaging

Whilst optical techniques can image multiple ridges, they cannot provide accurate information relating to height changes or the physical state of the ridges themselves. AFM is able to provide this, but the maximum scan size (100 µm) is below that of a single ridge (300 μm^4). In order to utilise the benefits of the AFM, composite AFM images are used to combine high resolution imaging with the ability to look at larger areas than on a single image. The images below use a false colour scheme representative of surface features heights, with the colour scale displayed in the legend for each image.

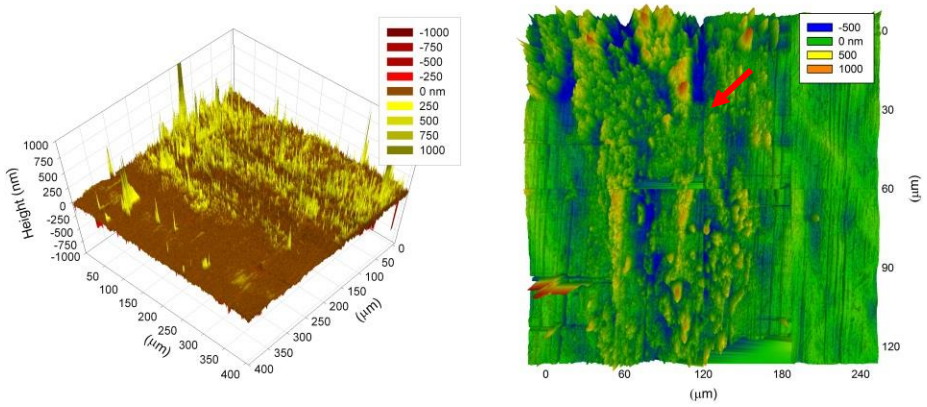

Figure 4.16 – Combined AFM data of fingerprint ridges on brass substrate. ***A)*** *sebaceous fingerprint on polished brass, stored in ambient conditions and aged 35 days, 16 AFM captures each of 100 µm in a 4 x 4 configuration;* ***B)*** *eccrine fingerprint on unpolished substrate, stored at ambient conditions for 9 days and then washed in warm soapy water, 8 AFM captures each of 60 µm in a 2 x 4 configuration.*

From the two images of ridges in Figure 4.16, it can be seen that the dotty and stalagmite nature of the ridges persists across them and is not merely found on the peripheries. There are areas within the fingerprint ridges that still show the substrate features on them as indicated in Figure 4.16B. Thus the deposit has not fully encompassed the area covered by the ridge sweat deposit. The ridge section shown in Figure 4.16A is of a complete ridge cross section, with the ridge being *ca*. 250 µm wide; whereas the ridge section shown in Figure 4.16B is of an

underdeveloped ridge since it is only *ca*. 100 µm wide. The narrower ridge could be a result of lack of material transferred in the deposition process or as a result of the post deposition treatment and storage conditions.

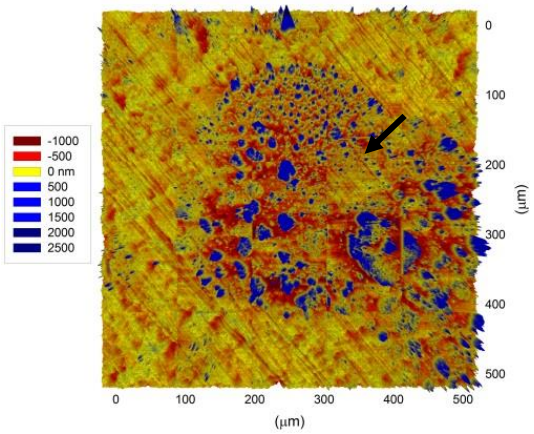

Figure 4.17 – Combined AFM data of a ridge ending from a sebaceous fingerprint on unpolished brass substrate, stored in a humid environment at 60°C for 5 days and then washed in warm soapy water. 25 scans are combined in a 5 x 5 arrangement, with each individual AFM scan being 100 µm x 100 µm.

As well as being able to study fingerprint ridge cross-sections, it is also possible to study ridge features and characteristics used for comparison purposes between fingerprint marks (see chapter 1, section 1.2.4 for more details). In Figure 4.17 a ridge end feature is shown, the edges of the ridge and the feature are clearly defined. As with Figure 4.16B, a clear section of exposed substrate is present in the midst of the ridge feature, showing characteristic manufacturing marks of the substrate (indicated). Again, the sweat deposit has not spread and fully encompassed the ridge area and as with previously presented AFM images, the ridge feature is comprised of clustered stalagmites. The height and compactness of these stalagmites varies across the feature and no clear pattern to this can be discerned.

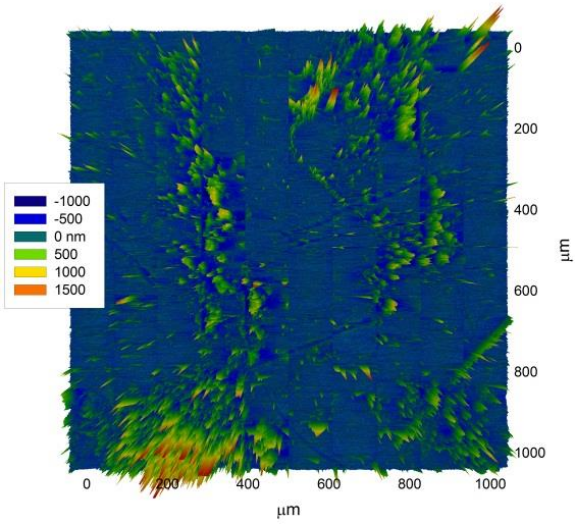

Figure 4.18 – Combined AFM scans showing two parallel ridges, from an eccrine fingerprint on polished brass substrate, stored in a humid environment at 50°C for 11 days. 100 AFM areas are combined in a 10 x 10 configuration, each individual AFM scan being 100 µm x 100 µm.

When looking at even larger areas obtained by multiple AFM capture areas, the discontinuous nature of the ridges can provide difficulties in identifying the fingerprint ridge areas. The image in Figure 4.18 shows two parallel ridges, running vertically. The left hand ridge at its widest point is over 300 µm wide, but for the majority of the captured area it is between 100-150 µm wide. The ridge on the right of the image is less continuous, with a visible break towards the bottom of the image, although this ridge is slightly wider than the one on the left, with a ridge width of ca. 200 µm. The ridges here show a sparser stalagmite configuration than seen in Figure 4.16 or Figure 4.17, although these ridges are equally visible by eye.

4.3 Summary

4.3.1 Overview of the Study of Fingerprints

There are two ways in which the sweat residue has been studied. The first is by optical means incorporating standard optical microscopes as well as DHM. The second is by measuring the topography by using a scanning probe, which can be considered a physical means of obtaining

information due to the mechanics of operation. Both forms have enabled characterisation of the sweat residue on the surface of brass as it ages. The optical methods are better utilised at observing whole ridge changes whereas the AFM has recorded the change of the deposit from fresh to aged.

From the different environments the samples have been subjected to, the warmer and more humid environments aided the development of a fingerprint, such that the fingerprint became visible on a much shorter timescale. Additionally, the final visualisation of the fingerprint was not compromised or distorted, regardless of storage environment.

4.3.2 Visually Observed Changes in Surface Features of Fingerprinted Substrates

Through optical measurements, the fingerprint deposit ridges can be seen to change from a trace material transfer to a fully visible distinguishable fingerprint. The faint spots visible shortly after deposition form linear ridges over time, which are much darker in colour than the substrate material. They stay confined to the areas of contact from the friction ridge skin and do not merge into neighbouring ridges.

The optical properties of the substrate (polished and un-polished surface finishes) do not have an impact on the visual appearance of the fingerprint marks. Furthermore, scratches and manufacturing marks present on the substrate do not mar the development of the ridges.

4.3.3 Physically Measured Changes of Fingerprinted Substrates

AFM observations show a change from a viscous tacky material to a much more solid material (Figure 4.5); they show compaction and solidification of the sweat deposit with aging. With the AFM, it has also been possible to observe changes on the sample surface that are not visible by optical means, such as the beginning of growth observed in section 4.2.3 and subsequently

4.2.4. The ridge as observed by eye, appears as a solid entity, however, the AFM has shown that in fact the fingerprint ridge marks are comprised entirely of dense packed stalagmite type features, with age they form larger clusters of material (Figure 4.16).

4.4 Conclusions

The optimum conditions for full visualisation in a short period of time appear to be exposure to a temperature of 60-80°C and 100% relative humidity. Under these conditions, a fingerprint can go from being a latent impression to a fully developed mark in less than twenty-four hours. Prolonged exposure to these conditions does not degenerate the fingerprint image. Less heat and less humidity also aid the development of the fingerprint, but not to the extent observed under optimum conditions. Both of these conditions are still preferable to the sample being exposed to ambient conditions; even after 9 days the visualisation of the fingerprint is far from clear. Exposure to higher temperatures can cause the substrate surface to degrade, giving rise to discolouration of non-fingerprinted regions and distracting from the fingerprint image.

The results of these studies give rise to the idea that something other than a physical interaction must be occurring. Without the addition of any other material, the fingerprint deposit goes from being invisible to the naked eye to a distinctive impression on the brass substrate. This realisation, coupled with the fact that these conditions favour corrosive mechanisms, suggests that the reason the fingerprint mark becomes more visible is because a corrosion reaction of the brass has occurred. The resultant visual marks are likely to be corrosion by-products.

4.5 References

1. S. Fieldhouse, *Forensic Sci. Int.*, 2011, **207**, 96-100.
2. R. S. Ramotowski, in *Advances in Fingerprint Technology*, eds. H. C. Lee and R. E. Gaensslen, CRC Press, Boca Raton, 2nd edn., 2001.
3. S. Sykes and J. W. Bond, *J. Forensic Sci.*, 2013, **58**, 138-141.
4. G. L. Thomas, *J. Phys. E. Sci. Instrum.*, 1978, **11**, 722-731.
5. E. Paterson, J. W. Bond and A. R. Hillman, *J. Forensic Sci.*, 2010, **55**, 221-224.
6. J. W. Bond, *J. Forensic Sci.*, 2008, **53**, 812-822.
7. A. J. Goddard, A. R. Hillman and J. W. Bond, *J. Forensic Sci.*, 2010, **55**, 58-65.
8. J. W. Bond, L. N. Eliopulos and T. F. Brady, *J. Forensic Sci.*, 2011, **56**, 506-509.
9. J. W. Bond, *J. Forensic Sci.*, 2009, **54**, 1034-1041.
10. J. W. Bond, *J. Forensic Sci.*, 2008, **53**, 1344-1352.
11. J. W. Bond, *J. Phys. D-Appl. Phys.*, 2008, **41**, 125502.
12. J. W. Bond, *Rev. Sci. Instrum.*, 2009, **80**, 075108.
13. J. W. Bond, *J. Phys. D-Appl. Phys.*, 2009, **42**, 235301.
14. J. W. Bond and C. Heidel, *J. Forensic Sci.*, 2009, **54**, 892-894.

Chapter Five:

Surface Chemical Analysis for the Interaction between Sweat Deposit and Brass Substrates

5.1 Outline

The topographical studies described in chapter 4 provided information relating to the *physical* characteristics of fingerprinted metal substrates. We now require surface sensitive *chemical* compositional information, for which X-ray photoelectron spectroscopy (XPS) is an ideal technique. Whilst other techniques are able to provide some compositional information, XPS has the advantage of being able to provide information relating to oxidation states of the substrate metal as well as the deposited material.

Previous studies outlined in chapter 1 section 1.1 suggest that the surface changes during the transformation from a latent fingerprint to a visible fingerprint. Certain conditions cause changes to occur in the substrate more than others, such as exposure to heat rather than aging at ambient temperature. Although research has been carried out as to the effects of fingerprints on metallic substrates[1-6], little work has been carried out in trying to analyse chemically the changes taking place on the substrate surface and, in particular, at the interface between the deposited material and the substrate.

XPS can be utilised in two modes, spatial and non-spatial XPS. Non-spatially resolved spectroscopy provides the average composition of the entire illuminated area, with all components represented in a single spectrum. The presence of multiple species in different spatial locations means that spectral peaks may require de-convolution to yield the individual components. Spatially resolved spectroscopy yields a set of individual spectra, with each spectrum representing one pixel in the spatially resolved image. Due to the smaller surface area for each spectrum, de-convolution is not always required. Although spatially resolved spectra should offer greater clarity for the changes at the interface, it can be harder to observe small changes in the kinetic energy of electrons from the elemental components, such as a change from Cu(0) to Cu(I). As a result, non-spatial and spatial XPS can be complementary and

can help explain peak formations observed in each. Further details on the fundamentals of XPS are given in section 2.3 of the methodology chapter.

Based on the findings from chapter 4, one can define the goals for XPS investigation of the surfaces. These include the effects on the substrate and sweat residue of fingerprint age and its exposure to heat and humidity. These are to be explored for sebaceous and eccrine sweat deposited on both polished and unpolished substrates. XPS offers the promise of information on the variation in copper/zinc ratio (surface depletion or enrichment) and oxidation state changes of the residual metal.

5.2 Results

5.2.1 Substrates Exposed to Ambient Conditions

Polished brass has been used for most of the studies as it is possible to ensure consistency of surface roughness for optical and physical surface and topographical measurements. However, the appearance of the brass substrate changes with polishing: it is not only more reflective, but there is a change to the colour. Polished brass has a lighter, more gold-like, colouring than unpolished brass. This change in colour could be due to a change in the surface chemical composition, most likely a change in the surface Cu:Zn ratio, but there could also be an oxidation state change of one or both of these metals, which could also influence the colour. If the chemical composition of the surface is significantly different between the polished and unpolished brass, then the nature of the interaction between the sweat deposit and the metal substrate may also differ. Therefore the surface chemical composition of polished and unpolished brass needs to be examined, both with and without sweat deposits, to investigate the changes to the surface Cu:Zn ratio as well as oxidation state changes with particular focus on the Cu $2p_{3/2}$, Zn $2p_{3/2}$, C 1s and O 1s regions of the XPS regions.

5.2.1.1 Non-Fingerprinted Substrates at Ambient Conditions

The first focus is to examine the metal in the absence of fingerprint sweat deposits.

Table 5.1 – Surface ratio of copper to zinc for non-fingerprinted brass substrates stored at ambient conditions

Surface Finish	Time stored at ambient conditions	Ratio of Cu:Zn*
Polished	3 weeks	1 : 1.12
Unpolished	5 weeks	1 : 0.25
Fresh Polished	>5 minutes	1 : 1.09

The surface Cu:Zn ratio of the polished and freshly polished brass substrates indicates a surface composition with more zinc than copper, yet in the bulk material, the composition of the brass is a 68:32 ratio of Cu:Zn. The abundance of zinc is likely to form a thick oxide coating across the surface and hence a more protective film. However, this zinc rich phase is susceptible to dezincification. Additionally, the zinc oxide species (ZnO) is susceptible to attack from Cl^- ions, which can be found in secreted sweat from salts such as NaCl and $CaCl_2$[7].

The surface ratio of unpolished brass shows an excess of copper: four times more copper is present on the surface than zinc. This abundance of copper explains why the visual appearances of unpolished and aged brass samples are of a darker colouring. The copper oxide layer that would form as a result of Cu(0) on the surface acts as a passivation layer.

* The surface ratio of Cu:Zn is calculated as specified in the experimental section. The bulk composition is 68%:32% (1:0.47)

The time frame difference between the polished and freshly polished samples is approximately three weeks. The polished samples (section 5.2.1.1) were prepared simultaneously with their fingerprinted counterparts (section 5.2.1.2) whereas the freshly polished specimen was polished onsite and inserted into the XPS vacuum immediately upon being prepared. The main differences one would expect to encounter are twofold: the first is the surface Cu:Zn ratio, whilst the second is the thickness of the oxide layer. The surface Cu:Zn ratio is close to 1:1, but still being slightly zinc rich as with the polished samples. Whilst oxide layers form on the sub-second scale, thicker layers may require longer to form and the immediate immersion into the UHV environment required for XPS may have hindered this from forming fully. Therefore part of the XPS measurement may be from the first few layers of the bulk material, unlike the older samples that would have a thicker oxide layer and so electrons would be emitted closer to the surface.

The results from Table 5.1 clearly demonstrate that the age and surface treatment vastly affect the surface of the brass samples. Polishing does not only produce a smoother and more reflective finish, but also one that is zinc rich. The variance in the surface Cu:Zn ratio between the freshly polished and aged polished samples is of interest. Most samples were fingerprinted shortly after polishing and one could deduce that at the time of deposition the surface encountered would resemble the freshly polished specimen rather than data retrieved from the non-fingerprinted regions. After deposition, the non-fingerprinted region of the brass surface would be expected to ‘mature’ and resemble that of the week old polished sample. However, the composition of the brass under the fingerprinted region may differ. This could cause a variation in Cu:Zn ratios across a surface, aside from that caused by interactions between deposited material and the substrate.

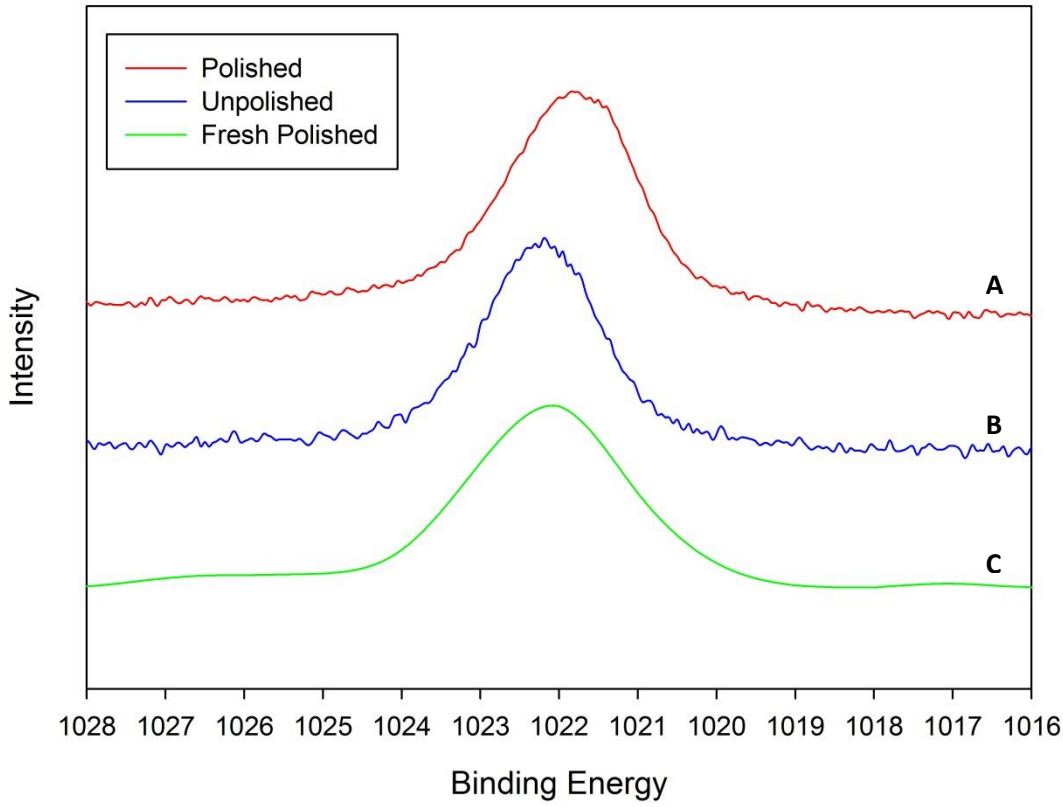

Figure 5.1 – XPS Zn $2p_{3/2}$ spectra of brass substrate stored at ambient conditions. ***A)*** *Polished and aged 3 weeks;* ***B)*** *Unpolished and aged 5 weeks;* ***C)*** *Polished onsite and immediately placed in UHV conditions.*

The shape and width of all of the zinc profiles seen in Figure 5.1 are similar. All 3 samples have a single peak but at slightly different positions. The aged polished sample (top red line in Figure 5.1) has a peak position of 1021.8 eV, the freshly polished sample (bottom green line) at 1022.1 eV and the unpolished sample (middle blue line) at the slightly higher value of 1022.2 eV. The binding energy position for the polished sample is characteristic of Zn(0)[8, 9] whereas the other two samples have peak positions more characteristic of Zn(II) as ZnO[8, 10, 11]. Although due to the same binding energy difference in the two peak positions, definitive species identification is not possible. The difference between the aged polished and the other two samples is surprising, the visual appearance of the freshly polished sample is brighter than the aged polished sample, which in turn is brighter than the unpolished sample. However, the data

shown above, suggests that the aged polished sample exhibits Zn(0) on/near the sample surface and yet the freshly polished sample is bound Zn(II).

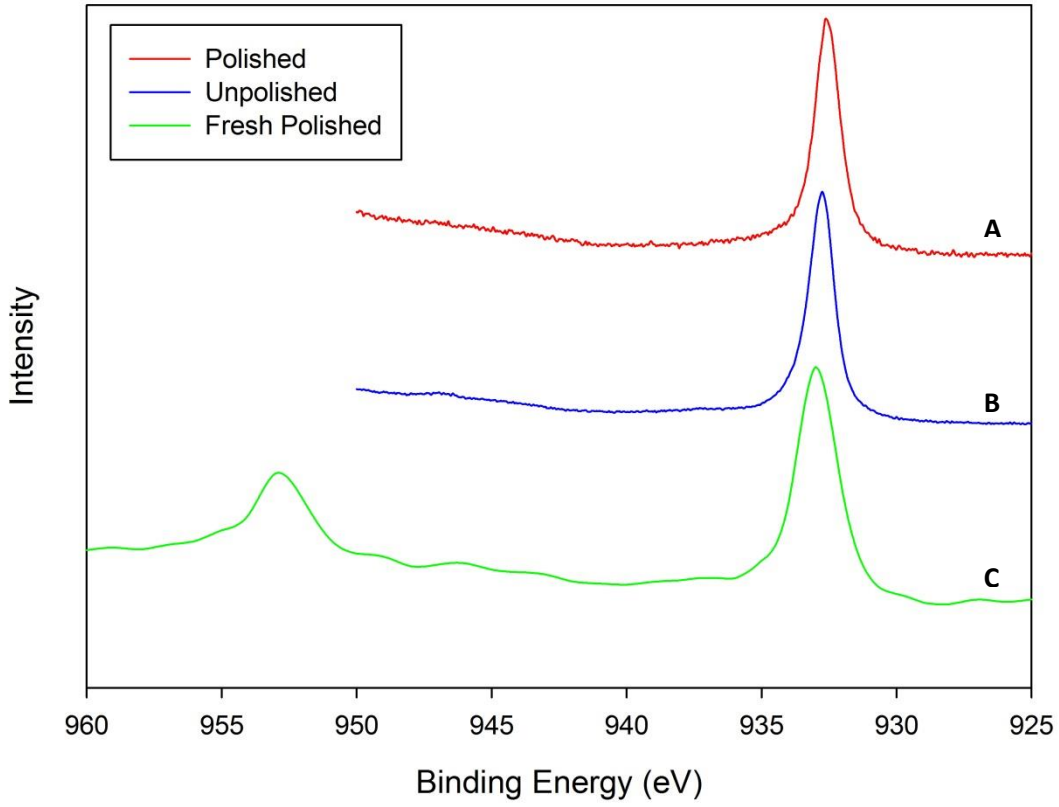

Figure 5.2 – XPS Cu $2p_{3/2}$ spectra of brass substrate stored at ambient conditions. ***A)*** *Polished and aged 3 weeks;* ***B)*** *Unpolished and aged 5 weeks;* ***C)*** *Polished onsite and immediately placed in UHV conditions.*

The copper spectra seen in Figure 5.2 are of slightly more interest than the zinc spectra as there is the presence of more than a single peak in the spectra. The prominent peak found between *ca*. 930 eV and 935 eV is the region for the Cu $2P_{3/2}$ signal, the peak between *ca*. 950-960 eV is for the Cu $2p_{1/2}$ signal; the peaks in between these are satellite signals and are not always related to the copper species present. Peak shifts of the $Cu2p_{3/2}$ and $Cu2p_{1/2}$ can give an indication of the oxidation states present on the surface. Occasionally the shift is more apparent in one region than the other. In the Cu $2p_{3/2}$ region, the binding energy of Cu(I) is the lowest of the three oxidation states of copper and depending on bond can be found between

932.0 and 932.5 eV; Cu(0) is of a higher energy value, between 932.5 and 932.9 eV, whereas Cu(II) is higher still, from 933.3 to 935.5 eV. In the Cu $2p_{1/2}$ region, this pattern is again replicated, with Cu(I) found at 952.3 eV, Cu(0) at 952.5 eV and Cu(II) at 953.6 eV[8]. A mixture of oxidation states present on/near the surface will cause a signal to be generated for each of them. Whilst identification of the different oxidation states present is entirely possible, deducing the exact identify of the bound species is not as reliable from a single XPS region due to smaller differences in binding energy values.

The spectra for the aged polished and unpolished samples display very narrow single Cu peaks, shown as the top and bottom lines in Figure 5.2, found at 932.6 eV and 932.7 eV respectively. A peak at this position is typical for a material containing Cu(I) as Cu_2O[8, 12, 13] or Cu(0)[9, 12, 14-16]. The freshly polished sample has a single narrow peak at 933.0 eV, predominately indicating Cu(0)[10]. However, the $Cu2p_{1/2}$ region for the freshly polished sample has an unsymmetrical peak, meaning that two overlapping peak profiles are present; this split is from signals for either Cu(0)[8] or Cu(I) as Cu_2O[8] and Cu(II) as CuO[8]. A review of the spectrum for this sample shows a slight signal at the base of the prominent peak around 934.9 eV, which can be assigned as Cu(II) as $Cu(OH)_2$[13, 16, 17]. The aged polished sample has the lowest binding energy value for the copper species found but it is not a dissimilar value to that of the unpolished sample, due to the difference in surface appearance as well as surface composition, a larger difference in the copper spectra was expected. Surprisingly, the freshly polished copper sample exhibited two distinct oxidation states for copper, Cu(0) and Cu(II); the Cu(0) is most likely a result of surface removal, so the bulk composition extends closer to the surface.

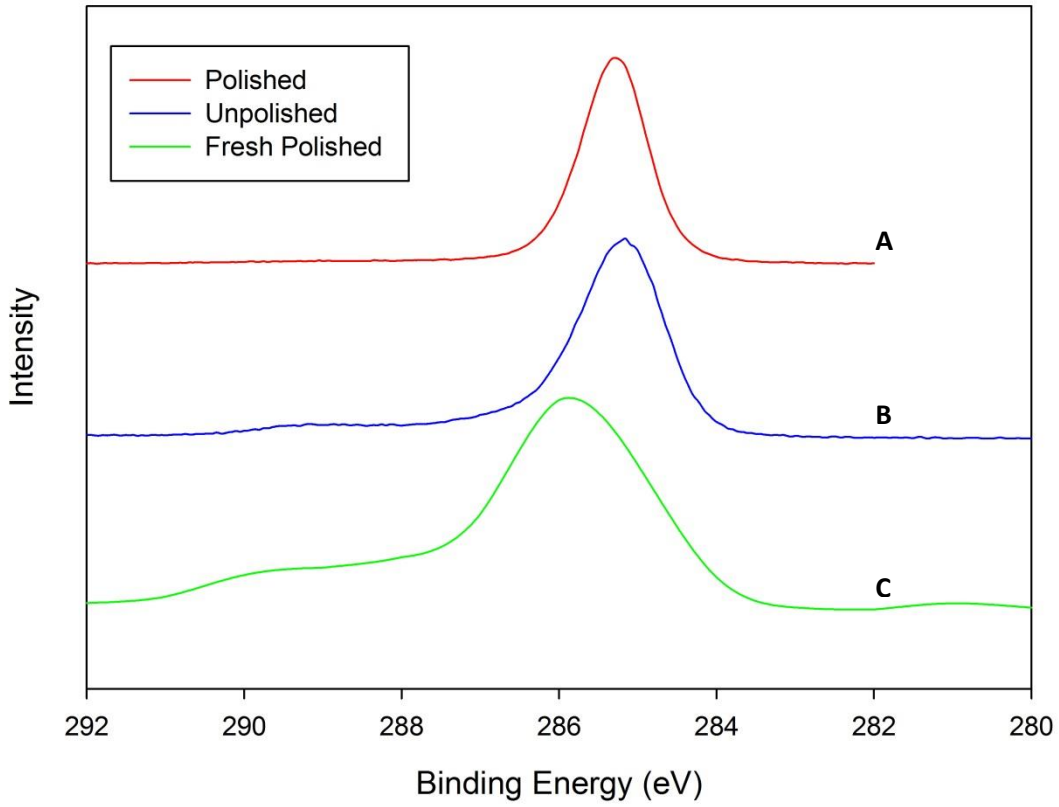

Figure 5.3 – XPS C 1s spectra of brass substrate stored at ambient conditions. ***A)*** *Polished and aged 3 weeks;* ***B)*** *Unpolished and aged 5 weeks;* ***C)*** *Polished onsite and immediately placed in UHV conditions.*

The aged polished and unpolished samples, seen above in Figure 5.3, have broad carbon peaks at 285.2 ±0.1 eV; this binding energy value is typical of hydrocarbons and alkane chains[18-20]. The freshly polished sample has a broad peak at 285.8 eV, slightly shifted to a higher binding energy value, this higher energy value is typical of predominately alkyl carbons[10, 19, 21, 22]. The freshly polished sample also has two small signals at a higher binding energy value than the main peak, found at *ca.* 291 eV and 288 eV. The signal at 288.0 eV indicates the presence of carbonyl groups[19, 23-26], possibly a remnant of un-evaporated or residual acetone used in the cleaning and polishing process. The peak at 291.0 eV is attributed to short carbon chains, such as ethane and methane[27]. Of the signals present in the C 1s region, very few signals are of much significance on non-fingerprinted substrates as the freshly polished sample displays signs

of acetone and the others of residual atmospheric carbon signals. The carbon region is of much greater interest when investigating the effects of fingerprinted substrates, with regard to distinguishing the two different sweat types used.

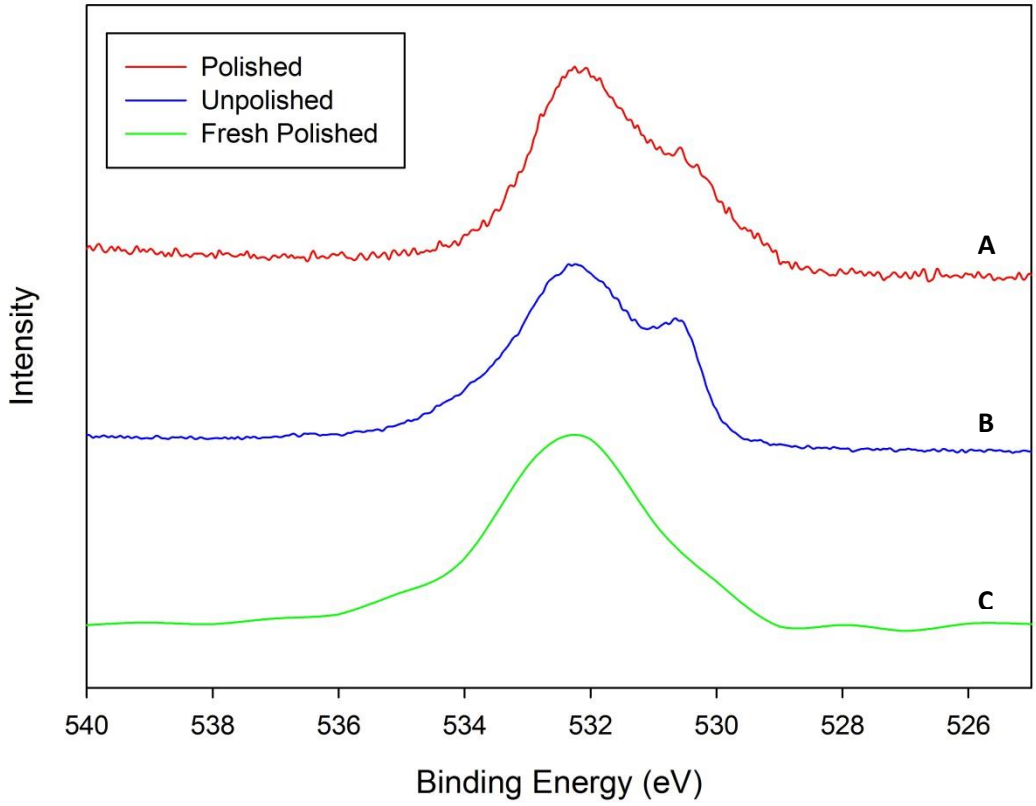

Figure 5.4 – XPS O 1s spectra of brass substrates stored at ambient conditions. ***A)*** *Polished and aged 3 weeks;* ***B)*** *Unpolished and aged 5 weeks;* ***C)*** *Polished onsite and immediately placed in UHV conditions.*

The three oxygen profiles seen in Figure 5.4 are different and contain multiple signals. The aged polished and unpolished multiple signals are more obvious, with additional peaks clearly seen at lower binding energies than the main signal. The additional peak in the freshly polished sample is less obvious; it is mainly detectable by observing the symmetry of the peak profile and can be seen at a slightly higher binding energy than the main signal. The aged polished sample signals are indicative of H_2O or OH (532.2 eV)[28, 29] and CuO or Cu_2O (530.5 eV)[12, 13, 30]; the presence of a copper oxide was expected and supported by the indication of Cu_2O from

the Cu $2p_{3/2}$ region. However, the peak indicating H_2O or OH was unexpected. The metal spectra do not support the presence of metal-OH bonds, nor does the carbon profile conclusively support COH species. Therefore, one must conclude that H_2O is the more likely candidate for this signal assignment. Additionally, peaks were found in all three of the samples that indicated water presence.

The unpolished profile main signal is the water signal mentioned above. As with the polished sample, the second peak for the unpolished sample is at *ca.* 530.6 eV and is again attributable to either CuO or Cu_2O[12, 30]. The presence of Cu_2O is more likely as this can be corroborated from the copper spectrum in Figure 5.2. The freshly polished oxygen profile has the main peak at 530.2 eV typical of metal oxides ZnO[31, 32] or Cu_2O[33-35].

Considering the abundance of zinc in both the surface Cu:Zn ratio of the polished and freshly polished samples, it is surprising that the ZnO signal is virtually undetectable when compared to the more prominent copper oxide signals. ZnO is typically found at slightly lower binding energies than the copper oxides, although some experiments have reported overlaps of the two metal oxide signals[8].

5.2.1.2 Fingerprinted Substrates at Ambient Conditions

The fingerprint sweat deposit is expected to alter the surface composition because there is not only the presence of additional material but this material is capable of interacting chemically with the substrate surface, which would result in at least a change to chemical bonds and oxidation states. Additionally, as suggested by the examination of differently aged polished brass samples (section 5.2.1.1), the substrate surface may contain two different states of the brass material. One is under the fingerprinted material and the second is the substrate left

exposed; one would expect these to differ in at least the amount of each component present if not oxidation states as well, irrespective of the effect that the sweat deposit may have had.

Table 5.2 – Surface ratio of copper to zinc for fingerprinted brass substrate stored at ambient conditions

Sample finish and deposition type	Time stored at ambient conditions since preparation	Surface ratio of Cu:Zn
Polished; sebaceous	4 weeks	1 : 0.58
Polished; eccrine	5 weeks	1 : 1.12
Polished; fresh eccrine	>5 minutes	1 : 0.52

The surface Cu:Zn ratios for the aged sebaceous and aged eccrine sweat deposited onto brass substrates in Table 5.2 are vastly different. The sebaceous deposited sample has a large abundance of copper on the surface whereas the aged eccrine deposited sample has a slight abundance of zinc. The samples had the same delay between polishing and deposition of a fingerprint. However, the sebaceous deposition was studied several weeks sooner after deposition than the eccrine deposited sample. This additional time that the eccrine sample spent being exposed to ambient conditions appears to be the largest contributor to the difference in Cu:Zn ratios. The difference between copper and zinc being most abundant on the surface can largely be discounted as a difference between the type of sweat deposit, since the fresh eccrine deposited sample ratio closely resembles the aged sebaceous deposited sample and not the aged eccrine deposited sample. However, neither the sebaceous or fresh eccrine deposited samples have ratios that would be expected from ratios suggested by the polished substrates seen in Table 5.1, following the comparison to the bare substrate; one would expect all fingerprinted samples (Table 5.2) to be zinc rich since they are on polished substrates. The only surface finish types to contain an abundance of copper on the surface of

the non-fingerprinted samples were the aged unpolished ones. The explanation for this could be that the deposited material has affected the substrate in such a way as to change the Cu:Zn surface composition present but only on the deposited areas or that the whole surface was in some way affected by the presence of the sweat deposit. Since the ratios in Table 5.2 are midway between those for the unpolished and polished samples from Table 5.1, an average of the fingerprinted and non-fingerprinted regions may be displayed. The only way to resolve this would be to perform spatially resolved XPS and examine the differences between the fingerprinted and non-fingerprinted regions (see Figure 5.11 below).

All the fingerprinted samples would be expected to have at least two environments present on the sample surface for fingerprinted and non-fingerprinted regions. One would expect to see these two different regions reflected in the XPS spectra for all elements providing the deposited material has chemically interacted with the brass substrate.

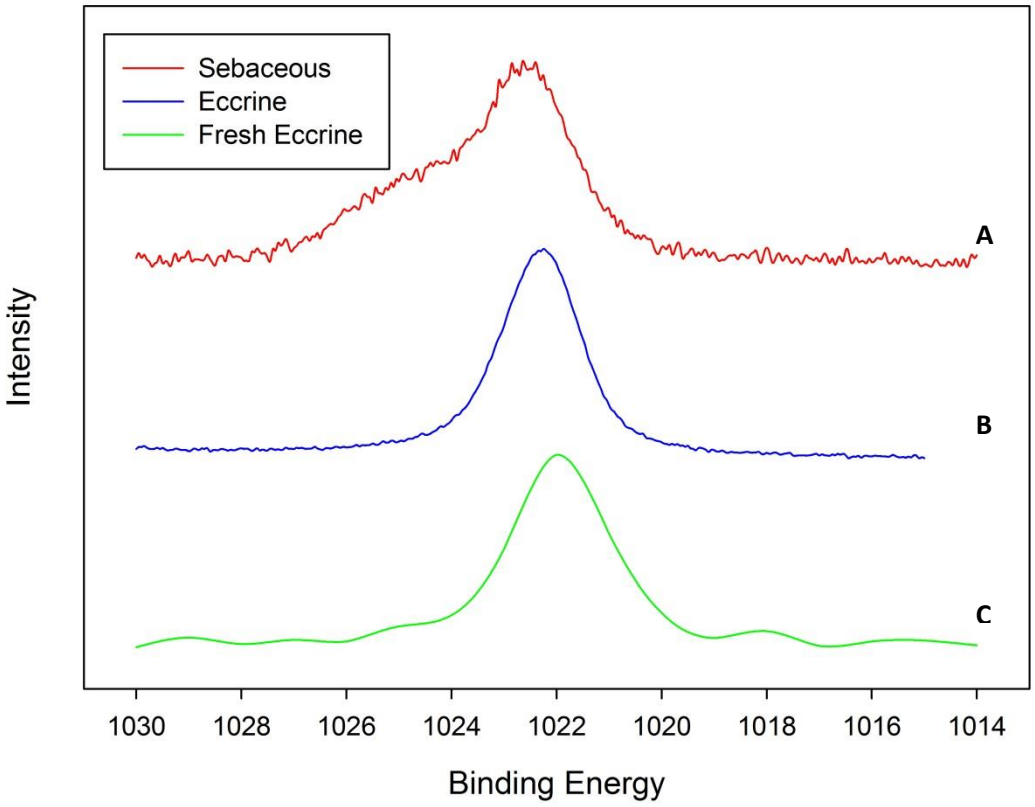

Figure 5.5 – XPS Zn $2p_{3/2}$ spectra of fingerprinted brass substrate stored at ambient conditions. ***A)*** *Sebaceous deposit;* ***B)*** *Eccrine deposit;* ***C)*** *Fresh eccrine deposit.*

The aged and fresh eccrine deposited samples seen in Figure 5.5 have very similar zinc profiles, both are smooth symmetrical peaks positioned at 1022.2 eV and 1022.0 eV respectively, identified as Zn(II) present as ZnO[8, 10, 11] rather than Zn(0)[8-10] due to its reactive nature and matching those from the bare substrates in Figure 5.1. However, the sebaceous deposited sample has two signals, both at higher binding energy values than either of the eccrine samples. The sebaceous deposited sample peaks are at 1022.5 eV and 1023.8 eV; the peak at 1022.5 eV is at binding energy values associated with zinc hydroxides[36] rather than oxides and the peak at 1023.8 is $ZnCl_2$[36]. The lack of a ZnO oxide peak in the sebaceous deposited sample was surprising since this is the most common zinc product found in the other samples examined. The existence of $ZnCl_2$ was also unexpected since sebaceous sweat does not

typically contain chloride components and so must be present as a contamination from eccrine based sweat already on the finger prior to deposition[37].

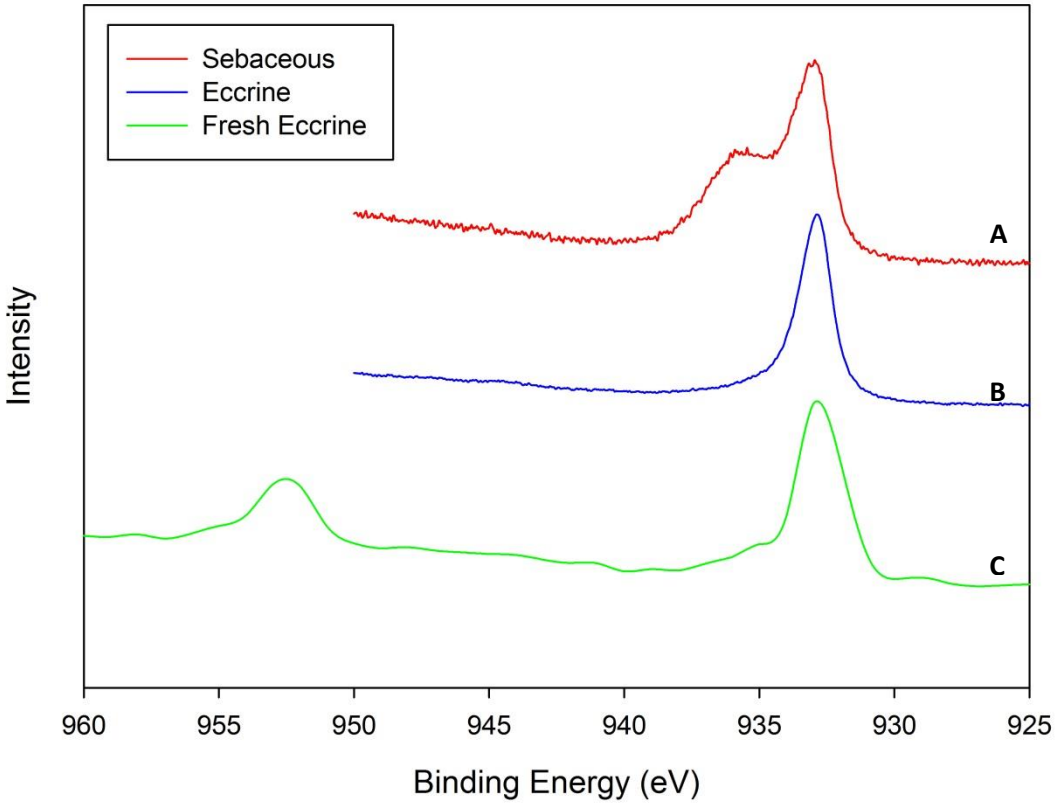

Figure 5.6 – XPS Cu $2p_{3/2}$ and $2p_{1/2}$ spectra of fingerprinted brass substrate stored at ambient conditions. ***A)*** *Sebaceous deposit;* ***B)*** *Eccrine deposit;* ***C)*** *Fresh eccrine deposit.*

As seen in Figure 5.6, the sebaceous deposited sample spectrum shows two clear signals, indicating at least two different chemical bonds for the copper species. The main peak for all three samples is at 932.9 ±0.1 eV: this binding energy value is typical of elemental copper[10, 14, 15]. The additional peaks in the spectra for the sebaceous and fresh eccrine samples also match in terms of energy value at 935.4 eV and can be assigned to $Cu(OH)_2$[16]. These signals are at higher binding energy values than the non-fingerprinted substrates (Figure 5.2), although nominally for the main signals (shift of *ca.* 0.2 eV), this indicates the presence of more copper material in the Cu(II) state than the Cu(0) and no Cu(I) present at all. The aged eccrine

deposited sample has a narrow symmetrical peak indicating a single copper environment, whereas the fresh eccrine has an additional peak at a higher binding energy than the main peak. Whilst the peaks in Figure 5.6 are not of Cu_2O oxides (*ca.* 932.5 eV)[8, 12, 13, 30], they are not of a high enough energy to represent CuO signals (*ca.* 933.7 eV)[8, 10, 12, 13, 16, 17, 30]. This could possibly be due to an equal mixture of several signals resulting in a single observable peak, although the narrow peaks and de-convolution dispute this.

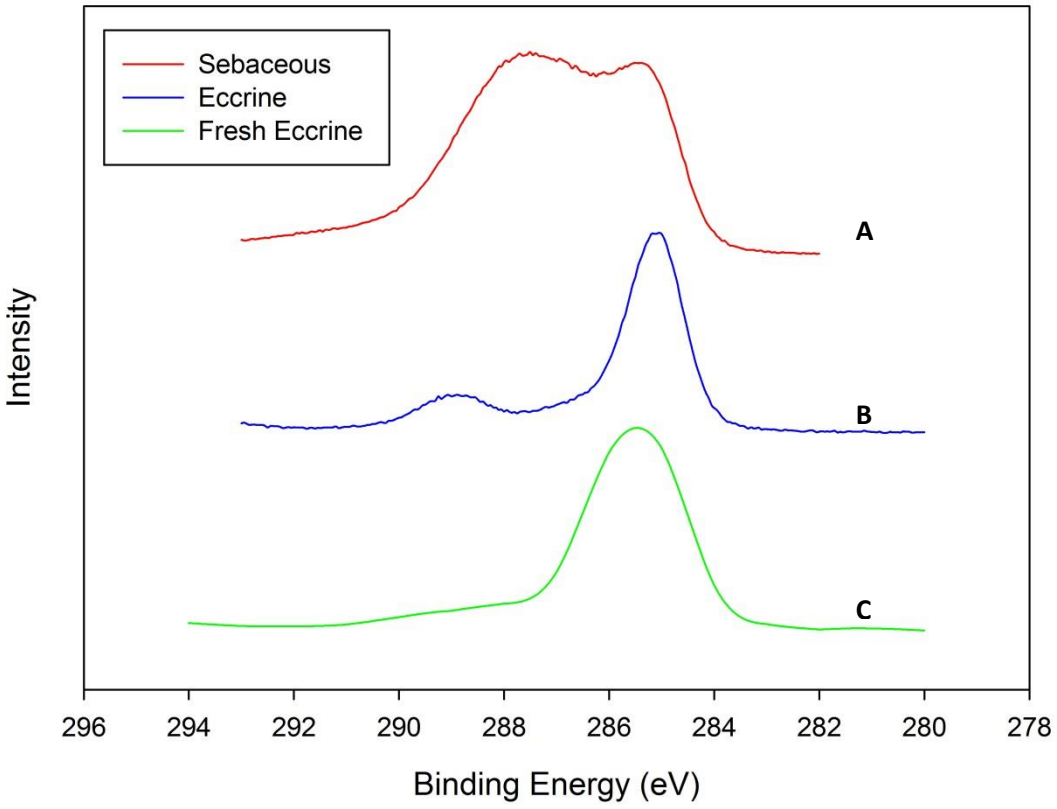

Figure 5.7 – XPS C 1s spectra of brass substrate stored at ambient conditions. ***A)*** *Sebaceous deposit;* ***B)*** *Eccrine deposit;* ***C)*** *Fresh eccrine deposit.*

The carbon spectrum for the aged eccrine sample has a main peak at 285.1 eV and a second signal at 288.9 eV as seen in Figure 5.7. The fresh eccrine sample has a slightly broader peak than the aged eccrine sample, as well as being at a higher energy value, 285.5 eV. These signals (285.1 eV, 285.5 eV and 288.9 eV) are all for carbon species as either C-C or C-H bonds[18-22, 38, 39].

The sebaceous sample has a carbon profile with multiple strong signals, creating the broad double peaked feature observed above in Figure 5.7. As sebaceous sweat is oil based (opposed to water based) it is expected that there would be many different environments of carbon. The main signals can be found at 285.2 eV, 286.7 eV, 288.2 eV and an additional smaller peak at 290.4 eV. The signal at 285.2 eV is a hydrocarbon[18-20]; 286.7 eV is of methyl groups on carbon chains[10, 19]; 288.2 eV is typical of carbons in carbonyl groups[24-26] and 290.4 eV is a carbon in an aromatic ring[27]. Although both eccrine and sebaceous sweat types contain carbon based compounds, both these XPS spectra and previous research[37] clearly shows that the sebaceous sweat contains more prominent and complex carbon species when compared to eccrine sweat. XPS is able to differentiate between the two sweat types and could be spatially mapped based on these carbon components.

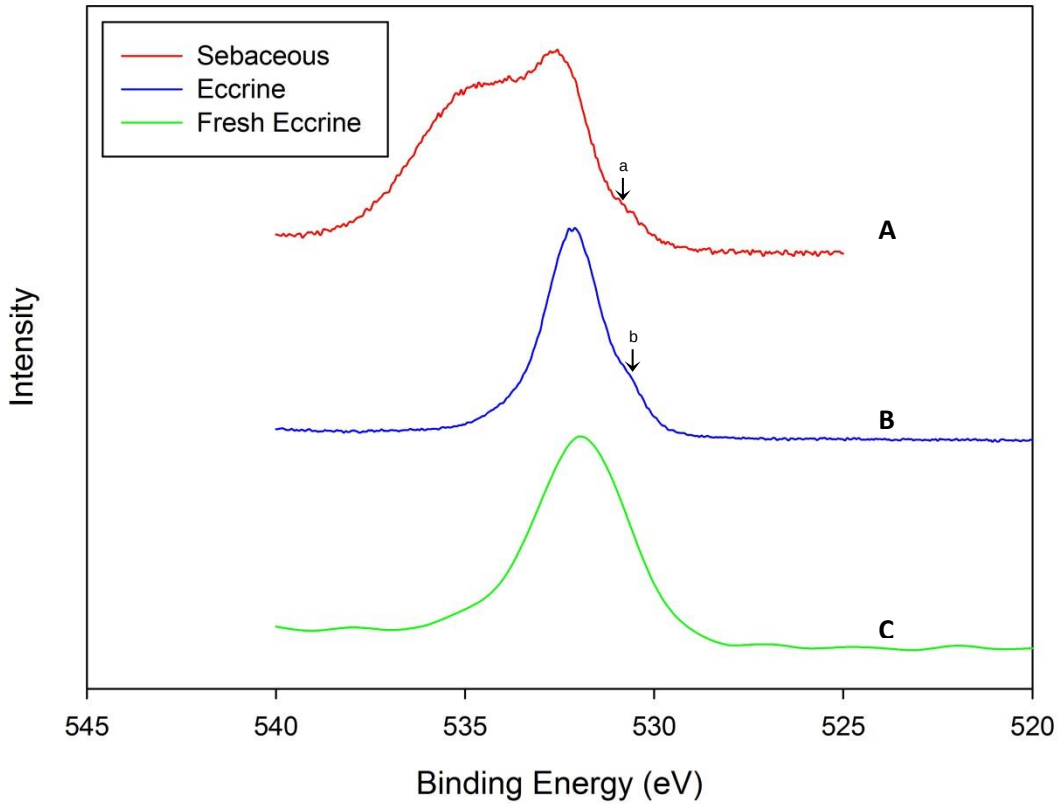

Figure 5.8 – XPS O 1s spectra of brass substrate stored at ambient conditions. ***A)*** *Sebaceous deposit;* ***B)*** *Eccrine deposit;* ***C)*** *Fresh eccrine deposit.*

In the O 1s spectra in Figure 5.8, one would expect a peak for each oxygen species identified by the three previous sets of spectra shown for these samples (zinc, copper and carbon). Additionally one would expect signals relating to the oxygen containing species present in the sweat deposits. Eccrine sweat is predominately water-based, so peaks identifying water molecules would be expected; small signals for fresh sweat deposits should also show traces of OH species, as either hydroxides or alcohols as well carboxylates, based on the composition of the sweat (Chapter 1, section 1.2.2). Sebaceous-based sweat would not contain a water molecule signal but would be expected to show peaks relating to functional groups such as esters, carboxylates, alcohols and other oxygen containing functional groups. The components and functional groups that may be detected in oxygen spectra will be similar between the two sweat types, the main difference being their relative intensities; the water signal in eccrine sweat would be expected to be nearly 100 times stronger than peaks representing other oxygen containing components since eccrine sweat is comprised of 98% water. In sebaceous sweat, just under half the composition is dominated by triglycerides and so the presence of carboxylates or ester groups would be expected in O 1s spectra.

The aged eccrine deposited sample has a prominent O 1s peak at 532.2 eV, as seen in Figure 5.8, and a smaller peak seen as a disruption to the symmetry of the main peak at 530.5 eV (point 'b'). These peaks can be assigned to oxygen in H_2O[29] and either CuO[30] or Cu_2O[12, 13], respectively. The presence of the water molecule is expected as outlined above. The fresh eccrine deposited sample only contains a single symmetrical signal at 532.0 eV, too low an energy value to be attributed to H_2O as expected but typical of OH species[28, 40, 41], but neither copper or zinc hydroxide species are found near this binding energy value. The lack of a signal for a water molecule was unexpected, since one would expect a strong H_2O signal in a fresh sweat deposit. The sebaceous deposited sample shows a broad, multi-signal peak. The main signal has a binding energy value of 532.4 eV and the secondary signal is at 534.8 eV. There is

also a slight imperfection to the slope of the lower binding energy side, indicating a third signal at *ca.* 531 eV ('a'). The signal at 532.4 eV is most likely attributed to a hydroxyl species in carbon chains[10, 11], possibly from the fatty acid chains present. The signal at 534.8 eV indicates an ether oxygen, again in carbon chains[10, 19]. The lower energy peak at *ca.* 531 eV is oxygen in $Cu(OH)_2$[12]. The copper hydroxide species suggest by the O 1s region is supported by the copper $2p_{3/2}$ region in Figure 5.6 for the sebaceous sweat deposited sample. However, the aged eccrine deposited sample did not have a corresponding signal in the copper region but since the copper spectrum only yielded elemental copper, it is that which is most likely mis-assigned, perhaps as two small equally sized signals with one each for Cu(I) and Cu(0). The metal oxide signal was weak for the non-fingerprinted substrates as well (Figure 5.4), but would still be expected to be seen in all three of the above fingerprinted samples.

5.2.1.3 Spatially Resolving Fingerprints on Substrates at Ambient Conditions

In the data presented above, differences can be observed between both sweat types as well as the non-fingerprinted substrates. However, this does not provide information relating to the spatial location when multiple species are revealed, such as seen in the oxygen (Figure 5.8) and carbon (Figure 5.7) spectra for sebaceous sweat on brass substrates. Using XPS in spatial mode can provide some answers as to whether the metal oxidation state is the same across the region studied by taking spectra at 4 µm intervals across the sample, but in order to spatially resolve the species, a sacrifice has to be made by decreasing the resolution of the binding energy. Therefore identification of the different signals present is much harder to discern.

Although data for fresh sebaceous deposit on brass substrate was absent from the non-spatially resolved data set in section 5.2.1.2, limited spatially resolved data are presented below in Figure 5.9. Not all elemental regions are reported because of the low intensities of signals for some of the regions. From Table 5.2, it is clear that there is a relatively small

amount of surface zinc reported for aged sebaceous and fresh eccrine deposit, therefore the signal was too weak to acquire a usual spatial spectrum for zinc regions. The same was true for oxygen regions.

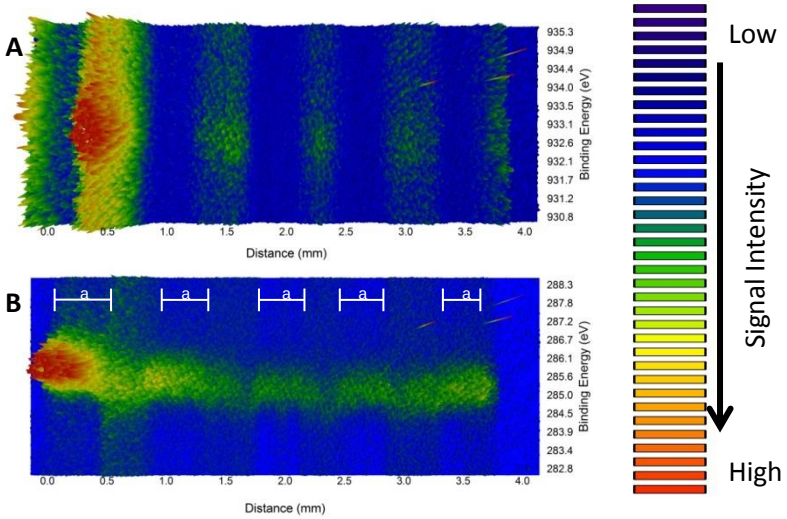

Figure 5.9 – Spatially resolved XPS images for fresh sebaceous sweat deposit on brass substrate, placed under UHV conditions immediately after deposition, with intensity scale bar on the right. ***A)*** *Copper* $2p_{3/2}$ *region;* ***B)*** *Carbon 1s region.*

The spatially resolved data shown in Figure 5.9 have binding energy variations shown in the y-axis and the spatial variation is shown laterally (x-axis). The third dimension (z-axis) is the relative intensity of the signals at each point, represented by a colour scale (seen on the right of Figure 5.9), with dark blue (red) being the lowest (highest) intensity present. The blue colour generally represents the background or baseline in relation to any peaks observed; in some regions the background level may be higher due to a much higher background intensity of all XPS signals. Depending on the intensity of the peaks, the colour on the highest point may vary from green through to red. The centre of the peak is sometimes a colour representative of a more intense signal, but where there is no colour variation present, the midpoint of the band can be taken as the peak position.

Where present, the carbon signal from the sample swamped the signals from the other elements and so made peak positions as well as copper to zinc ratios hard to identify and quantify. Above in Figure 5.9, the carbon and copper profiles can be seen to exist at separate spatial locations; where copper is found, the carbon signal is weaker than elsewhere. The regions where a strong carbon signal is present are areas of sweat deposit (labelled 'a'), the thickness of this sweat deposit means that the background signal level is lower on these ridge regions, resulting in the dark blue colour in the copper profile. Even where the furrows are (the gaps between the ridges present on the fingertip), significant traces of carbon can still be found alongside a very weak copper signal. The fact that some peaks and features could be observed on the copper profile but not the zinc due to relative intensities matches the findings displayed in Table 5.2. Although the aged sebaceous deposited sample at ambient conditions had multiple clear signals in the carbon 1s region (Figure 5.7), in the spatial profile above, a broad single peak is found between 285.0 eV and 285.6 eV, which only corresponds to the hydrocarbon energy value (285.2 eV) reported in the non-spatial data.

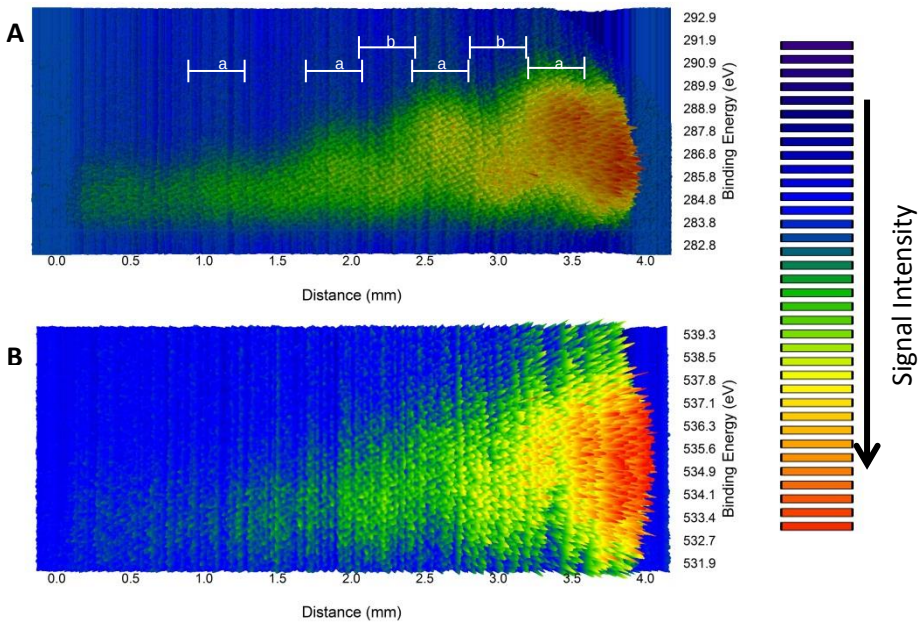

Figure 5.10 – Spatially resolved XPS images for sebaceous sweat deposit on brass substrate aged 10 days, stored at ambient conditions. ***A)*** *Carbon 1s region;* ***B)*** *Oxygen 1s region.*

As the metallic signals were quite weak and it was difficult to discern any notable spatially varying features, they have been omitted from Figure 5.10. However, the oxygen and carbon profiles observed in Figure 5.10 both show binding energy values that vary with spatial location. The presence of multiple signals was also observed in Figure 5.7 for carbon and Figure 5.8 for oxygen. The carbon profile is cleaner and it is easier to observe the spatial variance, at least in part due to it having a higher number of counts. The middle of the higher energy bands seen in the carbon profile in Figure 5.10A occur periodically (labelled with an 'a') and are *ca.* 400 μm wide. These bands are slightly wider than the suggested values of 300 μm for ridges and furrows[42] and this could be due to the proposed values being measured optically whereas the XPS is more surface sensitive and could detect trace materials present that are optically invisible. The slight broadening of one feature causes the narrowing of the other and could be attributed to ridges lying non-perpendicularly to the detector. Without the presence of the metallic signals, it becomes more problematic to discern which region is the ridge or furrow. However, since the oxygen position varies slightly and metallic oxides have a generally lower binding energy value than carbon based oxygen, it is possible to make some deductions. The locations where carbon signals have lower binding energy values (regions labelled 'b') coincide with the lower binding energy values for oxygen. One can deduce that these are the locations of the fingerprint furrows. Therefore, the laterally broader peaks at the higher binding energy values in both the carbon and oxygen profiles are associated with the ridge regions. The presence of carbon across the entire sample surface has been observed in all spatial profiles obtained, but is most prominent in the above Figure 5.10A, in which two clear binding energy states for the carbon can be seen. Low binding energy values for carbon suggest alkane compounds are present, whereas higher values suggest non-alkyl and/or long chain based carbon atoms. The presence of these alkane based carbons outside of deposited regions is difficult to conclusively explain; any residue from compounds used in the cleaning process (such as acetone) would also exhibit peaks at higher binding energy values.

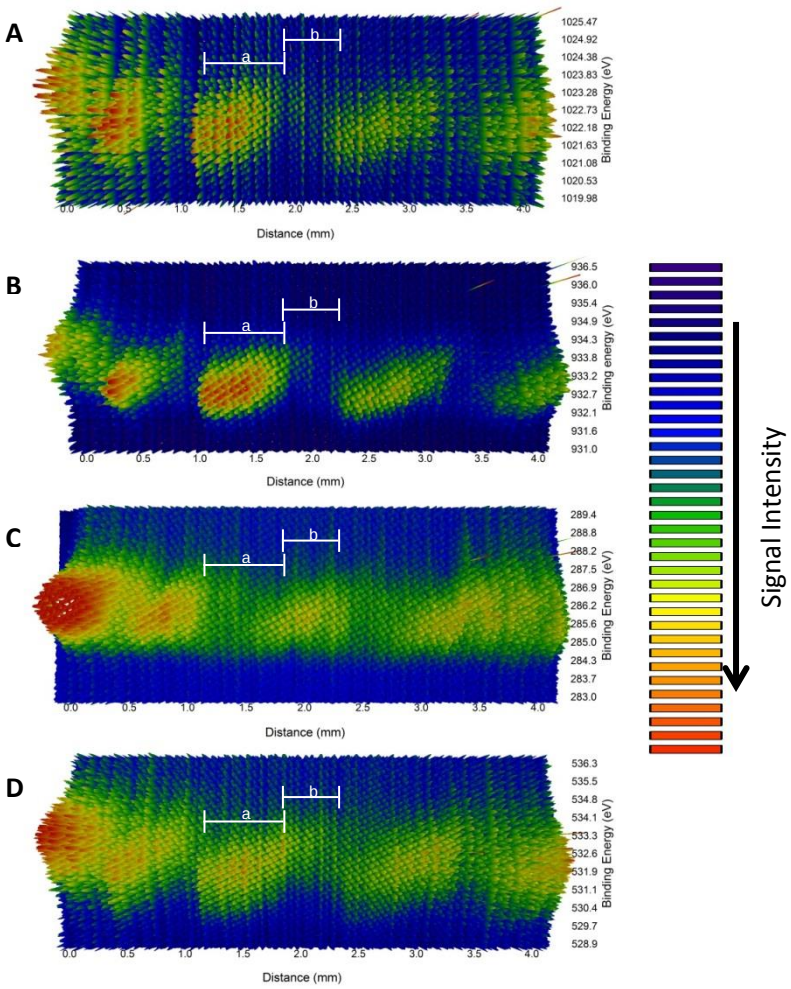

Figure 5.11 – Spatially resolved XPS images for fresh eccrine sweat deposit on brass substrate, placed under UHV conditions immediately after deposition. ***A)*** *Zinc $2p_{3/2}$ region;* ***B)*** *Copper $2p_{3/2}$ region;* ***C)*** *Carbon 1s region;* ***D)*** *Oxygen 1s region.*

Figure 5.11, above, shows several elemental spatial profiles for fresh eccrine sweat deposited onto a brass substrate. Both the carbon and oxygen profiles can be seen to have slight signals across the whole area examined, but have sections of stronger signals (shown by yellow and red colours) at specific spatial locations. The oxygen and carbon peaks do not fully align in the spatial domain. The carbon peaks appear where no copper or zinc are observed but the oxygen peaks seem to lie at the interface between these. The fingerprint ridges are the areas where the carbon signals are strongest (labelled 'b'), since this element is found in excreted sweat, and the furrows or gaps between the ridges are where the copper and zinc signals are prominent (labelled 'a'), since they are not attenuated by the deposit. In the deposited areas,

the sweat deposit is sufficiently thick to obscure the metallic signals, indicating that the fresh deposit is greater than 10 µm thick[43, 44]. The size of the ridges and furrows are all in the order of several hundred micrometres but the exact figure varies across the captured region; this variation is an indication that a series of ridges were not fully perpendicular to the measurement as the window is several millimetres wide and so non-perpendicular ridges would be seen with overlaps to spectra in the ridges and furrows as well as inconsistencies in their dimensions. Some variations in the binding energy of the peaks in all the elemental regions can be seen, most prominently in the oxygen and copper profiles. In the copper profile, Figure 5.11B, this could be attributed to the transition between Cu(I) or Cu(0) to Cu(II), although the formation of each signal is surprising. Each signal segment (either ridge or furrow) starts off at the same low binding energy and increases with increasing lateral distance (left to right). The reason for this pattern is not known but is also observed in the oxygen profile. In the case of oxygen (Figure 5.11D), the lower binding energy is found at the same lateral position as the metallic signals and the higher binding energies in relation to the carbon. Since metal-oxygen bonds have a lower binding energy than water or carbon-oxygen for O 1s regions, this is not unexpected, although a multi-signal oxygen profile was not detected in the non-spatially resolved data of Figure 5.8.

5.2.2 Substrates Exposed to Humid Environments

Results from Chapter 4 showed that humid conditions decreased the time in which a latent fingerprint on brass would become visible. This increased speed of visualisation could occur through either the same interaction mechanics as at ambient conditions, or the increased moisture present could provide additional pathways subsequently generating different end products. XPS can provide insight to this point. If the reactions are merely accelerated, then XPS spectra would be similar to those in section 5.2.1, otherwise the spectra would be different and provide insight into the alternative processes occurring.

Table 5.3 – Surface ratio of copper to zinc for fingerprinted and non-fingerprinted substrates subjected to humid conditions

Sample finish and deposition type	Time stored at humid conditions	Ratio of Cu:Zn
Polished; sebaceous	5 days	1 : 0.87
Polished; eccrine	5 days	1 : 1.20
Polished; control	5 days	1 : 0.63

The eccrine deposited sample has a much higher zinc content than the other samples as seen in Table 5.3. Both the sebaceous deposited sample and control sample have a higher proportion of copper to zinc, with higher copper levels on the non-fingerprinted sample. The surface Cu:Zn ratio for the control sample does not resemble that for polished brass stored at ambient conditions, neither does it resemble that for unpolished brass substrate (Table 5.1). From the ambient conditions, polished brass exhibited much higher levels of zinc than copper. However, exposure to a humid environment favours a higher copper surface population. The humid conditions could enable the removal of zinc through dezincification[45], which would explain why lower zinc amounts are recorded on the surface, although the surface Cu:Zn ratio value for the eccrine deposited sample would dispute this scenario. As with the surface Cu:Zn for aged eccrine samples in ambient conditions (Table 5.2), the ratio for the eccrine deposited sample also shows higher levels of zinc. The surface zinc could be removed from the surface by the water content of the sweat residue, following a localised leaching mechanism. This removed surface zinc is then trapped in the residue and, whilst not present directly on the substrate, is still measureable from within the remnants of the fingerprint sweat deposit.

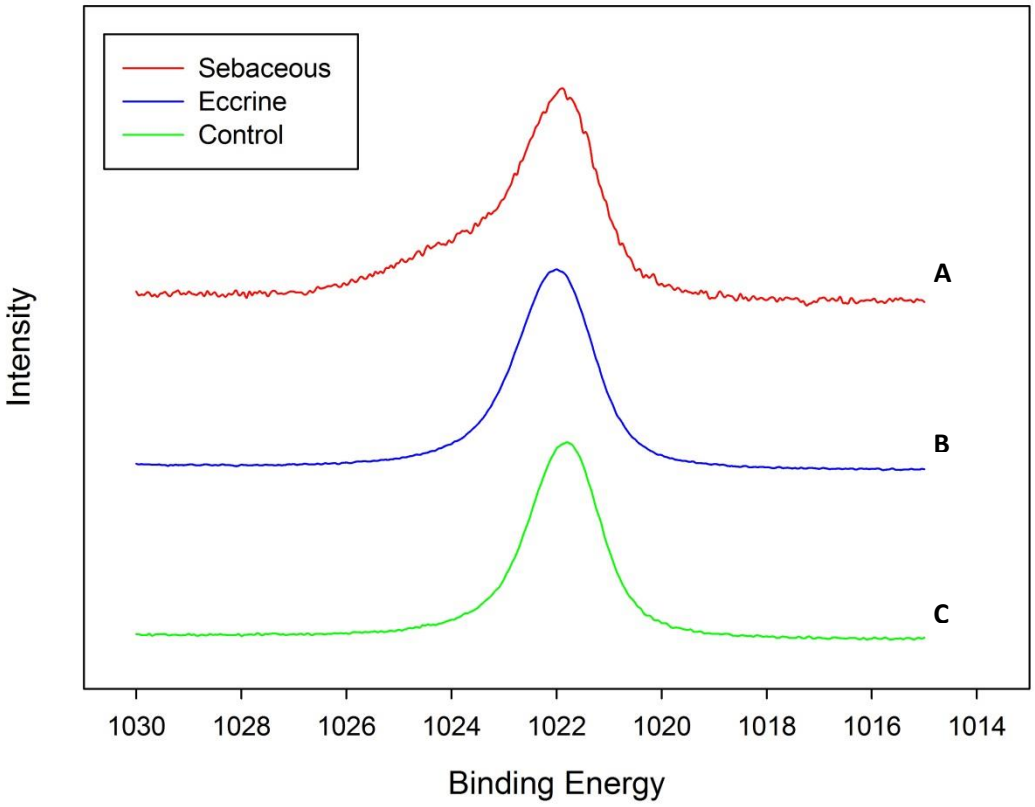

Figure 5.12 – XPS Zn $2p_{3/2}$ spectra of fingerprinted brass substrates subjected to humid conditions for 5 days. ***A)*** *Sebaceous sample;* ***B)*** *Eccrine sample;* ***C)*** *Control sample.*

In Figure 5.12, the eccrine deposited sample and the control sample both have a single, symmetrical peak at 1022 ±0.1 eV, this signal is either the zinc as Zn(0)[8-10] or ZnO[8, 10, 11], as the difference between the two states can be difficult to discern. The sebaceous deposited sample has two peaks, one of which is at 1022.0 eV as with the eccrine and control sample and the other has an energy value of 1024.0 eV and could be that of $ZnCl_2$[36]. The eccrine deposited sample and the control sample have similar profiles and peak energy values to both the non-fingerprinted and eccrine fingerprinted samples found in Figure 5.1 and Figure 5.5. The sebaceous profile differs in appearance from that of ambient sebaceous sample, mainly in that the second peak is smaller, but also with slightly shifted binding energy values. The presence of the zinc chloride signal being present in the sebaceous deposited sample rather than the

eccrine deposited sample is unexpected but was also observed for sebaceous deposited samples stored at ambient conditions (Figure 5.5), again the only explanation for its presence could be contamination from eccrine sweat yet this does not explain the lack of $ZnCl_2$ seen for the eccrine sweat spectrum in Figure 5.12.

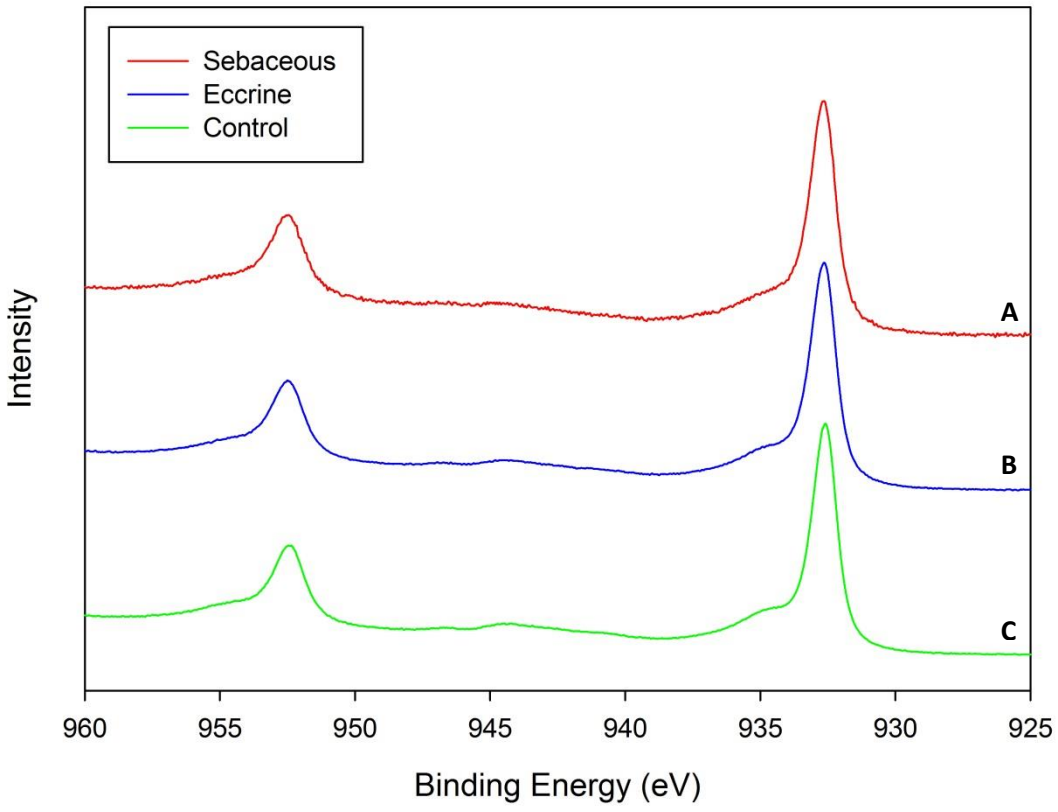

Figure 5.13 – XPS Cu $2p_{3/2}$ and $2p_{1/2}$ spectra of fingerprinted brass substrates subjected to humid conditions for 5 days. ***A)*** *Sebaceous sample;* ***B)*** *Eccrine sample;* ***C)*** *Control sample.*

Although there were differences in the zinc profiles for the three samples stored under humidified conditions (Figure 5.12), the copper profiles are nearly identical in appearance and peak positions (Figure 5.13). The main signal for all three samples in Figure 5.13 is a narrow peak at 932.6 eV, with an additional small peak at 935.2 eV. The additional peak is slightly bigger in the eccrine and control sample than the sebaceous sample. The main signal is at 932.6 eV and is either that of Cu_2O[8, 12, 13] or less likely that of Cu metal[12, 14-16]; the signal at 935.2

eV is $Cu(OH)_2$[16]. This suggests the presence of two different oxidation states for the copper species, both Cu(II) and either Cu(I) or Cu(0). This presence of the two different oxidation states present can also be seen in the Cu $2p_{1/2}$ region between 950 and 960 eV as an unsymmetrical peak, rather than a split peak. The fact that no difference in peak position can be discerned between the three samples suggests that the humid conditions have a greater impact on the surface composition and bound species than the presence of a fingerprint, regardless of sweat type deposited.

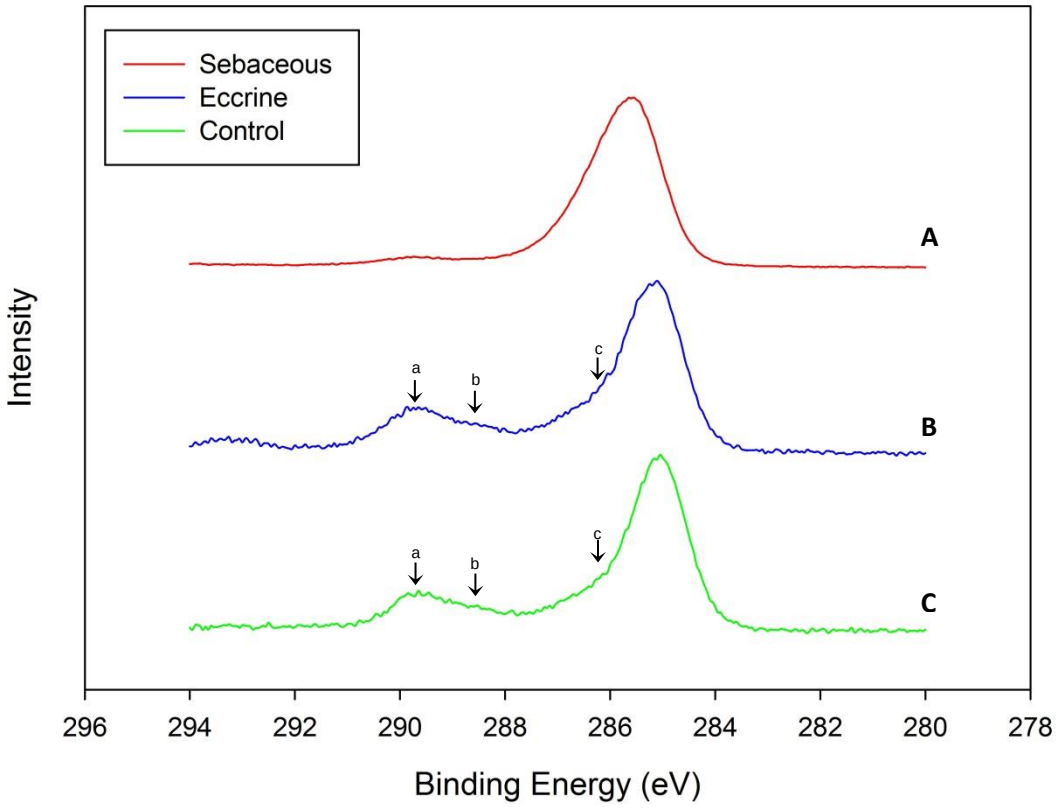

Figure 5.14 – XPS C 1s spectra of brass substrates subjected to humidified conditions for 5 days. ***A)*** *Sebaceous sample;* ***B)*** *Eccrine sample;* ***C)*** *Control sample.*

The carbon spectrum in Figure 5.14 for the sebaceous deposited sample contains fewer features than would be expected when compared to that observed for sebaceous sweat deposit stored at ambient conditions (Figure 5.7); this is due to the nature of sebaceous sweat

being oily and therefore contains non-alkyl and long carbon based chains. The sebaceous sweat deposited sample for humidified conditions contains a single peak at 285.5 eV, which is typical for aliphatic carbon chains [19, 21, 22]. The eccrine deposited sample and control sample exhibit similar profiles to each other, which is unexpected since the control sample is sweat-free. The main peak for both is at 285.0 eV and associated with hydrocarbon groups[18, 46]; the smaller peaks (in size order) are at binding energies of 289.7 eV ('a'), 288.5 eV ('b') and 286.2 eV ('c'), which could be carbonates (CO_3)[10, 47, 48], carbonyl groups[10, 20, 49] and carboxylate groups[25, 49-51] respectively. Whilst the presence of some of these functional groups would be expected in sweat residue, one would not expect to find the same carbon components on both the eccrine sweat based sample and the control sample. If a component or peak is present on the control sample that matches a fingerprinted sample, then it can be immediately discounted as a sweat component. In Figure 5.14, this means that as the spectra for the control and eccrine fingerprinted sample are similar, then the cause of the peaks is not sweat based. This is further corroborated as neither the spectra for aged or fresh eccrine deposited samples (Figure 5.7) match the spectral identities seen in Figure 5.14.

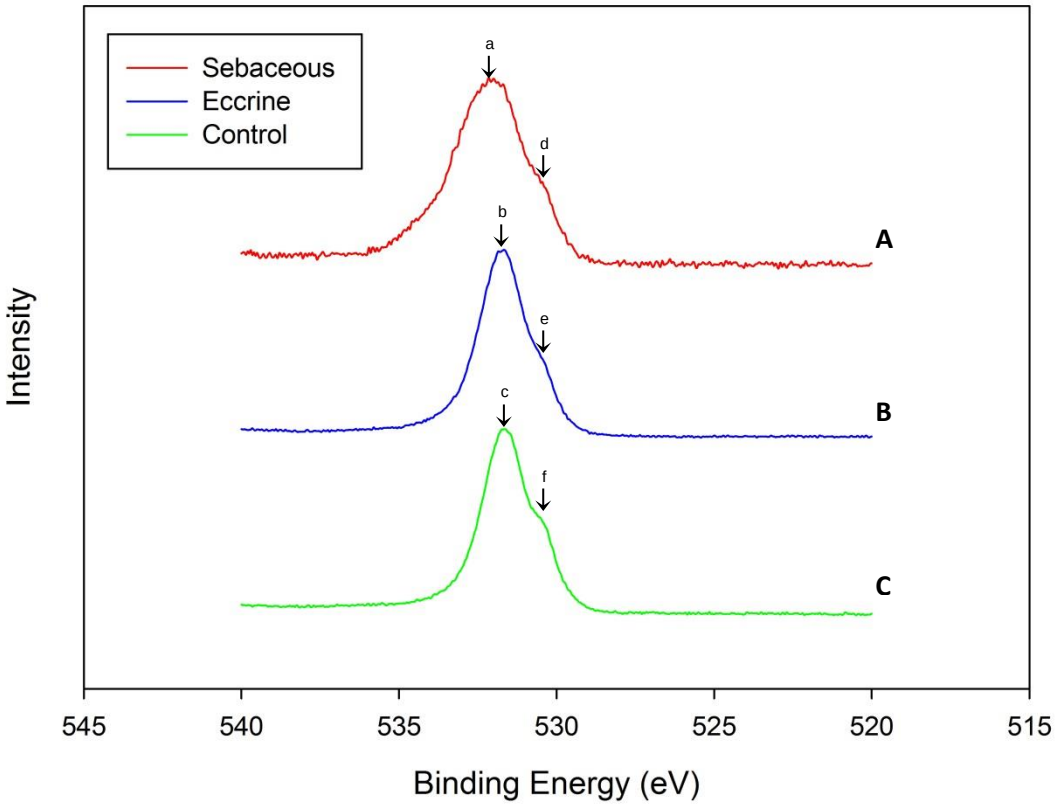

Figure 5.15 – XPS O 1s spectra of brass substrate subjected to humidified conditions for 5 days. ***A)*** *Sebaceous sample;* ***B)*** *Eccrine sample;* ***C)*** *Control sample.*

As with the zinc profiles in Figure 5.12, both the eccrine deposited and control samples have similar peak positions and appearances in the O 1s region. In Figure 5.15, both the eccrine and control samples have a main peak at 531.7 eV ('b' and 'c') and a smaller peak at 530.4 eV ('e' and 'f'). These peaks are hydroxyl[29, 52], possibly $Cu(OH)_2$[13], and copper oxide (CuO or Cu_2O)[13, 30] peaks, respectively. Both Cu_2O and $Cu(OH)_2$ were found in the Cu $2p_{3/2}$ region as well as the O 1s region, therefore each sample contains both the Cu(I) and Cu(II) oxidation states (Figure 5.13). Copper in the Cu(II) was not found on aged polished brass, but only on freshly polished brass. This indicates that the cause for the two different oxidation states of the copper is related to the effect that the sweat residue has on the surface. Either the freshly polished

brass surface is trapped beneath the sweat deposit and maintained in the Cu(II) state, or the sweat material has reacted with the copper and caused the formation of a Cu(II) species.

Although the peaks for the sebaceous sample in Figure 5.15 resemble those for the eccrine and control sample, the main peak is shifted to a slightly higher binding energy. The main peak is at 532.1 eV ('a'), compared to 531.7 eV for the eccrine and control samples, but the additional peak is at a similar position at 530.3 eV ('d'). The small peak at 530.3 eV can be assigned as a copper oxide signal[13, 30] and the main peak at 532.1 eV could either be a hydroxide[28] or water signal[29]. The spectrum for the sebaceous sample is less conclusive than the eccrine or control samples but it does not fully contradict the findings from the Cu $2p_{3/2}$ region since the presence of at least one oxidation state of copper is supported.

As with the clean substrate and fingerprinted substrates exposed to both ambient and humidified environments, there is little sign of the ZnO peak in the O 1s region despite the eccrine deposited and polished substrates exhibiting a higher level of surface zinc than copper. It is possible that the signals around 531.5 eV are caused by oxygen in both copper and zinc oxides[8]. As the spectrum for the eccrine fingerprinted sample and the control sample are very similar, it suggests that this environment has as much impact on the oxygen containing species present as the eccrine sweat deposit. This is plausible since eccrine sweat is predominately water-based (approximately 98%) and thus is not entirely different to the local environment.

5.2.3 Substrates Exposed to both Heat and Humidity

The surface composition, with regards to the amount of copper and zinc present, changes depending on the conditions and the type of sweat deposited onto the surface. Sebaceous sweat, fresh eccrine deposit and unpolished samples have a higher amount of copper than zinc present on the surface, whereas both polished ambient and aged eccrine fingerprinted

samples show the reverse and have more surface zinc than copper. From this, one would expect the application of heat as well as humidity would result in more surface copper than zinc for all but the eccrine deposited sample. However, this is not the case, as can be seen in below in Table 5.4.

Table 5.4 – Surface ratio of copper to zinc for fingerprinted and non-fingerprinted substrates subjected to heat (75°C) and 100% relative humidity

Sample finish and deposition type	Time stored in warm humid conditions since preparation	Ratio of Cu:Zn
Polished; sebaceous	6 hours	1 : 0.11
Polished; eccrine	6 hours	1 : 0.39
Polished; control	6 hours	1 : 0.77

The surface Cu:Zn ratios seen in Table 5.4 show a higher proportion of copper than zinc for all samples. Sebaceous deposited samples and polished control samples had more zinc than copper when exposed to humid conditions and the sebaceous deposited samples also had more zinc at ambient conditions. Eccrine deposited samples had more zinc than copper at both ambient and humid conditions, but with the heat and humidity conditions this has been reversed. Although the eccrine deposited sample had a higher proportion of zinc than the sebaceous deposited sample after exposure to both ambient (Table 5.2) and humid conditions (Table 5.3), this remains the same at these conditions despite both having more surface copper than zinc. The low level of surface zinc in Table 5.4 could be explained by dezincification; the higher level of zinc present, the more susceptible the sample is to dezincification[53]. In Table 5.1, the polished brass samples at ambient conditions had more surface zinc than copper; therefore the exposure to both heat and moisture must present a pathway for the removal of the zinc via the selective leaching pathway.

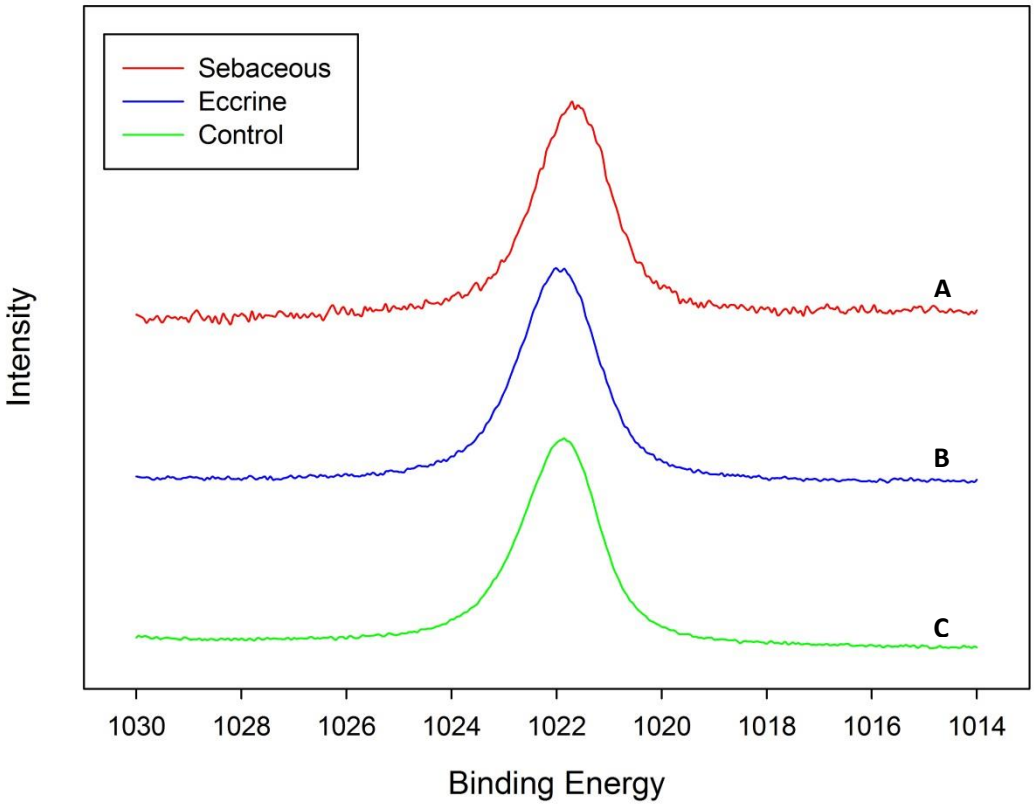

Figure 5.16 – XPS Zn $2p_{3/2}$ spectra of fingerprinted brass substrates subjected to heat and humid conditions. ***A)*** *Sebaceous sample;* ***B)*** *Eccrine sample;* ***C)*** *Control sample.*

Whilst all the spectra seen in Figure 5.16 show single symmetrical peaks, the sebaceous deposited sample peak position (1021.6 eV) is at a slightly lower binding energy value than either the control or eccrine deposited samples (1021.9 eV). This latter is associated with Zn(0)[8-10] whereas the former (1021.6 eV) is reported for ZnO[10]. Whilst the assignment for these peaks conflicts with the way in which copper oxidation states are determined, the binding energy separations for zinc species and its oxidation states are not as distinctly different or as well documented as in copper regions. The signal for the Zn(0) could stem from the Zn signal originating from the zinc in the bulk rather than purely on the surface. The ZnO signal is what would be expected if the zinc was present on the surface.

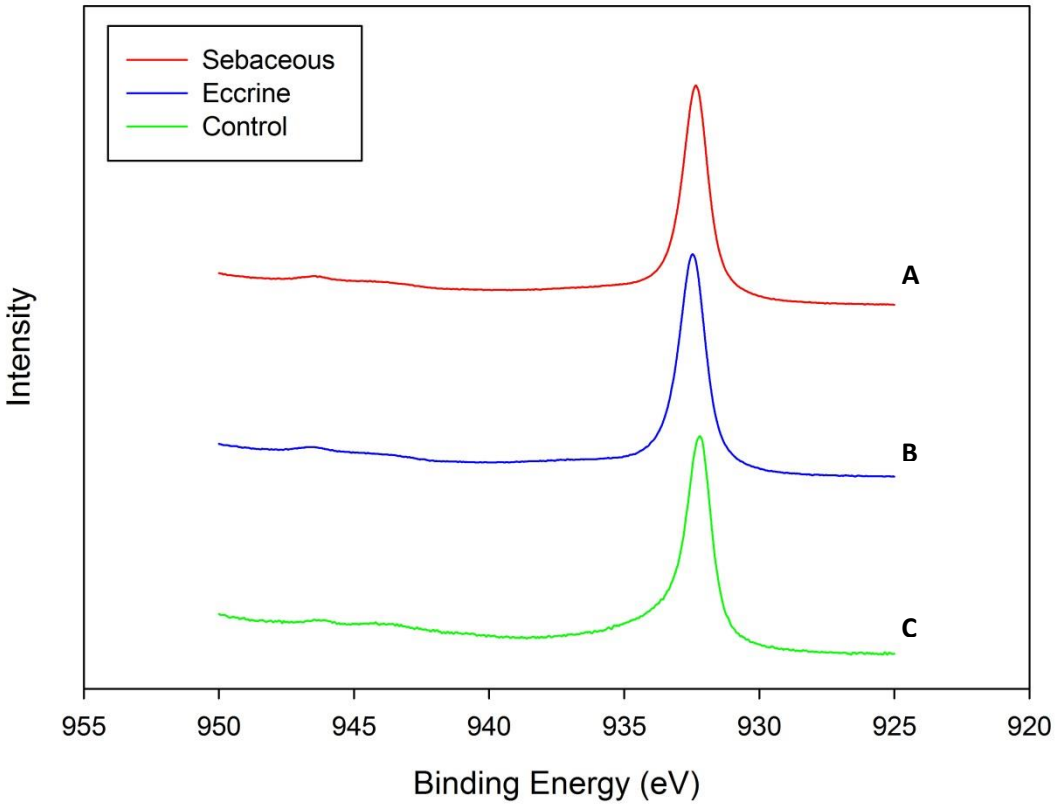

Figure 5.17 – XPS Cu $2p_{3/2}$ spectra of fingerprinted brass substrates subjected to heat and humid conditions. ***A)*** *Sebaceous sample;* ***B)*** *Eccrine sample;* ***C)*** *Control sample.*

The copper spectra for the eccrine and sebaceous deposited samples are similar, as seen in Figure 5.17. A single narrow peak is observed at 932.4 eV in both cases. The main signal at 932.4 eV is that of Cu(I), either copper in Cu_2O[8, 12, 13, 30] or CuCl[10], although Cu_2O is more likely, as no previous copper chloride product was found for fingerprinted samples stored in humid or ambient conditions. The control sample has a main peak at 932.2 eV and, despite being of lower binding energy than the fingerprinted samples, can also be attributed to Cu_2O[10, 11].

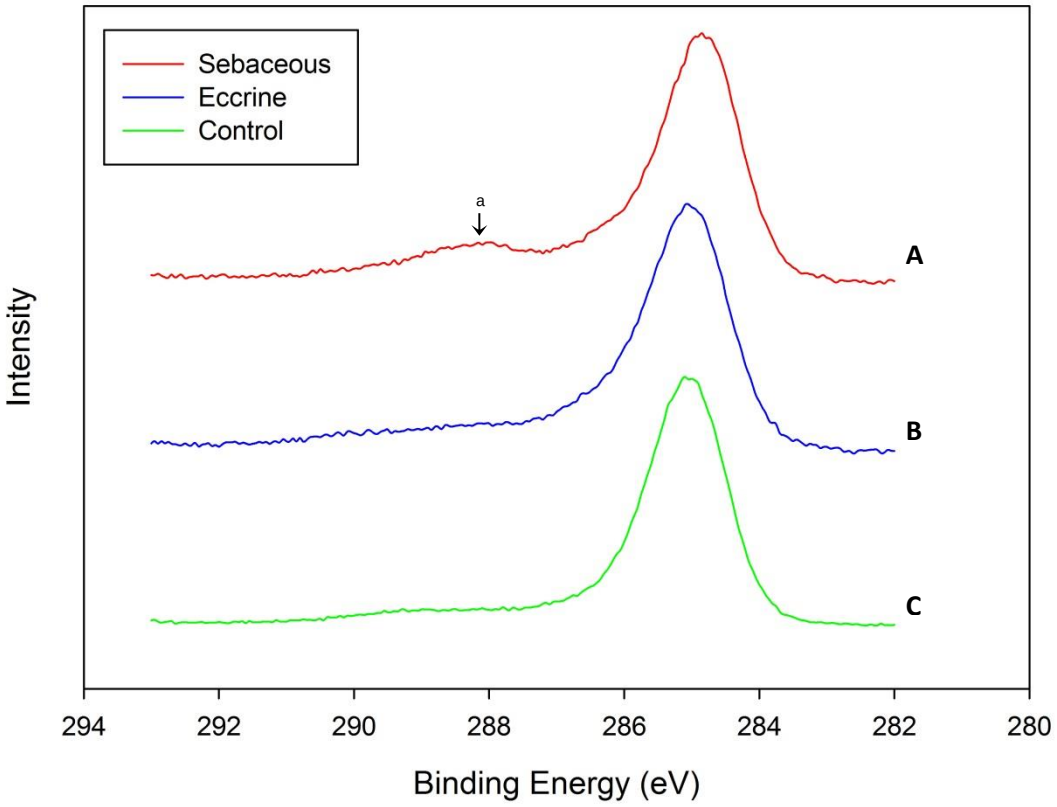

Figure 5.18 – XPS C 1s spectra of fingerprinted brass substrates subjected to heat and humid conditions. ***A)*** *Sebaceous sample;* ***B)*** *Eccrine sample;* ***C)*** *Control sample.*

Although sebaceous sweat consists of oily compounds that are not associated with removal by water, exposing sebaceous deposited samples to humid environments appears to cause a change to the residual deposit. Under ambient conditions (Figure 5.7), the carbon spectrum contained multiple signals with some associated with long carbon chains. However, in humid or warm humid conditions, the carbon spectrum is much less complex and only contains a single peak. In the latter conditions (Figure 5.18), the single peak for the sebaceous deposited sample is at 284.9 eV and represents carbon in alkane C-C bonds[18, 19, 22, 46, 50]. The small secondary peak seen for the sebaceous deposited sample in Figure 5.18 at 288.5 eV ('a') is typical of carbon in carbonyl bonds[20]. When combined with the first, the identification of the functional groups suggests an acetone like compound but due to acetones volatile nature, this

would be unlikely. Additionally, the alkyl and carbonyl groups could represent features present on many of the different components of the sebaceous sweat, including carboxylate containing compounds. The eccrine deposited sample and the control sample both have a single peak, found at *ca.* 285.0 eV, attributable to alkyl carbons[18-20, 22, 46, 50], but most likely from residual carbon.

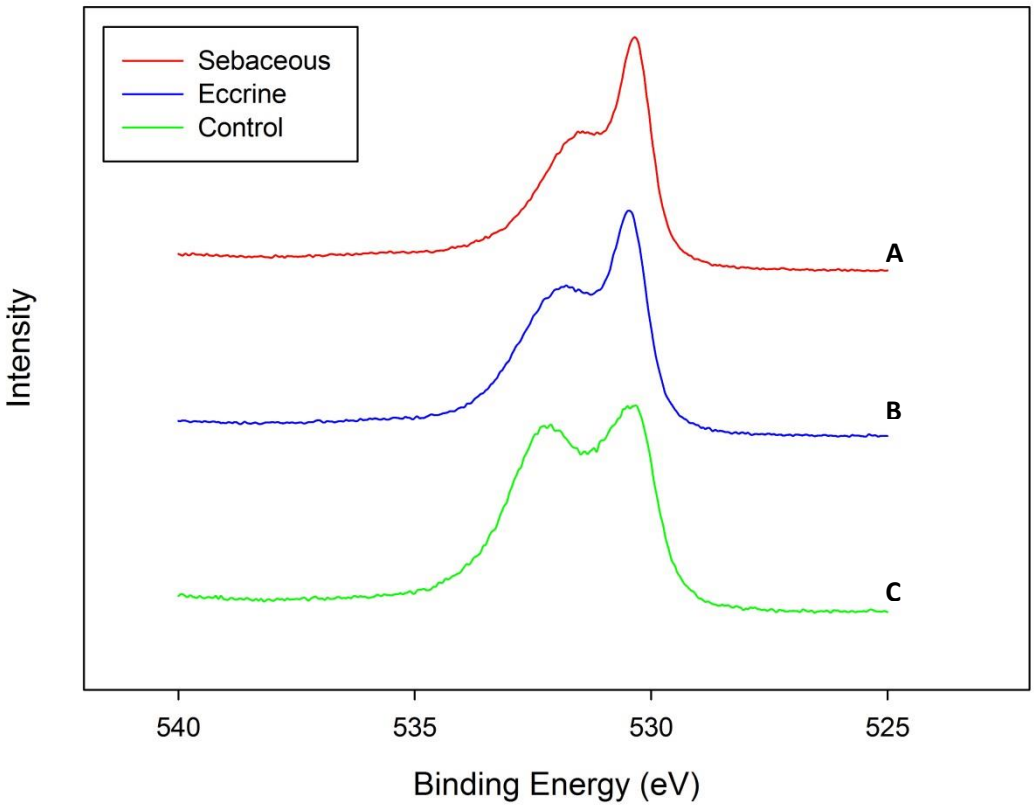

Figure 5.19 – XPS O 1s spectra of fingerprinted brass substrate subjected to heat and humid conditions. ***A)*** *Sebaceous sample;* ***B)*** *Eccrine sample;* ***C)*** *Control sample.*

All three of the spectra for O 1s, seen in Figure 5.19, are of multiple signal peak profiles, with each varying in peak position, relative intensities or both. The peak position of the lower energy signal in the eccrine deposited sample and control sample spectra is at 530.5 eV, whereas the sebaceous deposited sample exhibits a peak at 530.3 eV. This difference is small but potentially signifies a difference in the bound oxygen, as either CuO[30] or Cu_2O[10, 13]

respectively. The Cu_2O species matches those suggested in the copper spectra (Figure 5.17) but the CuO species is not supported by this. Due to the closeness of the energy values, it would be difficult to conclude conclusively the species present based on the O 1s signal alone, since the Cu $2p_{3/2}$ spectra offers a greater discrimination for copper oxidation states amongst copper oxides, based on binding energy separation. The second O 1s peaks for the eccrine and sebaceous deposited samples are aligned at 531.7 eV, an OH[13, 40] signal possibly $Cu(OH)_2$[13] although, again, this is not corroborated by the copper spectra from Figure 5.17. The control samples second peak is at a higher binding energy value than the other peaks present and is found at 532.4 eV, which is typical for H_2O[40, 54], a remnant of the storage environment. Strangely, in the O 1s spectrum for the sebaceous deposited sample there is no indication of the carbonyl bond proposed by the carbon spectrum in Figure 5.18A.

5.2.4 Substrates Exposed to Direct Heat

Whilst the warm humid conditions in section 5.2.3 were sufficient to cause dezincification of the surface, exposure to a direct heat source (a Bunsen flame) would cause local dehumidification effectively creating a dry environment on the sample surface. This would prevent any dezincification occurring since there would be no transit material to remove the zinc. The surface Cu:Zn ratio values given below in Table 5.5 strengthen this hypothesis.

Table 5.5 – Surface ratio of copper to zinc for fingerprinted and non-fingerprinted substrates subjected to direct heat by Bunsen flame for 40 seconds

Sample finish and deposition type	Time stored at ambient conditions before exposure to direct heat	Ratio of Cu:Zn
Polished; sebaceous	4 weeks	1 : 11.2
Polished; eccrine	4 weeks	1 : 9.58
Polished; control	4 weeks	1 : 18.6

After exposure to direct heat, the samples had a silvery sheen, as opposed to the typical appearance of brass. The silver appearance indicates a greater abundance of zinc on the sample surfaces, as demonstrated by the surface Cu:Zn ratios seen in Table 5.5. The sebaceous and eccrine deposited samples have approximately ten times more zinc than copper; the control sample has an even larger amount of zinc present. This difference seen between the fingerprinted and non-fingerprinted samples suggests that the deposited material could be protecting or preserving the substrate surface and preventing the level of change seen in exposed areas. With the samples exposed to direct heat, this is the only environment that causes the eccrine deposited sample to have exhibited a lower relative amount of zinc to copper than the sebaceous deposited sample. All previous eccrine samples (Table 5.2 to Table 5.4) portrayed surface compositions with the higher relative amounts of zinc than the sebaceous samples.

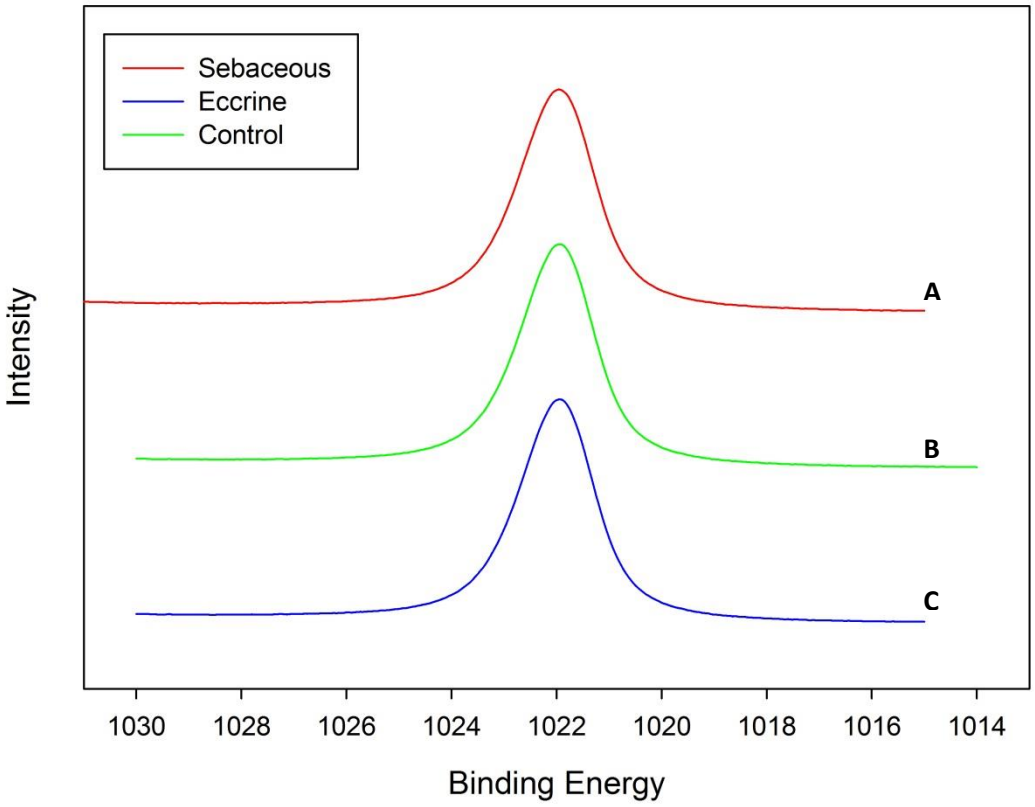

Figure 5.20 – XPS Zn $2p_{3/2}$ spectra of fingerprinted brass substrates subjected to direct heat. ***A)*** *Sebaceous sample;* ***B)*** *Eccrine sample;* ***C)*** *Control sample.*

All three samples have similar Zn $2p_{3/2}$ spectra, as seen in Figure 5.20. They show single symmetrical peaks at a binding energy of 1022 eV. This peak position can be assigned as either Zn(0)[8, 9] or Zn(II)[8, 10, 11], although, as the zinc is predominately on the surface, ZnO would seem to be more likely.

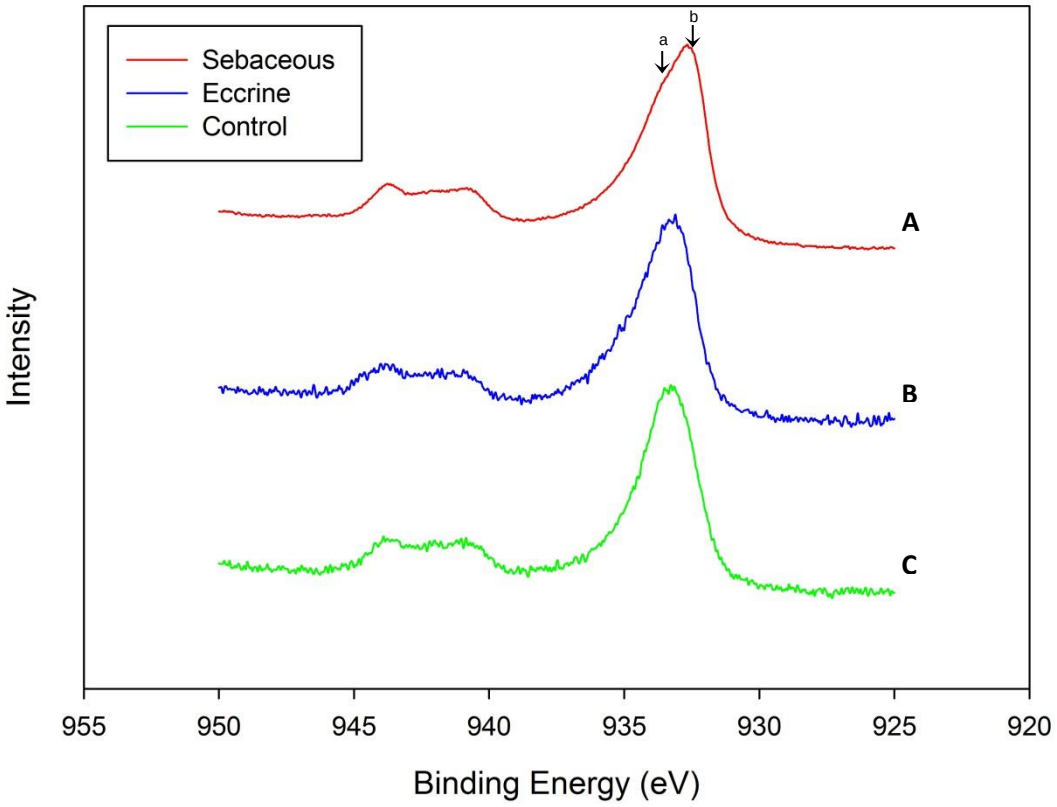

Figure 5.21 – XPS Cu $2p_{3/2}$ spectra of fingerprinted brass substrates subjected to direct heat. ***A)*** *Sebaceous sample;* ***B)*** *Eccrine sample;* ***C)*** *Control sample.*

In Figure 5.21, the Cu $2p_{3/2}$ spectra shows seemingly single peaks between 920-940 eV, but their width and unsymmetrical shape are characteristic of two components with similar binding energies. The sebaceous deposited sample has a peak at 933.8 eV ('a') and 932.6 eV ('b'), that at the higher binding energy being attributable to Cu(II) as CuO[8, 12, 13, 16, 17, 30]. The value at 932.6 eV is on the border between Cu(0)[9, 12, 16] and Cu(I)[8, 12, 13]. As XPS is surface sensitive, it is likely that the detected copper is oxidised rather than being in a zero oxidation state, therefore Cu(I) as Cu_2O[8, 12, 13] is more likely to be responsible for the second signal. The eccrine deposited sample and the control sample have very similar peak positions, which are distinctly different to that of the sebaceous deposited sample. The two peak positions for the eccrine deposited and control samples are 933.3 ±0.1 eV and 935.2 ±0.1 eV. These two signals

are both for Cu(II) products and can be assigned as CuO[10] and $Cu(OH)_2$[16] respectively. The eccrine deposit does not seem to have had as much effect on the surface composition as the sebaceous deposit, since its spectrum mirrors that of the control sample.

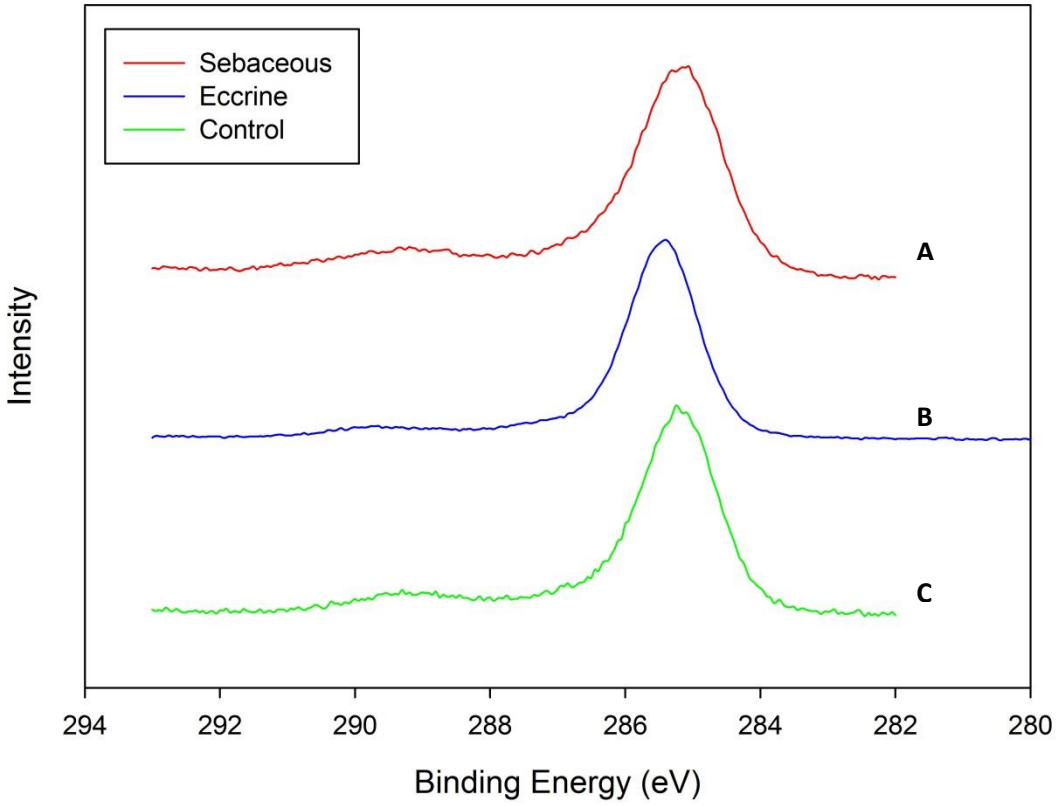

Figure 5.22 – XPS C 1s spectra of brass substrates subjected to direct heat for. ***A)*** *Sebaceous sample;* ***B)*** *Eccrine sample;* ***C)*** *Control sample.*

The data for the carbon profiles are similar for all samples exposed to direct heat, as seen in Figure 5.22, the peaks are similar in shape and position. The sebaceous and control samples have a peak at 285.2 eV, which is typical of alkane and hydrocarbon bonds[20]. The eccrine sample's peak is slightly higher at 285.4 eV, but still attributed to alkane-based carbons[20]. The carbon-based components of the sweat residue were likely to have been burnt off when exposed to the direct heat, thus the carbon signals detected can be attributed to background levels or burnt surface material.

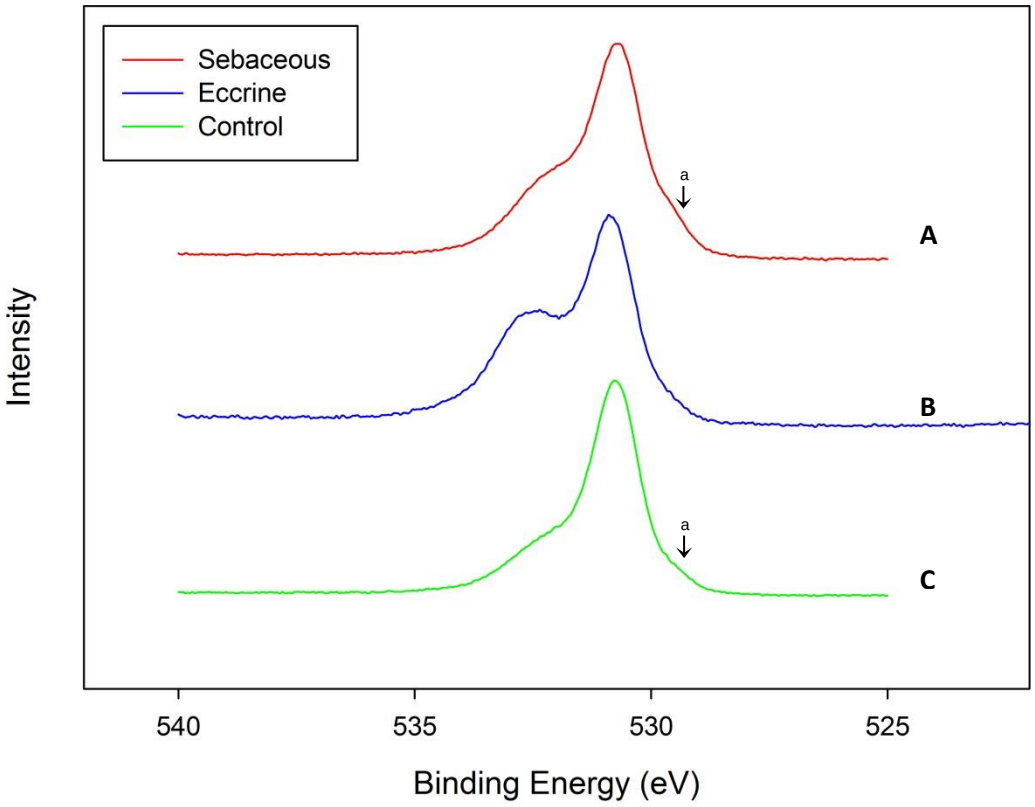

Figure 5.23 – XPS O 1s spectra of brass substrate subjected to direct heat. ***A)*** *Sebaceous sample;* ***B)*** *Eccrine sample;* ***C)*** *Control sample.*

The oxygen profiles in Figure 5.23 can be seen to have distinctive multiple peaks. All three samples have similar profiles, with the main peak at a lower binding energy than additional peaks. The sebaceous deposited sample has a peak shape and peak positions similar to that of the control sample, with peaks at 530.8 eV and 532.2 eV, which are attributable to oxygen in $Cu(OH)_2$[12] and water[29], respectively. A slight broadening can be seen at the base of the main peak for the sebaceous deposited sample around 529.5 eV ('a'), which is not as noticeable in the control sample. This binding energy value can be attributed to oxygen in either CuO[11] or ZnO[55] species, both of which are expected from the copper (Figure 5.21) and zinc (Figure 5.20) spectra. The eccrine sample has peaks at slightly different positions to the other two samples, with peaks at 532.5 eV, 530.8 eV and a small peak at 529.6 eV. The latter two match with

those found in the sebaceous and control samples and can be assigned in the same manner with binding energies of 530.8 eV being that of $Cu(OH)_2$[12] and 529.6 eV being either CuO[11] or ZnO[55]. The peak at 532.5 eV is of a higher energy value than the sebaceous or fingerprinted sample but can still be assigned as a water signal[40, 54]. The presence of a water molecule in any form is unexpected, as the samples were exposed to direct heat and placed under UHV conditions, one would assume that all surface moisture was removed. Although the Cu $2p_{3/2}$ spectrum (Figure 5.21) for the sebaceous fingerprinted samples suggested the presence of Cu_2O, a corresponding peak for this species was not present in the O 1s spectrum. This implies that the signal detected in Figure 5.21 was in fact due to Cu(0).

5.2.4.1 Spatially Resolved Fingerprinted Substrates

For the sebaceous fingerprinted sample, the surface composition (Table 5.5), shows a small amount of copper present with respect to zinc. Consequently, the copper signal was too weak to reveal the lateral intensity variation (if any) when spatially resolved. The carbon signal for the sebaceous fingerprinted sample showed no peak position variation across the surface; since the non-spatially resolved spectrum for this sample (Figure 5.22) only showed a single carbon species, no spatially variation would be expected. Therefore, only the Zn $2p_{3/2}$ and O 1s regions are presented as being spatially resolved in Figure 5.24, below.

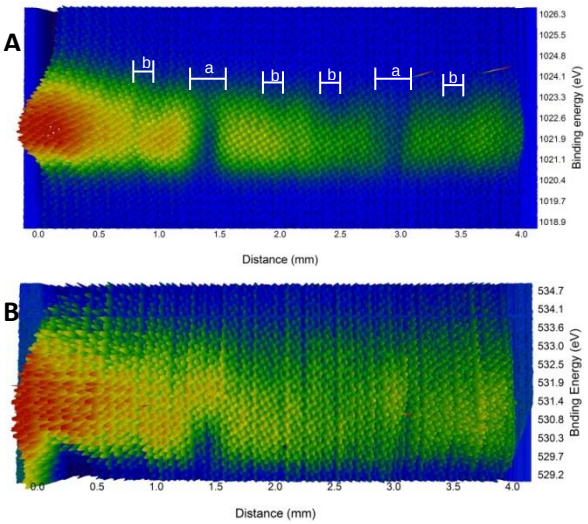

Figure 5.24 – Spatially resolved XPS images for sebaceous sweat deposit on brass substrate exposed to direct heat. ***A)*** *Zinc* $2p_{3/2}$ *region;* ***B)*** *Oxygen 1s region.*

For the sebaceous sample, the spatially resolved zinc profile contains more useful information than that displayed by the oxygen profile, in Figure 5.24. Two clear gaps can be seen in the zinc profile at areas labelled 'a', with other decreases in intensity seen as a narrowing of the band at fairly regular lateral intervals ('b'), approximately every 300 µm. Despite this, a single binding energy value for zinc is present at *ca.* 1022 eV, typical of Zn(II) and matching that observed in Figure 5.20. The oxygen band is quite broad but with a clear higher binding energy peak found where the gap in zinc is located. The furrow regions exhibit a much stronger signal than the ridge deposited material and the higher binding energy peaks in the oxygen are also portrayed as smaller peaks in the non-spatially resolved data (Figure 5.23).

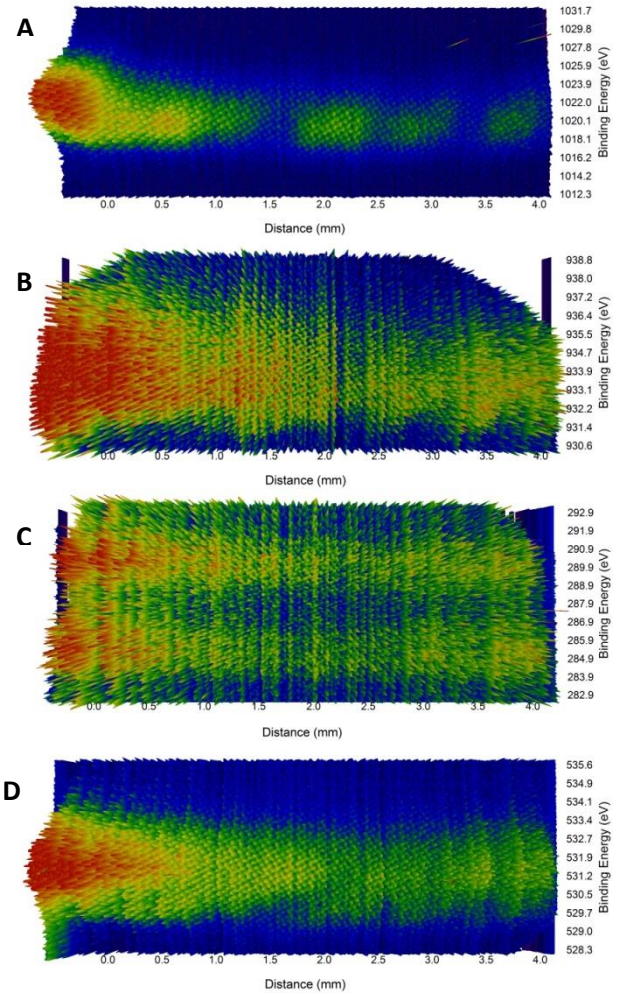

Figure 5.25 – Spatially resolved XPS images for eccrine sweat deposit on brass substrate exposed to direct heat. ***A)*** *Zinc $2p_{3/2}$ region;* ***B)*** *Copper $2p_{3/2}$ region;* ***C)*** *Carbon 1s region;* ***D)*** *Oxygen 1s region.*

The spatially resolved data for the eccrine fingerprinted sample exposed to direct heat is shown in Figure 5.25. Although the information displayed above is not as clear as in Figure 5.11, Figure 5.25 above shows similar features, with the gaps in the zinc profile matching peaks in the carbon profile. The ridges captured on the right hand side of the profiles must have been better aligned to the detector than those on the left, since the difference between regions is more discernible. However, the gap in the zinc profile around 1.5 mm matches a strong signal spike from the copper profile and this pattern is repeated at 3.5 mm. Whilst these measurements correspond to the x-axis in the figure, they are of an arbitrary scale and are therefore merely relative to the starting point of the data collection. These differences in the

metallic spatial locations could be due to the sweat deposit. In the control sample exposed to the Bunsen flame (Table 5.5), the surface Cu:Zn ratio was much more in favour of the zinc component than either of the fingerprinted samples. This suggested that the sweat deposit acted as a barrier and prevented the removal of copper from the surface. This can be confirmed by the spatially resolved data with the presence of copper in areas where the zinc level is decreased. Additionally, the copper appears to be in a higher oxidation state (higher binding energy value) in places with less zinc, meaning that Cu(II) is expected in regions with sweat deposit rather than exposed regions and explains the split peaks found in Figure 5.21.

Interestingly, the carbon profile in Figure 5.25 clearly shows two distinct signals found at *ca.* 290.5 eV and 285.5 eV, which would be aromatic carbons[27] and hydrocarbon chains[20] respectively. Spatial variations are not very apparent laterally, although the carbon signal is much weaker than the zinc or oxygen signals. This is because the sweat is mainly comprised of water and also exposure to the Bunsen flame may have burnt the remaining material, therefore the spatial location of peaks is harder to discern. Both the oxygen and zinc profiles show predominately single energy value signals, however, the oxygen band is quite broad in Figure 5.25 and could contain multiple components of similar intensities. This possible presence of multiple components was found in Figure 5.23, but the spatially resolved spectra shows no spatial differentiation or localisation of the different components present.

5.3 Summary

Throughout the chapter, comparisons were made with previous data sets. To facilitate these comparisons, tables showing consolidated data for surface Cu:Zn ratios, peak positions and their corresponding species are detailed below.

Table 5.6 – Consolidated surface Cu:Zn ratios for all environments and samples listed in this chapter

Control samples		Eccrine samples		Sebaceous samples	
Storage environment	**Cu:Zn ratio**	**Storage environment**	**Cu:Zn ratio**	**Storage environment**	**Cu:Zn ratio**
Ambient; Unpolished	1 : 0.25				
Ambient; Polished	1 : 1.12	Ambient	1 : 1.12	Ambient	1 : 0.58
Ambient; Fresh Polished	1 : 1.09	Ambient; fresh deposit	1 : 0.52		
Humid	1 : 0.63	Humid	1 : 1.20	Humid	1 : 0.87
Warm humid	1 : 0.77	Warm humid	1 : 0.39	Warm humid	1 : 0.11
Direct heat	1 : 18.6	Direct heat	1 : 9.58	Direct heat	1 : 11.2

From Table 5.6, the full range of surface Cu:Zn ratios can be seen. The ratio value is determined by one of two possibilities. The first is that the environment, rather than the presence of a fingerprint, dictates the samples surface Cu:Zn ratio. The second is that the effect of the fingerprint on the sample surface has a greater impact on the Cu:Zn ratio than the storage environment. Very few sample sets undisputedly belong solely to one of these classifications. An example is for samples exposed to direct heat (Bunsen flame). All samples in this category display ratios with far more zinc than copper present on the surface and yet there is still a fingerprint deposit effect as the two fingerprinted sample ratios are similar but distinctly different from the control sample.

As with the Cu:Zn ratios, XPS data for the samples is combined below. Again, the pattern present is the same two-fold hypothesis: which has the greater effect on sample surface species, the presence of a fingerprint or the storage environment.

Table 5.7 – Consolidated Zn $2p_{3/2}$ peak positions and peak identities

Control Samples			**Eccrine Samples**			**Sebaceous Samples**		
sample information	**B.E. position (eV)**	**Peak species**	**sample information**	**B.E. position (eV)**	**Peak species**	**sample information**	**B.E. position (eV)**	**Peak species**
Unpolished	1022.2	ZnO						
Polished	1021.8	Zn(0)	Ambient	1022.2	ZnO	Ambient	1022.5 1023.8	ZnOH $ZnCl_2$
Fresh Polished	1022.1	Zn(0) or ZnO	Ambient; fresh	1022.0	Zn(0) or ZnO			
Humid	1022.1	Zn(0) or ZnO	Humid	1022.1	Zn(0) or ZnO	Humid	1022.0 1024.0	Zn/ZnO $ZnCl_2$
Warm humid	1021.9	Zn(0)	Warm humid	1021.9	Zn(0)	Warm humid	1021.6	ZnO
Direct heat	1022.0	Zn(0) or ZnO	Direct heat	1022.0	Zn(0) or ZnO	Direct heat	1022.0	Zn(0) or ZnO

From Table 5.7, the similarities between eccrine fingerprinted samples and the control samples can be seen at all storage environments. In all cases, a single peak at 1022 ±0.2 eV is observed, this binding energy value is commonly reported as a typical value for both Zn(0) and ZnO species, making distinct identification difficult. With this single peak position being universally present, seemingly neither the presence of eccrine sweat nor storage environment has a considerable effect on the zinc species present. Conversely, the sebaceous fingerprinted samples have peak positions quite distinct from the eccrine and control samples for all storage environments, with the exception of exposure to direct heat, where a peak position at 1022.0 eV was found uniformly across all samples.

Table 5.8 – Consolidated Cu $2p_{3/2}$ peak positions and peak identities

Control Samples			Eccrine Samples			Sebaceous Samples		
sample information	**B.E. position (eV)**	**Peak species**	**sample information**	**B.E. position (eV)**	**Peak species**	**sample information**	**B.E. position (eV)**	**Peak species**
Unpolished	932.7	Cu_2O or CuO						
Polished	932.6	Cu_2O or CuO	Ambient	932.9	Cu(0)	Ambient	932.9 935.4	Cu(0) $Cu(OH)_2$
Fresh Polished	933.0 934.9	CuO, $Cu(OH)_2$	Ambient; fresh	932.9 935.4	Cu(0) $Cu(OH)_2$			
Humid	932.6 935.2	Cu_2O/Cu $Cu(OH)_2$	Humid	932.6 935.2	Cu_2O/Cu $Cu(OH)_2$	Humid	932.6 935.2	Cu_2O/Cu $Cu(OH)_2$
Warm humid	932.2	Cu_2O	Warm humid	932.4	Cu(I) as Cu_2O or CuCl	Warm humid	932.4	Cu(I) as Cu_2O or CuCl
Direct heat	933.3 935.2	CuO $Cu(OH)_2$	Direct heat	933.3 935.2	CuO $Cu(OH)_2$	Direct heat	933.8 932.6	CuO CuO/Cu(0)

The copper peak positions for the eccrine fingerprinted sample in Table 5.8 are affected more by the sweat deposit than environment when compared to the zinc data. At ambient conditions, the presence of fingerprint sweat in both sweat types has a greater affect than storage environment; this is also seen for samples stored in warm humid conditions. When the samples are stored in humid environments or exposed to direct heat, the environment has the greater impact on copper surface species present.

Table 5.9 – Consolidated C 1s peak positions and peak identities

Control Samples			Eccrine Samples			Sebaceous Samples		
sample information	**B.E. position (eV)**	**Peak species**	**sample information**	**B.E. position (eV)**	**Peak species**	**sample information**	**B.E. position (eV)**	**Peak species**
Unpolished	285.2	Alkyl						
Polished	285.2	Alkyl	Ambient	285.1 288.9	Alkyl Alkyl	Ambient	285.2 286.7 288.2 290.4	Alkyl Methyl C=O rings
Fresh Polished	285.8 291 288	Alkyl CH_3 C=O	Ambient; fresh	285.5	Alkyl			
Humid	285.0 289.7 288.5 286.2	Alkyl CO_3 C=O COOR	Humid	285.0 289.7 288.5 286.2	Alkyl CO_3 C=O COOR	Humid	285.5	Alkyl
Warm humid	285.0	Alkyl	Warm humid	285.0	alkyl	Warm humid	284.9 288.5	Alkane C=O
Direct heat	285.2	Alkyl	Direct heat	285.4	alkyl	Direct heat	285.2	Alkyl

The carbon components and compounds of sweat are varied between eccrine and sebaceous types. Whilst eccrine sweat does contain many carbon based components, such as carbonyls carboxylates and hydrocarbon chains, the main component of eccrine sweat is water (98%). Therefore, only traces of carbon products from sweat would be detectable on a sample surface and it is not surprising that carbon species for eccrine fingerprinted samples are similar to control samples in Table 5.9. Conversely, sebaceous sweat is mainly comprised of carbon containing compounds and includes the same functional groups mentioned for eccrine sweat as well as esters, ethers and aromatic rings. As can be seen in Table 5.9, the sebaceous species and peak positions for ambient conditions are distinctly different from the eccrine and control samples. However, in non-ambient conditions, the storage environment has affected the components present as peak positions are similar to eccrine and control samples.

Table 5.10 – Consolidated O 1s peak positions and peak identities

Control Samples			Eccrine Samples			Sebaceous Samples		
sample information	**B.E. position (eV)**	**Peak species**	**sample information**	**B.E. position (eV)**	**Peak species**	**sample information**	**B.E. position (eV)**	**Peak species**
Unpolished	530.6	CuO/Cu_2O						
Polished	532.2 530.5	H_2O/OH CuO or Cu_2O	Ambient	532.2 530.5	H_2O CuO or Cu_2O	Ambient	532.4 534.8 531.0	OH Ether $Cu(OH)_2$
Fresh Polished	530.2	ZnO/Cu_2O	Ambient; fresh	532.0	OH			
Humid	531.7 530.4	OH or $Cu(OH)_2$ CuO or Cu_2O	Humid	531.7 530.4	OH or $Cu(OH)_2$ CuO or Cu_2O	Humid	532.1 530.3	OH or H_2O CuO or Cu_2O
Warm humid	530.5	CuO	Warm humid	530.5	CuO	Warm humid	530.3	Cu_2O
Direct heat	530.8 532.2	$Cu(OH)_2$ H_2O	Direct heat	532.5 530.8 529.6	H_2O CuO $Cu(OH)_2$	Direct heat	530.8 532.2 529.5	$Cu(OH)_2$ H_2O CuO/ZnO

In Table 5.10 for the combined O 1s data, the environment has a large effect on peak positions due to the similarities between the different samples. The main variants expected would be relating to the sweat deposit, eccrine sweat is predominately water based and so a water signal would be expected for all eccrine fingerprinted samples. Sebaceous sweat would contain carbon based functional groups that incorporate oxygen, such as carbonyls, ethers, esters and carboxylates. However, very few of the expected species are seen in the data in Table 5.10. Eccrine fingerprinted samples have water peaks only at ambient stored and direct heated samples; sebaceous fingerprinted samples only show one carbon based functional group, being an ether peak, which is only seen at ambient storage environments. Whilst the sweat types do deviate from the peak positions for the control samples, peaks conclusively identifying sweat components are not discernible.

5.4 Conclusions

Polished substrates that appear brighter and are lighter in colour also have a lower amount of copper compared to duller and more gold-like substrates. Therefore this brighter appearance can be attributed to higher zinc levels, meaning the substrate is more susceptible to dezincification on local levels. Sebaceous sweat containing samples contain less surface zinc than eccrine sweat containing samples in the majority of environments that the samples were exposed to. Since eccrine sweat is 98% water it could allow dezincification to occur, but the zinc has not been fully removed from the top 10 nm of the sample surface. Also the fresh eccrine deposited sample exhibited similar surface Cu:Zn ratio values as sebaceous sample stored at ambient conditions. It should be noted that whilst the deposit was fresh, the sample was not. Furthermore, the fresh eccrine and sebaceous deposited samples exhibited surface Cu:Zn ratios similar to that of unpolished brass despite being deposited onto polished substrates.

Exposure to humid and warm humid environments caused a higher amount of surface copper to be present than at ambient conditions for the majority of samples. Additionally, sebaceous sweat containing samples had lower relative amounts of surface zinc than copper when compared to the eccrine sweat containing samples. Under humid conditions, the control sample exhibited the lowest amount of surface zinc, suggesting that surface rearrangement or dezincification could occur without hindrance from the sweat deposits, but if this was the case the water containing eccrine deposit would then also expect to yield a greater amount of copper than the sebaceous sample. The observed surface Cu:Zn ratios for the eccrine deposited sample were similar to those for ambient non-fingerprinted substrates for both ambient and humid conditions. This suggests that the eccrine sweat had little impact at ambient conditions and possibly preserved the surface at humid conditions. Exposure to direct heat by way of a Bunsen flame was the only environment that promoted zinc surface content;

the samples had a more silver-like appearance than previous ones and also had much greater zinc content. In these conditions, the sweat deposits can be seen to be affecting the surface composition, since the sweat deposited samples had half the relative amount of zinc than the control sample. As the surface Cu:Zn ratios for the fingerprinted samples were taken over a fingerprinted area, where the ridges and furrows cover approximately equal areas, this means that half the studied area contains fingerprinted sections, whereas the other half is equivalent to non-fingerprinted or control-like samples. Therefore, one could suggest that as the surface Cu:Zn ratio for these fingerprinted samples are midway between ambient fingerprinted and direct heated control samples; consequently, this ratio is the result of two types of surface environments being present. Where there is no fingerprint trace, the surface is characteristic of non-fingerprint directly heated samples. However, where fingerprint material is present, the surface ratio is more characteristic of fingerprinted ambient samples and thus the surface copper species has been preserved by the sweat deposit.

The data for the zinc peak positions were similar for all eccrine and control samples, suggesting that the eccrine sweat had little impact on the surface zinc compounds. Only sebaceous fingerprinted samples had Zn $2p_{3/2}$ peaks significantly higher than the 1022 eV values reported for the majority of samples, regardless of storage conditions. In these two instances the sebaceous fingerprinted samples twice reported values above 1023 eV, a region associated only with zinc halide compounds. This is unexpected since chloride ions are found only in eccrine sweat and not in sebaceous sweat, their presence here could only come from traces of eccrine sweat still present on the fingerprint prior to rubbing in the sebaceous rich regions of the body (hair line and nose), yet these values were not seen for samples containing eccrine sweat. Like the zinc values, the reported values for copper $2p_{3/2}$ regions were largely the same, despite the different environments used. The binding energy difference between non-fingerprinted and fingerprinted samples under ambient conditions was a binding energy

increase of several electron volts, although humid environments produced similar binding energy values to those for the non-fingerprinted ambient samples. After exposure to direct heat, the copper surface species appeared to change, with higher binding energy values reported for the peaks present. These copper surface species were not the same as ones found at ambient conditions, this suggests that the increased temperatures to which the samples were exposed were significant enough to cause a change in the surface copper species present, as well as decreasing its presence on the sample surfaces.

The peaks present in the organic spectra did not always provide as much useful information as those found in the metallic spectra. Residual signals for carbon were seen throughout the samples, around a binding energy value of 258.2 eV. The carbon spectrum seen for sebaceous sweat under ambient conditions is what one would expect for sebaceous sweat under all conditions. However, both heat and humidity seem to alter the carbon compounds found despite them being of an oily nature. The carbon spectra for both eccrine sweat and the control samples were generally the same. This is not surprising since eccrine sweat consists of mostly water or inorganic compounds. The spectra for oxygen were expected to generally yield at least two distinct peaks, with one each for copper and zinc oxides and at least one additional one for oxygen-containing compounds in the sweat deposits. For eccrine deposits, a signal for water compounds was found in far fewer environments than expected. Either the water present in the sweat was interacting with the metals in the substrate and/or it had evaporated under UHV conditions.

The spatial profiles have shown that localisation of the elements observed in non-spatial spectra does occur. The spatial profiles can show this localisation and separation clearly but cannot always provide as clear information relating to localised oxidation state changes. This is potentially the result of sacrificing binding energy resolution to obtain clearer lateral

resolution and collecting data on a narrower area. The copper and zinc compounds can be seen to have much lower intensity in sites where carbon is present, suggesting that the remaining sweat deposit is sufficiently thick to block the metal signals. Whilst oxygen can be seen to change intensity laterally, this is not always linked exclusively to the fingerprinted or non-fingerprinted regions. As oxygen naturally exists in both, this is not surprising.

Under ambient conditions, the differences present in O 1s and C 1s spectra between the sweat types could allow one to identify the type of sweat present. Sebaceous sweat is easier to characterise than eccrine sweat, due to eccrine sweat being predominately water based, determining regions containing fingerprint sweat residue and non-fingerprint areas is possible by spatially resolving the spectra. Even after exposure to direct heat, the surface species of fingerprinted samples differ from control samples and spatially resolving surface species is still possible. From the different species observed on the sample surfaces between control and fingerprinted samples, there is strong indication that the sweat interaction causes chemical changes to the surface.

5.5 References

1. J. W. Bond, *J. Forensic Sci.*, 2008, **53**, 1344-1352.
2. J. W. Bond, *J. Forensic Sci.*, 2008, **53**, 812-822.
3. J. W. Bond, *J. Phys. D-Appl. Phys.*, 2008, **41**, 125502.
4. J. W. Bond, *J. Forensic Sci.*, 2009, **54**, 1034-1041.
5. J. W. Bond, *Rev. Sci. Instrum.*, 2009, **80**, 075108.
6. J. W. Bond and C. Heidel, *J. Forensic Sci.*, 2009, **54**, 892-894.
7. O. Jensen and E. Nielsen, *Acta Derm.-Venereol.*, 1979, **59**, 139-143.
8. S. Maroie, G. Haemers and J. J. Verbist, *Appl. Surf. Sci.*, 1984, **17**, 463-467.
9. L. Ley and M. Cardona, *Photoemission in Solids II: Case Studies*, Springer-Verlag, Berlin, 1979.
10. C. D. Wagner, W. M. Riggs, L. E. Davis and J. F. Moulder, *Handbook of x-ray photoelectron spectroscopy: a reference book of standard data for use in x-ray photoelectron spectroscopy*, first edn., Physical Electronics Division, Perkin-Elmer Corp., 1979.
11. D. Briggs and P. Seah, *Practical Surface Analysis: Auger and X-ray photoelectron spectroscopy*, Wiley, 1990.
12. N. S. McIntyre and M. G. Cook, *Anal. Chem.*, 1975, **47**, 2208-2213.
13. T. L. Barr, *J. Phys. Chem.*, 1978, **82**, 1801-1810.
14. P. Marcus and M. E. Bussell, *Appl. Surf. Sci.*, 1992, **59**, 7-21.
15. H. M. Liao, R. N. S. Sodhi and T. W. Coyle, *J. Vac. Sci. Technol. A-Vac. Surf. Films*, 1993, **11**, 2681-2686.
16. L. S. Dake, D. E. King and A. W. Czanderna, *Solid State Sci.*, 2000, **2**, 781-789.
17. T. L. Barr, *J. Vac. Sci. Technol. A-Vac. Surf. Films*, 1991, **9**, 1793-1805.
18. V. Wiertz and P. Bertrand, in *ICPSI - 2, Polymer-Solid Interfaces : From Model to Real Systems*, eds. J.J. Pireaux, J. Delhalle and P. Rudolf, Universitaires de Namur, Namur, 1998, pp. 485-499.
19. D. T. Clark and H. R. Thomas, *J. Polym. Sci. Pol. Chem.*, 1978, **16**, 791-820.
20. N. Moncoffre, G. Hollinger, H. Jaffrezic, G. Marest and J. Tousset, *Nucl. Instrum. Methods Phys. Res. Sect. B-Beam Interact. Mater. Atoms*, 1985, **7-8**, 177-183.
21. P. Sundberg, R. Larsson and B. Folkesson, *J. Electron Spectrosc.*, 1988, **46**, 19-29.
22. J. Charlier, V. Detalle, F. Valin, C. Bureau and G. Lecayon, *J. Vac. Sci. Technol. A-Vac. Surf. Films*, 1997, **15**, 353-364.
23. D. Rats, L. Vandenbulcke, R. Herbin, R. Benoit, R. Erre, V. Serin and J. Sevely, *Thin Solid Films*, 1995, **270**, 177-183.
24. P. Y. Jouan, M. C. Peignon, C. Cardinaud and G. Lemperiere, *Appl. Surf. Sci.*, 1993, **68**, 595-603.
25. S. Delpeux, F. Beguin, R. Benoit, R. Erre, N. Manolova and I. Rashkov, *Eur. Polym. J.*, 1998, **34**, 905-915.
26. C. Bichler, T. Kerbstadt, H. C. Langowski and U. Moosheimer, *Surf. Coat. Technol.*, 1997, **97**, 299-307.
27. R. Larsson, B. Folkesson and J. Sadlej, *Spectrosc. Lett.*, 1991, **24**, 671-680.
28. A. M. Beccaria, G. Poggi and G. Castello, *Brit. Corros. J.*, 1995, **30**, 283-287.
29. W. P. Yang, D. Costa and P. Marcus, *J. Electrochem. Soc.*, 1994, **141**, 2669-2676.
30. V. I. Nefedov, D. Gati, B. F. Dzhurinskii, N. P. Sergushin and Y. V. Salyn, *Zhurnal Neorg. Khimii*, 1975, **20**, 2307-2314.
31. J. C. Otamiri, A. Andersson, S. L. T. Andersson, J. E. Crow and G. Ye, *J. Chem. Soc.-Faraday Trans.*, 1991, **87**, 1265-1271.
32. E. Agostinelli, C. Battistoni, D. Fiorani, G. Mattogno and M. Nogues, *J. Phys. Chem. Solids*, 1989, **50**, 269-272.

33. G. Schon, *Surf. Sci.*, 1973, **35**, 96-108.
34. T. Robert, M. Bartel and G. Offergeld, *Surf. Sci.*, 1972, **33**, 123-130.
35. C. E. Dube, B. Workie, S. P. Kounaves, A. Robbat, M. L. Aksu and G. Davies, *J. Electrochem. Soc.*, 1995, **142**, 3357-3365.
36. L. S. Dake, D. R. Baer and J. M. Zachara, *Surf. Interface Anal.*, 1989, **14**, 71-75.
37. R. S. Ramotowski, in *Advances in Fingerprint Technology*, eds. H. C. Lee and R. E. Gaensslen, CRC Press, London, 2nd edn., 2001, pp. 64-95.
38. J. L. Droulas, T. M. Duc and Y. Jugnet, *Le Vide, les couches minces*, Société française du vide, 1991.
39. N. M. D. Brown, J. A. Hewitt and B. J. Meenan, *Surf. Interface Anal.*, 1992, **18**, 187-198.
40. A. S. Lim and A. Atrens, *Appl. Phys. A-Mater.*, 1990, **51**, 411-418.
41. B. Stypula and J. Stoch, *Corros. Sci.*, 1994, **36**, 2159-2167.
42. G. L. Thomas, *J. Phys. E. Sci. Instrum.*, 1978, **11**, 722-731.
43. E. A. Leone and A. J. Signorelli, in *A Guide to Materials Characterisation and Chemical Analysis*, ed. J. P. Sibilia, Wiley-VCH, New York, 2nd edn., 1996, pp. 221-235.
44. P. W. Atkins, *Physical Chemistry*, 5th edn., Oxford University Press, Oxford, 1995, pp. 617-619.
45. M. G. Fontana, McGraw-Hill Book Co, Singapore, Int. edn., 1987, pp. 240-243.
46. D. S. Campbell, H. J. Leary, J. S. Slattery and R. J. Sargent, *IBM General Technology Division (ed.), Essex Junction, VT 05452,* , 1981, 328.
47. G. Fierro, G. M. Ingo and F. Mancia, *Corrosion*, 1989, **45**, 814-823.
48. W. Kowbel and C. H. Shan, *Carbon*, 1990, **28**, 287-299.
49. J. J. Pireaux, M. Chtaib, Q. T. Le and R. Caudano, *Le Vide, les couches minces*, Société française du vide, 1991.
50. S. Contarini, S. P. Howlett, C. Rizzo and B. A. De Angelis, *Appl. Surf. Sci.*, 1991, **51**, 177-183.
51. L. N. Boi, M. Thompson, N. B. McKeown, A. D. Romaschin and P. G. Kalman, *Analyst*, 1993, **118**, 463-474.
52. I. Olefjord, B. Brox and U. Jelvestam, *J. Electrochem. Soc.*, 1985, **132**, 2854-2861.
53. M. G. Fontana, McGraw-Hill Book Co, Singapore, Int. edn., 1987, pp. 39-152.
54. S. Jin and A. Atrens, *Appl. Phys. A-Mater.*, 1987, **42**, 149-165.
55. Y. Kaneko and Y. Suginohara, *J. Jpn. Inst. Met.*, 1977, **42**, 285.

Chapter Six:

Surface Analysis of Sweat Deposit on Brass Substrate Following Post-Deposition Treatments

6.1 Outline

The data presented in Chapters 4 and 5 focused primarily on fingerprint deposits on polished brass substrates with no external surface interactions aside from storage environments. However, in some circumstances the fingerprints may have been altered after deposition and before examination. This could be from attempts at removal to hide their presence or as a result of being exposed to the elements. In the former case, one may try to wipe clean a contacted surface or, on more mobile items, one may try to wash away the evidence of contact. Additionally, the removal of fingerprints is not always related to crime or evidence. In laboratory studies of fingerprints, a virgin or clean surface is required to irrefutably study the effects on fingerprints on a variety of surfaces. If one cannot ensure that the surface is clean, then all conclusions drawn from the samples in question are disputable. Patterson *et al.*[1] investigated this aspect on a visual level, examining the relative ease or difficulty in removing fingerprints from samples, whilst the majority of removal treatments inhibited the recovery of the fingerprints by conventional techniques, the fingerprint could still be visualised by the application of heat.

The sample surface finish is expected to have an impact on the visual nature of the fingerprint, as a smooth polished substrate would have a uniform surface finish with regards to colouration and optical reflection. An unpolished substrate may not have a uniform colouration and will also have visible markings from manufacturing processes which may adversely affect surface optical properties. Whilst one may expect all evidence relating to brass substrate to be of an unpolished nature, with polished substrates used only in laboratory studies for ease of examination, this is not the case. Brass has many applications, and whilst these will not all use the same alloy composition or ratio of copper to zinc, they will exhibit similar properties with regards to their interaction with fingerprints under certain conditions. Polished brass is routinely used for furnishings, musical instruments and door knobs as well as

latches and locks, whereas unpolished brass is used for cartridge cases of a range of ammunition as well as pipes used in plumbing.

In this section, fingerprinted brass substrates are examined using a variety of techniques to study the effects that different environments and surface treatments will have on both the visual nature of the fingerprint as well as the physical and chemical changes occurring.

6.2 Results

6.2.1 Polished and Unpolished Brass Substrates

Although both unpolished and polished brass substrates can be found as evidence, polished substrates have the advantage of easier detection of fingerprints or changes to the surface, whether by eye or by microscopic measurements, due to their more uniform surface appearance. Below in Figure 6.1 is a microscope image showing several ridges of a fingerprint but the two halves of the brass substrate have been treated differently.

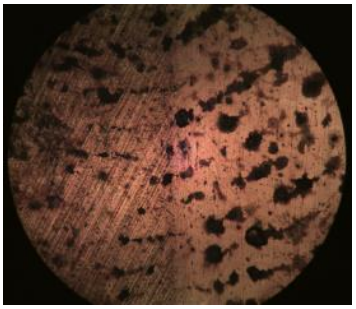

Figure 6.1 – Optical microscope image of an eccrine based fingerprint on brass substrate. Brass substrate on the left side was cleaned prior to deposition; the right side was polished as well as cleaned. Following deposition, the sample was stored at ambient conditions for 5 weeks and then subjected to water and acetone rinsing followed by being placed in an oven set to 100°C and then washed with warm water detergent.

In Figure 6.1, the fingerprint ridges can be seen as the dark curving lines flowing horizontally across the image. These ridges are still visible by eye despite attempts at removing them by

various washing treatments as well as heat treatment. The brass substrate was not uniformly prepared prior to the fingerprint deposit; one side was subjected to polishing whilst the other was left unpolished. In the left side on Figure 6.1, diagonally lying marks can be observed; these are the remnants of the manufacturing process used to generate the discs. Upon further study of Figure 6.1, two main aspects can be considered. The first is that the appearance of the brass on either side is vastly different; the polishing produces a lighter coloured background as well as being unperturbed by the manufacturing marks. This difference creates a better optical contrast for fingerprint deposit on polished rather than unpolished substrates. The second aspect is that the amount of observable fingerprint deposit differs between the polished and unpolished sides of the substrate. The left unpolished side has narrower black bands than on the right polished side; additionally they are less continuous and it is harder to follow the ridge lines. The cause of this difference in the appearance is not due to the fingerprint deposit itself, since it was deposited on both regions at the same time, comprising the same composition and being of eccrine sweat. Therefore, this visual difference of the ridges can be attributed to the interaction between the sweat deposit and the brass substrate. As the ridges are clearer on the right (polished) side of Figure 6.1, the sweat deposit on polished surfaces must therefore interact more strongly than on unpolished surfaces and subsequently more strongly resists attempts at removing the sweat deposit or fingerprint image. Therefore the question arises as to whether this effect observed is related to the chemical or physical surface differences in the polished and unpolished substrates. Additionally, one must also consider how washing and heat treatments affect fingerprinted substrates both chemically and physically with a view to potential post-treatment detection methods.

6.2.2 Fingerprints on Unpolished Brass Substrate

Fingerprints on unpolished brass substrates subjected to post-fingerprint deposition treatments are not as visibly apparent as on polished brass substrates as outlined above in

section 6.2.1. In this section, the effects of various post-deposition storage environments and treatments of eccrine and sebaceous sweat on brass substrates are examined.

If one were to intentionally remove fingerprints from an item, whether it is for sample preparation in a laboratory or related to criminal activity, in essence the procedure would be similar. Such removal techniques could include wiping or rinsing with a degreasing solution, such as White Spirit or acetone, or more abrasive cleaning including detergent or removal by heat. These treatments may affect the visual appearance of the print and/or its development by conventional enhancement techniques, which interact with either the substrate or the sweat deposit.

Storage of fingerprinted substrates in humid conditions produces a more visible print, as outlined in Chapter 4; also, aged fingerprints are more visually apparent than fresh deposits. In Figure 6.2, below, is a comparison of printed samples before and after post-deposition treatment.

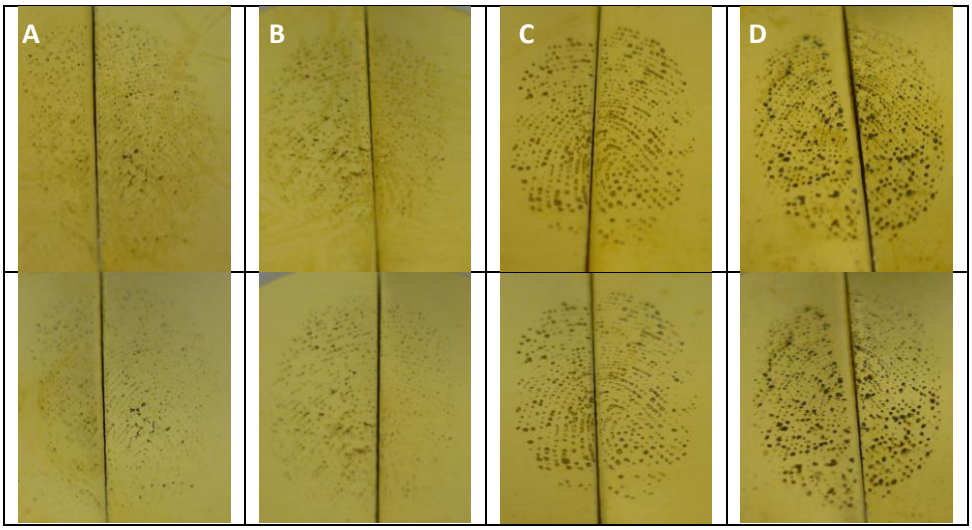

Figure 6.2 – Photographs of eccrine fingerprints on brass substrate, the top row is immediately prior to treatment with the bottom row being post-treatment. In each case, the left section was subjected to acetone rinse whilst the right was subjected to washing with warm water and detergent. ***A)*** *stored at ambient for 4 days;* ***B)*** *stored at ambient for 4 days;* ***C)*** *Stored at ambient for 9 days;* ***D)*** *stored in humid environment at ambient temperature for 9 days.*

In all four cases, the fingerprints on unprinted brass seen in Figure 6.2 are still detectable by eye and have not been fully removed by acetone or warm soapy water, although the remaining marks are unaffected by enhancement techniques such as black powder. From Figure 6.2C and D, a fingerprint mark can be seen both before and after washing, 9 days undisturbed in ambient produced a fingerprint that survived both washing treatments with only some visual fading occurring with the post treatment mark still having visible ridge details and features. The fingerprints that were aged only 4 days (A and B) were not as visible as the fingerprints aged 9 days prior to washing, but like C and D, these also faded slightly post-treatment. The fingerprint mark in B survived treatment by acetone better than washing with detergent and remnants of the fingerprint can be seen as a blemish to the brass substrate on the right side of the image.

From Chapter 4, warm humid conditions were shown to produce a more visual fingerprint on samples than storage at ambient conditions. With there still being visible remains of the

fingerprint after washing, there is the potential for a revival of the fingerprint by exposure to warm humid conditions.

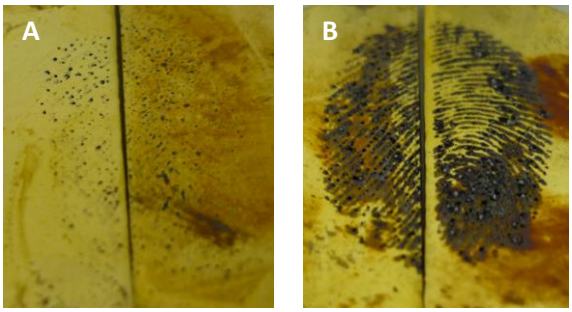

Figure 6.3 – Photographs of fingerprints on brass substrate. ***A)*** *same sample as in Figure 6.2A but subsequently subjected to 60°C and humid conditions for 5 days;* ***B)*** *after fingerprint deposition, immediately placed in a humid environment at 60°C.*

A comparison of fingerprinted samples exposed to warm humid environments is shown above in Figure 6.3. The right image (Figure 6.3B) has a much more obvious mark, the ridge lines are darker in colour and the whole mark is much more apparent, however this sample was not subjected to any treatment between being printed and placed in the above mentioned environment. In Figure 6.3A, a faint fingerprint can be observed: the ridge detail is thinner and less apparent than in Figure 6.3B, but an elliptical shape can be seen nonetheless. Being subjected to warm humid conditions post-washing has increased the visual nature when compared back to Figure 6.2A, thus confirming that despite washing, visual enhancement is still possible. The effect that these conditions had on the substrate is interesting; the warm humid conditions have darkened the substrate surface of the detergent wash far more than the acetone treated side, with a near uniform brown colouring. These brown marks can also be seen in the non-washed sample as well, but as large spots rather than a uniform covering. The explanation for this being observed on the washed sample could be that, despite being dried post-washing, some surface water remained and aided the dezincification process of the brass substrate. With the resultant colour changes to both the fingerprint ridge markings as well as

the substrate colour, it is likely that a change of chemical composition has occurred. Additionally, it is unclear as to whether or not the increased visibility of the ridge in the washed sample was brought about by remaining sweat residue, despite the washing, or a continuation of the process which started prior to removal of the sweat residue. In order to examine the possibilities, XPS data for the samples in Figure 6.3 are presented.

Table 6.1 – Surface ratio of copper to zinc for unpolished fingerprinted brass substrates exposed to different conditions

Sweat type	Post-deposition treatment	Ratio of Cu:Zn*
Sebaceous	Humid environment at 60°C for 5 days then washed in warm water and detergent	1 : 0.27
Eccrine	Ambient conditions for 4 days followed by detergent wash in warm water and then humid environment at 60°C for 5 days and washed again in warm water and detergent	1 : 0.39

Both Cu:Zn ratios in Table 6.1 show a far higher proportion of surface copper than zinc, when compared to the untreated samples in Chapter 5, the ratios are similar to those for unprinted unpolished substrate stored in ambient conditions (1:0.25) and that for polished eccrine subjected to 75°C in a humid environment (1:0.39). The samples in Table 6.1 were treated slightly differently, after fingerprinting; the first was placed immediately in a humid environment at 60°C whereas the second was first stored at ambient conditions for 4 days before being placed in the same warm and humid environment, with both being in this later environment for a period of 5 days. With the samples being unpolished and cleaned just prior to fingerprinting, it is unclear whether the differences observed in the ratio values are due to different surface compositions prior to fingerprinting or due to the difference in post fingerprinting treatment.

* The surface ratio of Cu:Zn is calculated as specified in the experimental section. The bulk composition is 68%:32% (1:0.47)

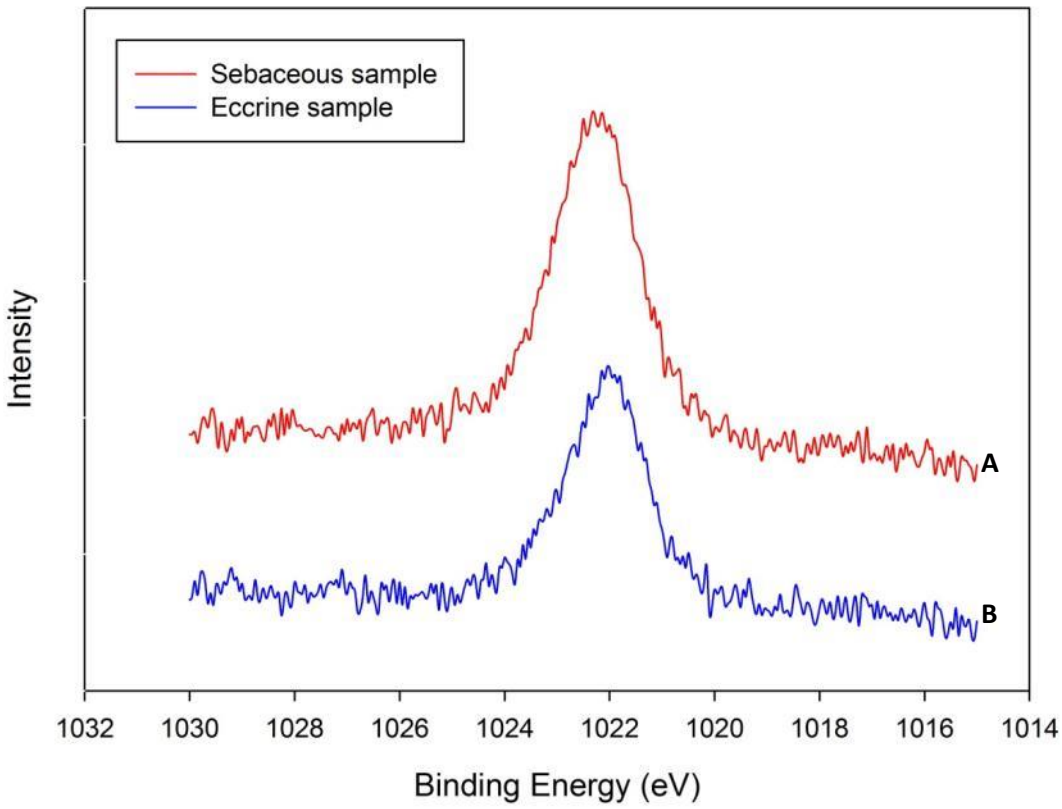

Figure 6.4 – XPS Zn $2p_{3/2}$ spectra of fingerprinted unpolished brass substrates. ***A)*** *sebaceous fingerprint stored in a humid environment at 60°C for 5 days then washed in warm water and detergent;* ***B)*** *eccrine fingerprint stored at ambient conditions for 4 days followed by detergent wash in warm water and then humid environment at 60°C for 5 days and washed again in warm water and detergent.*

Due to the Cu:Zn ratios reported above (Table 6.1), the XPS signal for zinc was fairly weak, hence the non-smooth sides seen on the peak profiles in Figure 6.4. Both peaks represent single identities for a Zn component at *ca.* 1022.1 eV, being characteristic of either Zn(0) or ZnO[2-4], however due to the poor separation of zinc oxidation states by XPS[5-7], it cannot be conclusively determined which is dominant, although since the zinc product is on/near the substrate surface, ZnO is intuitively more likely.

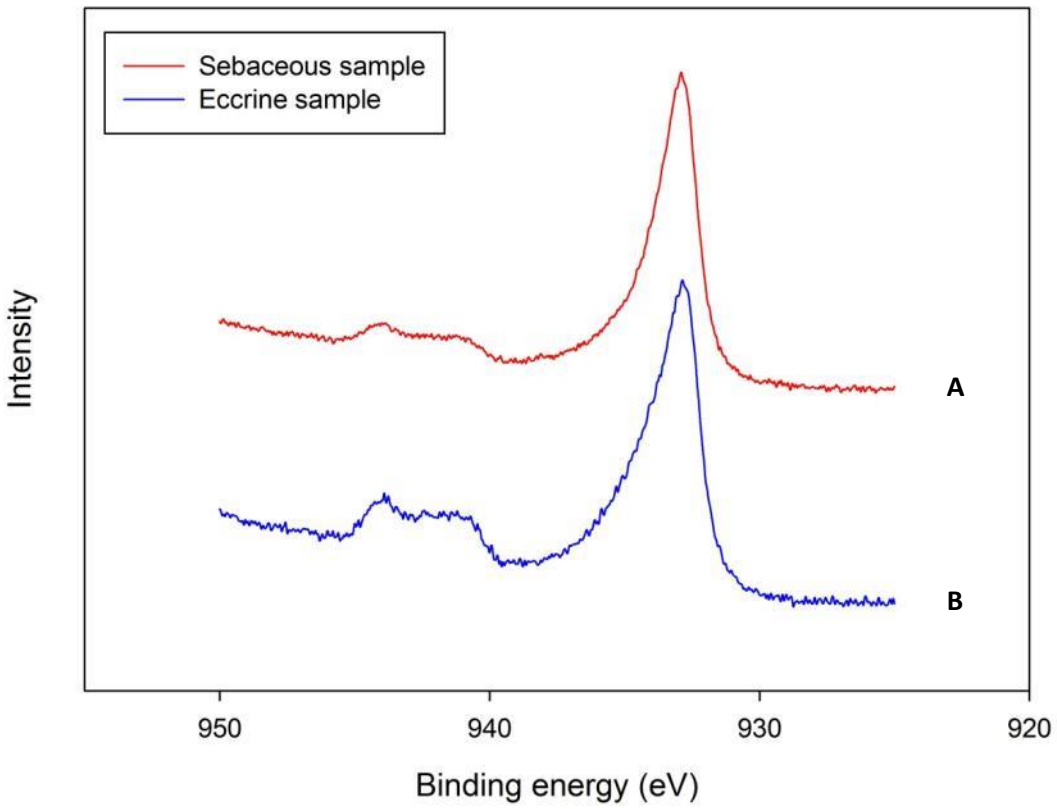

Figure 6.5 – XPS Cu $2p_{3/2}$ spectra of fingerprinted unpolished brass substrates. ***A)*** *sebaceous fingerprint stored in a humid environment at 60°C for 5 days then washed in warm water and detergent;* ***B)*** *eccrine fingerprint stored at ambient conditions for 4 days followed by detergent wash in warm water and then humid environment at 60°C for 5 days and washed again in warm water and detergent.*

Although the Cu $2p_{3/2}$ peak shapes in Figure 6.5 are similar, the energy signals responsible are slightly different. Figure 6.5A has two peaks at 933.9 eV and 932.9 eV attributable to CuO[8] and Cu(0)[2, 9, 10] respectively; both of these signals were commonly found on polished samples for various storage environments. Those found for Figure 6.5B were at 933.2 eV and 932.7 eV, in size order, these are CuO[2] and Cu(0)[2, 9, 10] respectively. In both cases, the Cu(0) signal is probably from the copper lying just below the sample surface. The CuO peak was also seen in the unpolished sample from chapter 5.

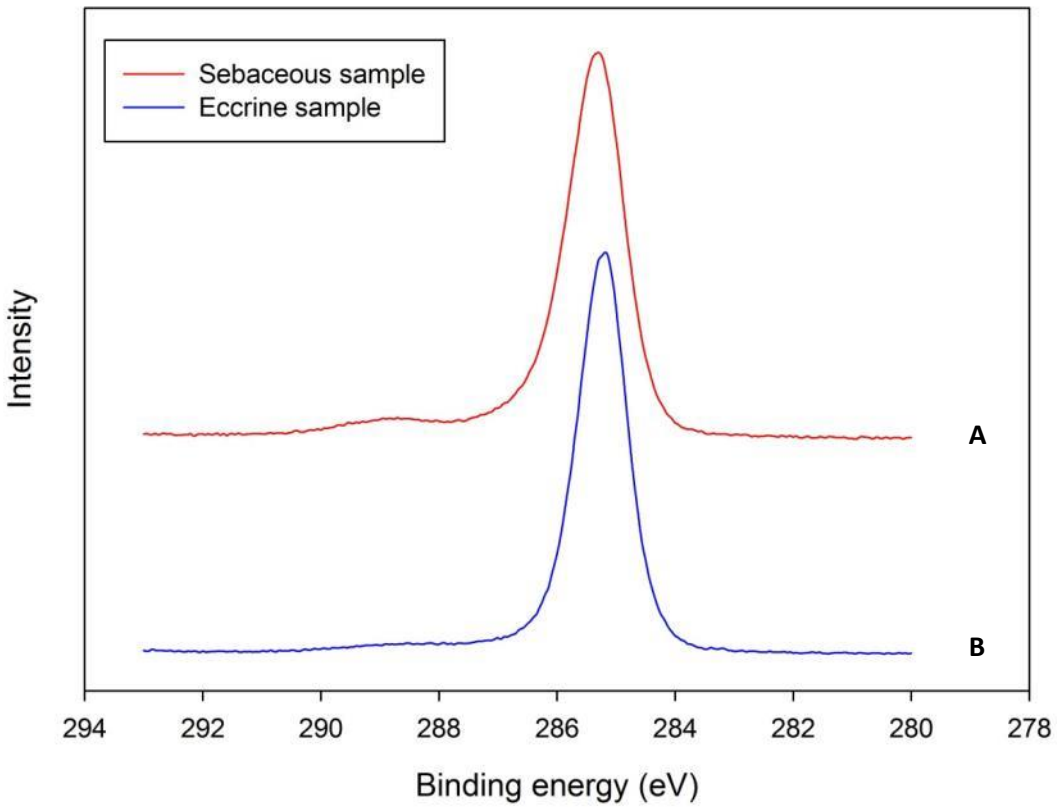

Figure 6.6 – XPS C 1s spectra of fingerprinted unpolished brass substrates. ***A)*** *sebaceous fingerprint stored in a humid environment at 60°C for 5 days then washed in warm water and detergent;* ***B)*** *eccrine fingerprint stored at ambient conditions for 4 days followed by detergent wash in warm water and then humid environment at 60°C for 5 days and washed again in warm water and detergent.*

The main prominent signal seen in the C 1s spectra (Figure 6.6) is at approximately the same binding energy position in both cases at *ca.* 285.3 eV; this binding energy is typical of hydrocarbons. Aside from this peak, very little else is present. There is a slight bump seen between 290 eV and 288 eV for the sebaceous sample, but of too low intensity to accurately determine the species responsible for it. The spectra here would suggest that the washing treatment has removed the sweat from the sample surface and therefore the visible fingerprint image must be due to at least one of the several oxidation states of copper identified above (Figure 6.5).

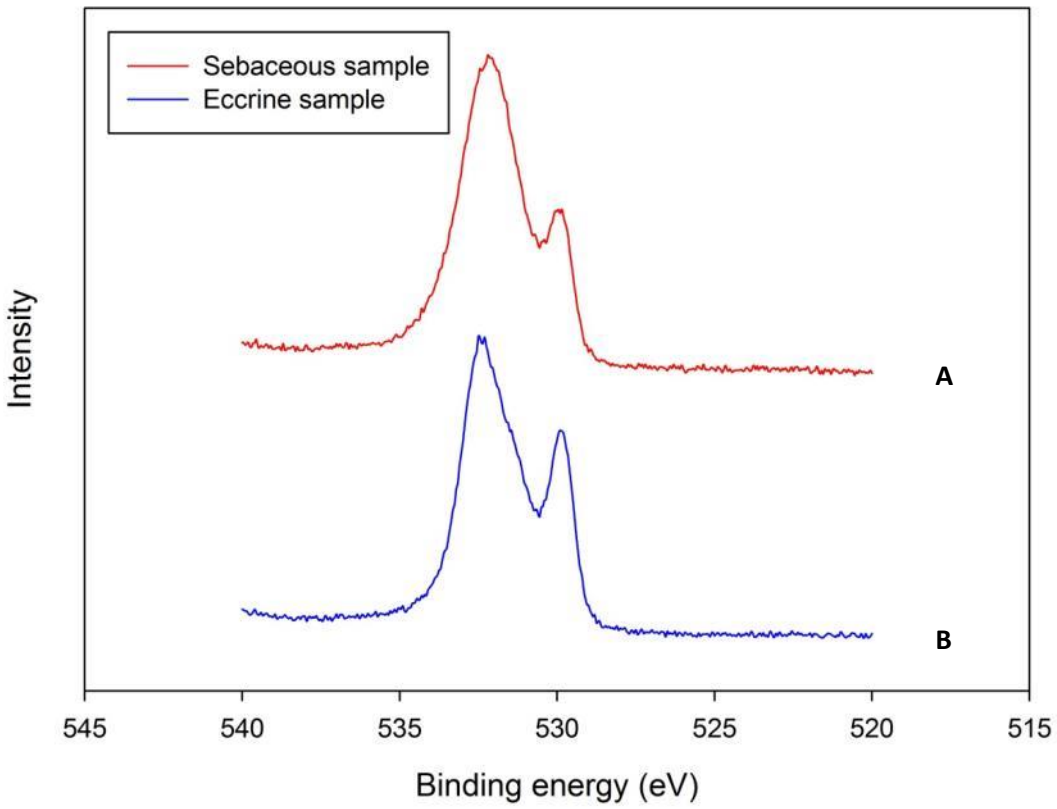

Figure 6.7 – XPS O 1s spectra of fingerprinted unpolished brass substrates. ***A)*** *sebaceous fingerprint stored in a humid environment at 60°C for 5 days then washed in warm water and detergent;* ***B)*** *eccrine fingerprint stored at ambient conditions for 4 days followed by detergent wash in warm water and then humid environment at 60°C for 5 days and washed again in warm water and detergent.*

Despite the outwardly similar shapes seen in the O 1s spectra of Figure 6.7, the two samples have distinctly different products responsible for them. The larger peak in Figure 6.7A is at 532.1 eV and is that of H_2O[13] or OH[14-16]. The main peak in Figure 6.7B is made of two different signals at 531.9 eV and 532.6 eV, which are OH[14-16] and H_2O[15, 17] species. The smaller peak is found at 529.8 eV and is that of ZnO[8]. Aside from this last peak identification, there are no detectable peaks in the range between 530 eV and 531 eV, which is the typical energy range one would expect to find copper oxide products[2, 8, 11, 18-23], whereas the zinc oxides are generally found slightly either side of this but still not encompassed by the peak values above.

6.2.3 Eccrine Fingerprints on Polished Brass Substrate at Ambient Conditions

Fresh eccrine deposit on most surfaces is a latent (invisible) mark. Even after several days the fingerprint is not always visible, but the application of heat and humidity can still reveal the fingerprint (chapter 4, section 4.2.5). This natural enhancement is not unique to polished brass substrates and is also applicable to unpolished ones (chapter 4, section 4.2.1). The image below (Figure 6.8) shows the development of a latent eccrine print to visible one by exposure to a warm humid environment.

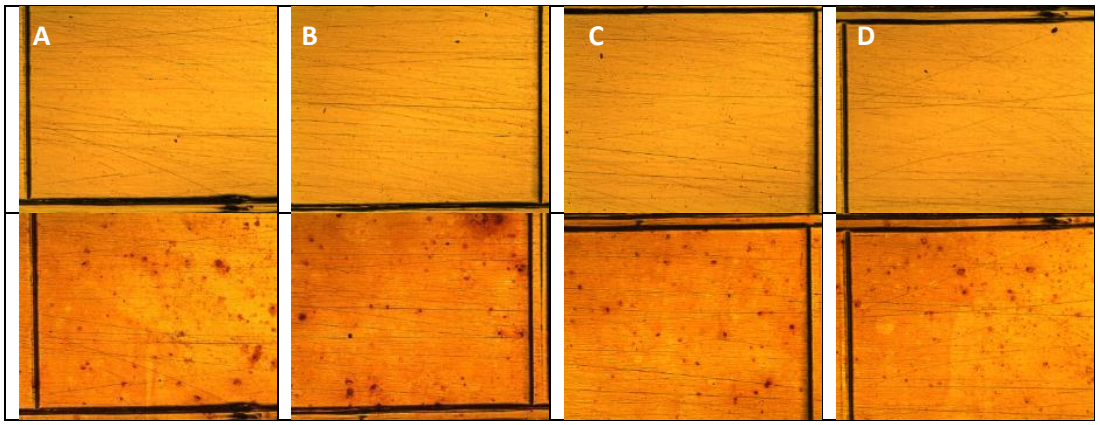

Figure 6.8 – Optical microscopy images of four different areas of a fingerprint on brass substrate; top row is after 7 days stored at ambient conditions; bottom row is the same area following exposure to 80°C and humid conditions for one hour.

Although distinct ridge lines may not be observable in the microscopy images of Figure 6.8, an obvious visual change to the sample surface has occurred. The majority of the sample has darkened slightly and, from the findings in chapter 5, this suggests an increase in surface copper content. Additionally, a seemingly random collection of small dark dots can be seen: these are the beginnings of the formation of the ridge lines which comprise the fingerprint. What this collection of images portrays is that eccrine deposit can persist as a latent mark for a considerable amount of time but can still be *revived* by warm and humid conditions to show fingerprint details.

As with the eccrine fingerprint unpolished samples in Figure 6.2, polished samples are also affected by post-deposition treatments such as washing processes. Below are a series of DHM images showing the change caused to small sections of ridges by washing the samples.

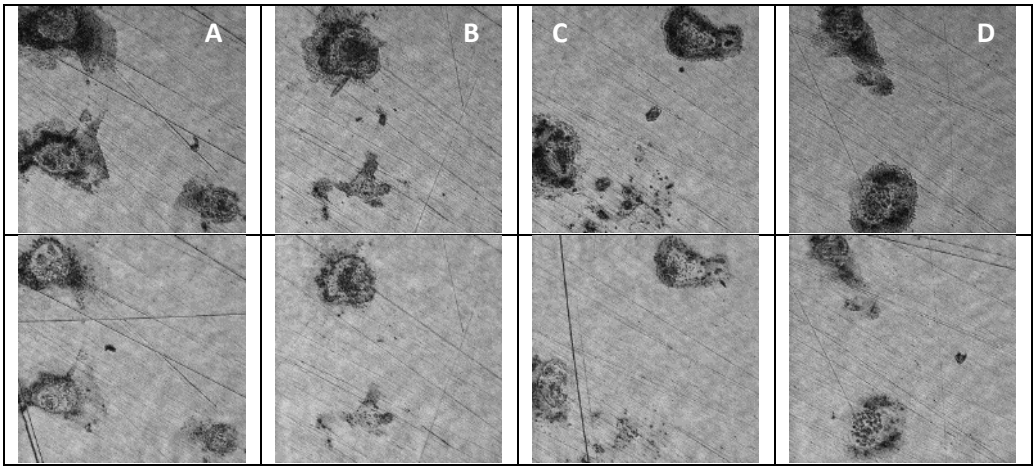

Figure 6.9 – DHM intensity images 4 different areas of an eccrine fingerprint deposit on polished brass substrate; top row is after 8 days at ambient conditions; bottom row are the same areas but after the sample was washed in warm water with detergent. All images are 450 µm wide.

The features in Figure 6.9 may not be recognisable as fingerprint ridges, but they are small sections of them. In each case the amount of material found is reduced but not fully removed by washing in warm soapy water, thus showing the persistent nature of the sweat residue. The core shape of the features, seen as darker marks in the top image, remain after the washing procedure but as less dense surface material. The lighter material stretching and filling these core features is reduced to almost unobservable levels by the washing process.

If a longer time frame was presented for the maturing of the fingerprint, one would expect the undisturbed mark to be visible, as seen in Chapter 4, and if this mark was more visible, one would expect it to also be more resilient to remove based upon the images in Figure 6.8 and Figure 6.9. The fingerprinted sample featured below was aged for 35 days before attempts at removing the deposit were made.

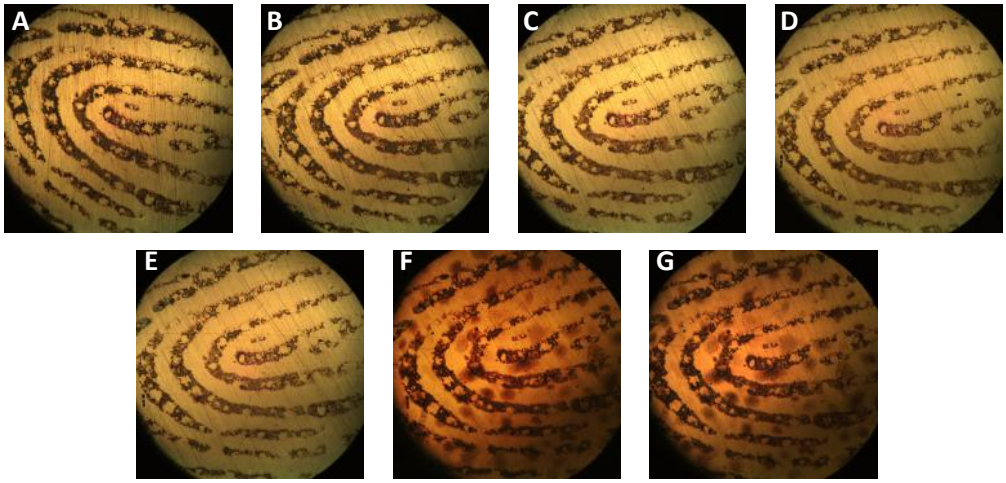

Figure 6.10 – Optical microscope images of an eccrine fingerprint core pattern on polished brass substrate. ***A)*** *after 35 days at ambient conditions;* ***B)*** *after wiping with blue paper towel;* ***C)*** *after several rinses with acetone;* ***D)*** *after several rinses with warm water;* ***E)*** *after washing in warm water with detergent;* ***F)*** *after being placed in a humid environment at 80°C for one hour;* ***G)*** *a further two weeks at ambient condition following the heat and humidity environment.*

From Figure 6.10, very little change can be seen going from an undisturbed eccrine fingerprint to one that has been treated in four different ways (images A to E). Post-washing *revival* created a better visual contrast between the ridges and the substrate but also introduced new features in between the ridges, seen as dark brown blemishes. These are not dark or large enough to be confused with sections of ridges but do distract the eye away from the clearer ridges pre-*revival*. Allowing a further two weeks after the treatments before re-examining yielded no visually noticeable changes suggesting that the combination of washing treatments followed by heat treatment has effectively quenched further visualisation at ambient conditions. However, this lack of apparent change was not observed when imaged using the AFM, as shown below.

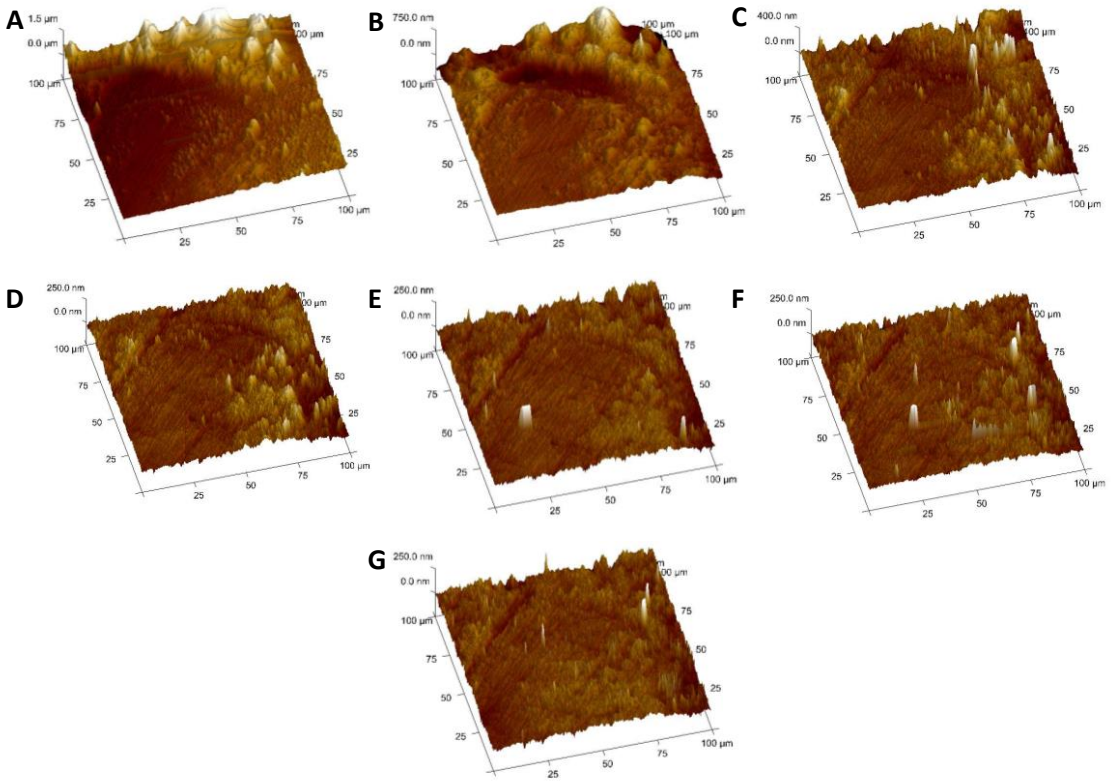

Figure 6.11 – AFM topographical images of an edge of a ridge section of the eccrine deposited fingerprint seen in Figure 6.10. ***A)*** *after 35 days at ambient conditions;* ***B)*** *after wiping with blue paper towel;* ***C)*** *after several rinses with acetone;* ***D)*** *after several rinses with warm water;* ***E)*** *after washing in warm water with detergent;* ***F)*** *after being placed in a humid environment at 80°C for one hour;* ***G)*** *a further two weeks at ambient condition following the heat and humidity environment. Lateral measurements are 100 µm, vertical measurements varies from 1.5 µm to 0.25 µm image dependent.*

The topographical images in Figure 6.11 show a decline in the height of features measured on the edge of a fingerprint ridge. As an aged but untouched deposit, some of the features in Figure 6.11A of the above figure are over a micrometre in height, surrounding a clear patch in the bottom left corner of the image. Wiping of the sample has approximately halved the height of the sweat material (Figure 6.11B) as well as giving a more uniform height to them. Rinsing the sample with acetone followed by rinsing with warm water (Figure 6.11C and D) has removed the majority of the sweat deposit with surface features not exceeding 200 nm, a fivefold reduction in height from the ambient stored sample. With so little remaining deposit, the effect of washing in warm soapy water cannot be fully observed; however it does reduce

the height of the features slightly and leaves a uniform height raised area like a plateau, surrounding the bare substrate. After the washing in warm soapy water, the sweat deposit area is approximately 100 nm high, less than 10% the height of the deposit before any removal methods were employed. However, despite this drastic reduction, there is not a great deal of difference observed for the print as a whole (Figure 6.10) rather than on the nanometre scale. This difference is linked to the processes occurring as well as the way in which the two techniques (one optical and one physical) report the information. Whilst the AFM is more than capable of monitoring and recording changes on the nanometre scale, as is the case above, the fact that these features are still visible by post treatment, despite the drastic reduction in the amount of sweat residue remaining, is due to the optical properties of ridge areas differing from that of the substrate. This optical difference could be caused by various factors, but most likely is the result of either the compacted remaining sweat deposit or the product of the interaction between the sweat and substrate surface prior to any washing or removal treatment. Although physical surface measurements show the majority of the sweat residue has been removed, the fingerprint image is still visible and features are easily distinguishable. This suggests that it is not just one of a physical nature, but also of a surface chemical change.

Table 6.2 – Ratio of copper to zinc for fingerprinted brass substrate stored at ambient conditions and then subjected to washing

Sweat type	Post-deposition treatment	Ratio of Cu:Zn
Eccrine	Ambient for 2 days and then washed in warm water and detergent	1: 0.82

The Cu:Zn ratio seen in Table 6.2 for the ambient washed sample has slightly more surface copper than zinc and this proportion does not closely resemble any values found in Chapter 5 for the untreated eccrine fingerprinted samples. As the sample was aged only two days before being washed with warm water and detergent, one would expect no further significant

changes to occur and so the Cu:Zn ratio should closely resemble that of bare substrate (ratio of 1:1.12) or aged eccrine deposit (ratio of 1:1.12). However, the Cu:Zn ratio measured is approximately half way between an aged polished sample and one with fresh eccrine deposit (1:0.52). This suggests that the exposed substrate may have aged as expected but the fingerprinted regions exhibit similar characteristics for those observed for the fresh eccrine deposit.

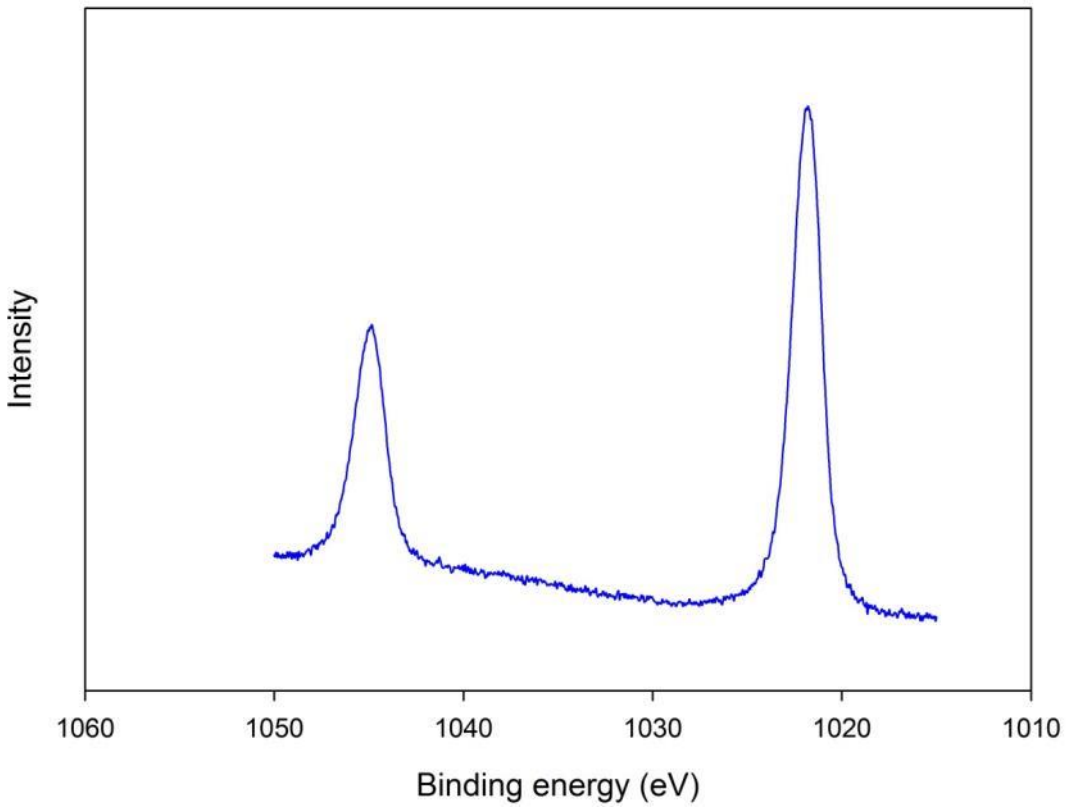

Figure 6.12 – XPS Zn $2p_{3/2}$ and $2p_{1/2}$ spectrum of an eccrine fingerprint on polished brass stored at ambient conditions for two days and then washed in warm water with detergent.

The detergent washed sample has two sets of single species peaks, as seen in Figure 6.12. The larger peak is a Zn $2p_{3/2}$ signal and is found at 1021.8 eV, attributable to Zn(0)[2, 4, 21] and the second observable peak is a Zn $2p_{1/2}$ signal and also attributable to Zn(0)[4] (1044.9 eV). The position for the peak seen in the $2p_{3/2}$ region is of a slightly lower binding energy than seen for

other single Zn species, by a few electron volts, thus supporting the notion of elemental zinc being present.

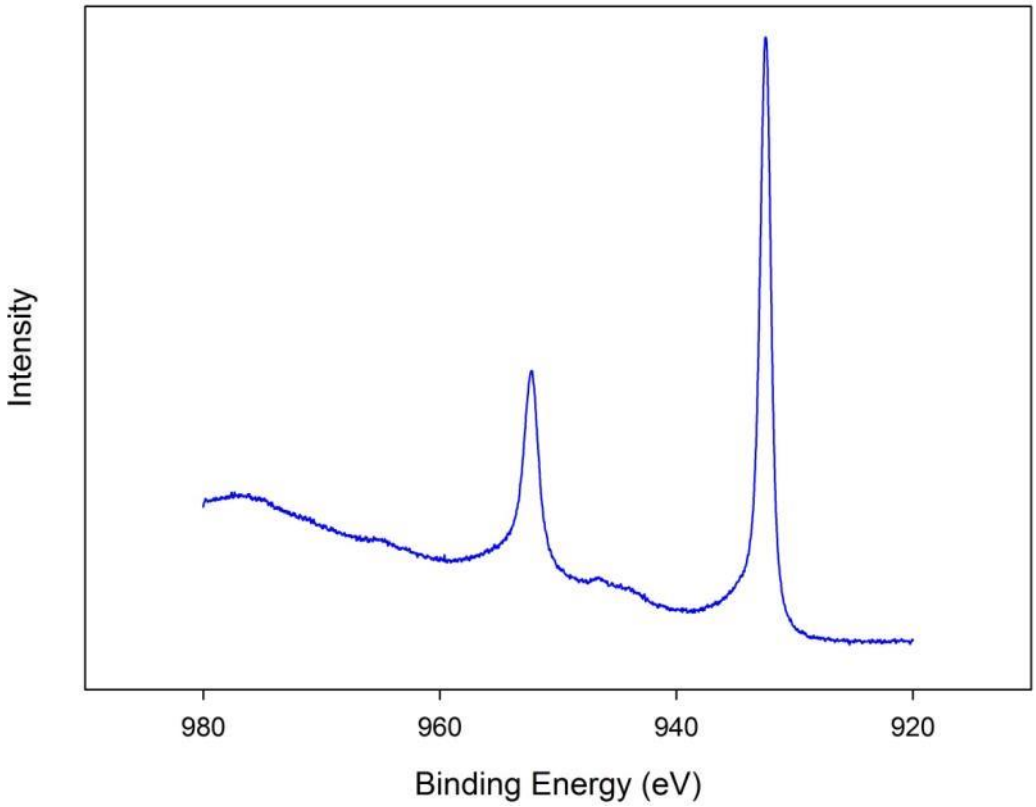

Figure 6.13 – XPS of Cu $2p_{3/2}$ and $2p_{1/2}$ spectrum of an eccrine fingerprint on polished brass stored at ambient conditions for two days and then washed in warm water with detergent.

In the Cu $2p_{3/2}$ spectrum of Figure 6.13, a large fairly symmetrical peak can be seen with a position of 932.5 eV and attributable to Cu_2O[4, 11, 23]. However, there is a very small second peak at 933.2 eV, at the base of the main peak, attributable to CuO[2]. The Zn $2p_{1/2}$ peak does not show a second oxidation state present but this is not surprising since the Cu(II) signal in the Cu $2p_{3/2}$ region is very small.

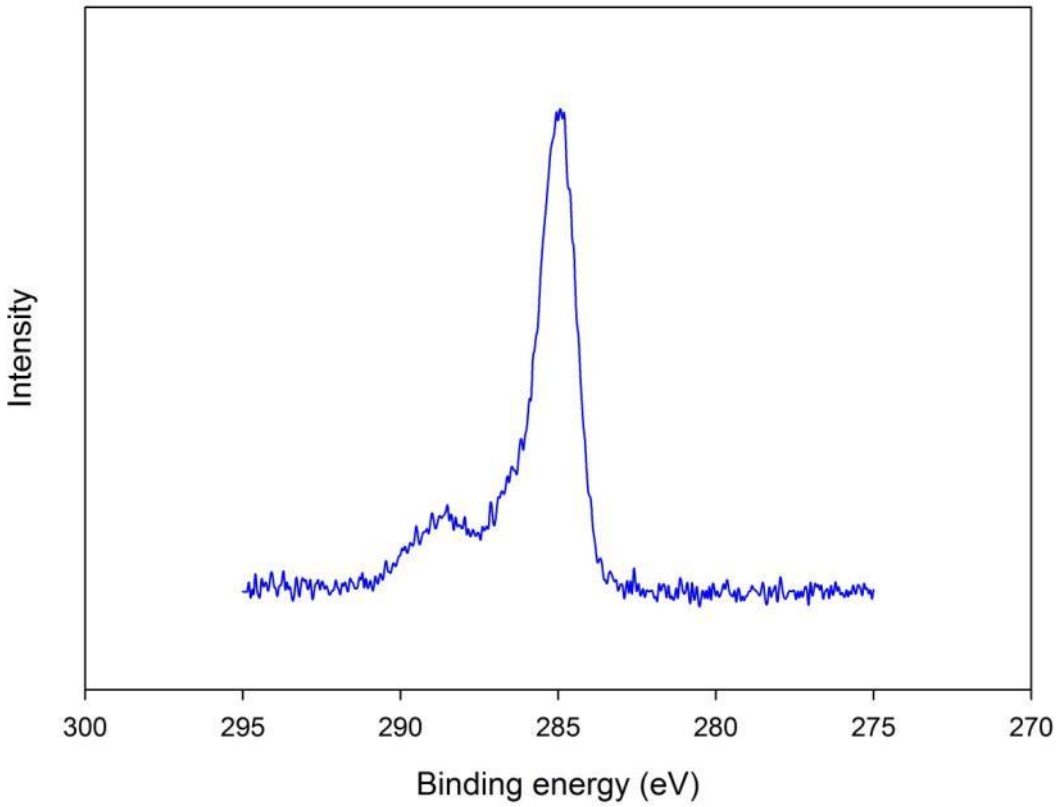

Figure 6.14 – XPS C 1s spectrum of an eccrine fingerprint on polished brass stored at ambient conditions for two days and then washed in warm water with detergent.

Two different peaks can be easily distinguished in the spectrum for the carbon region of this eccrine sample in Figure 6.14. However, a third is present between the two. The main signal is at 284.7 eV and is attributable to a hydrocarbon[25], the second peak on the shoulder on the main peak is found at 286.3 eV and is typical of carbon in C-O bonds[26-29], whilst the final peak is at 288.7 eV and is a signal for carbon in carbonyl groups[30]. Similarities between this carbon spectrum and others shown are present, mainly to eccrine samples exposed to ambient and humid conditions. This suggests that not all of the sweat residue is removed despite thorough washing in warm soapy water.

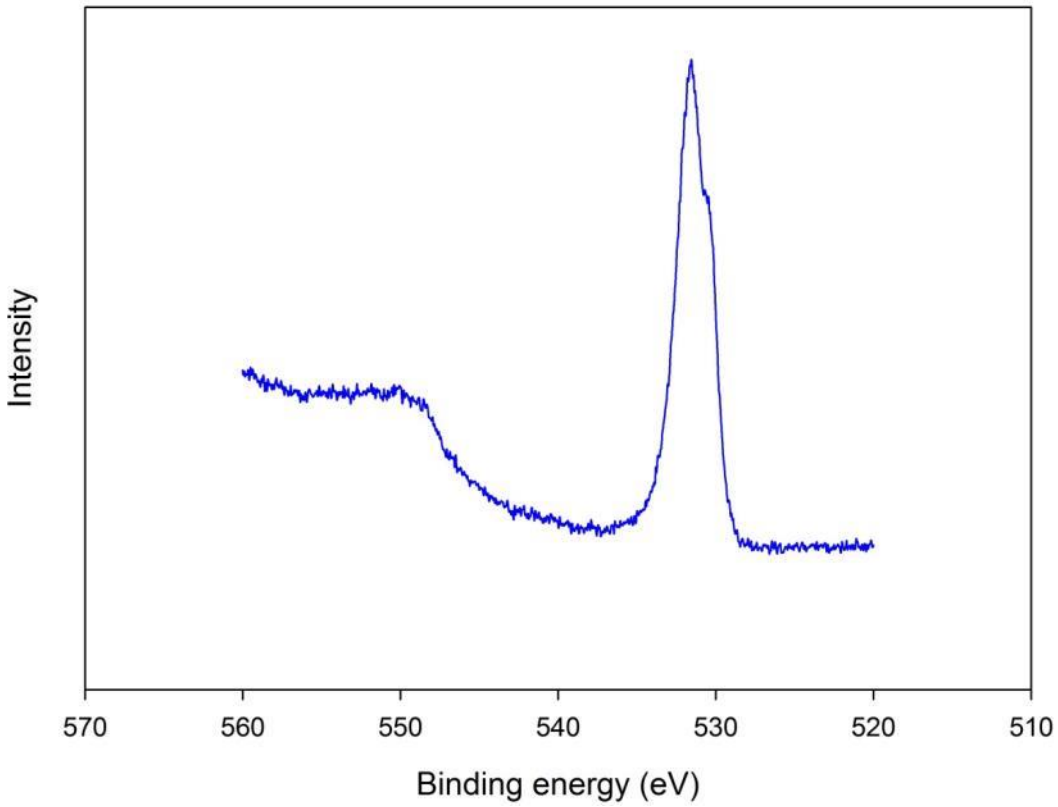

Figure 6.15 – XPS O 1s spectrum of an eccrine fingerprint on polished brass stored at ambient conditions for two days and then washed in warm water with detergent.

Whilst the carbon spectrum proposed the existence of carbon-oxygen bonds, the O 1s spectrum in Figure 6.15 has two main signals which only represent metal oxide bonds. These peaks are at 531.5 eV and 530.2 eV and are of CuO or ZnO[4] and Cu_2O[8, 11, 18-22], respectively. Correlation with the peaks found in the copper and zinc regions, with Zn(0) found in the zinc region, leaves the assignment as CuO and Cu_2O. However, the relative intensities of the peaks does not match, as one would expect a much smaller peak for the CuO product.

6.2.4 Eccrine Fingerprints on Polished Brass Substrates in Non-Ambient Storage Environments

Whilst storage of fingerprinted samples at ambient environments does not naturally enhance the visualisation of the fingerprint, it equally does not impede any subsequent enhancement process. Storage in warm humid conditions was been proven in chapter 4 (section 4.2.5) to promote the natural visualisation process of fingerprinted samples, but the effect on the sweat deposit and ease of removal have not yet been addressed.

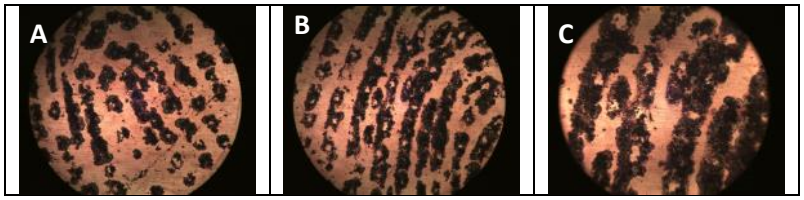

Figure 6.16 – Optical microscopy images of an eccrine fingerprint on polished brass substrate, stored in a humid environment at 50°C for 11 days and then washed with detergent and warm water. ***A)*** *core pattern of the fingerprint;* ***B)*** *outer ridges of the fingerprint;* ***C)*** *zoomed in on the centre of* ***B****.*

The fingerprint in Figure 6.16 has a good contrast between the ridges and the brass substrate, although they have a fairly dotty nature, more easily seen in Figure 6.16A of the core of the fingerprint pattern. Even with this dotty nature, it is still relatively easy to follow a single ridge across the image. Figure 6.16B is an area slightly away from the core and the ridges here can be seen to be more continuous but with holes present in them; these holes are the sweat pores and are approximately 100 µm in diameter. These conditions of a warm humid environment for a prolonged period (11 days), have caused not only the visualisation of the fingerprint pattern but also clearly show the 3rd level detail for identification features (see Chapter 1; Section 1.2.4 for further details). Additionally these clear features have also not been removed or damaged following washing in detergent and warm water, suggesting that the features present on the sample surface are of a permanent nature.

Storing an eccrine fingerprint at a slightly lower temperature (45° opposed to 50°C above) for a shorter period of time (4 days less) resulted in a fingerprint that was not fully visible. A faint trace of the fingerprint outline was visible as well as some discontinuous ridges. However, increasing the temperature to 80°C and maintaining the humid environment for a short duration brought about effects in line with previous findings, that increased temperature increases the rate of visualisation.

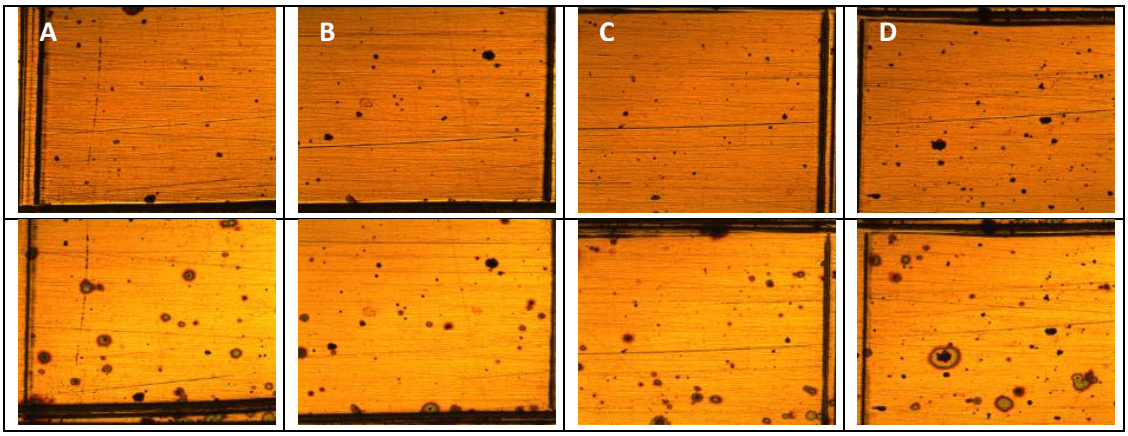

Figure 6.17 – Optical microscopy images of four different areas of a fingerprint on brass substrate; top row is after 7 days stored at 45°C in a humid environment; bottom row is the same area following exposure to 80°C and humid conditions for two and a half hours.

The top row of images shown in Figure 6.17 were taken after the sample was stored for 7 days at 45°C. More markings can be seen on the surface than if it was stored at humid conditions, but still not enough features are present to produce recognisable ridge lines. Increasing the temperature for a short duration did cause changes to the appearance of the markings in the top row: in Figure 6.17A, the small black dots have increased in size with the increase in temperature and some of the fainter dots have become distinctly visible but ridge lines are still not recognisable at this level of detail.

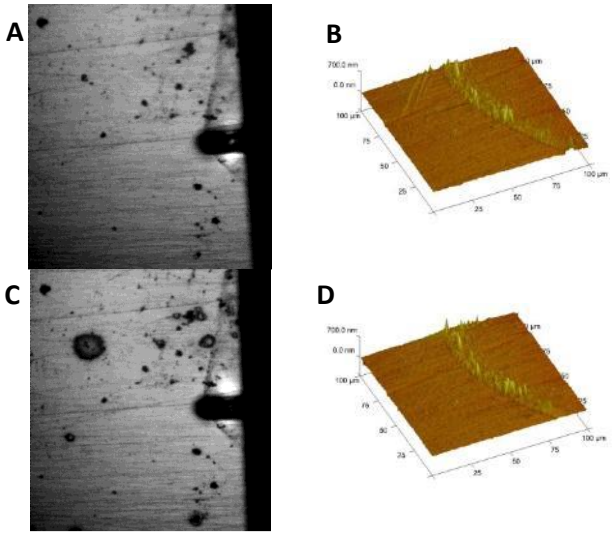

Figure 6.18 – Images of an eccrine fingerprint on polished brass substrate. ***A)*** *Optical image of sweat deposit after 7 days at 45°C in a humid environment;* ***B)*** *AFM topographical image of the area directly below the cantilever seen in* ***A****;* ***C)*** *Optical image of the same area as* ***A*** *but following exposure to 80°C and humid conditions for two and a half hours;* ***D)*** *AFM topographical image of the area directly below the cantilever seen in* ***C****. AFM images have lateral dimensions of 100 µm and a vertical height of 700 nm.*

Whilst changes can be seen in Figure 6.18 from images A to C, with the increasing size of the black dots as with Figure 6.17, the changes observed in the physical measurements are not as apparent. The AFM images in Figure 6.18B and D are of the solid curved line seen below the cantilever in Figure 6.18A and C. This feature has not noticeably changed in appearance optically with the increase in temperature and neither are significant changes seen in the AFM images. The features are of similar height, with the main band maintaining the same width and the density of the peak clusters has not changed. However, there is the addition of two new peaks in the band after the increase in temperature, which are now of equivalent height to the other features. Whilst this is a minor change, it is an indication that an increase in temperature from the original storage environment can still promote the occurrence in surface changes by decreasing the time frame in which they would have occurred.

In the above case, although the temperature was increased by 35°C, it is not as significant a temperature increase as going from ambient temperatures to exposure to a Bunsen flame.

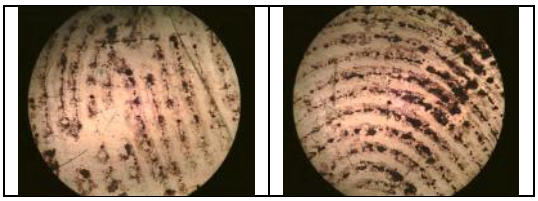

Figure 6.19 – Optical microscopy images of an eccrine fingerprint on polished brass substrate, stored at ambient temperatures but in a humid environment for 8 days and then subjected to exposure to a Bunsen flame for 30 seconds followed by washing in detergent and warm water.

Figure 6.19 shows clear ridge markings on the brass substrate. The ridges are not as solid or clearly resolved as with the sample in Figure 6.16. Some sweat pores can still be seen, although with difficulty, but the ridges and ridges feature are easily discernible. Prior to the exposure to the Bunsen flame, the humid storage environment had had little effect on the visualisation of the fingerprint, faint traces of contact could be seen but ridges and ridge features could not be recognised. Exposure to a blue Bunsen frame for a relatively short time period (seconds rather than hours for warm humid environments) caused a lightening of the brass substrate indicating a change in surface composition to a zinc rich phase as detailed in Chapter 5. Additionally, the fingerprint pattern was visually enhanced to the faint black markings seen above in Figure 6.19; washing of the fingerprint after exposure to the Bunsen flame had no noticeable effect on the visual nature of the ridge markings with them persisting with the clarity seen above. This reinforces the suggestion that whilst traces of the sweat deposit remain on the substrate surface, irrespective of storage environment, increasing the temperature will enhance the visual appearance of the fingerprint pattern.

The storage conditions and temperatures in this section varied significantly but all resulted in a visual and identifiable fingerprint image which persisted after washing of the sample.

However, the exact visual nature of both the fingerprint ridges as well as the substrate varied and so it is likely that chemical rather than physical differences are responsible for this variation.

Table 6.3 – Ratio of copper to zinc for polished fingerprinted brass substrates exposed to different conditions

Sweat type	Post-deposition treatment	Ratio of Cu:Zn
Eccrine	Humid environment at 50°C for 11 days and then washed with warm water and detergent	1 : 2.2
Eccrine	Humid conditions for 8 days and then exposed to a Bunsen flame for 30 seconds followed by washing in warm water and detergent	1 : 5.1

The ratios seen above in Table 6.3 do not match those found for untreated samples in chapter 5. Those subjected to the same Bunsen based heat treatment as the second sample in the table above had ratios on the order of 1:10 or above, here only 1:5 is seen. This suggests that the storage in humid conditions prior to exposure to the Bunsen flame had a significant impact on the surface composition of the sample, although the eccrine humid stored samples still exhibited a ratio favouring the zinc species. As this sample was not washed until after the Bunsen exposure and no visible difference was seen on the sample, it is strange that the Cu:Zn ratio is so different from the other values seen for similar conditions. The sample above that was subjected to warm humid conditions before being washed also has a ratio that does not fit the trend. Untreated samples stored in this manner for short periods exhibited a decrease in surface zinc compared to the ambient stored samples (ratio of 1:0.39 for warm humid samples compared to that of 1:1.12 for ambient samples), this sample displays the opposite. Although the washing regime is sufficient to remove surface residue, it is not aggressive enough to alter the surface composition of the substrate as depicted by both of the above samples. It is more

likely that is a result of the environments that were exposed to that the effect of the sweat deposit or washing treatments.

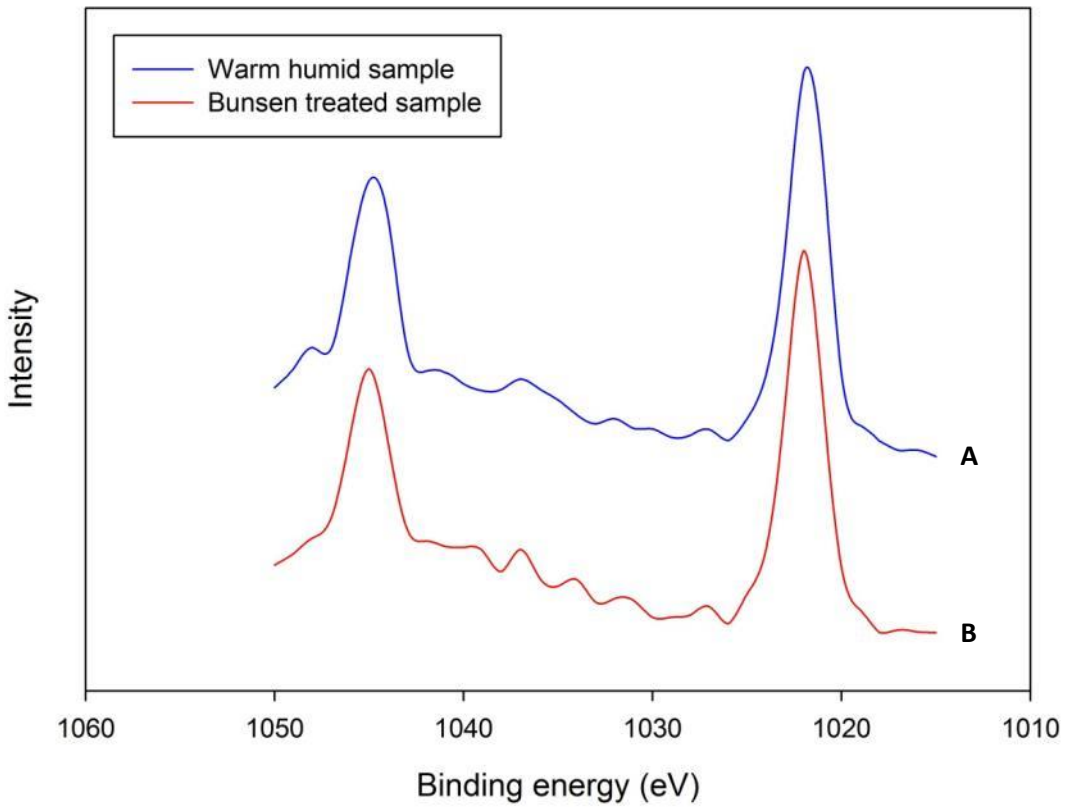

Figure 6.20 – XPS Zn $2p_{3/2}$ and $2p_{1/2}$ spectra of eccrine fingerprinted polished brass substrates. ***A)*** *stored in a humid environment at 50°C for 11 days then washed in warm water and detergent;* ***B)*** *stored in a humid environment at ambient temperature for 8 days and then exposed to a Bunsen flame for 30 seconds followed by washing in warm water and detergent.*

Whilst both spectra in Figure 6.20 have peaks in similar positions, both samples have a peak around 1022.1 eV, which can be assigned as either Zn(0) or ZnO[2-4, 24]. However, Figure 6.20A has a slightly broader peak, comprised of a second signal at 1022.7 eV, which can be assigned as $Zn(OH)_2$[31]. The signal for the Zn $2p_{1/2}$ product indicates the presence of a single oxidation state as Zn(II) due to its position at 1045.3 eV[4] and therefore the main signal is that of ZnO. The Bunsen treated sample (Figure 6.20B) has a single peak and the Zn $2p_{1/2}$ peak indicates that ZnO is present as the binding energy is 1045.1 eV[4], thus the main signal is also that of ZnO. The

presence of $Zn(OH)_2$ was not found in the untreated fingerprinted samples in Chapter 5 and so its occurrence must be the result of either the interaction between the sweat and the substrate or as a result of the treatment the sample was subjected to. The presence of ZnO is expected as zinc is the dominant surface metal present.

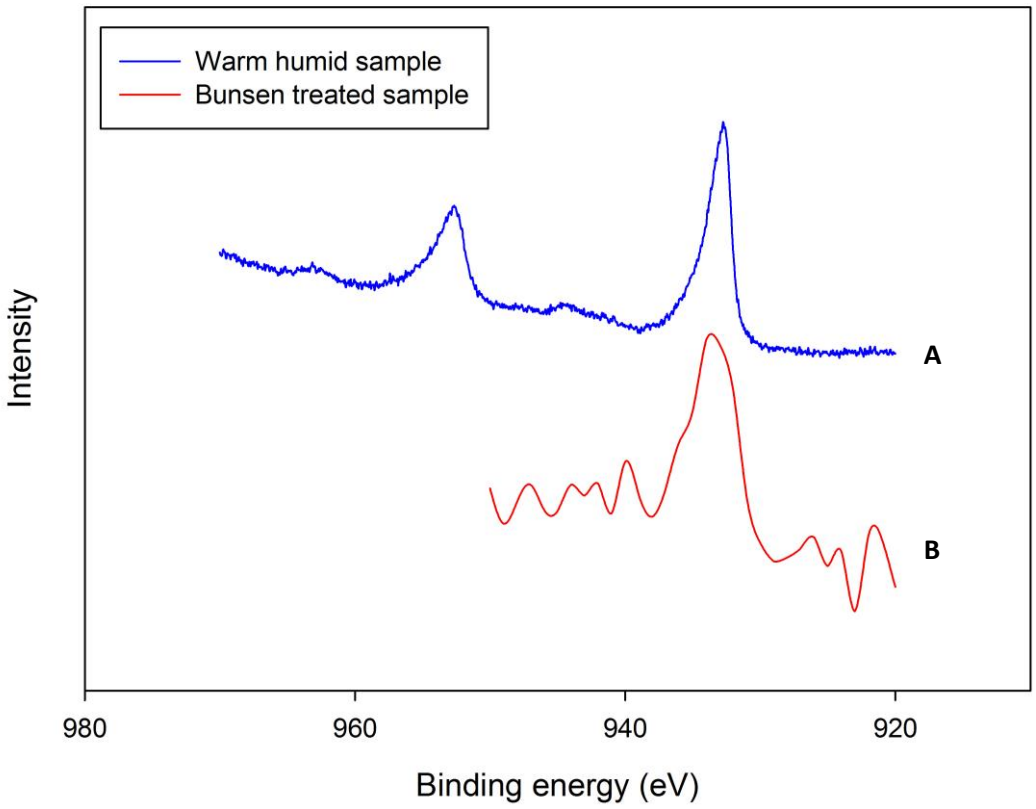

Figure 6.21 – XPS Cu $2p_{3/2}$ and $2p_{1/2}$ spectra of eccrine fingerprinted polished brass substrates. ***A)*** *stored in a humid environment at 50°C for 11 days then washed in warm water and detergent;* ***B)*** *stored in a humid environment at ambient temperature for 8 days and then exposed to a Bunsen flame for 30 seconds followed by washing in warm water and detergent.*

The spectrum for the Bunsen treated sample in Figure 6.21B is of very low intensity when compared to the zinc species, consequently the signal was magnified but the signal to noise ratio is unaffected and distracts from the peak present. This spectrum (Figure 6.21B) indicates a single peak at approximately 933.5 eV, which would be copper as CuO[4, 8, 11, 12, 23, 32]. The spectrum in Figure 6.21A is much clearer and shows a single main peak but with a smaller

signal at the base: these peaks are found at 932.8 eV and 934.0 eV, respectively. The main signal is found at 932.8 eV and is typical of Cu(0)[2, 9, 10]; the second much smaller signal is found at 934.0 and is CuO[8]. Additionally, a slight broadening of the $Cu2p_{1/2}$ signal can be seen which would support the presence of two different oxidation states for the copper species. Whilst the presence of such a prominent Cu(0) peak would be normally be surprising, as the Cu:Zn ratio favours the zinc species, the copper could be from just beneath the substrate surface and thus elemental copper rather than a copper oxide.

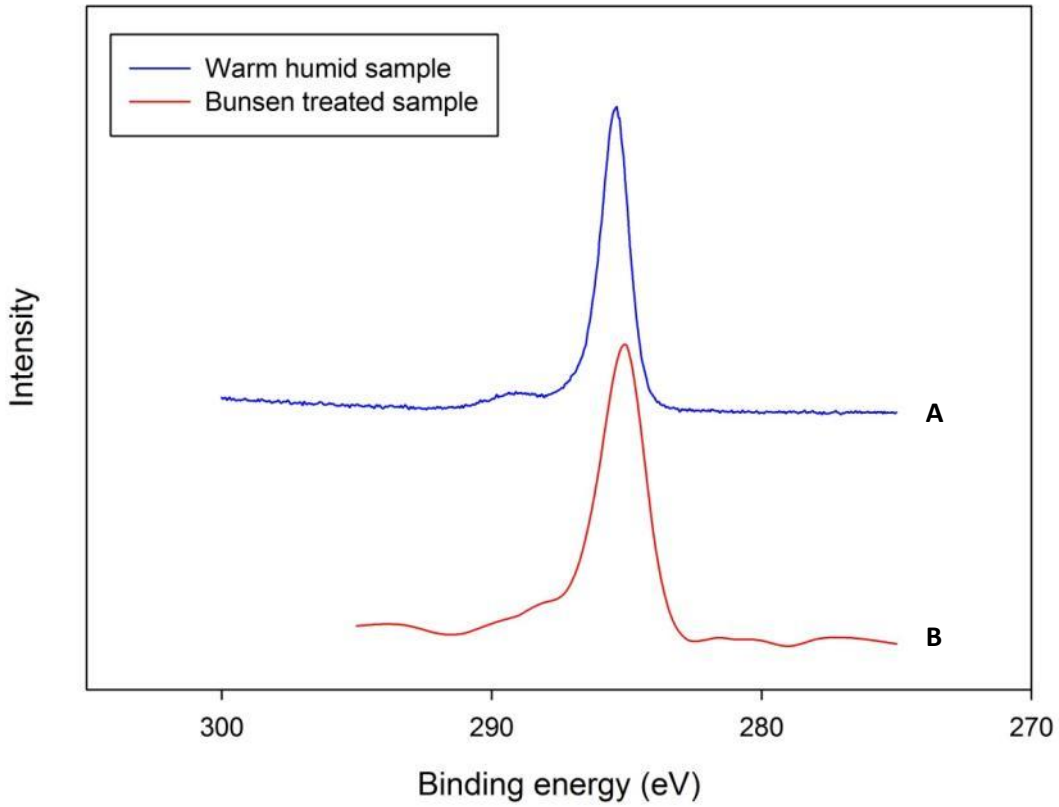

Figure 6.22 – XPS C 1s spectra of eccrine fingerprinted polished brass substrates. ***A)*** *stored in a humid environment at 50°C for 11 days then washed in warm water and detergent;* ***B)*** *stored in a humid environment at ambient temperature for 8 days and then exposed to a Bunsen flame for 30 seconds followed by washing in warm water and detergent.*

Both peaks in Figure 6.22 depict a prominent main signal, but with additional signals presence at much lower intensities. For the Bunsen treated sample (Figure 6.22B), the main signal is at

285.1 eV and is typical of alkane bonds[25, 33, 34], the second peak at 287.3 eV is of carbons in carbonyl bonds[34]. Neither of these strongly suggests the presence of eccrine sweat remaining on the sample surface. The other sample (Figure 6.22A) has peaks at 285.4 eV, 286.0 eV and 289.1 eV, which are alkane carbons[25], carbon in C-O bonds[26-29] and alkane carbons in a long carbon chain[34-36]. This set of peaks is slightly more indicative of remaining sweat residue although these values do not match any those found in the untreated samples in Chapter 5.

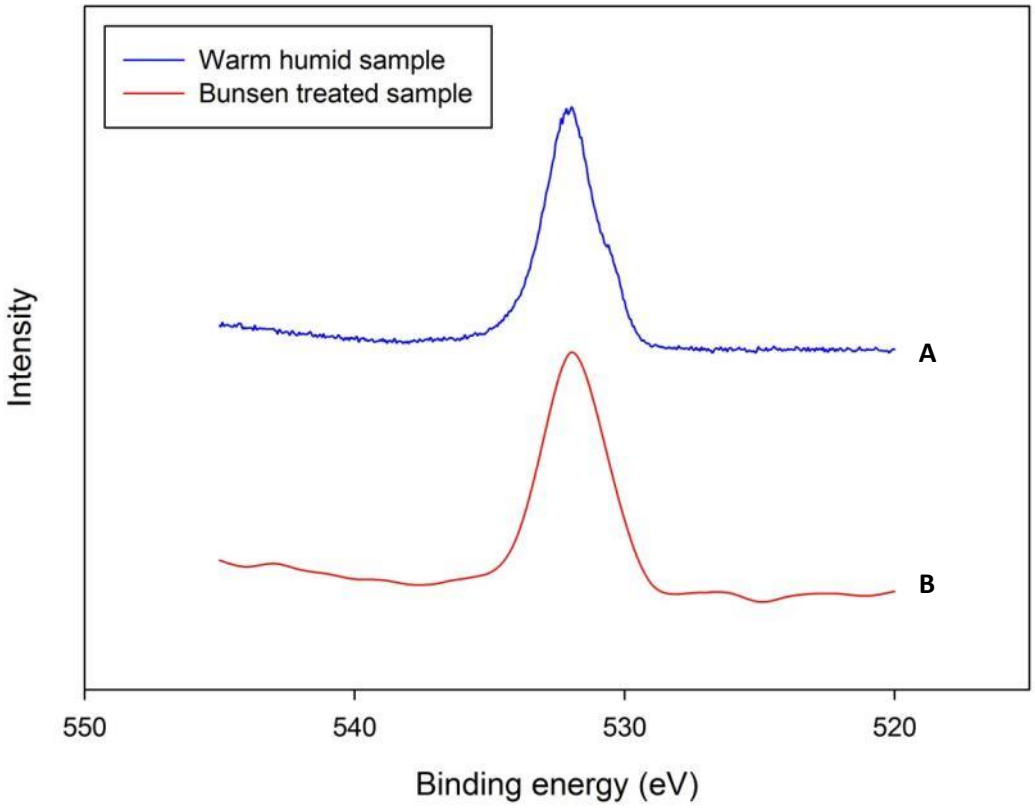

Figure 6.23 – XPS of O 1s spectra of eccrine fingerprinted polished brass substrates. ***A)*** *stored in a humid environment at 50°C for 11 days then washed in warm water and detergent;* ***B)*** *stored in a humid environment at ambient temperature for 8 days and then exposed to a Bunsen flame for 30 seconds followed by washing in warm water and detergent.*

The peak in Figure 6.23B is a single peak with a binding energy of 531.9 eV, typical of OH species[14-16]. There are no other peaks present which could indicate the presence of a metal oxide, as was found in Figure 6.7 as well. In Figure 6.23A, a slightly broad peak can be seen, the

major component is at 532.0 eV, with subsidiary peaks at 533.4 eV and 530.4 eV. The main peak is again that of an OH species[14-16], possibly $Zn(OH)_2$, which corroborates that found in Figure 6.20. The lower binding energy subsidiary signal (530.4 eV) is that of oxygen in either CuO[8, 11] or Cu_2O[2, 11] and the higher subsidiary signal (533.4 eV) is that of oxygen in either C-O bonds[2] or carbonyl bonds[2, 34].

6.2.5 Elemental Comparison between Sebaceous and Eccrine Fingerprint Deposits in Varying Conditions

Whilst the above data so far laid out in this chapter documents the effects of eccrine deposit on fingerprinted brass substrates, one must also consider the effects on sebaceous deposits. With eccrine sweat deposit being mostly water based, exposure to ambient and above ambient conditions would cause some evaporation of the residue, but the water can also aid corrosion processes by acting as an electrolyte. Conversely, sebaceous sweat is mainly comprised of oils and very little water, with that present being from eccrine sources. The oils and carbon based components present in the sebaceous sweat are not as conductive as water and so would not contribute significantly to any corrosion reactions. Additionally, one would expect the sweat residues to be affected differently by different washing or post-deposition treatment regimes, both chemically and physically.

Table 6.4 – Ratio of copper to zinc for polished fingerprinted brass substrates exposed to humid conditions

Sweat type	Post-deposition treatment	Ratio of Cu:Zn
Eccrine	Humid conditions for 7 days followed by washing with warm water and detergent	1 : 0.86
Sebaceous	Humid conditions for 7 days followed by washing with warm water and detergent	1 : 0.88

Both samples were stored in humid conditions for 7 days and then washed afterwards. The Cu:Zn ratios are very similar, with both showing a higher relative amount of copper than zinc. The values in Table 6.4 are not dissimilar to those found for a sebaceous sample in humid conditions (1:0.87) but are different to eccrine samples stored at ambient or humid conditions. In the case of previous eccrine fingerprinted samples (chapter 5), the Cu:Zn ratios showed a higher amount of zinc than copper (ambient and humid Cu:Zn ratios were 1:1.12 and 1.20 respectively). This lower than expected amount of surface zinc in Table 6.4, especially for the eccrine sample, was also seen for the ambient washed sample in Table 6.2 and to some extent in Table 6.3 as well, therefore it is apparent that the washing of the sample does have an effect on the ratio of Cu:Zn by skewing it towards copper.

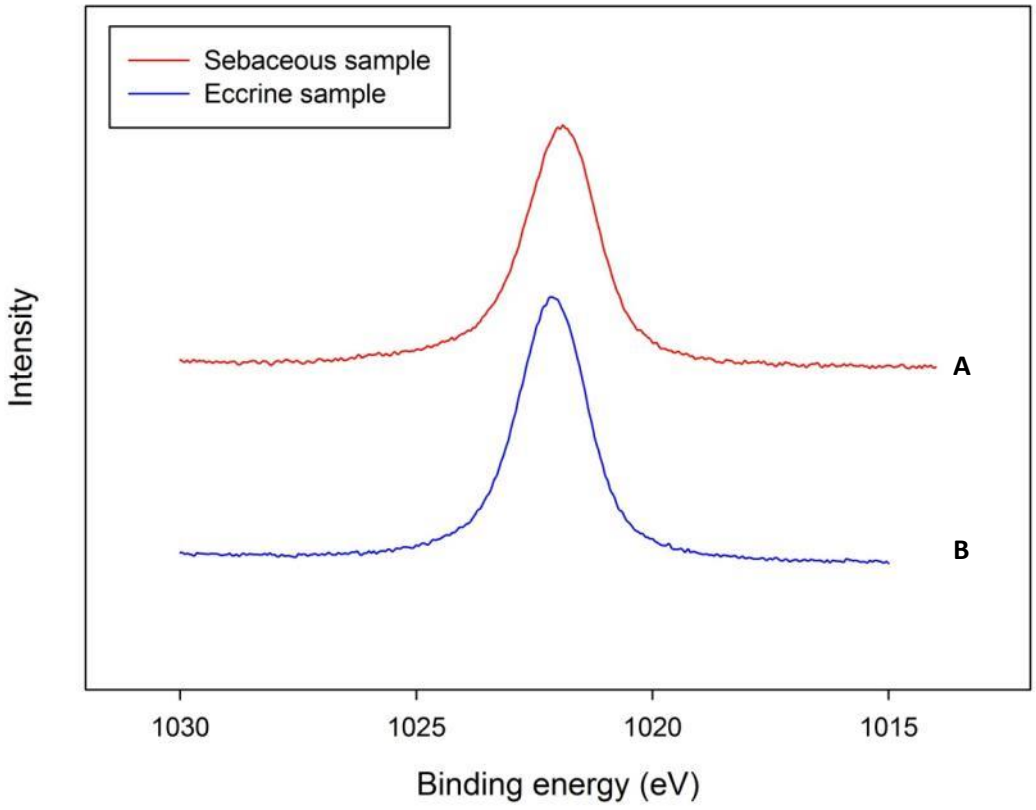

Figure 6.24 – XPS Zn $2p_{3/2}$ spectra of fingerprinted brass substrates stored in humid environments for 7 days followed by washing with warm water and detergent. ***A)*** *eccrine fingerprint deposit;* ***B)*** *sebaceous fingerprint deposit.*

Both of the peaks for the Zn2p$_{3/2}$ signal for the spectra in Figure 6.24 are of single species: the eccrine fingerprinted sample is at 1022.1 eV whereas the sebaceous fingerprinted sample is at 1021.9 eV. Although these values are fairly similar, they are at the limit of being able to discriminate different species and so it is possible to deduce that each contains a different oxidation state of zinc. The eccrine sample contains Zn(II) as ZnO[2-4] and the sebaceous sample has Zn(0)[2, 4, 24]. These binding energy values are similar to those seen in the humid samples in Chapter 5, where both were approximately 1022 eV.

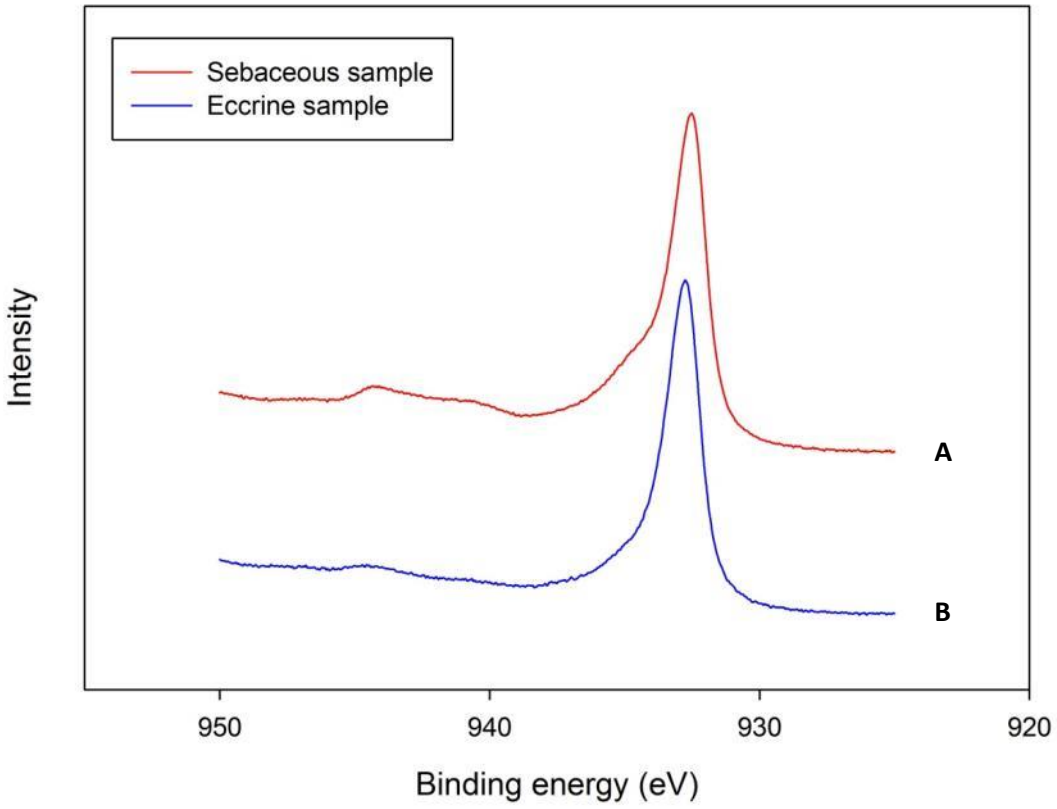

Figure 6.25 – XPS Cu 2p$_{3/2}$ spectra of fingerprinted brass substrates stored in humid environments for 7 days followed by washing with warm water and detergent. ***A)*** *eccrine fingerprint deposit;* ***B)*** *sebaceous fingerprint deposit.*

The eccrine fingerprinted sample in Figure 6.25 has a narrower peak than the sebaceous fingerprinted sample. However, both peaks contain more than a single species. The eccrine sample has the main peak at 932.8 eV, typical of Cu(0)[2, 9, 10], with the secondary subsidiary

peak at 933.8 eV, which is attributable to CuO[4, 8, 11, 12, 23, 32]. The sebaceous sample has the main peak at a slightly lower binding energy than the eccrine sample, at 932.5 eV, with subsidiaries found at 933.9 eV and 933.2 eV. The main peak (932.5 eV) is attributable to Cu_2O[4, 11, 23], the subsidiary at 933.9 eV is that of copper as CuO[2] and the last peak at 933.2 eV is that of copper as $Cu(OH)_2$[32]. The eccrine samples main peak being elemental copper is unexpected since it is the dominant substrate metal present, but the presence of Cu(II) species is the more common copper state found on the surface. Similarly, the sebaceous sample also has CuO present as well as a Cu(I) species and $Cu(OH)_2$, the presence of these latter two was also found in the samples stored in similar conditions without washing, as described in Chapter 5.

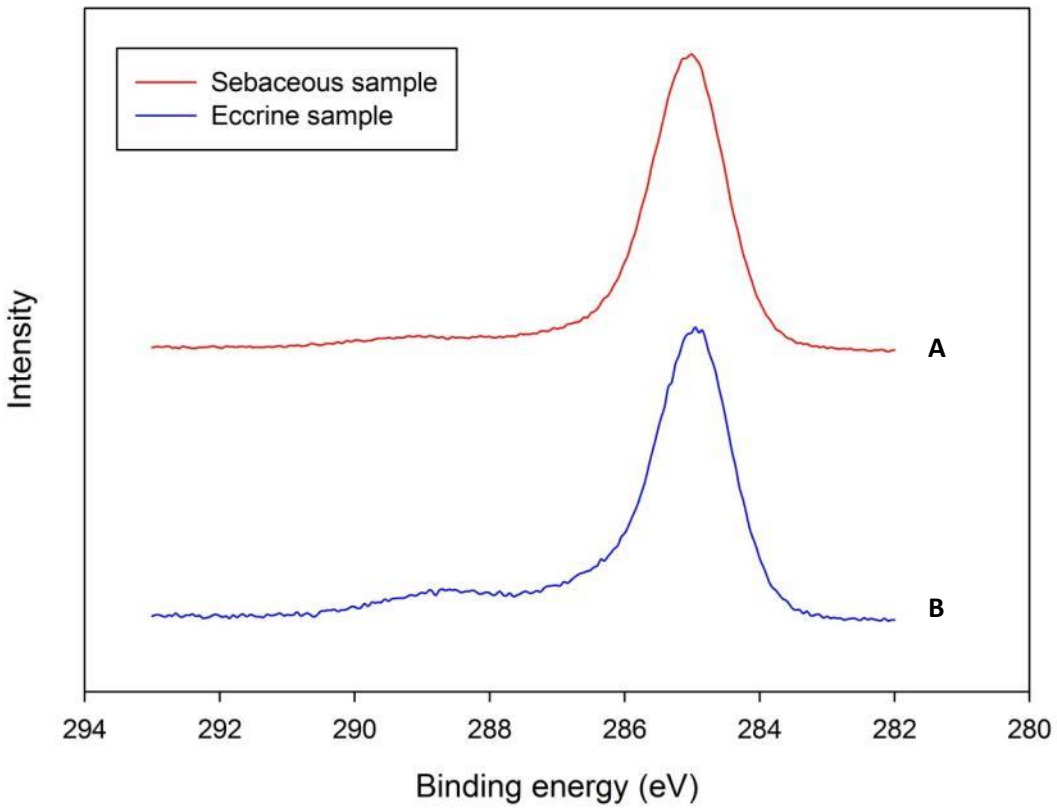

Figure 6.26 – XPS C 1s spectra of fingerprinted brass substrates stored in humid environments for 7 days followed by washing with warm water and detergent. ***A)*** *eccrine fingerprint deposit;* ***B)*** *sebaceous fingerprint deposit.*

The spectra showing the carbon region in Figure 6.26 show the presence of multiple peaks at slightly different binding energy values. The eccrine sample has peaks at 285.0 eV, 286.3 eV and 288.7 eV, which can be assigned as carbons in alkane bonds[25, 29, 33, 34, 37, 38], C-O bonds[26-29] and carbonyl bonds[25], respectively. The sebaceous sample has peaks at 284.8 eV, 285.6 eV, 288.9 eV and 288.3 eV, with the first 3 being assigned as carbon in alkane bonds in varying carbon chain lengths[29, 33-39] and the final being that of a carbonyl[27, 40, 41]. Whilst both have multiple peaks and profiles similar to that of the warm heated and washed eccrine sample in Figure 6.14, they are quite distinctive from the samples described in Chapter 5. It is therefore possible that whilst the fingerprint image remains, some of the sweat components are removed, revealing the deeper lying residue components.

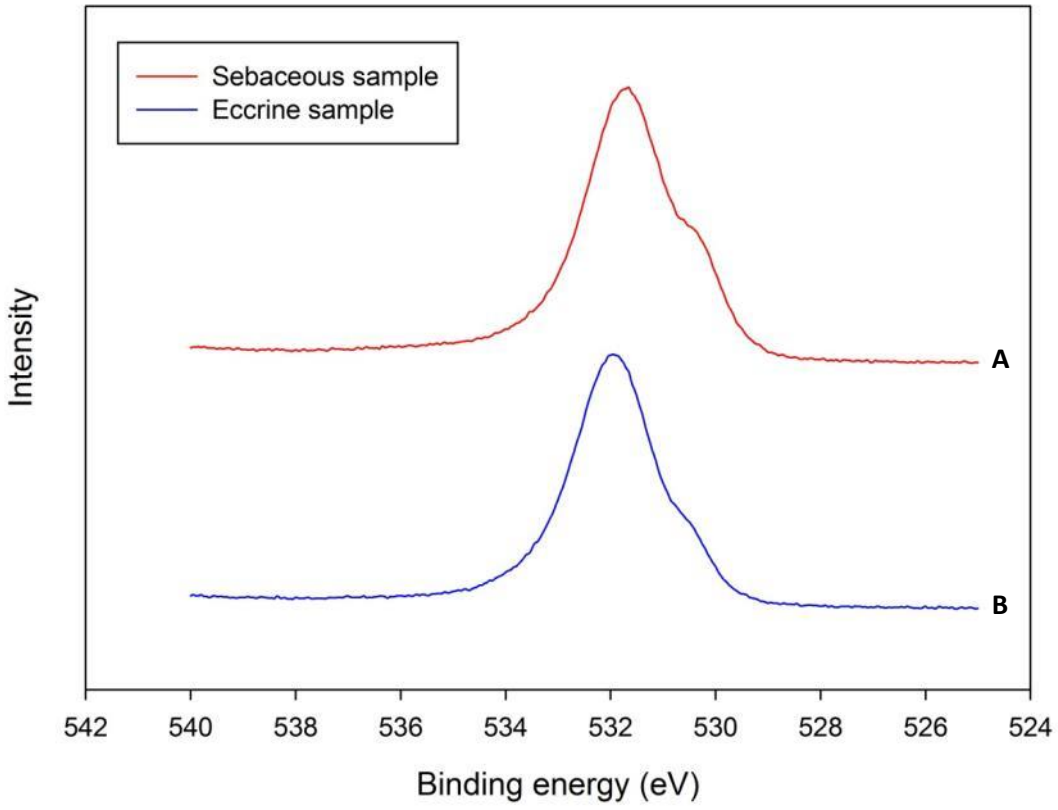

Figure 6.27 – XPS O 1s spectra of fingerprinted brass substrates stored in humid environments for 7 days followed by washing with warm water and detergent. ***A)*** *eccrine fingerprint deposit;* ***B)*** *sebaceous fingerprint deposit.*

The spectra for the O 1s region is shown in Figure 6.27, both samples have slightly broad peaks present with the main peak at a higher binding energy than the smaller additional peak. The eccrine sample has peaks at 532.0 eV and 530.3 eV, which are attributable to oxygen in OH[14-16] or H_2O[13] and Cu_2O[2, 8, 11] or CuO[8, 11] species. From the copper spectrum (Figure 6.25), CuO was also identified and so the second smaller peak is most likely that species. The sebaceous sample has peaks at 531.7 eV and 530.2 eV; the first is typical of OH[11, 13, 15, 42] or $Cu(OH)_2$[11] species and the latter could be either CuO[8, 11], Cu_2O[8, 18-22] or ZnO[8, 18-22]. As all three of these copper species were found in the copper spectrum Figure 6.25 for the sample, it is quite likely that all three are indeed present as there is little difference in binding energy values for the O 1s signals (compared to the Cu $2p_{3/2}$ signals) when differentiating between CuO and Cu_2O.

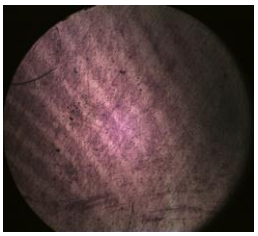

Figure 6.28 – Optical microscopy image of a sebaceous fingerprint on polished brass substrate stored in a warm (75°C) humid environment for two days and then washed with warm water and detergent. Image area is ca. 5.1 mm by 4.6 mm.

The optical microscopy image in Figure 6.28 shows several fingerprint ridges parallel to each other; the ridges are of a darker colour than the substrate material. In this instance, the ridges are wider than the gaps between them, most likely due to a firmer pressure used in the deposition process. As a result of this image, it is clear that the fingerprint mark is still fully visible despite being washed in warm soapy water. The level of visualisation of the fingerprint in this image is representative of the samples washed and stored in warm humid environments.

Table 6.5 – Ratio of copper to zinc for polished fingerprinted brass substrates exposed to warm humid conditions

Sweat type	Post deposition treatment	Ratio of Cu:Zn
Eccrine	Stored in a humid environment at 75°C for two days and then washed with warm water and detergent	1 : 0.94
Sebaceous	Stored in a humid environment at 75°C for two days and then washed with warm water and detergent	1 : 0.93

As both samples in Table 6.5 have very similar Cu:Zn ratios, it can be determined that the environment and conditions the samples have been exposed to have more bearing on the surface composition than the type of sweat present. These values and similarities in the values between the two samples follow the trend from Table 6.4. The values themselves suggest a near equal amount of copper and zinc present on the surface, a feature not seen for fingerprinted samples that were not subjected to any post deposition washing treatment (see chapter 5).

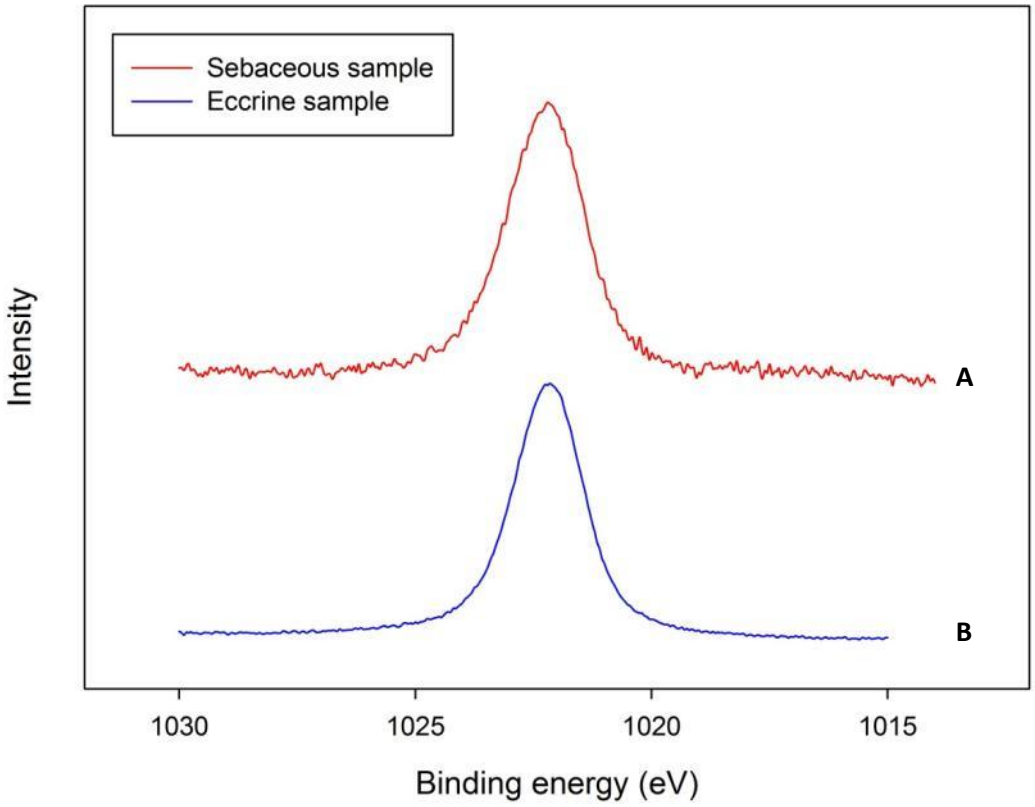

Figure 6.29 – XPS Zn $2p_{3/2}$ spectra for fingerprint samples stored in a humid environment at 75°C for two days and then washed with warm water and detergent, ***A)*** *sebaceous based fingerprint;* ***B)*** *eccrine based fingerprint.*

Both spectra in Figure 6.29 show single species zinc peaks at the same binding energy value of 1022.2 eV, this value is typically associated with Zn(II) as ZnO[2, 4]. No sign of Zn(0) species is present, unlike some Zn spectra for the fingerprinted samples (*ca*. 1021.9 eV).

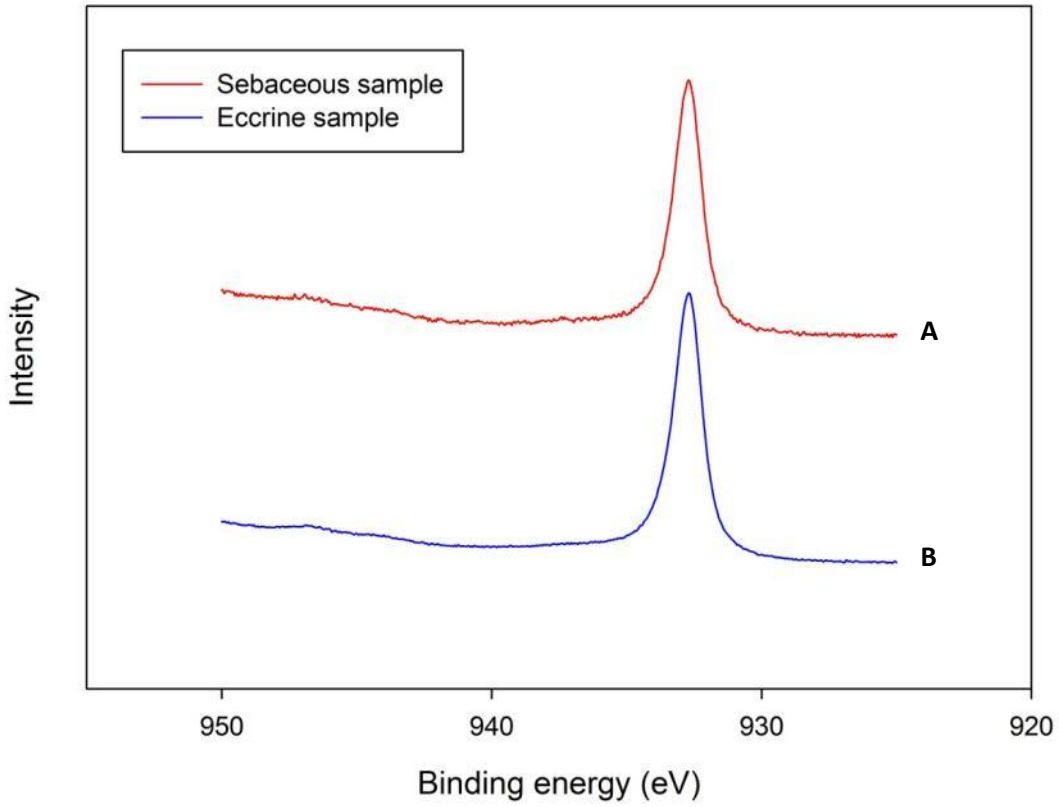

Figure 6.30 – XPS Cu $2p_{3/2}$ spectra for fingerprint samples stored in a humid environment at 75°C for two days and then washed with warm water and detergent, ***A)*** *sebaceous based fingerprint;* ***B)*** *eccrine based fingerprint.*

The peaks in Figure 6.30 have the same binding energy, 932.7 eV, so both represent the same copper species, namely Cu(0)[2, 9, 10, 24, 32]. Although it is unlikely that all of the surface copper would be in the elemental state, the position of the peak is firmly in the typical binding energy range for Cu(0) species.

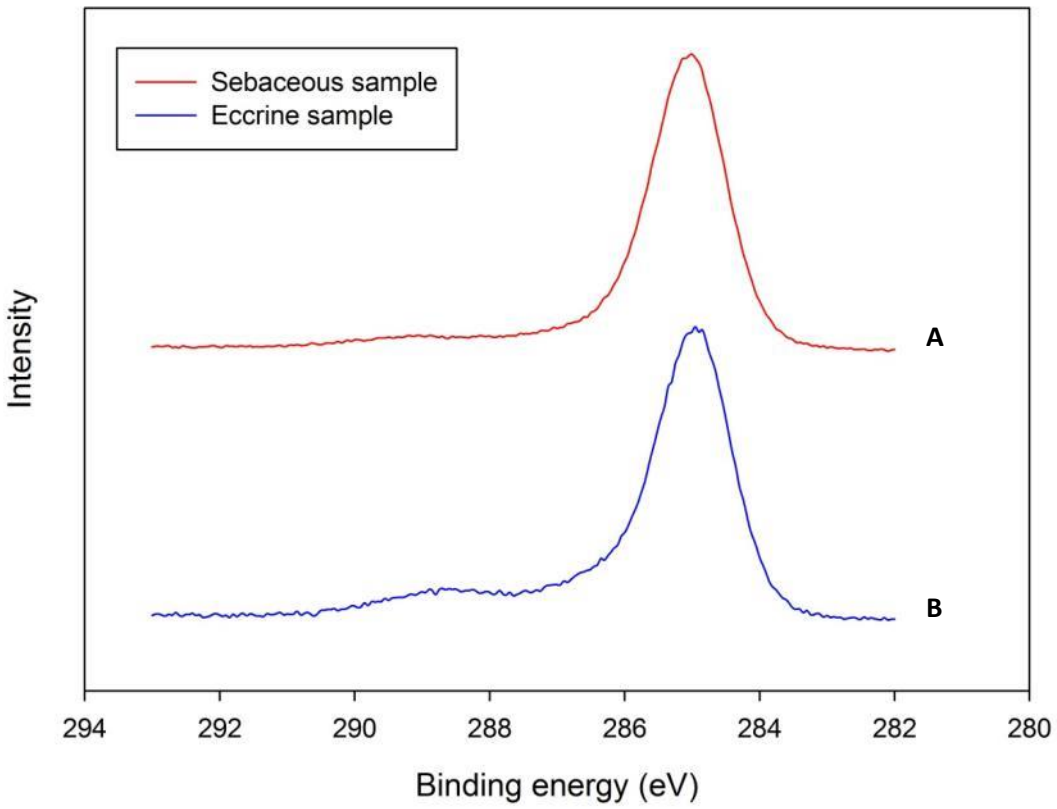

Figure 6.31 – XPS C 1s spectra for fingerprint samples stored in a humid environment at 75°C for two days and then washed with warm water and detergent, ***A)*** *sebaceous based fingerprint;* ***B)*** *eccrine based fingerprint.*

As with the copper and zinc spectra for these samples, the carbon spectra shown in Figure 6.31 also show single species main peaks with very similar binding energies: for the eccrine sample the peak is at 284.9 eV and for the sebaceous sample it is at 285.0 eV. Both these energy values are very similar and both represent carbons in alkane bonds[25, 29, 33, 34, 37, 38]. At higher binding energy values, a slight hump can be seen in both spectra at *ca.* 288.8 eV and 286.0 eV. The former is of carbon in carbonyl bonds[30] and the latter is typical of carbon in C-O bond types, most likely as C-OH[2, 33]. As both the eccrine and sebaceous fingerprinted samples have the same species present, it is unlikely this is remnants of sweat residue after the washing process. It is possible that the peaks present represent remnants of the surfactant from the

detergent used to wash the samples, surfactants have long uniform carbon chains with a carboxylate group on the end, which covers the three identified species.

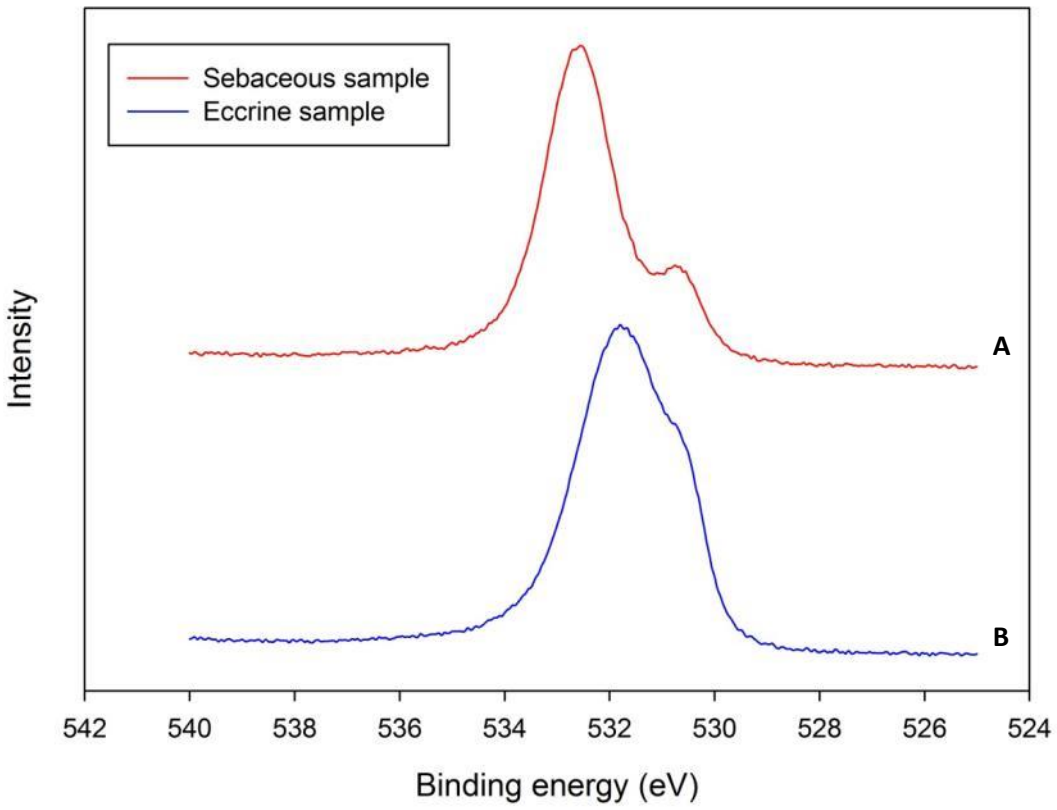

Figure 6.32 – XPS O 1s spectra for fingerprint samples stored at 75°C for two days and then washed with warm water and detergent, ***A)*** *sebaceous based fingerprint;* ***B)*** *eccrine based fingerprint.*

After the similarities seen in the zinc, copper and carbon spectra for the two samples, the O 1s spectra in Figure 6.32 show distinct differences, the peaks have different shapes and reside at slightly different energy values. The eccrine sample has a broad unsymmetrical peak which contains three signals, found at 531.8 eV, 530.5 eV and 533.8 eV, these are oxygen in OH[11, 13, 15, 42] or $Cu(OH)_2$[11] species, CuO or Cu_2O[8, 11, 23] and lastly oxygen in a C-O bond[2, 34]. The sebaceous sample has peaks at 532.6 eV, 530.7 eV and 534.2 eV, which are oxygen in H_2O[15, 17], in a copper species as either CuO[8, 23] or Cu_2O[8, 23] and lastly in a C-O bond[30]. As both copper spectra in Figure 6.30 indicated the presence of Cu(0) alone, it is surprising that the O 1s suggests

otherwise. The presence of a C-O bond in both instances partially matches with that identified in the carbon spectra (Figure 6.31), but signals for a carbonyl species were not seen in the O 1s spectra.

Table 6.6 – Ratio of copper to zinc for polished fingerprinted brass substrates wiped or washed before storage in a warm humid environment

Sweat type	Post deposition treatment	Ratio of Cu:Zn
Eccrine	Wiped with paper towel and then placed in a humid environment at 75°C for 20 hours followed by washing with warm water and detergent	1 : 1.18
Sebaceous	Wiped with paper towel and then placed in a humid environment at 75°C for 20 hours followed by washing with warm water and detergent	1 : 0.6
Eccrine	Washed with warm water and detergent and then placed in a humid environment at 75°C for 20 hours followed by washing with warm water and detergent	1 : 0.83
Sebaceous	Washed with warm water and detergent and then placed in a humid environment at 75°C for 20 hours followed by washing with warm water and detergent	1 : 0.83

Cu:Zn ratios for the samples that were washed and then stored in warm humid conditions in Table 6.6 are similar to those reported for humid stored and washed samples (Table 6.4) or warm humid stored and then washed samples (Table 6.5). In these two instances, the ratios showed a slight copper majority. The anomalies lie with the samples that were wiped before storage in warm humid conditions. The eccrine sample has more surface zinc than copper and the Cu:Zn ratio is more in line with that for aged eccrine fingerprinted samples at ambient and humid conditions than that for eccrine samples exposed to warm and humid conditions. The wiped sebaceous sample, whilst having the least amount of zinc, has a ratio similar to that of sebaceous samples at ambient conditions rather than humid or warm humid conditions.

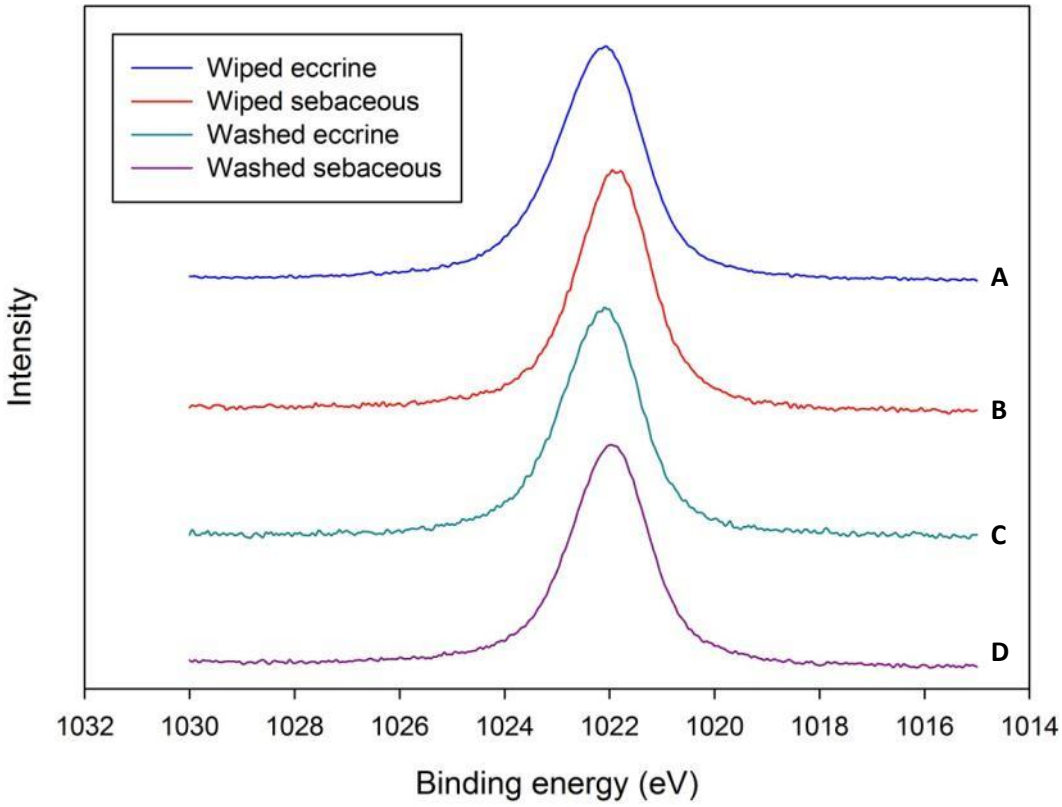

Figure 6.33 – XPS Zn $2p_{3/2}$ spectra of fingerprinted brass substrates treated in different manners before storage in a warm humid environment. ***A)*** *eccrine fingerprinted sample wiped with paper towel and then placed in a humid environment at 75°C for 20 hours, followed by washing with warm water and detergent;* ***B)*** *sebaceous fingerprinted sample wiped with paper towel and then placed in a humid environment at 75°C for 20 hours, followed by washing with warm water and detergent;* ***C)*** *eccrine fingerprinted sample washed with warm water and detergent and then placed in a humid environment at 75°C for 20 hours, followed by washing with warm water and detergent;* ***D)*** *sebaceous fingerprinted sample Washed with warm water and detergent and then placed in a humid environment at 75°C for 20 hours, followed by washing with warm water and detergent.*

All four samples in Figure 6.33 have similar peak profiles of a single zinc species, although the peak position varies slightly. The sebaceous wiped sample has the lowest binding energy (1021.9 eV), which is similar to that for the sebaceous washed sample (1020.0 eV). This peak position is typical of Zn(0)[2, 4, 24]. The two eccrine samples have a peak position of 1022.2 eV, more characteristic of Zn(II) as ZnO[2]. In this case the sweat type seems to have a distinct

bearing on the zinc species and its oxidation state: both the sebaceous samples contain Zn(0) whereas the eccrine have ZnO.

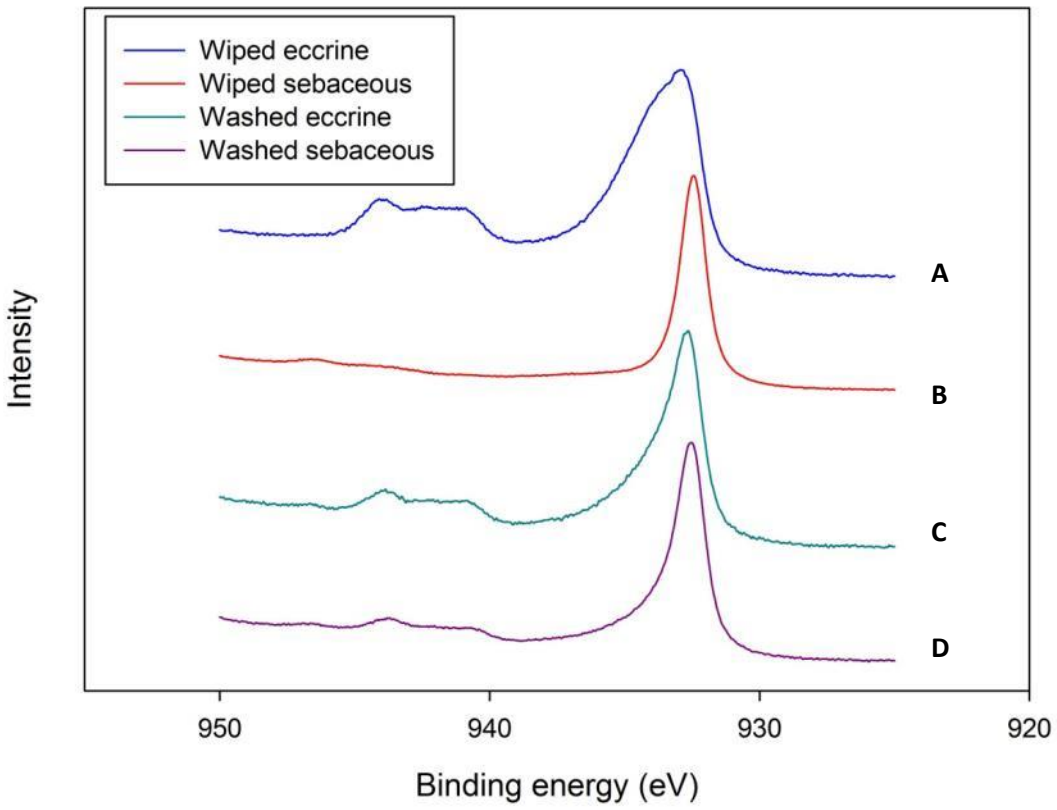

Figure 6.34 – XPS Cu $2p_{3/2}$ spectra of fingerprinted brass substrates treated in different manners before storage in a warm humid environment. ***A)*** *eccrine fingerprinted sample wiped with paper towel and then placed in a humid environment at 75°C for 20 hours, followed by washing with warm water and detergent;* ***B)*** *sebaceous fingerprinted sample wiped with paper towel and then placed in a humid environment at 75°C for 20 hours, followed by washing with warm water and detergent;* ***C)*** *eccrine fingerprinted sample washed with warm water and detergent and then placed in a humid environment at 75°C for 20 hours, followed by washing with warm water and detergent;* ***D)*** *sebaceous fingerprinted sample Washed with warm water and detergent and then placed in a humid environment at 75°C for 20 hours, followed by washing with warm water and detergent.*

In the spectra in Figure 6.34, each sample has a slightly broad peak in the main Cu $2p_{3/2}$ region (930-935 eV), the features in the satellite region (940-945 eV) vary in height in the washed samples but is only present in the eccrine wiped sample. The peaks in this region (940-945 eV)

can be identified as CuO satellites[43]. The main peak for the eccrine wiped sample is at 932.8 eV and the smaller peak is at 934.0 eV, these are attributable to copper in Cu(0)[2, 9, 10, 24] and CuO[8, 23, 32]. The sebaceous wiped sample has peaks at 932.4 eV and 933.7 eV, which are copper in Cu(I) as either CuCl[2] or Cu_2O[4, 8, 11, 23] and CuO[4, 8, 11, 12, 23, 32], respectively. The presence of a CuCl species was also found for fingerprinted sample stored in warm humid environments (chapter 5, section 5.2.3), in this washed series, CuCl was not found in the eccrine deposited sample. The eccrine washed sample has two peaks, one at 933.9 eV and the other at 932.7 eV; this latter is the same as in the eccrine wiped sample and is Cu(0)[2, 9, 10, 24] whilst the former is copper in CuO[4, 8, 11, 12, 23, 32]. Last, the sebaceous washed sample has three peaks found at 933.0 eV, 932.5 eV and 935.2 eV, which are most likely copper in Cu(0)[2, 9, 10], Cu_2O[4, 8, 11, 23] and $Cu(OH)_2$[32], respectively. Some elemental copper is expected, since that lying close beneath the thin oxide layer would also be detected.

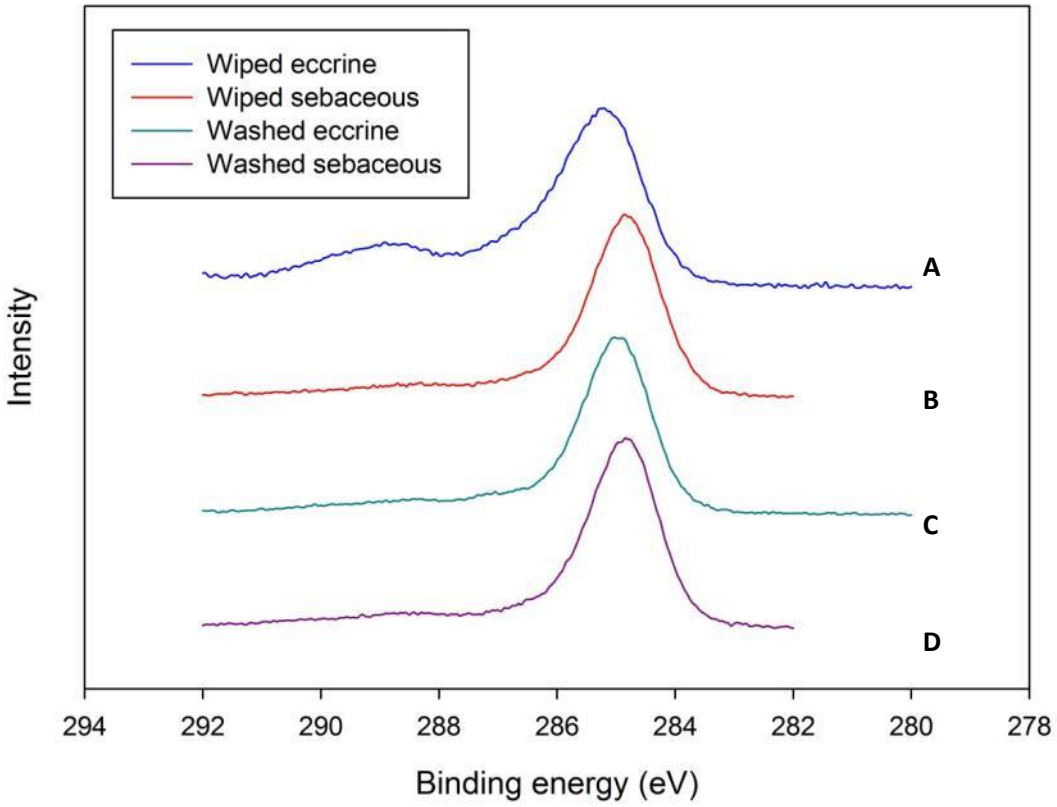

Figure 6.35 – XPS C 1s spectra of fingerprinted brass substrates treated in different manners before storage in a warm humid environment. ***A)*** *eccrine fingerprinted sample wiped with paper towel and then placed in a humid environment at 75°C for 20 hours, followed by washing with warm water and detergent;* ***B)*** *sebaceous fingerprinted sample wiped with paper towel and then placed in a humid environment at 75°C for 20 hours, followed by washing with warm water and detergent;* ***C)*** *eccrine fingerprinted sample washed with warm water and detergent and then placed in a humid environment at 75°C for 20 hours, followed by washing with warm water and detergent;* ***D)*** *sebaceous fingerprinted sample Washed with warm water and detergent and then placed in a humid environment at 75°C for 20 hours, followed by washing with warm water and detergent.*

Each spectrum in Figure 6.35 has a main peak at approximately 285 eV and subsidiary peaks at higher binding energies. The peak position varies from 284.8 eV for the sebaceous samples to 285.0 eV for the eccrine samples; in both cases these binding energy values are characteristic of carbon in alkanes[25, 29, 33, 34, 37]. The eccrine wiped sample has the other peaks at 288.9 eV and 286.2 eV, which are attributable to carbon in alkanes[34-36] and in C-O[26-29], respectively. The

eccrine washed sample has the additional peaks at 286.4 eV, 288.4 eV and 289.9 eV, which are attributable to carbon in C-O[2, 29, 41], carbonyl bonds[25] and possibly in carbonate[44, 45]. The wiped sebaceous sample has the subsidiary peaks at 286.3 eV, 288.2 eV and 289.4 eV, which are attributable to carbon in C-O[26-29], carbonyls[27, 40, 41] and ethyl carbonyls[30]. The washed sebaceous sample has the additional peaks at 285.8 eV and 288.6 eV, which are possibly carbon in aldehyde[39] and carbonyl[30] groups. The subsidiary peaks for each sample have varying energy values and subsequently varying identities, however, the amount of these present is minimal when compared to the intensity of the main peak.

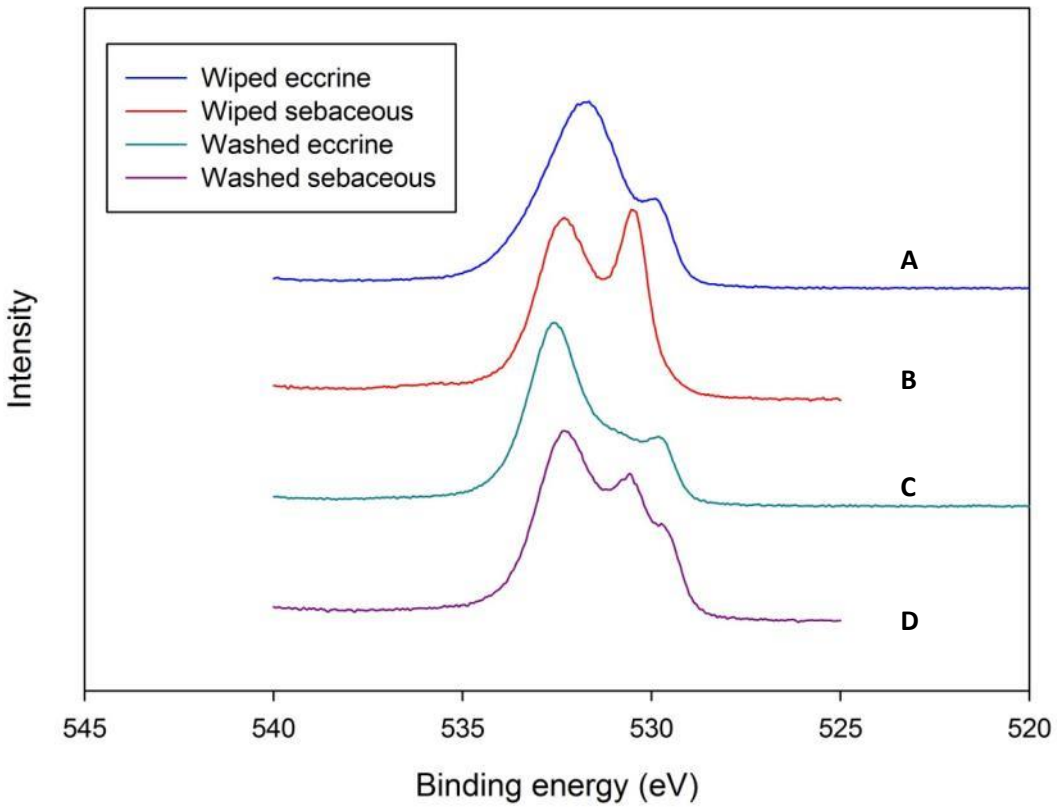

Figure 6.36 – XPS O 1s spectra of fingerprinted brass substrates treated in different manners before storage in a warm humid environment. ***A)*** *eccrine fingerprinted sample wiped with paper towel and then placed in a humid environment at 75°C for 20 hours, followed by washing with warm water and detergent;* ***B)*** *sebaceous fingerprinted sample wiped with paper towel and then placed in a humid environment at 75°C for 20 hours, followed by washing with warm water and detergent;* ***C)*** *eccrine fingerprinted sample washed with warm water and detergent and then placed in a humid environment at 75°C for 20 hours, followed by washing with warm water and detergent;* ***D)*** *sebaceous fingerprinted sample Washed with warm water and detergent and then placed in a humid environment at 75°C for 20 hours, followed by washing with warm water and detergent.*

Each spectrum in Figure 6.36 shows broad peaks containing multiple signals. Each spectrum and set of peaks has a different binding energy position and shape, with the shape being governed by the position of each peak present as well as their relative intensities. The wiped eccrine sample only has two components present, compared to the other samples having three components present, and these two can be found at 531.8 eV and 529.8 eV, which are

attributable to oxygen in either OH[11, 15] or $Cu(OH)_2$[11] and CuO[18, 20, 43]. CuO was also found in the copper spectrum (Figure 6.34) for the wiped eccrine sample, but $Cu(OH)_2$ was not. The washed eccrine sample had three peaks at 532.6 eV, 530.8 eV and 529.7 eV, which are attributable to oxygen in H_2O[13], $Cu(OH)_2$ and CuO[18, 20, 43] or ZnO[8]. Whilst a H_2O and a CuO or ZnO signal are expected, with the latter two matching assignments in Figure 6.34 and Figure 6.33, a $Cu(OH)_2$ species was not observed in the copper spectrum. The sebaceous wiped sample had peaks at 532.3 eV, 530.5 eV and 529.4 eV, which are typical of oxygen in H_2O[13], CuO or Cu_2O[23] and CuO[3] or ZnO[46] respectively. As the copper spectrum (Figure 6.34) for this sample reported the presence of both CuO and Cu_2O, the peaks found here are likely to be those as well, additionally the assignment of a ZnO peak here would not match the Zn(0) state reported in the zinc spectrum (Figure 6.33). The washed sebaceous sample peaks have very similar binding energy values to that of the wiped sebaceous sample, all within 0.1 eV. These three peaks can therefore be assigned in the same manner, as oxygen in H_2O[13], CuO or Cu_2O[23] and CuO[3] or ZnO[46] respectively. This washed sebaceous sample had copper signals for Cu_2O and Cu(0) as well as $Cu(OH)_2$ in the Cu 2p spectrum (Figure 6.34), the first corroborates with the O 1s findings but the latter does not, nor does the ZnO match the Zn(0) species proposed by the zinc spectrum (Figure 6.33). This leaves potentially three species that cannot be collaborated by the different XPS spectra (ZnO or CuO from O 1s and $Cu(OH)_2$ from Cu $2p_{3/2}$), meaning that at least one spectrum had peak positions incorrectly assigned. One possibility would be that the zinc species is actually ZnO rather than Zn(0), although this is not supported by the Zn $2p_{3/2}$ spectrum in Figure 6.33. Thus, the second possibility is that the Cu(II) species identified in Figure 6.34 is actually that of CuO rather than $Cu(OH)_2$, but again the binding energy position of the peaks conflict with this.

6.3 Summary

To facilitate comparisons between the data sets displayed in this chapter, tables showing consolidated data covering Cu:Zn ratios, peak positions and their corresponding species are detailed below. The data described in this chapter has covered a variety of conditions, for this reason, the data is displayed in two separate tables for each section. The first set compares unpolished and polished treated surfaces as well as basic environments for predominately eccrine fingerprinted samples. The second set comprises a comparison between pairs of eccrine and sebaceous fingerprinted samples that were treated similarly.

Table 6.7 – Consolidated surface Cu:Zn ratios for fingerprinted samples on polished and unpolished brass substrates exposed to a range of conditions and treatments

Substrate information	Storage conditions	Treatment	Additional storage conditions	Second treatment	Cu:Zn Ratio
Sebaceous; Unpolished	Humid 60°C	Detergent wash			1 : 0.39
Eccrine; Unpolished	Ambient	Detergent wash	Humid 60°C	Detergent wash	1 : 0.27
Eccrine; Polished	Ambient	Detergent washed			1 : 0.82
Eccrine; Polished	Humid 50°C	Detergent washed			1 : 2.2
Eccrine; Polished	Humid	Bunsen		Detergent washed	1: 5.1

The general trend for the majority of samples follows that suggested by the unwashed samples discussed in chapter 5. As with the unpolished control sample in Table 5.6 (1:0.25), the unpolished samples in Table 6.7 also show a higher amount of surface copper than zinc. The ambient polished and washed eccrine sample has a slight majority of surface copper (1:0.82), whereas non-washed samples in similar conditions had a higher proportion of surface zinc. The reason for this slight change could be the removal of zinc from the surface through selective leaching, with the washing step providing the carrier liquid. The two results that go slightly against the trend in chapter 5 are the last two listed. Warm humid conditions seemed to

promote an increase in surface copper, whereas with a washing step following the storage, an excess of surface zinc is seen. The fingerprinted sample treated by Bunsen flame had surface Cu:Zn showing a large excess of zinc as expected from chapter 5 and the lighter appearance of the sample. Whilst this ratio isn't as large as non-washed eccrine samples treated in a similar way (1:9.6), this could be explained by some surface zinc being removed by the washing process, possibly by selective leeching.

Table 6.8 – Consolidated surface Cu:Zn ratios for fingerprints on polished brass substrates, showing a comparison between eccrine and sebaceous samples

Treatment after deposition	Storage conditions	Treatment after storage	Cu:Zn ratio	
			Eccrine	Sebaceous
None	Humid	Detergent washed	1 : 0.86	1 : 0.88
None	Humid 75°C	Detergent washed	1 : 0.94	1 : 0.93
Wiped	Humid 75°C	Detergent washed	1 : 1.18	1 : 0.6
Detergent washed	Humid 75°C	Detergent washed	1 : 0.83	1 : 0.83

From the data displayed in Table 6.8, it can clearly be seen that for the majority samples, the storage environments and treatments had more affect on the surface Cu:Zn ratios than the sweat type present. In all but one case, there is an excess of surface copper to zinc, but still more surface zinc present that suggest by the bulk composition (1:0.47). The only exception to this case is the fingerprint printed samples that were subjected to being wiped shortly after deposition; the eccrine sample has a zinc majority on the surface, whereas the sebaceous sample has a copper majority. The wiping process would have spread some of the deposit across the surface and so one would expect the water based eccrine sample to be to have dezincification occur, with the leeched material removed by the washing process. However, this would lead to a ratio that was the opposite of what is seen above.

Table 6.9 – Consolidated Zn $2p_{3/2}$ peak positions and peak identities for fingerprinted samples on polished and unpolished brass substrates exposed to a range of conditions and treatments

Substrate information	Storage conditions	Treatment	Additional storage conditions	Second treatment	Peak position	Species
Sebaceous; Unpolished	Humid 60°C	Detergent wash			1022.1	Zn/ZnO
Eccrine; Unpolished	Ambient	Detergent wash	Humid 60°C	Detergent wash	1022.1	Zn/ZnO
Eccrine; Polished	Ambient	Detergent washed			1021.8	Zn(0)
Eccrine; Polished	Humid 50°C	Detergent washed			1022.1 1022.7	Zn/ZnO $Zn(OH)_2$
Eccrine; Polished	Humid	Bunsen		Detergent washed	1022.1	Zn/ZnO

The Zn 2p3/2 peak positions for all of the samples in Table 6.9 are similar to what would be expected based on previous work (Chapter 5), however the main exception is the presence of a $Zn(OH)_2$ species. For this eccrine washed sample the O 1s spectrum also has a corroborating peak suggesting such a species. Even with a low proportion of Zn for the unpolished eccrine sample, the peak position is more normally associated with ZnO than Zn(0), suggesting that the detected zinc species are present on the surface rather than just below.

Table 6.10 – Consolidated Zn $2p_{3/2}$ peak positions and peak identities for fingerprints on polished brass substrates, showing a comparison between eccrine and sebaceous samples

Sweat type	Treatment after deposition	Storage conditions	Treatment after storage	Peak position	Species
Eccrine	None	Humid	Detergent washed	1022.1	ZnO
Sebaceous	None	Humid	Detergent washed	1021.9	Zn(0)
Eccrine	None	Humid 75°C	Detergent washed	1022.2	ZnO
Sebaceous	None	Humid 75°C	Detergent washed	1022.2	ZnO
Eccrine	Wiped	Humid 75°C	Detergent washed	1022.2	ZnO
Sebaceous	Wiped	Humid 75°C	Detergent washed	1021.9	Zn(0)
Eccrine	Detergent washed	Humid 75°C	Detergent washed	1022.2	ZnO
Sebaceous	Detergent washed	Humid 75°C	Detergent washed	1020.0	Zn(0)

The peak positions in Table 6.10 also reflect similar findings, the majority of samples producing peaks with binding energy values associated more with ZnO than Zn(0). Several sebaceous samples have a slightly lower binding energy position, more characteristic of Zn(0) despite the surface composition proportionally containing more zinc than the bulk composition.

Table 6.11 – Consolidated Cu $2p_{3/2}$ peak positions and peak identities for fingerprinted samples on polished and unpolished brass substrates exposed to a range of conditions and treatments

Substrate information	Storage conditions	Treatment	Additional storage conditions	Second treatment	Peak position	Species
Sebaceous; Unpolished	Humid 60°C	Detergent wash			933.9 932.9	CuO Cu(0)
Eccrine; Unpolished	Ambient	Detergent wash	Humid 60°C	Detergent wash	933.2 932.7	CuO Cu(0)
Eccrine; Polished	Ambient	Detergent washed			932.5 933.2	Cu_2O CuO
Eccrine; Polished	Humid 50°C	Detergent washed			932.8 934.0	Cu(0) CuO
Eccrine; Polished	Humid	Bunsen		Detergent washed	933.5	CuO

The majority of copper species found in Table 6.11 were CuO, with some Cu(0) also found. The CuO would be the predominate surface species, with the Cu(0) being detected from just below the surface. There is one instance where a Cu(I) species was observed, in the case of an eccrine fingerprinted sample subjected to ambient conditions prior to washing. This binding energy value is on the border of values reported for Cu(0) and Cu(I) but more towards Cu(I) states, as there is also the presence of CuO, the other species could be either oxidised or elemental copper. Since this peak at 932.5 eV is the predominate one, with a surface Cu:Zn ratio suggesting a copper excess, the oxidised copper would be the more expected product.

Table 6.12 – Consolidated Cu $2p_{3/2}$ peak positions and peak identities for fingerprints on polished brass substrates, showing a comparison between eccrine and sebaceous samples

Sweat type	Treatment after deposition	Storage conditions	Treatment after storage	Peak position	Species
Eccrine	None	Humid	Detergent washed	932.8 933.8	Cu(0) CuO
Sebaceous	None	Humid	Detergent washed	932.5 933.9 933.2	Cu_2O CuO $Cu(OH)_2$
Eccrine	None	Humid 75°C	Detergent washed	932.7	Cu(0)
Sebaceous	None	Humid 75°C	Detergent washed	932.7	Cu(0)
Eccrine	Wiped	Humid 75°C	Detergent washed	932.8 934.0	Cu(0) CuO
Sebaceous	Wiped	Humid 75°C	Detergent washed	932.4 933.7	$CuCl/Cu_2O$ CuO
Eccrine	Detergent washed	Humid 75°C	Detergent washed	933.9 932.7	CuO Cu(0)
Sebaceous	Detergent washed	Humid 75°C	Detergent washed	933.0 932.5 935.2	Cu(0) Cu_2O $Cu(OH)_2$

The species found on the surface of the samples in Table 6.12 are slightly more varied than those in Table 6.11, however the eccrine fingerprinted samples only display either Cu(0) or both Cu(0) and CuO; it is the sebaceous fingerprinted samples that display the more varied species. The two instances where only Cu(0) was reported is very strange, the binding energy value strongly suggests a Cu(0) state, with narrow peaks (Figure 6.30), however, the copper species is also the dominate surface metal. For the sebaceous samples, the presence of multiple oxidation states or species for copper isn't in itself surprising, one would expect two states, with one with the oxidised surface copper and the other as either the underlying bulk material or an alternative oxidised copper. The humid washed sebaceous sample has two different oxidation states present, Cu(I) and Cu(II), suggesting that all the copper is oxidised and on the surface rather than just below. Although the presence of the copper hydroxide species is unusual, this is also supported by peaks seen for the O 1s data. The warm humid,

twice washed, sebaceous sample has all three oxidation states of copper present. The Cu(0) would mostly likely be below the surface, whereas the Cu(I) and Cu(II) species would be surface lying. Although, most surprisingly, this sample has no peak associated with the commonly found CuO species.

Table 6.13 – Consolidated C 1s peak positions and peak identities for fingerprinted samples on polished and unpolished brass substrates exposed to a range of conditions and treatments

Substrate information	Storage conditions	Treatment	Additional storage conditions	Second treatment	Peak position	Species
Sebaceous; Unpolished	Humid 60°C	Detergent wash			285.3	Hydrocarbon
Eccrine; Unpolished	Ambient	Detergent wash	Humid 60°C	Detergent wash	285.3	Hydrocarbon
Eccrine; Polished	Ambient	Detergent washed			284.7 286.3 288.7	Hydrocarbon C-O carbonyl
Eccrine; Polished	Humid 50°C	Detergent washed			285.4 286.0 289.1	Alkane C-O alkane
Eccrine; Polished	Humid	Bunsen		Detergent washed	285.1 287.3	Alkane carbonyl

The carbon species suggested by Table 6.13 shows predominately signals around 285 eV, typical for residual carbon or hydrocarbons. The presence of a peak here would be expected for the majority of C 1s spectra, regardless of being fingerprinted or not. There are several carbon-oxygen species suggested by the binding energy values of peaks in the C 1s spectra, however, very few of these were observed for the O 1s spectra. The lack of significant peaks is not surprising since the washing regime is designed to remove any soluble or adhered material and therefore the majority of the sweat deposit would also have been removed by this process.

Table 6.14 – Consolidated C 1s peak positions and peak identities for fingerprints on polished brass substrates, showing a comparison between eccrine and sebaceous samples

Sweat type	Treatment after deposition	Storage conditions	Treatment after storage	Peak position	Species
Eccrine	None	Humid	Detergent washed	285.0 286.3 288.7	Alkane C-O Carbonyl
Sebaceous	None	Humid	Detergent washed	284.8 285.6 288.9 288.3	Alkane Alkane Alkane carbonyl
Eccrine	None	Humid 75°C	Detergent washed	284.9 288.8 286.0	Alkane Carbonyl C-OH
Sebaceous	None	Humid 75°C	Detergent washed	284.9 288.8 286.0	Alkane Carbonyl C-OH
Eccrine	Wiped	Humid 75°C	Detergent washed	284.8 288.9 286.2	Alkane Alkane C-O
Sebaceous	Wiped	Humid 75°C	Detergent washed	285.0 286.3 288.2 289.4	Alkane C-O Carbonyl Ethyl carbonate
Eccrine	Detergent washed	Humid 75°C	Detergent washed	284.8 286.4 288.4 289.9	Alkane C-O Carbonyl Carbonate
Sebaceous	Detergent washed	Humid 75°C	Detergent washed	285.0 285.8 288.6	Alkane Aldehyde Carbonyl

The range of species found Table 6.14 suggests that the washing treatments are ineffective for the removal of the sweat residue. A variety of peaks are found at binding energy positions not associated with residual signals (285 eV), and therefore directly indicate surface species. As most samples have a carbonyl present, it could be proposed that is a remnant of the surfactant used in the cleaning process as surfactants have a long hydrocarbon chain with a carboxylic group on one end. The carboxylic component contains both the carbonyl (C=O) and hydroxyl groups (C-O).

Table 6.15 – Consolidated O $1s_{/2}$ peak positions and peak identities for fingerprinted samples on polished and unpolished brass substrates exposed to a range of conditions and treatments

Substrate information	Storage conditions	Treatment	Additional storage conditions	Second treatment	Peak position	Species
Sebaceous; Unpolished	Humid 60°C	Detergent wash			532.1 529.8	H_2O/OH ZnO
Eccrine; Unpolished	Ambient	Detergent wash	Humid 60°C	Detergent wash	531.9 532.6 529.8	OH H_2O ZnO
Eccrine; Polished	Ambient	Detergent washed			531.5 530.2	CuO/ZnO Cu_2O
Eccrine; Polished	Humid 50°C	Detergent washed			532.0 533.4 530.4	$Zn(OH)_2$ C-O CuO/Cu_2O
Eccrine; Polished	Humid	Bunsen		Detergent washed	531.9	OH

There is some overlap of ZnO and CuO peak positions in O 1s spectra, this comes about by having a shared oxide layer on the surface of the brass alloy; typically this is observed around 530 to 531 eV. The exact position of this peak is determined by the surface composition, oxidation states of the metal (principally copper in brass alloy) amongst other factors. Therefore, although specific peaks in the O 1s spectra may not be observed for every metal oxide species, they can still be present.

Table 6.16 – Consolidated O 1s peak positions and peak identities for fingerprints on polished brass substrates, showing a comparison between eccrine and sebaceous samples

Sweat type	Treatment after deposition	Storage conditions	Treatment after storage	Peak position	Species
Eccrine	None	Humid	Detergent washed	532.0 530.3	OH/H_2O Cu_2O/CuO
Sebaceous	None	Humid	Detergent washed	531.7 530.2	$Cu(OH)_2$ $CuO/ZnO/Cu_2O$
Eccrine	None	Humid 75°C	Detergent washed	531.8 530.5 533.8	$Cu(OH)_2$ CuO/CU_2O C-O
Sebaceous	None	Humid 75°C	Detergent washed	532.6 530.7 534.2	H_2O CuO/Cu_2O C-O
Eccrine	Wiped	Humid 75°C	Detergent washed	531.8 529.8	$Cu(OH)_2$ CuO
Sebaceous	Wiped	Humid 75°C	Detergent washed	532.3 530.5 529.4	H_2O CuO/Cu_2O CuO/ZnO
Eccrine	Detergent washed	Humid 75°C	Detergent washed	532.6 530.8 529.7	H_2O $Cu(OH)_2$ CuO/ZnO
Sebaceous	Detergent washed	Humid 75°C	Detergent washed	532.3 530.5 529.4	H_2O CuO/Cu_2O CuO/ZnO

The range of species reported for the O 1s data in Table 6.16 mostly supports the species proposed by the previous data seen in this summary section. The presence of the hydroxyl groups was also reported for C 1s species and the majority of the metal oxide species are corroborated by the relevant metal $2P_{3/2}$ spectral data. The unusual species not expected was a H_2O species, however this is most likely adsorbed water on the substrate surface rather than the water component of the sweat deposit.

6.4 Conclusions

Fingerprints deposited on substrates are more visually apparent if the substrate has a uniform and smooth finish. The fingerprint is more apparent on polished samples than unpolished samples while aging undisturbed; the residue is also easier to monitor and measure by visual

or physical means on polished surfaces. However, chemically only a few small differences were noticeable, such as the Cu:Zn ratio showing an excess of surface copper. Similar Cu and Zn species were observed in the $2p_{3/2}$ regions for both polished and unpolished samples, although the signal for Cu(0) was smaller for unpolished than polished fingerprinted substrates. Additionally, fingerprints on unpolished substrates were very resilient to removal by washing in warm water and detergent as well as the use of acetone. As with Paterson's[1] findings on unpolished discs, warm water and detergent did remove some sweat residue, sufficient for conventional powder techniques to not enhance the fingerprint, but upon exposure to a warm and humid environment, fingerprint ridge details became visible. This confirms that whilst washing the samples does remove some of the material, sufficient for them to be a latent/invisible fingerprint mark, sufficient material can remain for the fingerprint to be visualised by other means, including imaging by surface chemical species.

On polished substrates with eccrine fingerprints, the amount of residue removed by successive removal treatments was successfully monitored by physical measurements (AFM) and optical microscopic measurements (primarily DHM). Although large reductions in deposited material could be seen at both the nanoscale and microscopic level, only minimal changes were observed at the macroscopic level. Therefore the material removed was not necessarily the sole visual part of the fingerprint image and either trace components of the residue remain or a surface chemical change has occurred; there are indications that both occurred. Chemical analysis still has similar components present to those for undisturbed fingerprinted samples, which are also distinctly different from the unprinted substrates. The major surface chemical difference is in the Cu:Zn ratio: very few of the ratios observed were in line with either the non-fingerprinted substrates or their undisturbed fingerprinted counterparts in chapter 5.

Fingerprinted samples that were exposed to warm humid conditions, with temperatures in excess of 50°C, produced the most visible fingerprints and there was little impact on the appearance of the fingerprints regardless of whether they were washed before or after storage in this environment. Wiping of samples produced clear fingerprint images and the chemical analysis was in line with findings for the washed equivalents generally, with the main exception being the Cu:Zn ratio. The ratio amounts for these samples were inconsistent and displayed values outside of what was expected, whilst the washed samples had near identical Cu:Zn ratios despite being fingerprinted with different sweat types.

The washing of visible fingerprints may cause them to become latent, but traces can still be detected by physical or chemical means. The amount of material required to produce a visual fingerprint is less than 200 nm thick and with this amount remaining, not much loss of detail is found on the macroscopic level. Whilst, chemically, the fingerprint samples may have similar spectroscopic signatures and identities irrespective of post-deposition treatment, these differ from non-fingerprinted samples. Thus, traces of the contact can still be found after attempts to remove the fingerprints. With all this considered together, it is proven to be near impossible to remove all traces of fingerprints and therefore transfers of sweat material by washing with detergent or acetone. After these treatments, sufficient material remains for visualisation by a controlled heat environment is possible. If one wants to remove fingerprints from evidence or non-study materials, then washing will remove the fingerprints to a level undetectable with conventional enhancement techniques. However, the traces of the fingerprint can still be detected and consequently imaged by chemical spectroscopic techniques.

6.5 References

1. E. Paterson, J. W. Bond and A. R. Hillman, *J. Forensic Sci.*, 2010, **55**, 221-224.
2. C. D. Wagner, W. M. Riggs, L. E. Davis and J. F. Moulder, *Handbook of x-ray photoelectron spectroscopy: a reference book of standard data for use in x-ray photoelectron spectroscopy*, first edn., Physical Electronics Division, Perkin-Elmer Corp., 1979.
3. D. Briggs and P. Seah, *Practical Surface Analysis: Auger and X-ray photoelectron spectroscopy*, Wiley, 1990.
4. S. Maroie, G. Haemers and J. J. Verbist, *Appl. Surf. Sci.*, 1984, **17**, 463-467.
5. T. Kosec, D. K. Merl and I. Milosev, *Corros. Sci.*, 2008, **50**, 1987-1997.
6. I. Milosev, T. K. Mikic and M. Gaberscek, *Electrochim. Acta*, 2006, **52**, 415-426.
7. I. Milosev and H. H. Strehblow, *J. Electrochem. Soc.*, 2003, **150**, B517-B524.
8. V. I. Nefedov, D. Gati, B. F. Dzhurinskii, N. P. Sergushin and Y. V. Salyn, *Zhurnal Neorg. Khimii*, 1975, **20**, 2307-2314.
9. P. Marcus and M. E. Bussell, *Appl. Surf. Sci.*, 1992, **59**, 7-21.
10. H. M. Liao, R. N. S. Sodhi and T. W. Coyle, *J. Vac. Sci. Technol. A-Vac. Surf. Films*, 1993, **11**, 2681-2686.
11. T. L. Barr, *J. Phys. Chem.*, 1978, **82**, 1801-1810.
12. T. L. Barr, *J. Vac. Sci. Technol. A-Vac. Surf. Films*, 1991, **9**, 1793-1805.
13. W. P. Yang, D. Costa and P. Marcus, *J. Electrochem. Soc.*, 1994, **141**, 2669-2676.
14. A. M. Beccaria, G. Poggi and G. Castello, *Brit. Corros. J.*, 1995, **30**, 283-287.
15. A. S. Lim and A. Atrens, *Appl. Phys. A-Mater.*, 1990, **51**, 411-418.
16. B. Stypula and J. Stoch, *Corros. Sci.*, 1994, **36**, 2159-2167.
17. S. Jin and A. Atrens, *Appl. Phys. A-Mater.*, 1987, **42**, 149-165.
18. J. C. Otamiri, A. Andersson, S. L. T. Andersson, J. E. Crow and G. Ye, *J. Chem. Soc.-Faraday Trans.*, 1991, **87**, 1265-1271.
19. E. Agostinelli, C. Battistoni, D. Fiorani, G. Mattogno and M. Nogues, *J. Phys. Chem. Solids*, 1989, **50**, 269-272.
20. G. Schon, *Surf. Sci.*, 1973, **35**, 96-108.
21. T. Robert, M. Bartel and G. Offergeld, *Surf. Sci.*, 1972, **33**, 123-130.
22. C. E. Dube, B. Workie, S. P. Kounaves, A. Robbat, M. L. Aksu and G. Davies, *J. Electrochem. Soc.*, 1995, **142**, 3357-3365.
23. N. S. McIntyre and M. G. Cook, *Anal. Chem.*, 1975, **47**, 2208-2213.
24. L. Ley and M. Cardona, *Photoemission in Solids II: Case Studies*, Springer-Verlag, Berlin, 1979.
25. N. Moncoffre, G. Hollinger, H. Jaffrezic, G. Marest and J. Tousset, *Nucl. Instrum. Methods Phys. Res. Sect. B-Beam Interact. Mater. Atoms*, 1985, **7-8**, 177-183.
26. J. J. Pireaux, M. Chtaib, Q. T. Le and R. Caudano, *Le Vide, les couches minces*, Société française du vide, 1991.
27. S. Delpeux, F. Beguin, R. Benoit, R. Erre, N. Manolova and I. Rashkov, *Eur. Polym. J.*, 1998, **34**, 905-915.
28. L. N. Boi, M. Thompson, N. B. McKeown, A. D. Romaschin and P. G. Kalman, *Analyst*, 1993, **118**, 463-474.
29. S. Contarini, S. P. Howlett, C. Rizzo and B. A. De Angelis, *Appl. Surf. Sci.*, 1991, **51**, 177-183.
30. D. T. Clark and H. R. Thomas, *J. Polym. Sci. Pol. Chem.*, 1976, **14**, 1701-1713.
31. L. S. Dake, D. R. Baer and J. M. Zachara, *Surf. Interface Anal.*, 1989, **14**, 71-75.
32. L. S. Dake, D. E. King and A. W. Czanderna, *Solid State Sci.*, 2000, **2**, 781-789.

33. V. Wiertz and P. Bertrand, in *ICPSI - 2, Polymer-Solid Interfaces : From Model to Real Systems*, eds. J.J. Pireaux, J. Delhalle and P. Rudolf, Universitaires de Namur, Namur, 1998, pp. 485-499.
34. D. T. Clark and H. R. Thomas, *J. Polym. Sci. Pol. Chem.*, 1978, **16**, 791-820.
35. J. L. Droulas, T. M. Duc and Y. Jugnet, *Le Vide, les couches minces*, Société française du vide, 1991.
36. N. M. D. Brown, J. A. Hewitt and B. J. Meenan, *Surf. Interface Anal.*, 1992, **18**, 187-198.
37. J. Charlier, V. Detalle, F. Valin, C. Bureau and G. Lecayon, *J. Vac. Sci. Technol. A-Vac. Surf. Films*, 1997, **15**, 353-364.
38. D. S. Campbell, H. J. Leary, J. S. Slattery and R. J. Sargent, *IBM General Technology Division (ed.), Essex Junction, VT 05452,* , 1981, 328.
39. P. Sundberg, R. Larsson and B. Folkesson, *J. Electron Spectrosc.*, 1988, **46**, 19-29.
40. P. Y. Jouan, M. C. Peignon, C. Cardinaud and G. Lemperiere, *Appl. Surf. Sci.*, 1993, **68**, 595-603.
41. C. Bichler, T. Kerbstadt, H. C. Langowski and U. Moosheimer, *Surf. Coat. Technol.*, 1997, **97**, 299-307.
42. I. Olefjord, B. Brox and U. Jelvestam, *J. Electrochem. Soc.*, 1985, **132**, 2854-2861.
43. F. Parmigiani, G. Pacchioni, F. Illas and P. S. Bagus, *J. Electron Spectrosc.*, 1992, **59**, 255-269.
44. G. Fierro, G. M. Ingo and F. Mancia, *Corrosion*, 1989, **45**, 814-823.
45. W. Kowbel and C. H. Shan, *Carbon*, 1990, **28**, 287-299.
46. Y. Kaneko and Y. Suginohara, *J. Jpn. Inst. Met.*, 1977, **42**, 285.

Chapter Seven:

Conclusions and Future Work

7.1 Conclusions

The central theme of this thesis has been the nature of fingerprints on brass substrate, based on investigation of the interaction between the sweat deposit and the brass substrate. This was accomplished by examining the effects of storage environment and ageing of fingerprinted samples, with monitoring by optical, physical and chemical means. Secondly, the effects of post-deposition removal attempts were studied, including the extent to which different removal methods impact the sample surface in terms of physical and chemical changes of both the substrate and the fingerprint material.

Physical and optical monitoring of fingerprinted samples has enabled characterisation of the changes occurring in the sweat residue as it ages. The AFM showed that freshly deposited fingerprint material comprises densely packed stalagmites and that the residue becomes more compact with ageing. The natural visualisation and enhancement of the fingerprint mark is promoted by storage in warm (>50°C) humid environments, in these conditions a fingerprint can be revealed in several hours, as opposed to several weeks in ambient storage conditions.

Different storage environments also affect the chemical composition of the substrate. Warm humid environments caused a higher relative amount of surface copper to be present. The exception to this is exposure to a Bunsen flame, which increases the relative amount of surface zinc.

The surface Cu:Zn ratios and the peak positions obtained by XPS suggest the presence of two distinct environments on sample surfaces: one is created by the presence of the fingerprint deposit and the second is the non-fingerprinted areas (bare substrate). This is revealed by local binding energy variations in spatially resolved spectra and supported by multi-component peaks present in non-spatially resolved spectra. Although spatially resolved data shows this

localisation and separation, species identification is not always possible due to resolution limitations. However, this could be addressed by using longer acquisition times, either by having longer dwell times or by multiple energy scans. In the spatially resolved data, the copper and zinc intensity was lower where carbon was present, which indicates that the fingerprint material is sufficiently thick in order to block XPS signals; this is supported by AFM measurements. A binding energy peak position difference for zinc, copper and carbon was also observed between fingerprinted and control samples at ambient conditions. Although present to some extent in other storage environments (copper variations in warm humid environments), it was less noticeable.

The Cu:Zn ratios of fingerprinted samples represent averaged data from both the fingerprinted and non-fingerprinted regions of the sample. In instances where the deposit is sufficiently thick (>10 µm) to block the substrate signals, this would not alter the ratio value although it may be incorrectly reported (i.e. reported for fingerprint containing regions rather than just bare substrate). Interestingly, sebaceous sweat samples contained less surface zinc than eccrine sweat samples. As eccrine sweat is 98% water, dezincification of the substrate could be occurring, but the zinc products remain in the fingerprint material. Another possible reason for this could be species migration, as proposed by *Barr et al.*[1], the ZnO layer forms preferentially to any copper oxide species and zinc migrates to the surface, further increasing both the passivation layer as well as the proportion of zinc on the surface. As the samples ages, formation of copper oxide species begin along with diffusion of copper to the surface, thus older brass surfaces proportionally contain more copper than older surfaces. These aged brass surfaces are also darker in colour than fresh, further supporting this theory.

The carbon XPS spectra of ambient stored sebaceous fingerprint samples contained multiple components and were distinctive from both control and eccrine fingerprinted samples; although this was expected for all storage environments, this was not the case. The storage of sebaceous samples in non-ambient environments had a detrimental effect on the composition and components of the sweat material. The carbon and oxygen spectra for eccrine fingerprinted samples contained very few signals; this is not surprising since it is mostly water-based. Because of the differences in the components of the sweat types, as well as the relative amounts of each, it is possible to differentiate between them primarily when stored at ambient conditions.

Chemically, there is little difference between polished and unpolished brass surfaces, the primary difference being less elemental copper present on the surface of fingerprinted unpolished substrates for both fingerprinted and non-fingerprinted samples. In the fingerprinted samples that were treated before exposure to warm humid conditions, there is a marked difference in the binding energy position of zinc species. For both washed and wiped post-deposition treated samples, eccrine samples typically had a peak position 0.2 eV higher than sebaceous samples in the Zn $2p_{3/2}$ region.

As mentioned above, Barr *et al.*[1] proposed that in a brass alloy, the zinc will preferentially be oxidised before the onset of any copper oxidation; the oxidation of any copper species does not begin prior to near completion of the ZnO layer. Thus following this it is possible to determine the extent of formation of the natural passivation layer. Where Cu(0) is encountered, the passivation has not been completed, where no Cu(0) is found, either passivation is complete or a corrosion mechanism has occurred. The final formation of Cu(II) is more favourable than Cu(I) species, in fully oxidised surfaces a predominate Cu(II) species would be present. Therefore, in more oxidised samples (either induced by age or condition),

one would expect predominately Cu(II) species to be present. However, in most of the copper spectra there is the presence of more than a single oxidation state of copper. By viewing the spatial resolved XPS data, in most cases it can be seen that the non-fingerprinted surface contains mainly Cu(II) as CuO, the expected product of natural passivation. Although the peak signal is weaker for the fingerprinted regions in the spatial resolved spectra, it can be implied that the other copper species detected, primarily Cu(I), could be present in these regions.

Fingerprint residue on both polished and unpolished substrates is resilient to removal. AFM measurements show a large reduction in material after various post-deposition treatments, but there is little reduction in visual quality of the fingerprint. After washing in warm soapy water, a non-visible fingerprint can still be recovered by exposure to a warm humid environment. This finding is in contrast to that found by Paterson et al.[2], a similar washing procedure appeared sufficient to remove the fingerprint; however, the main difference is that they only attempted recovery using conventional techniques (powdering), whereas the recovery of fingerprints documented in this thesis has been based on developing a naturally enhanced image rather than applying foreign material. Washing before or after storage in a warm humid environment had little impact on the resultant visual quality of a fingerprint.

There are indications that the sweat deposit remains on the sample surface despite removal attempts. Additionally, this has caused localised surface chemical changes, since the surface species found on post-deposition treated fingerprinted samples were different to those found on control samples. In cases where the sample had been subjected to washing treatments and carbon spectra showed only a single peak (residual carbon), the copper spectra showed multiple oxidation states, which were uncharacteristic of the non-fingerprinted samples. The washing process also had a greater impact on surface Cu:Zn ratios than the sweat type whereas for non-treated samples there was a marked difference between the Cu:Zn ratio for

the two sweat types. Washing regimes create a difference in surface Cu:Zn composition; the reason for this is unknown. The colours of the samples are similar for both washed and unwashed samples despite the difference in Cu:Zn ratios; therefore the hypothesis is that the washing helped remove the de-zincified material.

It was found nearly impossible to remove all traces of the fingerprints from the brass without abrasion of the surface. In instances where the fingerprint was sub-visible or partially visible, components of the fingerprint material could still be detected chemically.

The findings detailed throughout this thesis have a significant impact on the protocols for laboratory experiments involving the study of fingerprints as well as new procedures for processing evidential items. In laboratory studies where samples are accidentally contaminated with fingerprints, they should be subjected to an abrasive cleaning regime; washing in warm soapy water without abrasion is not sufficient to remove all traces of the fingerprint deposit. With regards to evidential recovery, the work in this thesis has detailed how to identify trace components that are non-visible by eye as well as the ability to map these traces by means of chemical imaging.

7.2 Future Work

7.2.1 Overview

This thesis demonstrated the ability to study fingerprint deposit material on brass substrates. Whilst brass can be commonly found containing fingerprints in crime related situations, the brass found in those circumstances will not always be as smooth or flat as the model substrates used here. Also, there is a wider range of metal substrates that can be corroded by fingerprint deposition material. These considerations provide motivation for further study, outlined below with the inclusion of some preliminary work.

7.2.2 Extension to Other Metallic Substrates

Those metals that are susceptible to natural enhancement of fingerprints by corrosion pathways include copper and copper containing metals. For copper, the process of detection and imaging is similar to that used for brass; fingerprints on copper can be spatially resolved using XPS (shown in Figure 7.1).

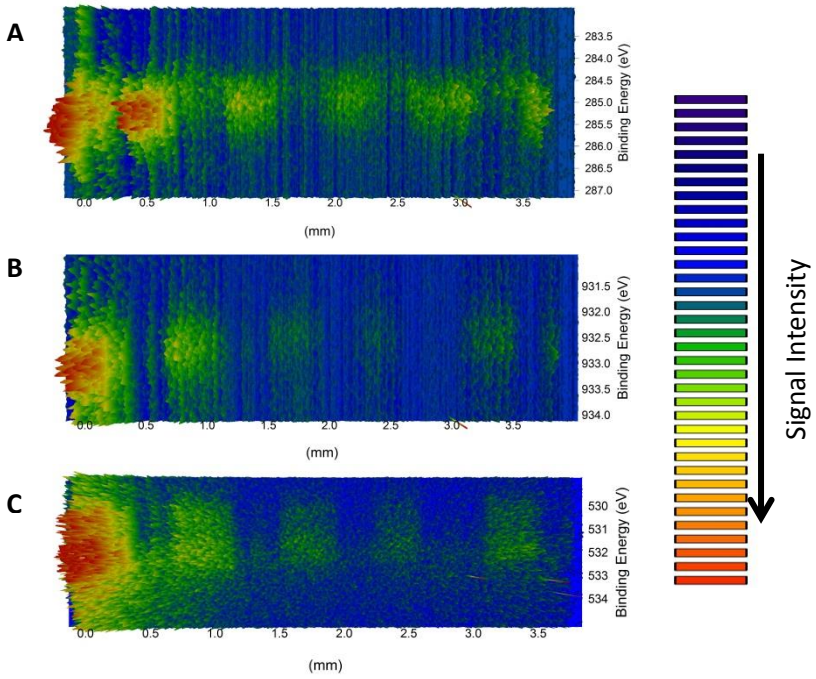

Figure 7.1 – Spatially resolved XPS images of an eccrine fingerprint on copper substrate. ***A)*** *Carbon 1s region;* ***B)*** *Copper $2p_{3/2}$ region;* ***C)*** *Oxygen 1s region.*

Whilst the ideal application is onto non-flat surfaces, this creates a variety of problems relating to surface geometry and sample size. It is possible to use physical and optical imaging techniques to study the surface of cartridge cases (Figure 7.2), but curve correction and precision turning apparatus would also be needed for it to be fully utilised.

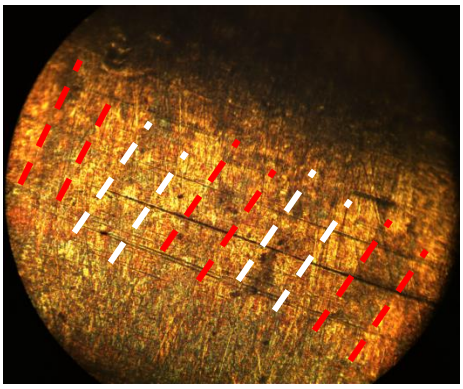

Figure 7.2 – Optical microscopy image of a fingerprint on a 9 mm Luger cartridge case (brass). The dashed sections indicate ridge markings.

7.2.3 Extension to Imaging by Sweat Residue

Whilst not the primary aim of this project, imaging of fingerprints on brass substrates was performed both using substrate variation (metal based bonds) and by the sweat deposited material. The XPS instrument used was only capable of spatially resolving in a single lateral dimension; however, more advanced instruments can resolve in both the *x* and *y* axes. Thus the instrument would be capable of providing a representative imaging resembling a whole fingerprint section rather than merely being able to deduce the presence of localised surface changes as a result of deposited fingerprint material. Two different techniques capable of doing this are Raman and FTIR spectroscopy, although these can image fingerprint material, they cannot image changes in metal substrates. Therefore, if the fingerprint could not be made visible by conventional enhancement techniques (principally dyes and powders) then an image may not be able to be generated by Raman (Figure 7.3) or FTIR (Figure 7.4). However, in these instances XPS may still be able to generate a fingerprint image based on metal oxidation or binding species changes.

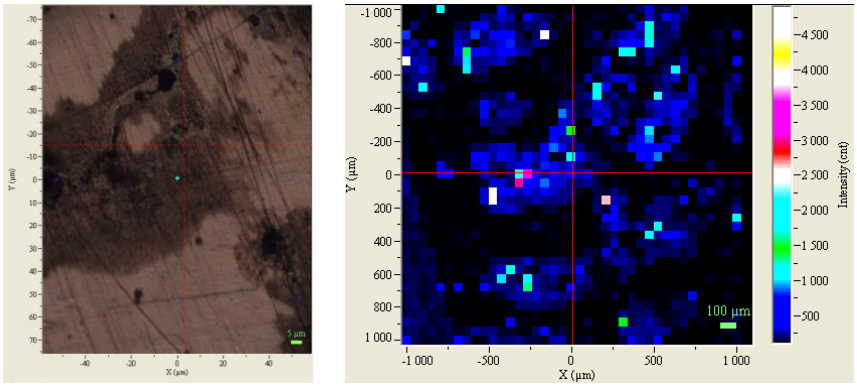

Figure 7.3 – Image of several eccrine fingerprint ridges on a brass substrate stored in ambient conditions. ***A)*** *optical image showing the point of origin of scan sequence;* ***B)*** *Raman spectral map of scanned area using peaks between 2100 cm^{-1} and 2250 cm^{-1}, spectra are acquired every 25 µm. Images were acquired using an Horiba Jobin Yvon Raman spectrograph.*

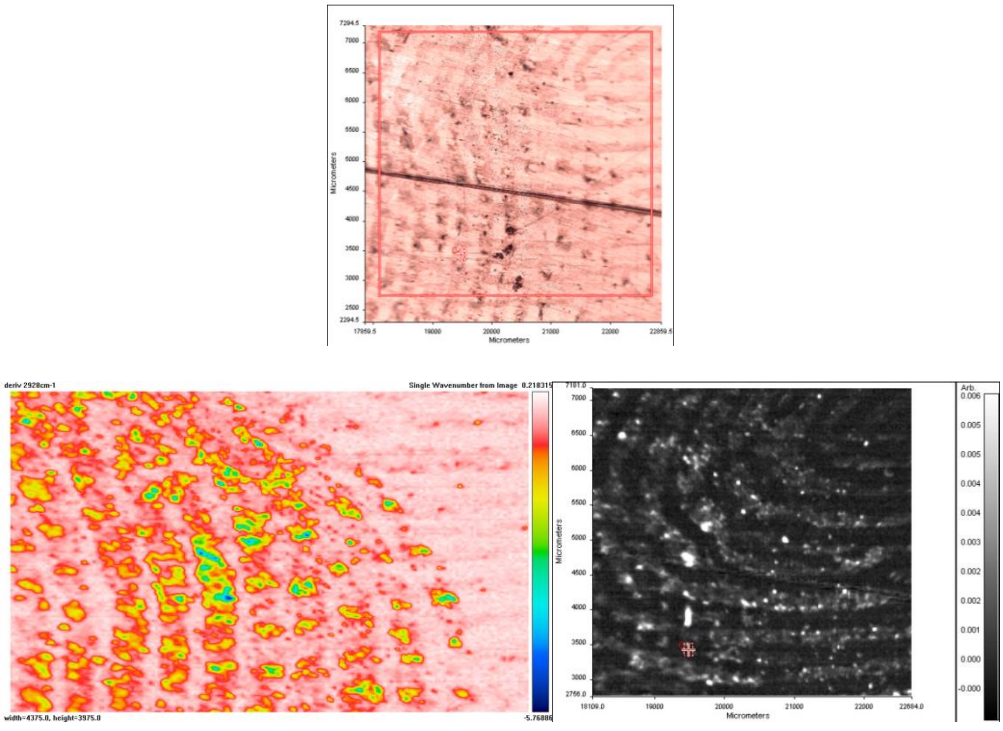

Figure 7.4 – Images acquired using an IR with spatial imaging features. ***A)*** *optical image showing two overlapping fingerprints and marks;* ***B)*** *selective imaging (2900-2920 cm^{-1}) of the right side mark in* ***A****;* ***C)*** *selective imaging (2950-3000 cm^{-1}) of the left side mark in* ***A****. Images were acquired using a Perkin Elmer Frontier FTIR with imaging capabilities.*

7.3 References

1. T. L. Barr and J. J. Hackenberg, *Applications of Surface Science*, 1982, **10**, 523-545.
2. E. Paterson, J. W. Bond and A. R. Hillman, *J. Forensic Sci.*, 2010, **55**, 221-224.

Appendix

A. Chemical Structures for Sweat Components

Urea:

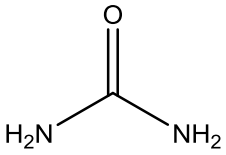

Lactate:

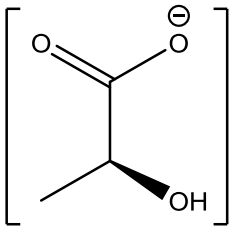

Amino Acid

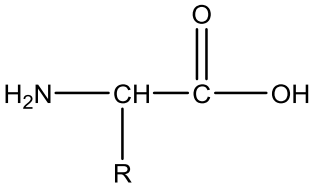

Fatty Acid (unsaturated):

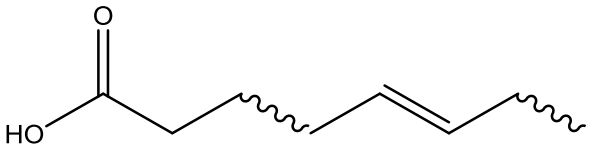

Fatty Acid (saturated):

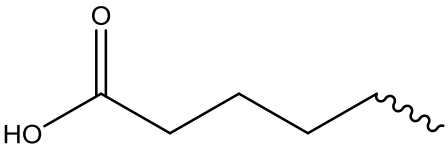

Glucose:

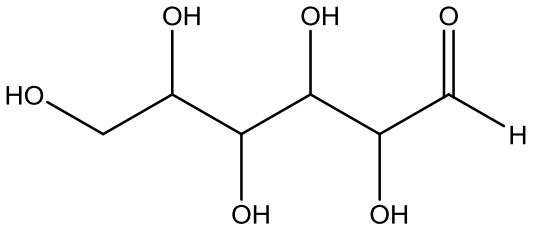

Triglycerides:

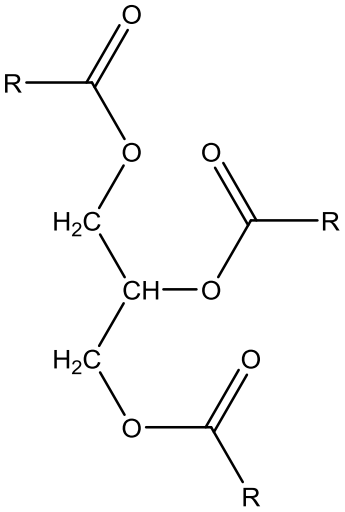

Furan:

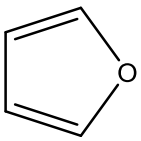

Wax Ester:

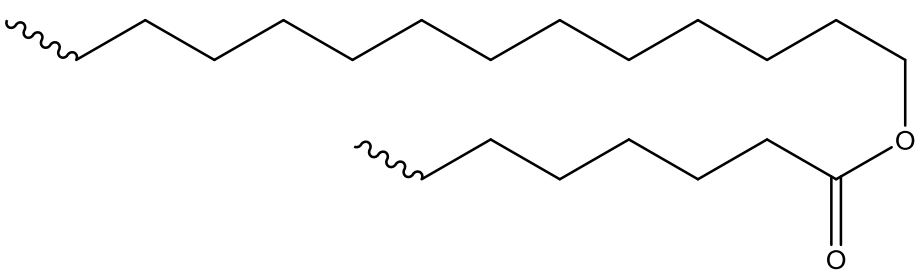

Squalene:

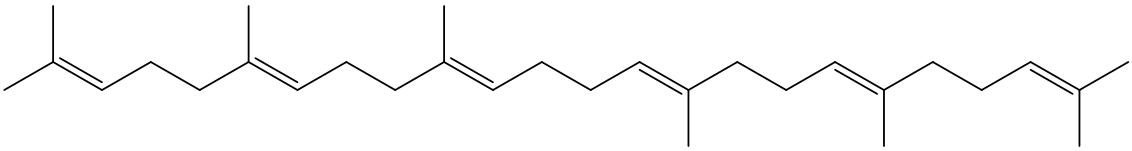

Cholesterol:

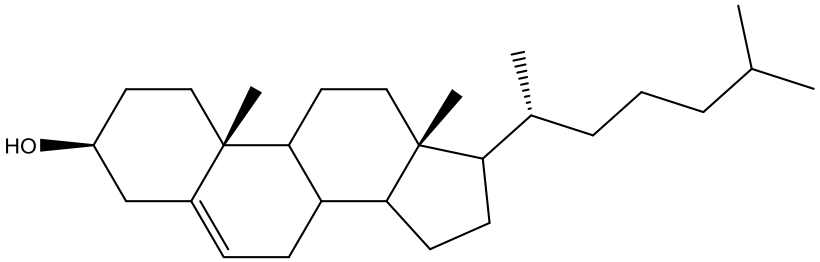

Cholesterol Ester:

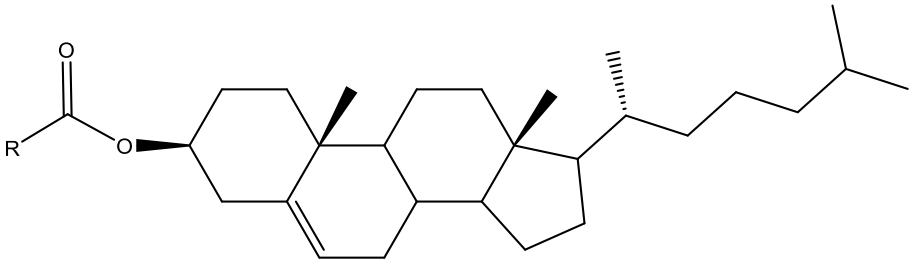

Piperidine:

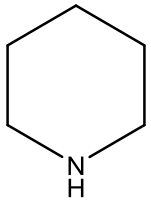

Pyrazine:

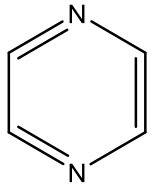

Pyridine:

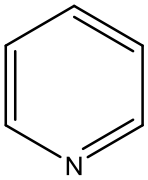

Pyrrole:

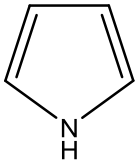

B. Fingerprint Patterns

B.1 UK classification System (Galton-Henry Model)

Depictions on the main fingerprint types used for classification of fingerprints in the UK, these classifications are based on the types primarily outlined by Galton and Henry.

B.1.1 Loops

Right:

Left:

An ulnar loop will enter and leave the fingerprint pattern from the opposite side of the hand to the thumb, pointing towards the ulnar bone in the forearm. A radial loop will enter and leave the fingerprint pattern in the direction of the thumb (radial bone). Without knowing which hand deposited the fingerprint, they can only be assigned as right and left loops; a right loop on the right hand would be an ulnar loop and a right loop on the left hand would be radial loop.

B.1.2 Arches

Arch:

Tented arch:

B.1.3 Whorl: plain, central pocket, double loop and accidental

Plain: Central pocket: Double loop:



An Accidental whorl is one that does not fit into any of the above categories, examples:


B.2 Vucetich's System

Pattern	Value	Short Description	
Arch	5	Vaulted/Normal	Plain arch type
	6	Left-inclined	Left sloping arch pattern
	7	Right-inclined	Right sloping arch pattern
	8	Tent-shaped	Tented arch type
	9	All others	Irregular arches that do not fit the above

Internal loop (ulnar loop)	5	Normal flow	standard loop pattern
	6	Invaded	Loop with additional features
	7	Interrogatory	Internal loop approximating a central pocket
	8	Hooked	External loop approximating a central pocket
	9	All others	Irregular loops that do not fit the above

Pattern	Value	Description	
External loop (radial loop)	5	Normal flow	standard loop pattern
	6	Invaded	Loop with additional features
	7	Interrogatory	Internal loop approximating a central pocket
	8	Hooked	External loop approximating a central pocket
	9	All others	Irregular loops that do not fit the above

Whorl	5	Normal	Plain or central pocket whorl
	6	Sinuous	Spiral based whorl
	7	Ovoid	Elongated plain or central pocket
	8	Hooked	Double core plain or central pocket types
	9	All others	Irregular whorls that do not fit the above

C. DHM

C.1 Interpretation of the Wavefront

In reflection configuration, the wavefront is deformed during the reflection (Figure 2.6B). The deformation with respect to the incident wave is called dephasing ($\Delta\phi$), as is measured in degree. For a homogeneous sample, this dephasing is can be used to determine height changes:

$$\Delta h \frac{\lambda \Delta \varphi}{4\pi n} \qquad \text{Equation C.1}$$

Where, Δh is the height of the sample and n the refractive index of the immersion medium (n=1 in air). However, a DHM does not measure the real dephasing but instead measures the *modulo* 2π.

$$\varphi_{DHM} = \left(\frac{\Delta h 4\pi n}{\lambda}\right) Mod 2\pi \qquad \text{Equation C.2}$$

Where the equidistance is 360° (2π),

$$equidistance = \frac{\lambda}{2n} \qquad \text{Equation C.3}$$

D. AFM Additional Information

D.1 AFM Probe Details

Probes used for all AFM measurements were: Veeco Probes model RTESP MPP-11100-10

1-10 Ωcm phosphorus (n) doped silicon, uncoated

Cantilever details: thickness: 3.5-4.5 µm; length: 115-125 µm, width: 30-40 µm

resonant frequency (f_o): 276 ±34 kHz, spring constant (k): 20-80 N/m

D.2 AFM Scan Settings

Scan settings for AFM data (unless specified otherwise) were:

Scan size: 100 µm

Scan rate: 0.6-0.8 Hz

Integral: 0.2

Proportional gain: 0.3

Amplitude: 0.8-1.0 V

E. Binding Energy: Positions and Species

E.1 Zinc (Zn $2p_{3/2}$)

Binding Energy (eV)	Oxidation state	Species
1021.6 – 1022.0	Zn(0)	Zn(0)
1022.0 – 1022.2	Zn(II)	ZnO
1022.5 – 1022.7	Zn(II)	$Zn(OH)_2$
1023.8 – 1024.0	Zn(II)	$ZnCl_2$

E.2 Copper (Cu $2p_{3/2}$)

Binding Energy (eV)	Oxidation state	Species
932.4	Cu(I)	CuCl
932.4 – 932.7	Cu(I)	Cu_2O
932.6 – 932.9	Cu(0)	Cu(0)
933.0 – 933.9	Cu(II)	CuO
934.9 – 935.4	Cu(II)	$Cu(OH)_2$
943.7 – 946.3	Cu(II)	CuO (satellite peak)

E.3 Carbon (C 1s)

Binding Energy (eV)	Species
285	Residual carbon
285 – 285.5	Hydrocarbons/Alkyl carbon
286.0 – 286.3	C-O/COOR
288.0 – 288.7	C=O
288.9	Alkyl carbon
289.7 – 289.9	CO_3
290.4	Aromatic carbons
291	Methyl

E.4 Oxygen (O 1s)

Binding Energy (eV)	Species
529.5 – 530.2	Metal oxides (ZnO/CuO/Cu_2O)
530.3 – 530.6	CuO/Cu_2O
530.8 – 531.0	$Cu(OH)_2$
531.5	ZnO/CuO
531.7 – 532.1	$Cu(OH)_2$/OH
532.0	$Zn(OH)_2$
532.1 – 532.2	H_2O
332.4	O in organic carbon compounds
532.2 – 532.6	H_2O
533.4 – 534.2	C-O